
**Structural and Biochemical Examination of the
PER1-PAS Domains and the CRY1/PER2 Complex
as Regulatory Elements of the Mammalian Circadian Clock**

Dissertation

der Fakultät für Biologie

der Ludwig-Maximilians-Universität München



vorgelegt von

Ira Christine Schmalen, MSc

München

08.07.2014

1. Gutachter: Prof. Dr. J. Soll

2. Gutachter: Prof. Dr. C. David

Betreuer: Prof. Dr. E. Wolf

Tag der mündlichen Prüfung: 12.09.2014

Eidesstattliche Erklärung

Ich versichere hiermit an Eides statt, dass die vorgelegte Dissertation von mir selbständig und ohne unerlaubte Hilfe angefertigt ist.

München, den

(Unterschrift)

Erklärung

Hiermit erkläre ich,

- dass die Dissertation nicht ganz oder in wesentlichen Teilen einer anderen Prüfungskommission vorgelegt worden ist.
- dass ich mich anderweitig einer Doktorprüfung ohne Erfolg **nicht** unterzogen habe.
- dass ich mich mit Erfolg der Doktorprüfung im Hauptfach und in den Nebenfächern bei der Fakultät für der (Hochschule/Universität) unterzogen habe.
- dass ich ohne Erfolg versucht habe, eine Dissertation einzureichen oder mich der Doktorprüfung zu unterziehen.

München, den.....

(Unterschrift)

Table of Contents

Abbreviations	7
List of Publications.....	9
Zusammenfassung	10
Summary	12
1 Introduction.....	14
1.1 Circadian Rhythms	14
1.2 Molecular Components and Mechanisms of the Mammalian Circadian Clock	17
1.3 The Circadian Clock and Metabolism.....	21
1.4 PERIOD (PER) Proteins – Prominent Members of the Mammalian Circadian Clock	24
1.4.1 Mutant Phenotypes Suggest Non-Redundant Mammalian PER Protein Functions	24
1.4.2 Domain Architecture/Functional Motifs of Mammalian PER Proteins.....	26
1.4.3 Posttranslational Modifications of Mammalian PER Proteins.....	28
1.4.4 PAS Domains: Signal Sensors and Interaction Platforms.....	29
1.5 CRYPTOCHROMES (CRY) – Blue Light Sensors and Transcription Repressors.....	31
1.5.1 Photolyases – Evolutionary Relatives of Cryptochromes	31
1.5.2 Classification, Domain Architecture and Light Sensitivity of Cryptochromes	32
1.5.3 Mammalian Cryptochromes and the Circadian Clock.....	34
1.5.4 Posttranslational Modifications of Mammalian CRY Proteins.....	36
1.5.5 Mammalian CRY and its Link to Metabolism.....	36
1.6 The CRY/PER Repressor Complex Drives Circadian Rhythms.....	38
1.6.1 Nuclear Localization of CRY and PER.....	38
1.6.2 The Molecular Mechanisms of Feedback Transcriptional Repression	39
2 Aims of the Thesis.....	42
3 Results	43
Publication I	43
Publication II	59

4 Extended Discussion	90
4.1 <i>In Vitro</i> Characterization of Mammalian PERIOD Proteins	91
4.2 A Conserved Tryptophan as Mediator of Clock PAS Interactions	91
4.3 Mammalian PER - a Heme Bound Signal Sensor or not?	94
4.4 Zinc Binding and Disulfide Bond Formation Regulates the mCRY1/mPER2 Core Complex	96
4.5 Helix α 22 Determines CRY Stability and Function.....	102
4.6 FAD and the mCRY1/mPER2 Complex	104
4.7 Composition and Dynamics of the CRY/PER Repressor Complex	105
5 Outlook.....	108
References.....	110
Acknowledgements	125
Curriculum Vitae.....	126

Abbreviations

AMPK	:	AMP-activated protein kinase
AMP	:	adenosine monophosphate
ar	:	arhythmic
At	:	<i>Arabidopsis thaliana</i>
ATP	:	adenosine triphosphate
bHLH	:	basic helix-loop-helix
BMAL1	:	<u>B</u> rain <u>M</u> uscle <u>A</u> RNT <u>L</u> ike 1
bZIP domain	:	basic leucine zipper domain
ccgs	:	clock-controlled genes
CLD	:	cytoplasmic localization domain
CLOCK	:	<u>C</u> ircadian <u>L</u> ocomotor <u>O</u> utput <u>C</u> ycles <u>K</u> aput, CLK
CK	:	casein kinase
CRY	:	CRYPTOCHROME
Cys	:	cysteine, C
DBP	:	D-site albumin promoter binding protein
Dm, d	:	<i>Drosophila melanogaster</i>
DNA	:	deoxyribonucleic acid
ds	:	days
E4BP4	:	E4 promoter binding protein 4
FAD	:	flavin adenine dinucleotide
FASPS	:	familial advanced sleep phase syndrome
FBXL3	:	F-box/LRR-repeat protein
FMN	:	flavin mononucleotide
GSK	:	glycogen synthase kinase
8-HDF	:	8-hydroxy-7,8-didemethyl-5-deazariboflavin
HRM	:	heme regulatory motif
hrs	:	hours
MAPK	:	mitogen-activated protein kinase

Mm, m	:	<i>Mus musculus</i> , mouse
MTHF	:	methenyltetrahydrofolate
NAD	:	nicotinamide adenine dinucleotide
NADP	:	nicotinamide adenine dinucleotide phosphate
NCoR/HDAC3	:	NR corepressor/ histone deacetylase 3
NES	:	nuclear export signal
NLS	:	nuclear localization signal
NPAS2	:	neuronal PAS domain protein 2
NR	:	nuclear receptor
PAS	:	<u>P</u> ER- <u>A</u> RNT- <u>S</u> IM
PER	:	PERIOD
pd	:	period
PHR	:	photolyase homology region
Pro	:	proline, P
PTM	:	posttranslational modification
RNA	:	ribonucleic acid
ROR	:	retinoic acid receptor-related orphan receptor
ROS	:	reactive oxygen species
RRE	:	receptor response element
SCF	:	<u>S</u> kp, <u>C</u> ullin, <u>F</u> -box protein complex
SCN	:	suprachiasmatic nucleus
Ser	:	serine, S
SIRT1	:	sirtuin 1
Thr	:	threonine, T
TIM	:	TIMELESS
Trp	:	tryptophan, W
ws	:	weeks
wt	:	wild type

List of Publications

1) Kucera N., **Schmalen I.**, Hennig S., Öllinger R., Strauss H. M., Grudziecki A., Wieczorek C., Kramer A., and Wolf E. (2012). Unwinding the differences of the mammalian PERIOD clock proteins from crystal structure to cellular function. *Proc Natl Acad Sci USA* 109, 3311–3316.

I.S. solved the crystal structure of mPER1 and designed and performed parts of the biochemical analysis of mPER1/2. She prepared the corresponding figures for the paper.

2) **Schmalen I.**, Reischl S., Wallach T., Klemz R., Grudziecki A., Prabu J.R., Benda C., Kramer A., Wolf E. (2014). Interaction of circadian clock proteins CRY and PER is modulated by zinc binding and disulfide bond formation. *Cell* 157, 1203 - 1215.

I.S. solved the crystal structure of mCRY1/mPER2 and designed, performed and evaluated all *in vitro* experiments. The manuscript was written by I.S., E.W. and A.K..

Remark:

The projects described in this thesis are collaborative achievements. Ira Schmalen performed all experiments mentioned above under the supervision of Prof. Dr. E. Wolf and received scientific suggestions and technical support from people in the lab. Based on the structural and biochemical analysis complementary cell-based assays and *in vivo* experiments have been collaboratively designed and were performed by the lab of Prof. Dr. A. Kramer at the Charité in Berlin.

I hereby confirm the above statements.

.....

Ira Schmalen

.....

Prof. Dr. E. Wolf

Zusammenfassung

Zirkadiane Uhren steuern 24 Stunden Rhythmen im Verhalten, im Stoffwechsel und in der Physiologie fast aller Spezies. PERIOD (PER) Proteine stellen eine essentielle molekulare Komponente für die Funktionalität aller bisher untersuchten Säugetieroszillatoren dar. Sie interagieren nicht nur mit Cryptochromen (CRY), sondern dienen auch als Plattform für die Interaktion mit zahlreichen weiteren Uhrenproteinen. Dadurch unterstützen PER1 und PER2 Cryptochrome (CRY1, CRY2) bei der negativen Regulierung der durch die Transkriptionsfaktoren CLOCK/BMAL1 gesteuerten Transaktivierung von Uhren- und Uhr kontrollierten Genen, während PER3 individuelle Funktionen in den Ausgangssignalwegen und den peripheren Uhren zugeschrieben werden.

Im Rahmen dieser Arbeit wurden die unterschiedlichen molekularen Mechanismen der PAS Domänen von mPER1 im Vergleich zu den PAS Domänen von mPER2 und mPER3 sowie die molekularen Details des mCRY1/mPER2 Komplexes mittels Röntgenstrukturanalyse und komplementären, biochemischen Methoden untersucht und im Kontext des zirkadianen Oszillators analysiert.

Die Kristallstruktur der PER1 PAS-Domänen zeigt, wie bereits im Falle von mPER2 und mPER3, ein nicht-kristallographisches Homodimer, welches auch in Lösung vorliegt. Das Homodimer wird durch Wechselwirkungen der antiparallelen PAS-B Domänen (PAS-B Trp Interface) und, anders als im Fall von mPER2 und mPER3, durch zusätzlich Interaktionen der beiden PAS-A Domänen stabilisiert (α C-Interface). Dies bedingt vermutlich die hohe Affinität des mPER1 Homodimers und unterstützt die, im Vergleich zu den PAS Domänen von mPER2 und mPER3, kompaktere und starrere Faltung von mPER1. Die geringe Flexibilität des mPER1 Homodimers limitiert sehr wahrscheinlich auch die Wechselwirkungen von mPER1 mit anderen Proteinen und Liganden und beschränkt so seine Funktionen. Dies zeigt sich in kleineren mPER1 Komplexen im Vergleich zu mPER2 und erklärt seine Rolle beim Kernimport von CRY/PER und seine im Vergleich zu mPER2 weniger dominante Rolle als Transkriptionskorepressor.

Die PAS-Domänen von PER sind an der Bildung des Repressorkomplexes im Zellkern beteiligt, jedoch sind sie nicht in die Bildung des dimeren CRY/PER Kernkomplexes involviert. Die Kristallstruktur von mCRY1/mPER2 zeigt, dass mPER2 großflächig mit seinen ≈ 100 C-terminalen Resten mit der α -helikalen Domäne von mCRY1 interagiert und dabei die

Bindestellen der E3 Ligase Komponente FBXL3 und der Transkriptionsfaktoren CLOCK/BMAL1 nicht aber die Bindetasche des Kofaktors FAD abdeckt. Auf der einen Seite stabilisiert PER dadurch CRY und schützt es vor dem proteolytischen Abbau durch FBXL3. Auf der anderen Seite behindert die Wechselwirkung mit PER CRY bei seiner Bindung an den aktiven CLOCK/BMAL1 Transkriptionskomplex. Überraschenderweise zeigt sich in der Kristallstruktur ein gemeinsam koordiniertes Zinkion an einer der vier Hauptbindestellen zwischen mCRY1 und mPER2, welches den Komplex stabilisiert. Ergebnisse aus *in vitro* und Zell-Assay Experimenten deuten auf ein Zusammenspiel dieser Zinkbindung und der Bildung von Disulfidbrücken in CRY bei der Regulierung des mCRY1/mPER2 Komplexes hin. Die Disulfidbrückenbildung von mCRY1 wird *in vivo* vermutlich durch den Redoxzustand der Zelle beeinflusst. Zusammenfassend gewährt die Kristallstruktur von mCRY1/mPER2 einen detaillierten Einblick in die Wechselwirkungen von CRY und PER. Dadurch entstehen neue Ideen, wie dieser Komplex möglicherweise den metabolischen Zustand der Zelle erkennt und dementsprechend agiert und wie das Zusammenspiel von CRY/PER mit anderen Uhrenproteinen die zirkadiane Uhr antreibt. Auf dieser Grundlage können weiterführende Experimente und die Entwicklung neuer Wirkstoffe, die auf die innere Uhr oder den Stoffwechsel zielen, geplant werden.

Summary

Circadian clocks account for rhythmic changes in behavior, metabolism and physiology of most species with respect to time of day. PERIOD (PER) proteins are essential components of the molecular mammalian oscillator. They do not only form complexes with cryptochromes (CRY) but also serve as a scaffold for the interaction of multiple proteins transferring timing to the latter. Thereby, PER is important for CRY mediated negative regulation of CLOCK/BMAL1-dependent transactivation of clock and clock-controlled genes. Nevertheless, mammalian PER proteins (PER1-3) seem to have distinct functions in the clock and related output pathways.

In the course of this thesis the different molecular mechanisms of the PAS domains of mPER1 in comparison with the PAS domains of mPER2 and mPER3 as well as the molecular details of the mCRY1/mPER2 complex were examined by crystal structure analysis and complementary biochemical methods. The results were further analyzed in the context of the circadian oscillator.

The crystal structure of the dual PAS domains of mPER1 shows, as in the case of mPER2 and mPER3, a non-crystallographic PAS homodimer, which is present in solution, too. The homodimer is stabilized by interactions of the antiparallel PAS-B β -sheet surfaces (PAS-B Trp interface) and, different from mPER2 and mPER3, by additional interactions between its PAS-A domains (α C-interface). These two interfaces are presumably responsible for the highly affine, more compact and inflexible fold of the mPER1 PAS domains in comparison to mPER2 and mPER3. Thereby, its molecular interaction and signaling capacity is limited which is probably reflected on the one hand in lower molecular weight of mPER1 complexes compared to mPER2 complexes and on the other hand explains its less dominant circadian roles in determination of CRY-PER localization and as transcriptional corepressor.

The PAS domains are required for transcriptional repressor complex formation; however, they are not involved in dimeric core CRY/PER complex formation. The crystal structure of mCRY1/mPER2 reveals that mPER2 winds with its \approx 100 C-terminal residues around the α -helical domain of mCRY1. Thus, it covers a large surface area which includes the binding sites of the E3 ligase complex component FBXL3 and the transcription factor BMAL1 but not the FAD cofactor binding pocket. Consequently, PER stabilizes CRY and shields it from FBXL3 mediated degradation on the one hand, and probably interferes with its binding to CLOCK/BMAL1 on the

other hand. Surprisingly, one of the four complex interfaces is mediated by a jointly coordinated zinc ion, which substantially stabilizes mCRY1-mPER2 interaction. Results from both *in vitro* and cell-based assays imply that mCRY1/mPER2 complex formation is probably regulated by an interplay of zinc binding and mCRY1 disulfide bond formation, which may be influenced by the redox state of the cell. Overall the crystal structure of mCRY1/mPER2 not only provides a detailed insight into CRY-PER interaction but also new ideas on how this complex might sense and act corresponding to the cellular/metabolic state and how the interplay with other clock components drives the circadian oscillator. This will guide the design of new experiments and the development of novel circadian and metabolic modulators in the future.

1 Introduction

1.1 Circadian Rhythms

Circadian rhythms are the extrinsic manifestations of an endogenous timing system and include approximately 24 hrs (circa diem: lat. approximately one day) rhythms in many physiological and behavioral processes. Developed as adaptation to the daily light/dark cycle they advantageously influence the activity and survival of organisms from all phyla and link regular environmental changes with the (temporal) molecular composition of organisms.

Circadian rhythms are associated with asexual development in *Neurospora crassa* (Loros and Dunlap, 2000), photosynthesis, leaf positioning and growth in plants (Yakir et al., 2006), locomotor activity, wake cycle and body temperature in animals and more precisely blood pressure, heart rate and hormone circulation in humans (Albrecht and Eichele, 2003; Hastings et al., 2007). Fundamental features of all these rhythms are I) persistence in the absence of external cues, i.e. they are free-running and self-sustained, II) entrainment to cyclic environmental stimuli like light, which allows for adaptation of the circadian period to about 24 hrs, and III) compensation for inappropriate signals like changing surrounding temperature or varying nutrition (Kramer and Meroow, 2013).

The origin of rhythmicity lies in so-called circadian clocks which commonly consist of three major components: an input pathway, a central oscillator and an output pathway (Eskin, 1979). The input pathway transduces “Zeitgeber” signals, the most prominent of which are light signals, to the oscillator which generates rhythms in RNA and protein levels based on autoregulatory feedback loops. The output pathways translate these rhythms into periodic biological processes (Figure 1). In mammals a hierarchal network of numerous oscillators exists with the master clock residing in the suprachiasmatic nucleus (SCN) in the hypothalamus (Bell-Pedersen et al., 2005). It is composed of coupled, synchronized neurons which all display self-sustained oscillations (Quintero et al., 2003). Indeed the selective destruction of the SCN results in complete loss of all circadian rhythms (Moore and Eichler, 1972; Stephan and Zucker, 1972), however, rhythmicity can be almost completely restored, including rhythmic locomotor activity, through grafting of a SCN. This leads to adoption of the donator rhythm (Ralph et al., 1990). Synaptic communication between its constitutive cells and integrity of the SCN allow for robust

molecular oscillation of the clock proteins, sustain rhythmicity even in absence of single clock genes and keep phase against environmental disturbances like restricted feeding (Damiola et al., 2000; Liu et al., 2007b; Yamaguchi et al., 2003).

The master pacemaker is uniquely entrained through light signals from the environment received via the retinohypothalamic tract (RHT) (Johnson et al., 1988). It is then responsible for synchronization of local peripheral clocks either directly through humoral and neuronal signaling or indirectly through regulation of sleep, body temperature and feeding (Balsalobre et al., 2000; 1998; Brown et al., 2002; Green et al., 2008). Peripheral clocks are found in almost all cells and tissues including the liver, lung, kidneys, etc. (Yoo et al., 2004). They are responsible for tissue specific rhythmic expression of genes (output). Some rhythmic outputs such as NAD^+ have been suggested to feedback to the clock and act as adjusting signals (Eckel-Mahan and Sassone-Corsi, 2009).

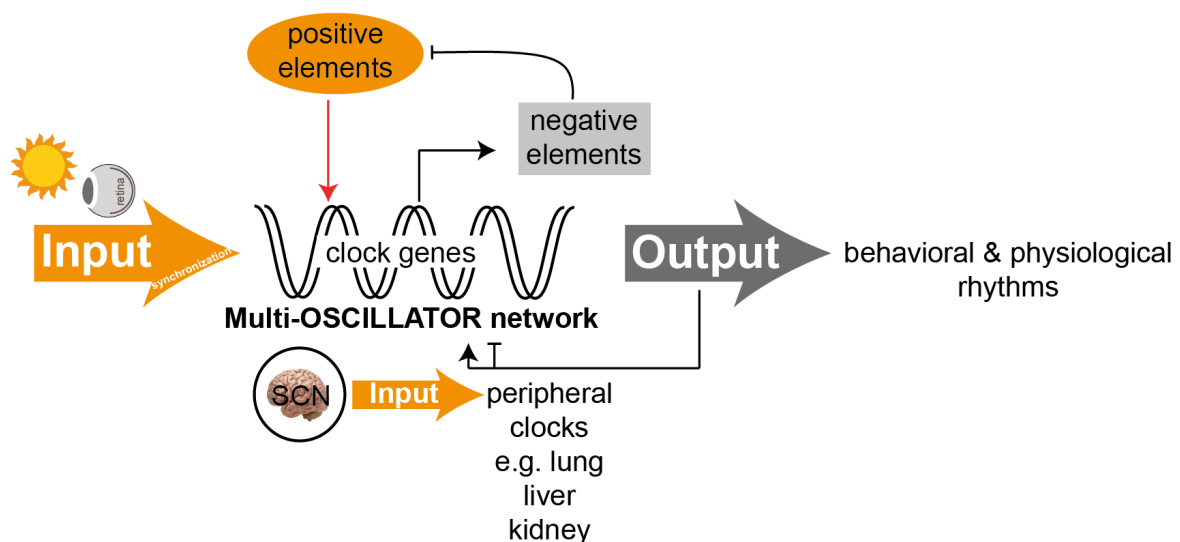


Figure 1: Principle components of the mammalian timing system (input, the 24 hrs clock, output). The mammalian circadian clock is composed of a multi oscillator network, in which the SCN is the central pacemaker. This master oscillator receives light signals (input) for synchronization with the daily 24 hrs light/dark cycle and accordingly produces endogenous circadian signals which serve to coordinate peripheral clocks (responsible for local outputs). Transcriptional autoregulatory feedback loops mediated through the interplay of positive and negative elements continuously drive all clocks. While the positive clock elements/proteins induce the expression of clock genes including the negative elements/proteins, these in turn “feedback” and inhibit the positive elements. Together all body oscillators generate rhythmic behavioral and physiological outputs (inspired from (Agostino et al., 2010; Liu et al., 2007a)).

The core clock genes and mechanisms are very similar in all body oscillators and are based on transcriptional autoregulatory feedback loops and specified to keep the 24 hrs time frame through posttranscriptional (Kojima et al., 2012) and posttranslational modifications (Gallego

and Virshup, 2007), chromatin remodeling (Grimaldi et al., 2009), directed subcellular localization (Vielhaber et al., 2001) as well as timed degradation of clock proteins (e.g. (Sahar et al., 2010; Yoo et al., 2013)). However, the expression levels, contributions and functions of core and peripheral clock and clock-controlled components are tissue specific. This manifests for example in a low convergence in oscillating transcripts between SCN, liver and heart. Only transcripts of integral clock genes that assure fundamental oscillator functionality are consistent (Panda et al., 2002; Storch et al., 2002).

1.2 Molecular Components and Mechanisms of the Mammalian Circadian Clock

The mechanistic principle behind circadian clocks is conserved, however, the core clock genes and corresponding proteins greatly vary across phyla.

The mammalian circadian clock, which was most intensively studied in rodents¹, is composed of feedback loops involving transcription and translation of specific core clock proteins (Figure 2). A circadian cycle is initiated by the transcription factors CLOCK (circadian locomotor output cycles kaput protein) (Antoch et al., 1997) (or its paralog NPAS2 (neuronal PAS domain protein 2) (DeBryne, et al., 2007)) and BMAL1 (brain and muscle Arnt-like protein-1) (Bunger et al., 2000; Gekakis et al., 1998) (positive elements, compare Figure 2). Both contain a bHLH (basic helix-loop helix) motif and two PAS (PER-ARNT-SIM) domains. While the PAS domains mediate their heterodimer formation (section 1.4.1), CLOCK and BMAL1 bind to E/E'-box elements in the DNA of clock and clock-controlled genes via their bHLH domain (Huang et al., 2012). Thereby, they activate transcription of the negative clock components PERIOD (PER, paralogs 1, 2 and 3) and CRYPTOCHROME (CRY, paralogs 1 and 2) as well as the so-called clock-controlled genes (ccgs). This cascade contributes to the rhythmic output of circadian proteins and their targets. The accumulated PER and CRY proteins form degradation protected complexes in the cytoplasm. These complexes then enter the nucleus where they interact with the CLOCK/BMAL1 complex and repress transcription (Lowrey and Takahashi, 2004). Hence, they negatively influence their own transcription (negative feedback). At the end of the cycle PER and CRY are degraded via the ubiquitin-proteasome pathway and CLOCK/BMAL1 mediated transcription is restored.

Resetting and synchronization of the circadian cycle with the environment is achieved through Ca²⁺-dependent protein kinase signaling pathways and subsequent activation the cAMP/Ca²⁺ response element-binding (CREB) protein which binds to corresponding elements in the promoters of for instance *Per1* and *2* and induces expression in response to a light signal (Golombek and Rosenstein, 2010; Hastings and Herzog, 2004). Recruitment of the histone acetyltransferases CREB-binding protein (CBP) and its homolog p300 (amongst others) to the CLOCK/BMAL1 complex restarts a new transcription cycle (Koike et al., 2012; Lee et al., 2010).

¹ Next to the *Drosophila* oscillator, the mammalian oscillator is best studied today. Rodents, in particular mice, serve as model organism. Therefore, this study focuses on mouse (*mus musculus*) clock proteins, which show a very high sequence similarity/ identity with clock proteins from humans (*homo sapiens*).

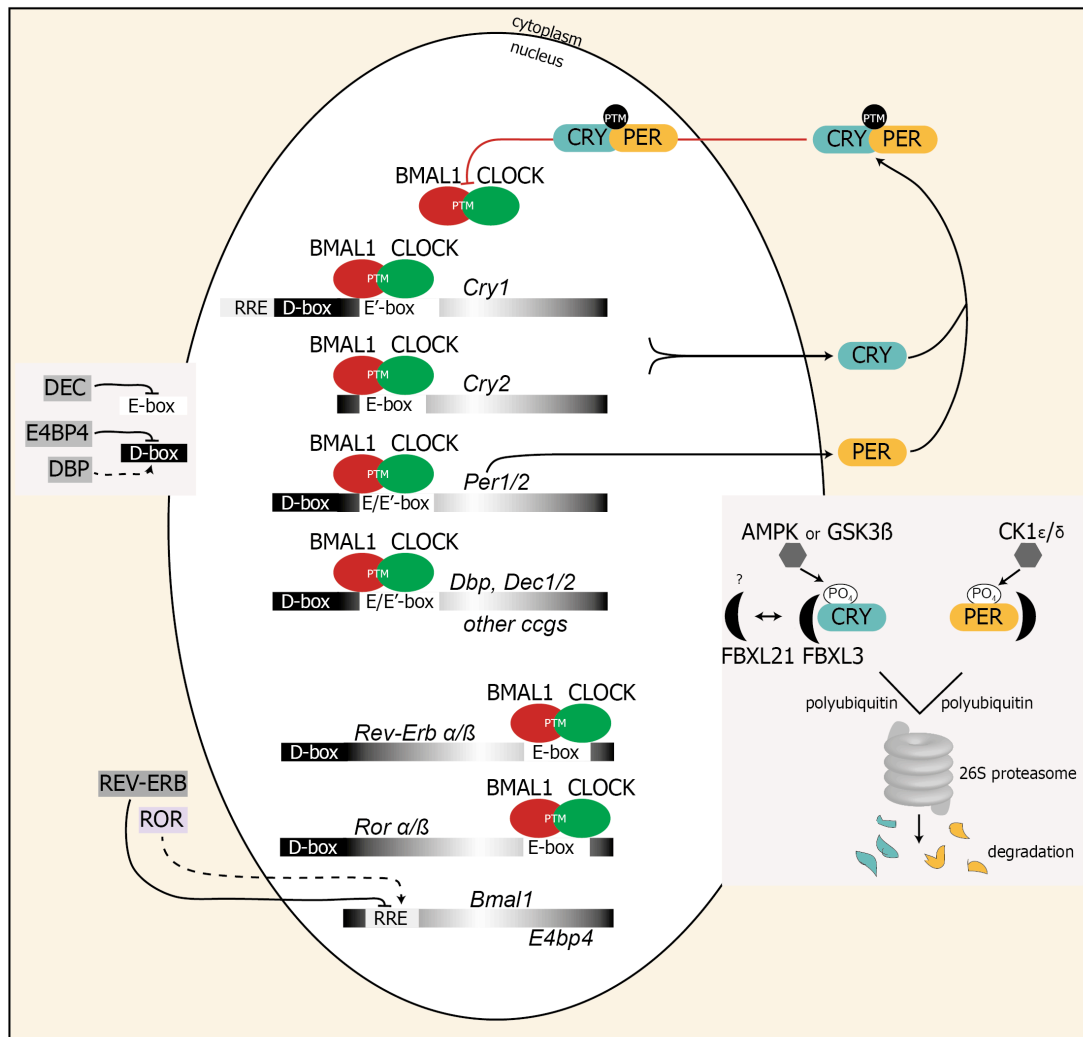


Figure 2: Illustration of the molecular components of the mammalian circadian clock. The CLOCK/BMAL1 complex (green/red) binds to the E/E'-boxes in the DNA of clock and clock controlled genes and regulates their transcription. Resulting CRY and PER proteins (cyan/orange) dimerize and translocate to the nucleus where they inhibit CLOCK/BMAL1 initiated transcription and consequently their own transcription (negative feedback). A delay in CRY/PER mediated feedback is established through two additional accessory feedback loops in one of which the orphan nuclear receptors REV-ERB and ROR regulate BMAL1 transcription amongst others through binding to RRE sites. Transcription factors DBP and E4BP4 further regulate the clock on the transcriptional level via binding to D-box elements in the DNA of several clock genes. Transcriptional repression is terminated through degradation of CRY and PER via the ubiquitin proteasome pathway; PTM: posttranslational modification (modified from (Kramer and Merrow, 2013)).

To ensure flexibility and ≈ 24 hrs coverage of the circadian clock, the above described core feedback loop is assisted by numerous side processes. Transcription activation through CLOCK/BMAL1 depends on the phosphorylation by casein kinase I ϵ (CK1 ϵ), glycogen synthase kinase 3 β (GSK3 β) and mitogen-activated protein kinase (MAPK) (Eide et al., 2002; Sahar et al., 2010; Sanada et al., 2002) as well as posttranslational histone modifications. Histone modifications are achieved through acetylation by CLOCK itself (Doi et al., 2006) or other

chromatin modifying activities resulting in (de)phosphorylation, (de)acetylation, (de)methylation, etc. of histones (Curtis et al., 2004; Etchegaray et al., 2003).

CLOCK/BMAL1 activity on E-box containing genes (*Per1*, *Dbp*, *REV-ERBa*) is further suggested to be delayed through the transcriptional corepressor DEC1, whose expression is conversely controlled by the core loop. It modulates BMAL1/CLOCK activity either through binding with its bHLH DNA binding domain to E-box elements or through interaction with BMAL1 (Nakashima et al., 2008). Furthermore, regulation of CRY/PER cellular localization as well as timed degradation of CRY and PER via the ubiquitin proteasome pathway account for supplemental precision.

In a second transcriptional feedback loop the retinoic acid-related orphan nuclear receptors ROR (paralogs α , β and γ) and REV-ERB (paralogs α and β), whose expression is reversely fine-tuned by the CLOCK/BMAL1 heterodimer through their E-box elements, control circadian *Bmal1* expression (Clock is constitutively expressed in the SCN and cycles in peripheral clocks (Lowrey and Takahashi, 2004)). ROR and REV-ERB support the clock through their competitive binding to the retinoic acid-related orphan receptor response elements (RRE), however, they are insignificant for rhythmicity. While REV-ERB represses *Bmal1* transcription through recruitment of the NCoR/HDAC3 complex, ROR activates *Bmal1* transcription (Akashi and Takumi, 2005; Guillaumond et al., 2005; Preitner et al., 2002). RRE elements are also contained in the DNA of *Clock*, *Npas2*, *Cry1*, *E4bp4* and *Ror*.

Lately a second accessory feedback loop was suggested which involves the antagonistically acting bZIP transcription factors DBP (D-site albumin promoter binding protein) and E4BP4 (E4 promoter binding protein 4). They act on D-box elements in the promoter of their target genes including *Per1-3*, *Rev-Erb*, *Ror* and *Cry1* (Ueda et al., 2005; Yamajuku et al., 2011). Indeed, Ukai-Tadenuma et al. reported from cell culture assays that phase delay in *Cry1* transcription is ensured through the combination of D-Box, E-box and RRE elements in the DNA of *Cry1* and constitutes the prerequisite for an efficient clock (Ukai-Tadenuma et al., 2011).

Nevertheless, findings from Menet et al. recently modified the influence of *de novo* transcription and instead strengthened the importance of posttranscriptional modifications for the circadian cycle. Using a genome-wide sequencing approach of nascent RNA they showed that only half of the rhythmically transcribed clock-controlled genes indeed show a rhythmic mRNA pattern. In contrast, about two-thirds of all rhythmic mRNAs even did not show rhythmic transcription and the DNA binding profile of CLOCK/BMAL1 did not fit to the time point of

transcription of their target genes (Menet et al., 2012). Few examples of transcription independent circadian cycles are described in literature, too, including the autoregulatory phosphorylation cycle of cyanobacterial Kai proteins. Most recently, circadian rhythms in the cysteine redox state of peroxiredoxins, rhythmic hemoglobin dimer (oxidized, Fe(III)) - tetramer (reduced, Fe(II)) transitions, and oscillations in the level of NADH/NADPH in anucleate human red blood cells have been described as consistent in the absence of transcription. However, they are most probably initiated by and somehow interconnected with the transcriptional circadian elements (O'Neill and Reddy, 2011).

1.3 The Circadian Clock and Metabolism

The circadian clock is linked to metabolic homeostasis. Indeed, among the rhythmically regulated genes there is a profound number of rate limiting genes involved in e.g. glucose homeostasis as well as lipid and xenobiotic metabolism in the liver (Panda et al., 2002). Correspondingly, mice with disrupted clock genes are prone to metabolic disorders. Shift work, which distracts the natural circadian rhythm, is associated with an increased occurrence of metabolic syndrome in humans (De Bacquer et al., 2009).

However, there is emerging evidence that metabolic output reciprocally contributes to circadian timing, too. Especially peripheral oscillators are affected by feeding and hence metabolism. Indeed, restricted feeding changes the phase of circadian gene expression in peripheral organs independent from the master clock in the SCN which keeps phase according to daytime (Damiola et al., 2000). It is mainly unclear by which means this food entrainment of peripheral clocks happens. However, it resembles light resetting of the central pacemaker and consequently suggests a reciprocal link between the circadian clock and metabolism.

Glucose, which resets the circadian clock in cell assays (Hirota et al., 2002), or food stimulated hormones such as Ghrelin (LeSauter et al., 2009) are discussed to entrain the peripheral circadian clocks according to feeding. The redox and metabolic state of the cell, which is for example represented by the coenzyme NAD^+/NADH ratio, impacts the circadian oscillator (Figure 3). Reduced NADH enhances DNA binding of CLOCK/BMAL1 and NPAS2/BMAL1, respectively, while oxidized NAD^+ attenuates at least NPAS2/BMAL1 DNA binding capacity *in vitro* (Rutter et al., 2001). Furthermore, circadian gene expression is affected in different ways by the NAD^+ dependant (histone) deacetylase SIRT1: It interacts with CLOCK and deacetylates its partner BMAL1 (Nakahata et al., 2007). Thereby, SIRT1 attenuates interaction BMAL1 with its repressor CRY1 (Hirayama et al., 2007). Secondly, it deacetylates PER2, the second key component of the transcription repressor complex, which supports its degradation (Asher et al., 2007). Consequently, SIRT1 compromises CLOCK/BMAL1 transcriptional activity. Moreover, it deacetylates Lys9 and Lys14 of histone H3 and thereby counterbalances the histone H3 acetylation function of CLOCK. As both acetylation of BMAL1 and histone H3 are associated with the acetylation function of CLOCK at different time points, SIRT1 probably acts as a regulator for CLOCK (Nakahata et al., 2007). SIRT1 also deacetylates

and regulates other proteins like PGC1 α (PPAR γ coactivator α) which is involved in gluconeogenesis (Rodgers et al., 2005). PGC1 α further functions as a transcriptional coactivator of ROR proteins which positively regulate *Bmal1* expression (Liu et al., 2007c). Strikingly, SIRT1 activity is inhibited by the reduced form of NAD $^+$ (NADH) as well as by the NAD $^+$ consumption and deacetylation side product NAM (nicotinamide) and thus generates a feedback loop on its enzymatic function. SIRT1 in interaction with CLOCK/BMAL1 controls the expression of NAMPT (nicotinamide phosphoribosyltransferase), a key enzyme in the salvage pathway of NAD $^+$ biosynthesis, and thereby the production of its functionally important cofactor (Nakahata et al., 2009). Consequently NAD $^+$ levels and SIRT1 activity rhythmically fluctuate.

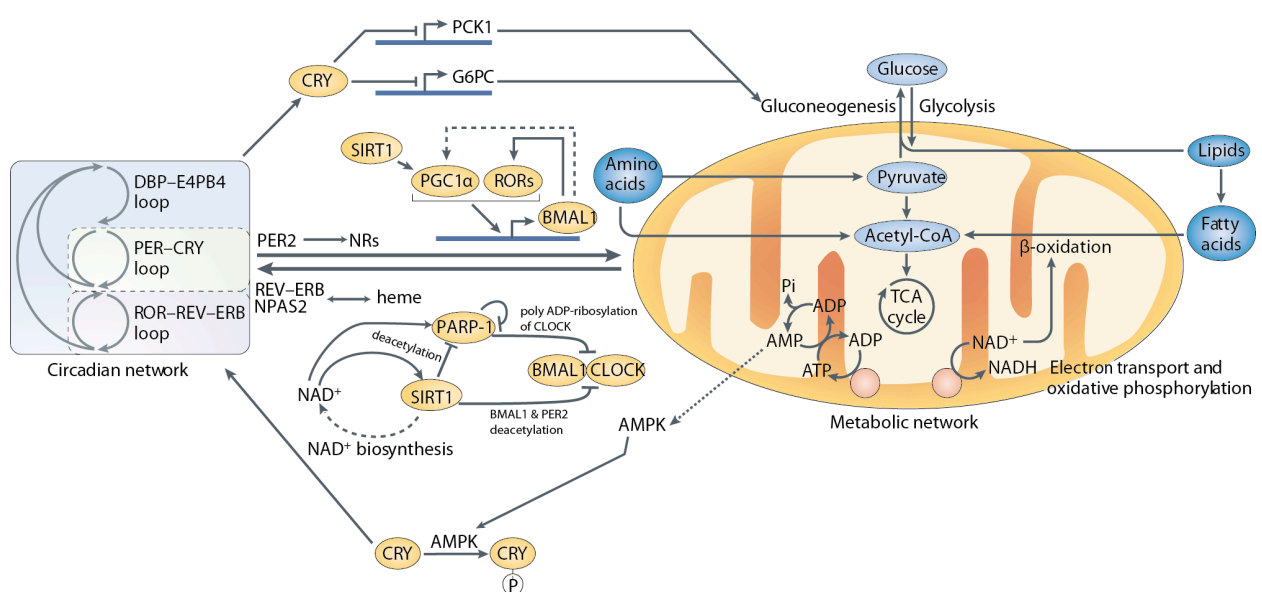


Figure 3: Schematic illustrating the interconnections of the circadian clock and metabolism (for detailed description see text). CRY1 regulates glucose homeostasis through negative regulation of gluconeogenic gene expression. Conversely, CRY1 is targeted for degradation through AMP-activated protein kinase (AMPK) (see section 1.5). PER2 supposedly interacts with certain nuclear receptors and modulates their (metabolic) functions (see section 1.4); (modified from (Zhang and Kay, 2010)).

As NAD $^+$ levels also regulate SIRT3, a mitochondrial deacetylase modulating oxidative enzymes, the circadian oscillator probably reciprocally impacts mitochondrial oxidative metabolism, too (Peek et al., 2013). Moreover, PARP-1 (poly (ADP-ribose) polymerase 1) interacts with CLOCK and impairs the interaction of CLOCK/BMAL1 with DNA through poly-ADP ribosylation. Like SIRT1 it depends on NAD $^+$ for synthesis of the ADP ribose molecules and thereby functions in response to the cellular redox state (Asher et al., 2010). Interestingly, the AMP/ATP ratio, which

reflects the cellular energy state, regulates activity of AMPK (AMP-activated protein kinase), which influences the circadian oscillator by stimulation of increasing intracellular NAD^+ levels and consequently SIRT1 activity (Cantó et al., 2009). Moreover, AMPK also regulates CRY stability through phosphorylation (section 1.5).

Apart from ROR several other nuclear receptors like REV-ERB or PPAR, which traditionally regulate genes involved in glucose or lipid metabolism, are involved in maintenance of the circadian oscillator. They sense and function in dependence of a ligand, which is often a small metabolite or hormone, and thereby translate the metabolic state of the cell into circadian gene expression. For instance REV-ERB binds the metabolite heme which can sense both diatomic gases and the cellular redox state. Interestingly, it was shown that REV-ERB α reversely modulates the synthesis of heme in a negative feedback loop and thereby also impacts on cellular energy metabolism (Wu et al., 2009).

Moreover, many nuclear receptors (e.g. TR α , PPAR, ERR, REV-ERB, ROR, etc.) are rhythmically expressed in metabolic organs like the liver, adipose tissue and muscle (Yang et al., 2006), and in this way reciprocally link the circadian clock with metabolism (Figure 3).

1.4 PERIOD (PER) Proteins – Prominent Members of the Mammalian Circadian Clock

The *Per* gene and its importance for the circadian clock was first described in *Drosophila* where the change in the free-running circadian period could be associated with mutations in the *dPer* gene. The observation that both the rhythmic cycling of *dPer* mRNA and protein as well as the regulation of these rhythmic accumulations by PER itself later suggested that PER functions in a feedback loop within the clock (Hardin, 2011). In mammals, three homologous *Per* genes were subsequently identified and named *Per1*, *2* and *3*, respectively (Albrecht et al., 1997; Shearman et al., 1997; Sun et al., 1997; Tei et al., 1997; Zylka et al., 1998b).

1.4.1 Mutant Phenotypes Suggest Non-Redundant Mammalian PER Protein Functions

Analysis of wheel locomotion activity, which is recorded as behavioural read-out of the oscillator, of corresponding *Per* mutant mice revealed the importance of PER proteins for the mammalian circadian oscillator.

In constant darkness (free-running clock condition) the knockout of either *mPer1* or *mPer2* still allows the clock to continue oscillation for several cycles, however, with a changed periodicity and, in most cases, leads to arrhythmicity over time. *Per2* mutant mice on average show a more severe phenotype compared to *Per1* mutant mice (for example (Zheng et al., 1999) and (Zheng et al., 2001) or (Bae et al., 2001) or (Brown et al., 2005a), see Figure 4A). Mice with a disruption of both *Per1* and *Per2* consistently show an immediate arrhythmic behaviour which is also reflected on the molecular level (Bae et al., 2001; Zheng et al., 2001). In contrast, PER3 deficient mice show only mild alterations in their locomotor activity (Shearman et al., 2000a).

Compared to wheel running locomotor activity, following circadian rhythms in tissue and individual cell cultures unravels differences between the individual central and peripheral oscillators and visualizes the influence of intercellular interactions on rhythmicity. Here, *Per3*^{-/-} SCN explants cycle with a slightly shorter period than wild-type and thereby mirror locomotor activity results, which is also the case for *Per1* (Liu et al., 2007b) (Figure 4B). However, tissue explants of several peripheral organs (e.g. liver, lung, etc.) from PER3 deficient mice show an altered circadian period and phase while corresponding fibroblasts show a shortened period

only and, for instance, tissue explants from kidney are not affected at all (Liu et al., 2007b; Pendergast et al., 2012). Lung explants, fibroblasts (in culture or individual cells) and single neurons from *Per1* mutant mice as well as fibroblasts from *Per2* mutant mice become arrhythmic and/or display unstable rhythms of low amplitude followed by arrhythmicity, respectively (Liu et al., 2007b). On the whole this shows that all three mammalian PER proteins have a unique function in circadian timing and can only partially compensate for one another. Especially PER1 and PER2 impact on circadian rhythmicity while PER3 only influences peripheral clocks.

A

Gene	Allele	Mutant phenotype	References
<i>mPer1</i>	<i>Per1^{brdm1}</i>	1 hrs shorter pd 0.4 hrs shorter pd	Zheng et al., 2001 Brown et al., 2005
	<i>Per1^{ldc}</i>	0.5 hrs shorter pd/ arrhythmic (over 2 ws)	Bae et al., 2001
	<i>Per1^{-/-}</i>	0.5 hrs shorter pd/ arrhythmic	Cermakian et al., 2001
<i>mPer2</i>	<i>Per2^{brdm1}</i>	1.5 hrs shorter pd/ arrhythmic (over 2-18 ds) 0.8 hrs shorter pd/ arrhythmic over time	Zheng et al., 1999 Brown et al., 2005
	<i>Per2^{ldc}</i>	0 - 0.5 hrs shorter pd/ arrhythmic (over 0-3 ws)	Bae et al., 2001
<i>mPer1/ mPer2</i>	<i>Per1^{ldc}/Per2^{ldc}</i> <i>Per1^{brdm1}/Per2^{brdm1}</i>	arrhythmic arrhythmic arrhythmic	Bae et al., 2001 Zheng et al., 2001 Brown et al., 2005
<i>mPer3</i>	<i>Per3^{-/-}</i>	0 - 0.5 hrs shorter pd	Shearman et al., 2000

B

Gene	Allele	Cellular phenotype	Tissue phenotype	References
<i>mPer1</i>	<i>Per1^{ldc}</i>	fibroblasts, SCN neurons: arrhythmic	SCN: wt; lung: arrhythmic	Liu et al. 2007b
<i>mPer2</i>	<i>Per2^{ldc}</i>	fibroblasts: arrhythmic	-----	Liu et al. 2007b
<i>mPer3</i>	<i>Per3^{-/-}</i>	fibroblasts: short pd	SCN, lung: short pd	Liu et al. 2007b

Figure 4: Overview of the effects of PER proteins on the circadian oscillator. **A)** *Per* mutation affects wheel running locomotion of mice. Different *Per* mutant mice and corresponding locomotion phenotypes as read-out of the free-running clock from different sources are listed; brdm1: in frame deletion of 82 amino acids in PAS-B of mPER2 and deletion of exons 4-18 in *mPer1* gene (protein comprises only amino acids 1-124 of mPER1, assumed null mutations; (modified from (Ko and Takahashi, 2006))); **B)** Cell and tissue phenotypes observed in a reporter gene assay as a result of mutated mouse *Per* genes; pd: period; (modified from (Lowrey and Takahashi, 2011)).

1.4.2 Domain Architecture/Functional Motifs of Mammalian PER Proteins

The mammalian PER proteins comprise about 1200 amino acids. Comparative sequence analysis of mPER1-3 reveals a 46% sequence identity of mPER1 and mPER2 but only 36% and 37% identity with mPER3, respectively. Sequence analysis also reveals a nuclear localization sequence (NLS), several nuclear export sequences (NES) as well as a cytoplasmic localization domain (CLD).

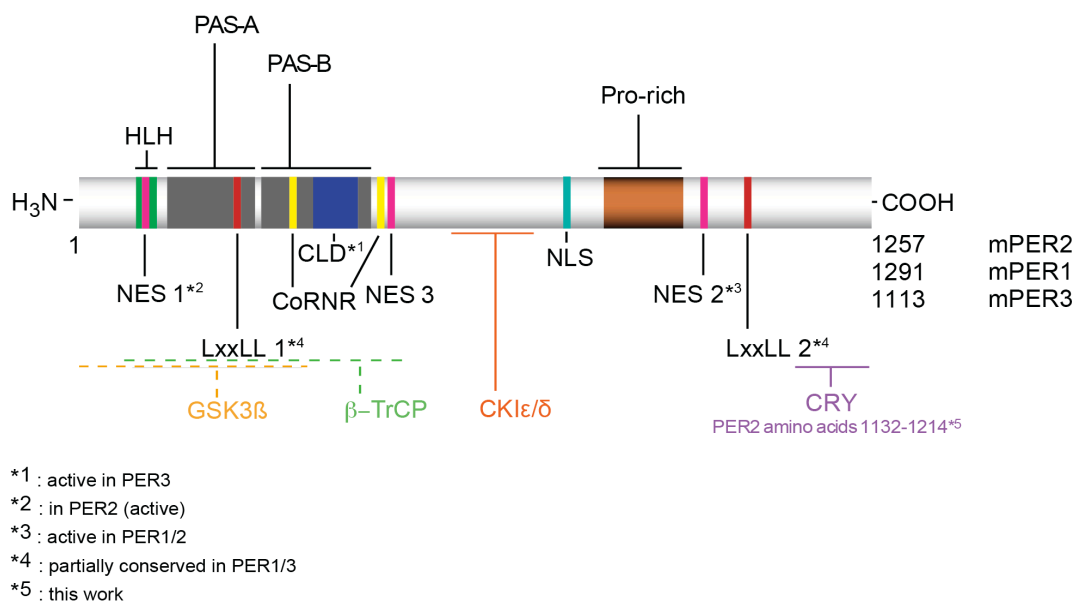


Figure 5: Domain structure and mapped interaction sites of mammalian PER proteins (mouse proteins are exemplarily shown) which belong to the PAS (PER-ARNT-SIM) family of proteins. A predicted helix-loop-helix (HLH) domain is located N-terminal of PAS-A. Sequence analysis further depicted several subcellular localization sequences (NES, NLS, CLD) as well as potential proline-rich (Pro-rich) interaction motifs and typical nuclear receptor coregulator binding motifs (LXXLL and CoRNR). The CK1 β/ϵ binding site (orange) together with several phosphorylation sites was mapped to the central region of the proteins. The C-terminal domain of PER comprises the CRY interaction domain (violet) which was specified to residues 1132-1252 of mPER2 in this work (adapted from (Ripperger and Albrecht, 2011)).

Regions of highest sequence identity include two N-terminal PAS domains (section 1.4.4) which mediate homo- and heterodimer formation of PER proteins (Yagita et al., 2000; Zylka et al., 1998a). Apart from the PAS domains, secondary structure prediction suggests that PER proteins are intrinsically mainly unfolded. The domain architecture of mPER1-3 is shown in Figure 5. So far interaction sites for CRY, located in its C-terminus (residues 917-1257 of mPER2), and several kinases were mapped on PER. CRY importantly stabilizes PER, prevents ubiquitination and its subsequent degradation (Lee et al., 2001; Yagita et al., 2002). Moreover, the interaction of PER2 with both CLOCK and BMAL1 have been suggested without precise mapping of the

interaction sites (Chen et al., 2009; Kiyohara et al., 2006; Langmesser et al., 2008; Sato et al., 2006).

Importance of PAS domains for PER functionality is underlined by the observation that mice homozygous for a deletion of 82 amino acids in the PAS-B domain of mPER2 display a shorter free running circadian period which is followed by a complete loss of rhythmicity (Figure 4A). In addition, these mice suffer from impaired DNA damage responses and increased tumor development rates (Fu et al., 2002).

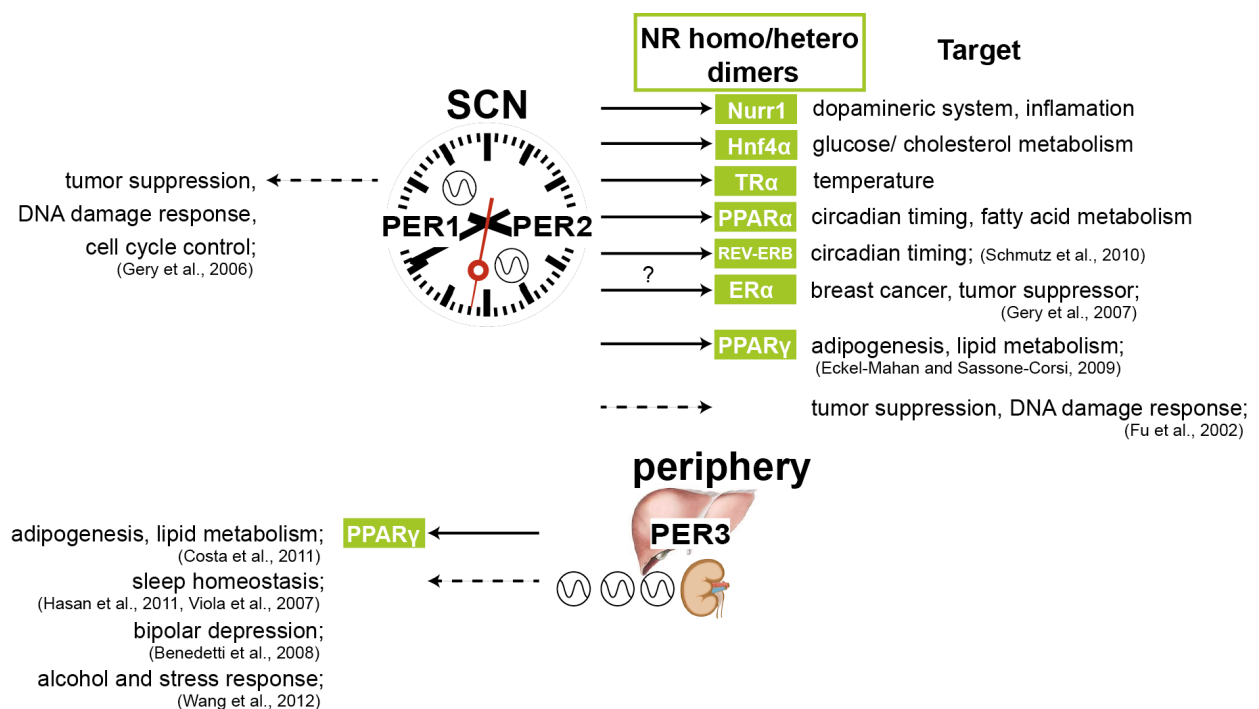


Figure 6: Roles of mammalian PER proteins outside the circadian oscillator. Both PER1 and PER2 are described to act as tumor suppressors while polymorphisms of the *Per3* gene are associated with sleep and behavioral disorders; black arrows: suggested interactions of PER protein with nuclear receptors and their implications (inspired from (Ripperger and Albrecht, 2011)).

PER PAS domains depict sequence motifs which are usually involved in coregulator binding to nuclear receptors; in particular a LxxLL co-activator motif and two CoRNR co-repressor motifs. An additional LxxLL motif is found in the C-terminus of the PER proteins (as 1050-1054 of mPER2). Interestingly, it was recently suggested that mPER2 (rather than mPER1) interacts via its PAS LxxLL motifs with REV-ERBα and PPARα (replaces RORα in the liver and activates BMAL1 expression) and acts as a coregulator of BMAL1 transcription in the liver. A regulation of PER2 on BMAL1 transcription was already suggested from a study in mutant mPER2^{Brdm1} mice in

which *Clock* remains unaffected but *Bmal1*, *Cry* and *Per* RNA rhythms are blunted (Shearman et al., 2000b). Moreover, interaction of mPER2 with HNF4 α , TR α , PPAR γ and to some extent with NURR1 und ROR α was shown (Schmutz et al., 2010).

mPER3 was described to interact via its PAS domains with the nuclear receptor PPAR γ . This interaction supposedly represses the PPAR γ activity and thereby inhibits adipogenesis. Since nuclear receptors are involved in numerous physiological processes, they potentially constitute another link of the circadian oscillator and metabolism through interaction with PER (Costa et al., 2011). These non-core clock functions of PER and others are summarized in Figure 6.

1.4.3 Posttranslational Modifications of Mammalian PER Proteins

PER proteins are targets of and depending on casein kinase 1 δ and ϵ (CK1 δ / ϵ) as well as glycogen synthase kinase 3 β (GSK3 β). The importance of phosphorylation for circadian timing is implicated in patients suffering from familial advanced sleep phase syndrome (FASPS) which is characterized by a shortened circadian period, early sleep onset and early awakening. The patients show a changed PER2 phosphorylation pattern either due to a mutation in the CK1 ϵ phosphorylation target Ser662_{PER2}, which is mutated to glycine, or due to a T44A missense mutation in the gene of the PER2-phosphorylating CK1 δ . Both mutations are associated with hypophosphorylation of PER2 which alters its cellular localization and stability (Toh et al., 2001; Vanselow et al., 2006) and/or, in case of S662G mutation, reduced PER2 transcription (Xu et al., 2006). In the Syrian Tau hamster a T178C substitution in CK1 ϵ accelerates the circadian cycle due to an affected kinase activity which changes PER endurance (Gallego and Virshup, 2007; Meng et al., 2008). Furthermore, polymorphisms of the *Per3* gene, which are implicated in the delayed sleep phase syndrome (DSPS), are also associated with a changed CK1 phosphorylation pattern (Ebisawa et al., 2001).

Thus on the one hand, CK1 δ/ϵ targets PER for degradation through phosphorylation and subsequent ubiquitinylation by the SCF^{TRCP} E3 ubiquitin ligase complex (Camacho et al., 2001; Eide et al., 2005; Shirogane et al., 2005). On the other hand, phosphorylation by casein kinase 1 ϵ (Lee et al., 2001; Takano et al., 2000; 2004) and GSK3 β (shown for mPER2, (Iitaka et al., 2005)) is involved in determination of cellular localization of PER which is important for feedback and rhythmicity.

1.4.4 PAS Domains: Signal Sensors and Interaction Platforms

PAS domains are named according to sequence homology in *Drosophila* proteins PERIOD and developmental regulator single-minded (SIM) and the vertebrate aryl hydrocarbon receptor nuclear transporter (ARNT) and comprise 100-130 amino acids which, despite low sequence identity among PAS domains, adopt a characteristic fold (Figure 7A). This fold is composed of five antiparallel β -strands and several flanking α -helices. LOV (light-oxygen-voltage, “PAS” phototropin-like photosensor domain) (Crosson et al., 2003) and potentially Cache (mostly extracellular domains of signalling proteins) (Anantharaman and Aravind, 2000) domains present subsets of the PAS fold.

PAS domains are found in both prokaryotes and eukaryotes either as a single or as pairwise domains (PAS-A/ PAS-B) and are often N-terminal components of signal transduction proteins. They either serve as signal sensors for environmental (or more precisely for changes in e.g. oxygen, light, redox potential, metabolites) or structural changes or as signal transmitters and protein interaction platforms. Consequently, some PAS domains bind cofactors in their core such as heme, FMN, FAD, small metabolites, polycyclic or halogenated aromatic hydrocarbons (PAH/HAH) or metal ions (Henry and Crosson, 2011).

In many cases PAS domains are linked to signal transducing effector domains including histidine or serine/threonine kinases, phosphodiesterases, ion channels and transcription factors (Möglich et al., 2009). In fact, the eukaryotic bHLH-PAS transcription factors belong to the best studied PAS proteins and include ARNT, HIF α (hypoxia inducible factor- α), AHR and SIM, which are involved in hypoxia and xenobiotic response pathways and neurogenesis, respectively. Furthermore, this group of transcription factors involves the mammalian circadian transcription factors NPAS, CLOCK and BMAL1. PERIOD proteins, however, do not contain a traditional effector domain and are not associated with a classical signaling function of their PAS domains at least according to current knowledge. Numerous other clock proteins also comprise PAS domains including WC1/2 (WHITE-COLLAR 1/2) and VVD (VIVID) from *Neurospora*, CYCLE, PER and CLOCK from *Drosophila* as well as the photoreceptors PHOT1/2 (phototropin 1/2) and ZTL (ZEITLUPE) from *Arabidopsis*. Thereby, PAS proteins accomplish a prominent role in biological timing.

Finally, PAS domains mediate formation of both homo- and heterodimers as well as higher oligomers through variable PAS packings (Figure 7B). Thereby, they can provide more surfaces

for accessory interactors. Signal transduction and specificity of PAS interactions is amongst others mediated through quaternary structure changes (Möglich et al., 2009).

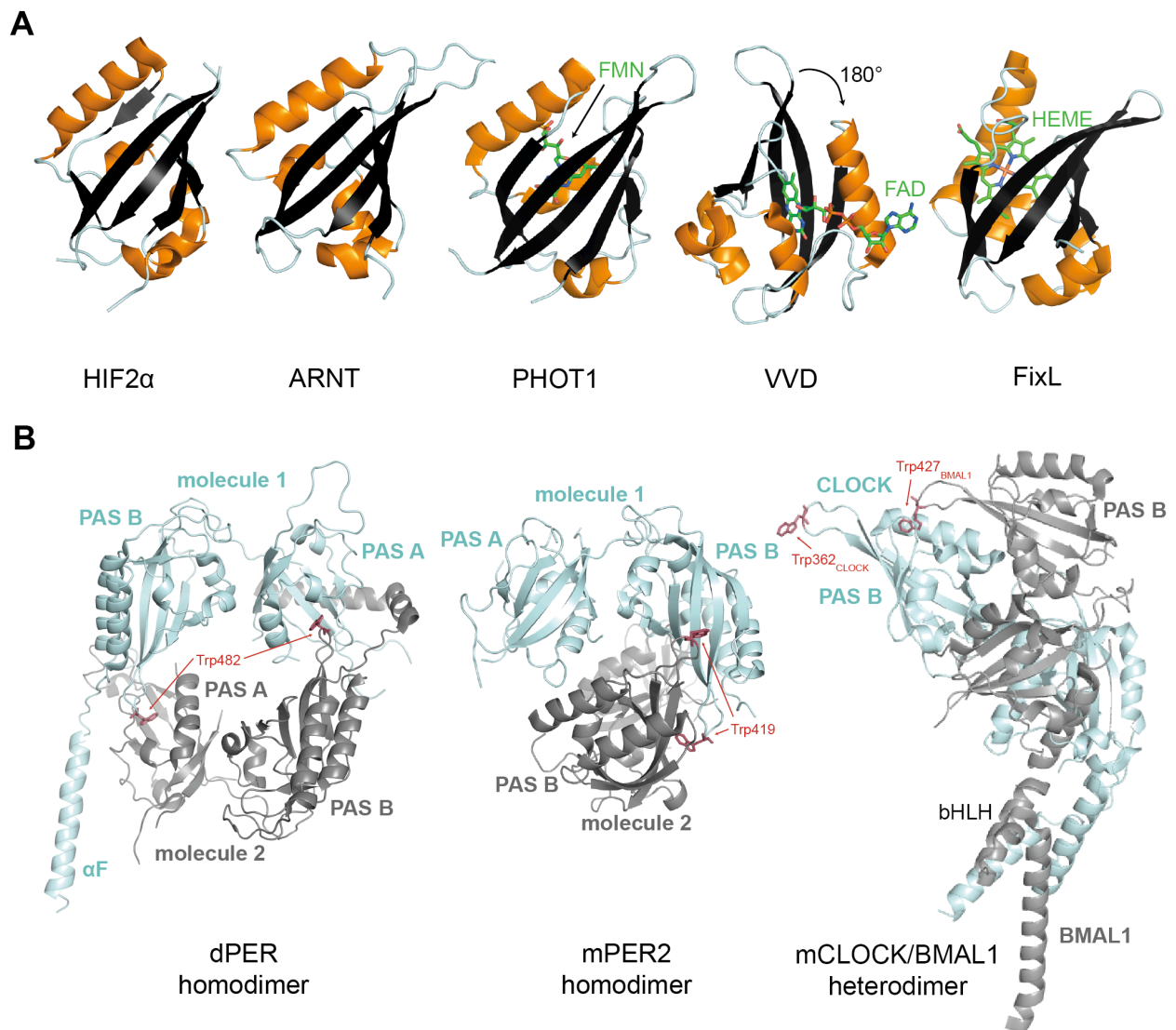


Figure 7: The well-conserved PAS domain fold visualized by a subset of crystal structures (pdb). **A)** Single PAS domains; from left to right: PAS-B domains of the bHLH transcription factors HIF2 α and ARNT (4GHI), (middle) PAS-A (also called LOV1) of the plant blue light photoreceptor PHOT1 (phototropin 1 bound to FMN) (2Z6C), PAS domain of fungal blue-light photoreceptor VIVID (VVD) bound to FAD (2PD7), (right) PAS domain of oxygen sensor histidine kinase FixL (1D06) from *Sinorhizobium meliloti* bound to heme; (modified from (Bersten et al., 2013)). **B)** Crystal structure of the dPER (232-572) (1WA9, open conformation), mPER2 (170-473) (3GDI) and mCLOCK/mBMAL1 (4F3L) dual PAS dimers. dPER dimerization is mediated through interactions of the PAS-A and PAS-B with the PAS-B and PAS-A domain of the dimerising molecule (PAS-A - Trp482 - PAS-B interface), respectively, and through the essential interaction of PAS-A with the C-terminal α F-helix of the second molecule (Yildiz et al., 2005). The mPER2 homodimer is sufficiently stabilized through an antiparallel PAS-B β -sheet interface comprising the conserved Trp419 (PAS-B Trp419 interface) (Hennig et al., 2009). The mCLOCK/mBMAL1 heterodimer is mediated through pair wise interactions of the corresponding PAS-A, PAS-B and bHLH domains (Huang et al., 2012).

1.5 CRYPTOCHROMES (CRY) – Blue Light Sensors and Transcription Repressors

Cryptochromes were first described in plants where they regulate development and growth as blue light photoreceptors. Today cryptochromes are known in all kingdoms of life except archaea but mainly in plants and animals. They are structurally closely related to photolyases and together represent the photolyase-cryptochrome protein family.

1.5.1 Photolyases – Evolutionary Relatives of Cryptochromes

Photolyases are classified either as CPD-photolyases or 6-4-photolyases. They catalyse in a light dependant reaction the repair of cyclobutane pyrimidine and (6-4) pyrimidine-pyrimidone DNA dimers, respectively.

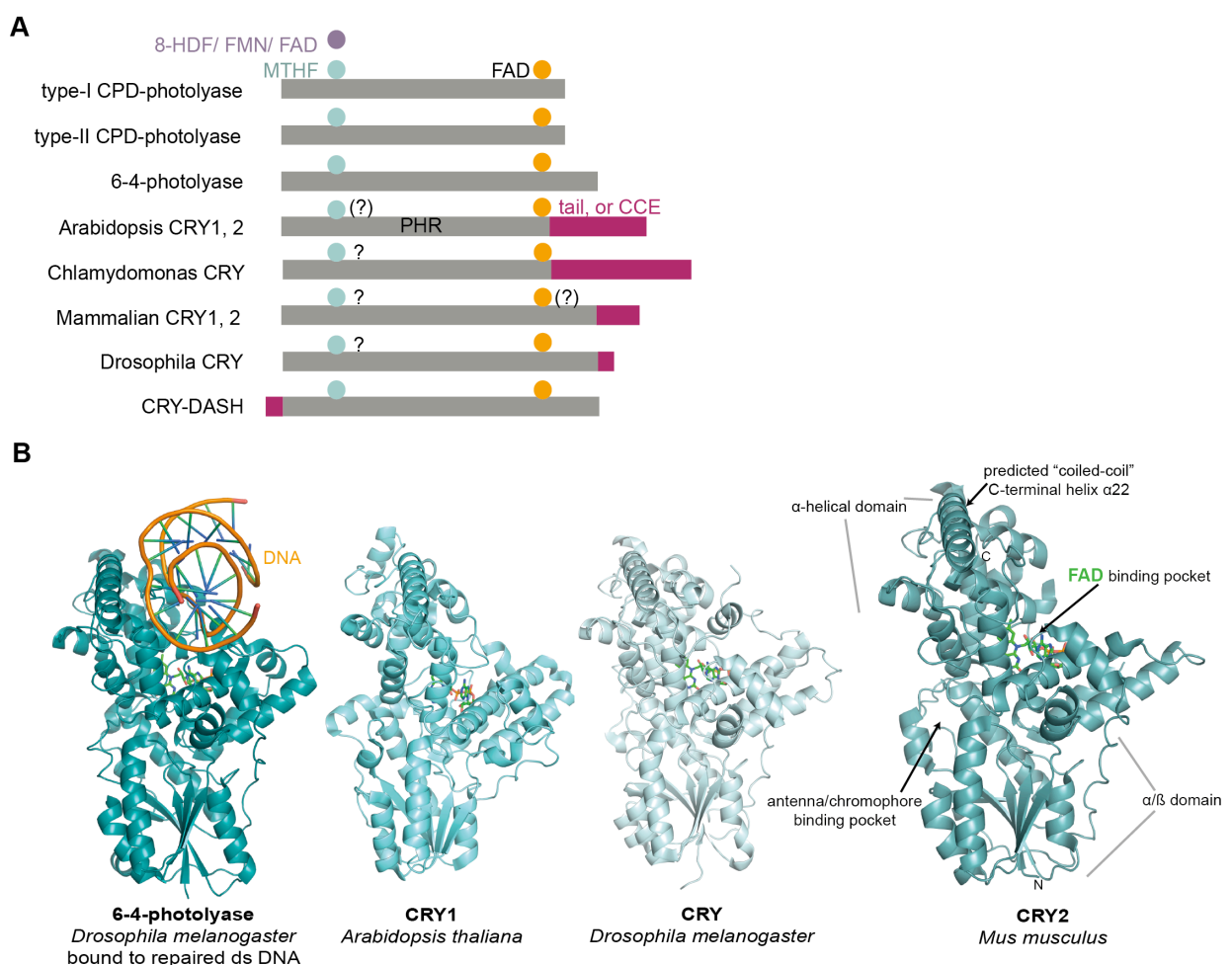


Figure 8: The cryptochrome/photolyase protein family **A)** Domain architecture of photolyases and cryptochromes and their known cofactors (modified from (Cashmore et al., 1999)); **B)** Structural conservation among photolyases and the PHR of cryptochromes; crystal structures shown (pdb): DmPhotolyase (3CVY), PHR AtCRY1 (1U3C), full-length DmCRY (4JZY), PHR MmCRY2 (4I6G), all FAD bound.

Next to the catalytically active cofactor FAD they contain a surface exposed light harvesting chromophore; either MTHF (methenyltetrahydrofolate) or, in case of class-I CPD-photolyases, 8-HDF (8-hydroxy-7,8-didemethyl-5-deazariboflavin, F0), FAD (Fujihashi et al., 2007) or FMN (Klar et al., 2006). Cryptochromes and photolyases share a similar “photoactive” domain (called photolyase homology region (PHR) in CRY, \approx 500 amino acids), but they differ in a C-terminal tail, which is unique to cryptochromes (Figure 8A) (Cashmore et al., 1999). The crystal structures of several CPD- and 6-4-photolyases and various cryptochromes impressively visualize this structural relation (also compare Figure 8B). The photolyase domain is composed of a N-terminal α/β domain and a C-terminal α -helical domain. Accordingly, cryptochromes are able to bind FAD and MTHF as cofactors, however, most have lost photolyase activity and act as signal transducers. An exception are DASH-cryptochromes, which can repair single stranded DNA. Nevertheless, hCRY2 retained weak DNA binding capacity which is augmented by the presence of a 6-4 DNA photoproduct (Ozgur and Sancar, 2003).

1.5.2 Classification, Domain Architecture and Light Sensitivity of Cryptochromes

Cryptochromes are classified into three groups: I) the classical blue light sensitive plant cryptochromes (CYR1 and CRY2), II) DASH-cryptochromes, and III) animal cryptochromes. The latter are further categorized as type I cryptochrome photoreceptors (e.g. dCRY) or type II light independent cryptochromes (mammalian CRY1/2 or monarch butterfly CRY2). Strikingly, they all differ in the length of their predicted unordered and practically non-conserved C-terminal tails (N-terminal in DASH-CRY). The cryptochrome tails are suggested to operate in signal transduction and effector binding (e.g. AtCRY1/2, dCRY). To fulfil their signalling function light sensing cryptochromes undergo photoreduction.

In photolyases the blue light dependant photoreaction of flavin, which is also called photoactivation, serves to accumulate the FAD cofactor in the fully reduced and active form FADH^- . Hence, light activated, semireduced FADH° receives electrons (with few exceptions) via an intramolecular electron transfer chain composed of three highly conserved tryptophans (Figure 9). According to current knowledge light sensing cryptochromes bind fully oxidized FAD_{ox} in the dark, resting state. Light initiates reduction to the semireduced radical anion FAD° in insect CRYs and to the semireduced neutral anion FADH° in plant CRYs. As in the case of

photolyases this happens via a tryptophan triad and converts CRY into the putative signalling state (Figure 9) (Chaves et al., 2011).

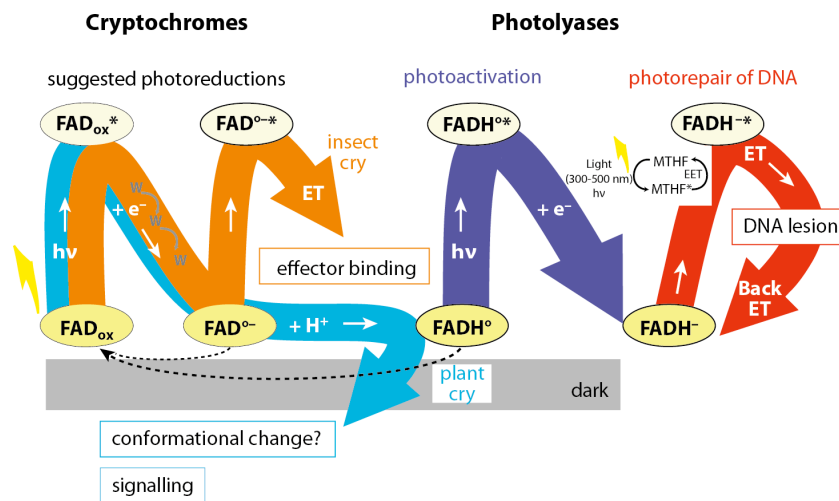


Figure 9: Overview of the light reactions of cryptochromes (left) and photolyases (right). Cryptochromes bind oxidized FAD in the dark state which is reduced to the semireduced anion radical (FAD^{o-}) in insects and semireduced neutral radical (FADH^o) in plants for signal transduction upon light sensing (photoreduction). Photolyases undergo photoactivation to accumulate FAD in its fully reduced state (FADH⁻) which is needed for DNA repair. In a second photoreaction the light harvesting chromophore (e.g. MTHF) transfers excitation energy to FADH^{o*}. An electron is then transferred from the excited, high energy FADH^{o*} to the DNA lesion which is subsequently resolved; hv: photon absorption; ET: electron transfer; EET: excitation energy transfer; W: tryptophan (modified from (Chaves et al., 2011)).

In *Drosophila* cryptochrome acts as blue light photoreceptor that synchronizes the clock with the daily light-dark cycle. In the current model photoreduction of FAD induces a conformational change in the dCRY C-tail which consequently allows for dCRY interaction with dTIM and F-box protein JET (JETLAG), which is part of the SCF E3 ubiquitin ligase complex. This induces proteasomal degradation of dTIM and dCRY and thereby both resetting and light synchronization of the clock (Ozturk et al., 2011; Peschel et al., 2009).

While FAD is well established as chromophore in light sensitive cryptochromes, convincing evidence for MTHF or another second chromophore and its functional role *in vivo* is missing for most cryptochromes. At least in the case of plant and animal cryptochrome spectroscopic data implies MTHF, and excludes F0, as second chromophore (Berndt et al., 2007; Malhotra et al., 2001; Ozgur and Sancar, 2003; Selby and Sancar, 2012). However, different from plant and animal cryptochromes the crystal structure of recombinantly expressed DASH cryptochrome

from *Arabidopsis thaliana* clearly depicts MTHF as one potential second chromophore in DASH cryptochromes (Huang et al., 2006).

1.5.3 Mammalian Cryptochromes and the Circadian Clock

In mammals two *Cry* homologs have been identified, *Cry1* and *Cry2*. Analysis of the corresponding knockout mice revealed a shorter and longer free running period for mutant *Cry1* and *Cry2* mice, respectively (Thresher et al., 1998; van der Horst et al., 1999; Vitaterna et al., 1999). These results of *Cry* knockout mice are also reflected on the single cell or tissue level for *Cry2*^{-/-}. However, knockout of *Cry1* causes arrhythmicity at the single cell level and tissue explants from peripheral clocks, which is unexpected from the behavioural studies (Liu et al., 2007b; Yagita et al., 2001). Although these opposing effects of mutations on the circadian period suggest opposing or least different functions of CRY1 and CRY2 in the circadian oscillator, both CRY1 and CRY2 repress transcriptional activity of the CLOCK/BMAL1 heterodimer through interaction in cell assays (Griffin, 1999; Kume et al., 1999).

A

Gene	Allele	Mutant phenotype	References
<i>Cry1</i>	<i>Cry1</i> ^{-/-}	1 hrs shorter pd	van der Horst et al., 1999 Vitaterna et al., 1999
<i>Cry2</i>	<i>Cry2</i> ^{-/-}	1 hrs longer pd	van der Horst et al., 1999 Thresher et al., 1998 Vitaterna et al., 1999
<i>Cry1/Cry2</i>	<i>Cry1</i> ^{-/-} / <i>Cry2</i> ^{-/-}	arrhythmic	van der Horst et al., 1999 Vitaterna et al., 1999
<i>Per2/Cry1</i>	<i>Per2</i> ^{brdm1} / <i>Cry1</i> ^{-/-}	arrhythmic	Oster et al., 2002
<i>Per2/Cry2</i>	<i>Per2</i> ^{brdm1} / <i>Cry2</i> ^{-/-}	0-0.4 hrs shorter pd	Oster et al., 2002

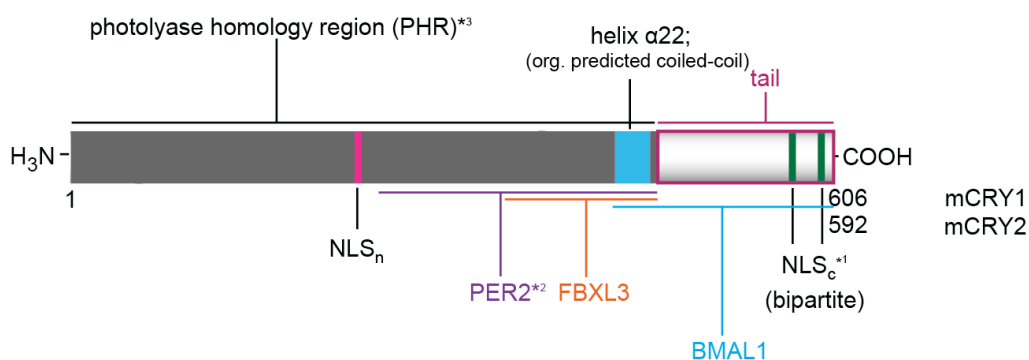
B

Gene	Allele	Cellular phenotype	Tissue phenotype	References
<i>mCry1</i>	<i>Cry1</i> ^{-/-}	fibroblasts, SCN neurons: arrhythmic	SCN: short pd; lung, liver, cornea: arrhythmic	Liu et al. 2007b
<i>mCry2</i>	<i>Cry2</i> ^{-/-}	fibroblasts, SCN neurons: long pd	SCN, lung, liver, cornea: long pd	Liu et al. 2007b
<i>mCry1/mCry2</i>	<i>Cry1</i> ^{-/-} / <i>Cry2</i> ^{-/-}	fibroblasts: arrhythmic	SCN, lung, liver, cornea: arrhythmic	Liu et al. 2007b Yagita et al., 2001

Figure 10: Overview of the effects of CRY proteins on the circadian oscillator. **A)** In *Cry* knockout mice wheel running locomotion as read-out of the free-running circadian clock (in constant darkness) is affected. Results from different studies are shown; (modified from (Ko and Takahashi, 2006)); **B)** Summary of cell and tissue phenotypes observed from deletion of *Cry* genes in reporter gene assays; pd: period (modified from (Lowrey and Takahashi, 2011)).

However, the repressor strength of CRY1 is described superior to CRY2 in cellular assays. This is supported by the observation that *Per2^{brdm1}/Cry2^{-/-}* mice display robust circadian rhythms while *Per2^{brdm1}/Cry1^{-/-}* mice are arrhythmic (Anand et al., 2013; Oster et al., 2002). Like single knockout mice double *Cry1^{-/-}/Cry2^{-/-}* knockout mice show a wild-type like rhythmicity under regular light-dark conditions, but they completely lose behavioural and molecular rhythmicity in the dark indicating that CRY1 and CRY2 are at least partially redundant (Okamura et al., 1999; van der Horst et al., 1999; Vitaterna et al., 1999) (Figure 10).

Recently it has been suggested that CRY1 and CRY2 are sequentially required for distinct phases in repressing or delaying CLOCK/BMAL1 mediated transcription (Koike et al., 2012). CRY1 and CRY2 mainly differ in their C-terminal tails, which are, together with the preceding PHR C-terminal helix $\alpha 22$ (formerly predicted coiled-coil), involved in but not sufficient for transcriptional repression (Chaves et al., 2006). It has been suggested that the differential amino acid composition of CRY1 and CRY2 C-tails as well as modification of the C-terminus of BMAL1 through timed acetylation by CLOCK (Hirayama et al., 2007) regulates the different interactions of CRY1 and CRY2 with BMAL1 and their inhibitory effects on the CLOCK/BMAL1 complex (Czarna et al., 2011). The BMAL1 interaction site on CRY probably partially overlaps with the PER interaction site on CRY, which was mapped to residues in helix $\alpha 22$ of mCRY2 and which are also conserved in mCRY1 (Ozber et al., 2010) (Figure 11).



*1 : amino acids 585 to 602 in mCRY1, amino acids 559 to 588 in mCRY2

*2 : this work

*3 : mCRY1 [1-496], mCRY2 [1-514]

Figure 11: Domain structure and mapped interaction sites of mammalian CRY proteins (mouse proteins shown as representative). They contain a N-terminal, highly conserved photolyase homology region, which is completed by helix $\alpha 22$, a formerly predicted coiled-coil. Their C-terminus contains a mostly non-conserved, highly flexible tail, which supposedly regulates interaction with BMAL1. Nuclear localization of CRY is determined by its NLS sequences.

In contrast to *Drosophila* CRY, mammalian CRY1 and CRY2 are integral, light independent regulators of the circadian clock. Nevertheless, there is an increasing number of reports that does not exclude an additional FAD/light dependant function of mammalian cryptochromes anymore. For instance, human CRY2 and monarch butterfly type II CRY can rescue magnetosensitivity in dependence of blue-light in mutant flies which lack functional dCRY (Foley et al., 2011; Gegear et al., 2010). Human CRY, which is overexpressed in insect cells, undergoes photoreduction in response to blue light. Moreover, it is proteolysed in a light dependant manner in transgenic flies implying that mammalian cryptochromes are light responsive *in vivo*, too (Hoang et al., 2008).

1.5.4 Posttranslational Modifications of Mammalian CRY Proteins

Mammalian cryptochromes are regulated by phosphorylation. Phosphorylation by MAPK alters CRY transcriptional repression on CLOCK/BMAL1 in transfection assays (Sanada et al., 2002). Subsequent phosphorylation by DYRK1A (dual specificity tyrosine-phosphorylated and regulated kinase 1A) and GSK3 β of Ser557 and Ser553 in the C-tail specifically targets mCRY2 (not conserved in mCRY1) for degradation (Harada et al., 2005; Kurabayashi et al., 2010) through a yet unknown mechanism. Contradictory, phosphorylation of Ser588 in the C-tail apparently stabilizes mCRY1 (Gao et al., 2013).

The SCF^{FBXL3} E3 ubiquitin ligase complex ubiquitinates mammalian CRY which is followed by proteasomal degradation. Recently, it was determined that AMPK (AMP-activated protein kinase) promotes this destabilization of mCRY1 (and probably mCRY2) through phosphorylation (Lamia et al., 2009). Indeed, Ser71 phosphorylation enhances FBXL3 binding but weakens PER2 binding to CRY1 in co-immunoprecipitation assays. Thus, FBXL3 and PER2 probably competitively determine CRY stability through binding to the same site on CRY. The recently published crystal structure of the mCRY2/FBXL3/SKP1 complex reveals that FBXL3 interacts with the FAD binding pocket, the C-terminal helix α 22 and the C-terminal lid of mCRY2 (Xing et al., 2013).

1.5.5 Mammalian CRY and its Link to Metabolism

As a target of AMPK, whose activity adapts to the cellular AMP to ATP ratio, CRY1 links the

circadian clock with metabolism and the energy state of the cell (Lamia et al., 2011). In agreement with that, glucose deprivation in a cell assay activated AMPK, destabilized CRY and altered circadian rhythmicity. In contrast, CRY1 influences glucose homeostasis by regulation of gluconeogenesis during fasting. It can modulate GPCR (G protein coupled receptor) activity through interaction with the $G_s\alpha$ subunit of the G-protein (Zhang et al., 2010). This supposedly inhibits, according to Zhang et al., accumulation of cAMP in response to glucagon in a circadian manner and consequently reduces the phosphorylation status and activity of CREB (cAMP response element-binding protein) which mediates gluconeogenic gene expression of e.g. *G6pc* (glucose-6-phosphatase) and *Pck1* (phosphoenolpyruvate carboxykinase-1), respectively (Zhang et al., 2010). Moreover, CRY1 and CRY2 are stimulated by glucocorticoids to interact with the glucocorticoid receptor (GR). Thereby, they negatively regulate the GR induced gene expression (but not inflammatory genes) and specifically repress the expression of the gluconeogenetic enzyme *Pck1* in the liver. Consequently, mice which lack cryptochromes are more prone to glucocorticoid-induced hyperglycaemia and suffer from high glucose doses (Lamia et al., 2011). Strikingly, in insulin resistant mice overexpression of CRY1 in the liver leads to lower blood glucose concentrations and enhances insulin sensitivity (Zhang et al., 2010).

1.6 The CRY/PER Repressor Complex Drives Circadian Rhythms

The principle of negative feedback originates from studies of the *Drosophila* circadian clock where it was convincingly demonstrated that dPER/dTIM complex formation is both important for their nuclear localization and repression of its own transcription through interaction with the transcription factors CLOCK and CYCLE (Dunlap, 1998).

In mammals, however, CRYs were established instead of TIM as the second transcriptional feedback repressors next to PERs whereby the mammalian oscillator mechanistically diverges from the *Drosophila* oscillator. As for PER, cryptochrome RNA and protein levels oscillate in various tissues in a daily manner driven by CLOCK and BMAL1 binding to the E-box elements in their promoters. Results from co-immunoprecipitation, yeast two hybrid screens and biochemical analysis imply the direct interaction of CRY and PER as well as their interaction with CLOCK and BMAL1. Moreover, cellular reporter gene assays provide clear evidence for the joined capacity of CRY and PER to feedback and negatively regulate CLOCK/BMAL1 mediated transcription. Finally, Sato et al. identified CLOCK and BMAL1 mutations in a molecular genetic screen in mammalian cells which prohibit direct interaction with CRY1. As a consequence, arrhythmic phenotypes are observed due to uncoupling of CLOCK/BMAL1 from CRY mediated transcriptional repression. Thereby, it was proven that I) transcriptional feedback is required for a functional mammalian clock and II) cryptochromes most probably mediate mammalian negative feedback in collaboration with PER in a time dependent manner (Gekakis et al., 1998; Griffin, 1999; Jin et al., 1998; Kume et al., 1999; Reppert and Weaver, 2001; Sato et al., 2006; Shearman et al., 1997). This also explains the complete behavioral and molecular arrhythmicity of *Per1^{-/-}/Per2^{-/-}* and *Cry1^{-/-}/Cry2^{-/-}* double knockout mice (compare Figure 4A and Figure 10A).

1.6.1 Nuclear Localization of CRY and PER

To allow for negative feedback, CRY and PER proteins have to be located in the nucleus. Although controversial results have been reported about the cellular localization of PER proteins in cell systems, their cellular localization appears to be decided by both regulated nuclear import as well as export of proteins. A combination of one nuclear localization signal (NLS) and several nuclear export signals (NES) as well as e.g. phosphorylation dependent masking of these determines mPER 1-2 localization (Vielhaber et al., 2001; Yagita et al., 2002).

mPER3 further contains an active cytoplasmic localization domain (CLD) (Yagita et al., 2000) (Figure 5). Nevertheless, cellular localization of PERs is additionally influenced by heterodimerization of PER proteins with each other which not only enhances their stability but also probably causes the structural masking and unmasking of certain localization signal sequences and thereby controls activation of transport in or out of the nucleus, respectively (Loop and Pieler, 2005; Yagita et al., 2000). Cellular localization of CRY1 (and probably CRY2), however, was found to be determined by two NLS sequences and influenced by its predicted coiled-coil region at the C-terminus of its PHR which contains PER interaction sites (Chaves et al., 2006). In fact, CRY and PER largely depend on each other in nuclear localization as they form heterodimeric CRY/PER or tetrameric CRY (2)/ PER (2) complexes (Kume et al., 1999; Loop et al., 2005; Shearman et al., 2000b) or trimeric CRY/PER/CK1 δ/ϵ complexes which are targeted by phosphorylation for nuclear transport (Lee et al., 2001). PER, and especially PER1, abundance seems to be the limiting factor for nuclear localization of CRY/PER since PER1 deficient mice show lower nuclear levels of PER2 and CRY1 in SCN cells despite unaltered circadian gene expression (Bae et al., 2001). It is likely that only combined NLS sequences from both CRY and PER suffice to counteract the NES sequences of PER and thereby shift CRY/PER from the cytoplasm to the nucleus (Chaves et al., 2006; Miyazaki et al., 2001). Nuclear abundance is further augmented by the mutual stabilization of PER and CRY through interaction (Yagita et al., 2002).

1.6.2 The Molecular Mechanisms of Feedback Transcriptional Repression

The mechanisms underlying CRY/PER mediated negative transcriptional feedback repression are still obscure. It most likely bases on physical CRY/PER protein-protein interactions with CLOCK/BMAL1 (Langmesser et al., 2008) promoted by e.g. posttranslational modifications like BMAL1 acetylation by CLOCK (Hirayama et al., 2007). Inhibition of transcriptional activity is related to impaired phosphorylation patterns of CLOCK/BMAL1, disruption of the CLOCK/BMAL1/(DNA) complex and modification of coregulator binding (Dardente et al., 2007; Sato et al., 2006; Ye et al., 2011).

Likewise, an ongoing discussion exists about the individual impact of CRYs and PERs on negative transcriptional feedback repression. Early studies on the role of CRY in the mammalian circadian clock report crucial effects of CRY in transcriptional repression of CLOCK/BMAL1 and

only mild effects of PER (Kume et al., 1999). More recent studies with cell transfection assays also postulate the potent influence of CRY on CLOCK/BMAL1 inhibition (Dardente et al., 2007). Similarly biochemical data suggest that only CRY1 and not CRY1/PER2 or PER2 alone can bind to CLOCK/BMAL1 on DNA. Complementary cell assays in the same study show that CRY1 destabilizes the CLOCK/BMAL1/DNA complex and represses transcription independently of PER (Ye et al., 2011). Interestingly, results from Chen et al. instead suggest that rhythmic PER2 abundance is not only the limiting factor for active repressor complex formation but also driving cyclic CLOCK/BMAL1 repression. Indeed, they observe that constitutive expression of PER2 disrupts the rhythmic clock gene and endogenous PER protein expression in cultured fibroblasts and in mouse liver *in vivo*; and that mice lose rhythmic locomotor activity upon PER2 overexpression in their brain. Coimmunoprecipitation results from the same study indicate that PER2 serves as a “bridge” for the transcriptional repressor CRY1 in its interaction with CLOCK/BMAL1. (Chen et al., 2009). This, however, would contradict the observation that PER interferes with CRY binding to CLOCK/BMAL1 on DNA (Ye et al., 2011) and biochemical data report a direct interaction site of CRY1 and BMAL1 (Czarna et al., 2011).

CLOCK/BMAL1 inhibition probably needs more than solely CRY and PER and represents a collaborative and constitutive process in which the CRY/PER core complex recruits enzymes and other protein machineries, which modify CLOCK/BMAL1 transcriptional control. PER1 and PER2 associated complexes, which were harvested and purified from mouse tissues at circadian time of repression, are huge (> 1 megadalton) (Brown et al., 2005b). Analysis showed that they contain, next to common circadian clock proteins (CRY1/2, PER1-3, CLOCK, BMAL1, casein kinase 1 δ/ϵ) (Padmanabhan et al., 2012), DNA- and RNA-binding proteins (NONO) and histone methyltransferases (subunit WDR5, HP1 γ -Suv39h), which probably support CRY/PER transcriptional repression through histone methylation (Brown et al., 2005b; Duong and Weitz, 2014). As deacetylation and methylation of histone H3K9 are often collaboratively associated with the transcriptionally repressed chromatin state, identification of PSF (polypyrimidine tract-binding protein-associated splicing factor) in PER complexes makes sense; it recruits the SIN3 histone deacetylase complex to the site of CLOCK/BMAL1 mediated transcription (Duong et al., 2011). It was shown previously that rhythmic acetylation and deacetylation of histones and chromatin remodeling at the promoters of clock genes allows for cyclic CLOCK/BMAL1 transcriptional activity (Etchegaray et al., 2003). As CLOCK contains an active histone

acetyltransferase domain (Doi et al., 2006) itself, PSF and the subsequent recruitment of SIN3 HDAC probably reverses CLOCK histone modifications.

The sequential identification of RNA helicases DDX5 and DHX9, RNA polymerase II, pre mRNAs and other factors involved in transcriptional elongation as well as DNA/RNA helicase SETX, which mediates transcriptional termination, in CRY/PER complexes suggests that the repressor complex not only inhibits transcription initiation. It supposedly also blocks SETX action at the *Cry* and *Per* transcription termination sites which results in RNA polymerase accumulation on the DNA and reduces transcription reinitiation (Padmanabhan et al., 2012).

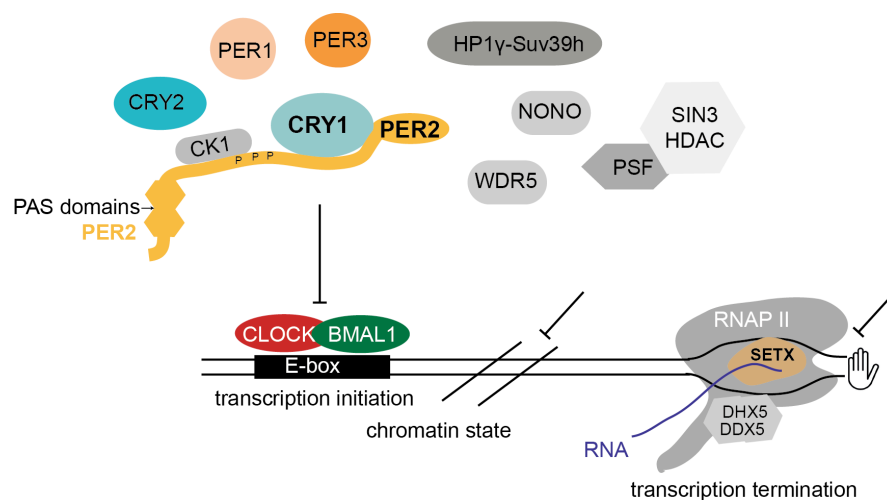


Figure 12: Identified components of nuclear PER1/2 complexes. They target CLOCK/BMAL1 mediated transactivation, chromatin state and transcription termination for inhibition of circadian transcription.

These studies suggest that inhibition of CLOCK/BMAL1 mediated transcription is a multistep mechanism involving different protein assemblies. PER (most probably PER2 or PER1) serves as a scaffold for a dynamic multiprotein complex including CRYs. The interaction capacity of PER proteins probably brings cryptochrome and other corepressors close to their targets to mediate transcriptional feedback mechanisms which render the CLOCK/BMAL1 transactivation complex temporally nonfunctional (Figure 12). Whether transcriptional repression attenuates affinity of CLOCK and BMAL1 for DNA or not is unclear. Recent studies, however, imply a negative impact of CRY1 on CLOCK/BMAL1 DNA binding capacity and rhythmic binding of CLOCK/BMAL1 to DNA (Koike et al., 2012; Ripperger and Schibler, 2006; Ye et al., 2011). Interestingly, PER/TIM repressor activity in the *Drosophila* circadian clock presumably also involves dissociation of CLOCK/CYCLE from DNA in a two step mechanism involving PER-CLOCK interactions (Menet et al., 2010).

2 Aims of the Thesis

Strikingly, many aspects of the mechanistic details behind the circadian clock and especially behind the CRY/PER complex are still poorly understood. Our knowledge bases on experimental observations but hardly ever provides precise interconnecting explanations for observed phenomena. Solely, biochemical assays and high resolution crystal structure analysis of mammalian clock complexes will unravel step by step the direct protein-protein interactions, dynamics and mechanisms that account for driving the circadian oscillator. This will allow in the future to selectively treat clock or clock-related disorders which become more and more prominent because of lifestyle based irregular sleep patterns and the predominance of artificial light.

This study specifically addresses the molecular biology of PER within the circadian clock using a structural and biochemical approach. More precisely, the following questions should be answered: What are the reasons for the distinct functions of mammalian PER1-3 and how do these become noticeable? How do the N-terminal PAS domains of PER contribute to clock; are they potential chemical and/or structural signal sensors or only plain protein interaction platforms? How is the interaction between mammalian CRY1 and PER2 mediated and regulated? How does PER contribute to CRY stability and its repressor function? How does the CRY/PER complex account for negative feedback in the mammalian circadian clock? Finally, what do we learn from structural insights about the biology of the mammalian circadian clock?

Therefore, the mammalian PER proteins (or fragments) alone or in complex with CRY should be expressed, purified and crystallized. Based on the structural information, mutational analysis and complementary biochemical experiments are designed to verify the complex structure in solution and to test for the influence of potential ligands. Furthermore, complementary and model proofing cell assays and *in vivo* studies are performed in collaboration.

3 Results

Publication I

Kucera N., **Schmalen I.**, Hennig S., Öllinger R., Strauss H. M., Grudziecki A., Wieczorek C., Kramer A., and Wolf E. (2012). Unwinding the differences of the mammalian PERIOD clock proteins from crystal structure to cellular function. *Proc Natl Acad Sci USA* 109, 3311–3316.

→ Crystal structure and analysis of homodimeric mPER1 (PAS-A and B)

Unwinding the differences of the mammalian PERIOD clock proteins from crystal structure to cellular function

Nicole Kucera^{a,1}, Ira Schmalen^b, Sven Hennig^{a,1}, Rupert Öllinger^c, Holger M. Strauss^{d,2}, Astrid Grudziecki^c, Caroline Wiczorek^{a,3}, Achim Kramer^c, and Eva Wolf^{b,4,5}

^aMax Planck Institute of Molecular Physiology, Department of Structural Biology, Otto-Hahn-Strasse 11, 44227 Dortmund, Germany; ^bMax Planck Institute of Biochemistry, Department of Structural Cell Biology, Am Klopferspitz 18, 82152 Martinsried, Germany; ^cNanolytics, Gesellschaft für Kolloidanalytik mbH, Am Mühlenberg 11, 14476 Potsdam, Germany; and ^dLaboratory of Chronobiology, Charité—Universitätsmedizin Berlin, 10098 Berlin, Hessische Strasse 3-4, 10115 Berlin, Germany

Edited by Gregory A. Petsko, Brandeis University, Waltham, MA, and approved January 4, 2012 (received for review August 16, 2011)

The three PERIOD homologues mPER1, mPER2, and mPER3 constitute central components of the mammalian circadian clock. They contain two PAS (PER-ARNT-SIM) domains (PAS-A and PAS-B), which mediate homo- and heterodimeric mPER-mPER interactions as well as interactions with transcription factors and kinases. Here we present crystal structures of PAS domain fragments of mPER1 and mPER3 and compare them with the previously reported mPER2 structure. The structures reveal homodimers, which are mediated by interactions of the PAS-B β -sheet surface including a highly conserved tryptophan (Trp448_{mPER1}, Trp419_{mPER2}, Trp359_{mPER3}). mPER1 homodimers are additionally stabilized by interactions between the PAS-A domains and mPER3 homodimers by an N-terminal region including a predicted helix-loop-helix motive. We have verified the existence of these homodimer interfaces in solution and inside cells using analytical gel filtration and luciferase complementation assays and quantified their contributions to homodimer stability by analytical ultracentrifugation. We also show by fluorescence recovery after photobleaching analyses that destabilization of the PAS-B/tryptophan dimer interface leads to a faster mobility of mPER2 containing complexes in human U2OS cells. Our study reveals structural and quantitative differences between the homodimeric interactions of the three mouse PERIOD homologues, which are likely to contribute to their distinct clock functions.

circadian clock | PAS domains | PERIOD proteins | protein interactions

In mammals many physiological, behavioral, and biochemical processes are regulated in a day-time dependent (circadian) manner. The approximately 24 h period is generated by a circadian clock, which is operated by molecular feedback loops. In the main feedback loop, the bHLH (basic-helix-loop-helix)-PAS (PER-ARNT-SIM) transcription factors mBMAL1/2, mCLOCK, and NPAS2 activate the expression of three PERIOD proteins (mPER1, mPER2, and mPER3) as well as two cryptochromes, mCRY1 and mCRY2. The mPER and mCRY proteins inhibit their own transcription, completing the circle of negative feedback. The daily regulated expression of mBMAL1 is ensured by a stabilizing feedback loop, in which the heme binding nuclear receptor REV-ERB α/β represses mBMAL1 expression, whereas ROR- α/β activates it (1, 2). Recently, nontranscriptional circadian oscillations of peroxiredoxin oxidation-reduction, hemoglobin dimer-tetramer transitions, and NADH/NADPH oscillations have been described in human red blood cells, which are interconnected with the transcriptional feedback loops in nucleated cells (3, 4).

The PERIOD proteins and the transcription factors mBMAL1/2, mCLOCK, and NPAS2 contain two tandemly organized PAS domains (PAS-A and PAS-B). The PAS domains mediate homo- and heterodimeric interactions between the mPER homologues (5–8) as well as interactions of the mPERs with mBMAL1/2, mCLOCK, and NPAS2 (9–12). These interactions regulate the stability and cellular localization of the mPERs and modulate the activity of

the mBMAL1/mCLOCK transcription factor complex. Additionally, the PAS domains of NPAS2, mCLOCK, and mPER2 have been reported to bind heme (13–16). In the circadian clock, mPER1 and mPER2 proteins are found in large protein complexes, likely establishing multiple interactions via their PAS domains, the central CK1 ϵ/δ binding domain and the C-terminal mCRY binding region (17–19).

Studies with mPER knockout mice showed that mPER1 and mPER2 are more essential for circadian rhythmicity than mPER3 (20–22). mPER2 appears to positively regulate the expression of clock genes (*mper1*, *mper2*, *mCRY1*, *mbmal1*) in vivo (20, 21), possibly by interacting with REV-ERB α and thereby modulating its effect on mBMAL1 transcription (23). In contrast, mPER1 knockout leads to decreased peak amounts of mPER2 and mCRY proteins in the nucleus, suggesting that mPER1 regulates their stability and/or nuclear entry through protein-protein interactions (20). The subtle effect of mPER3 deficiency on circadian behavior implies that mPER3 is more important for output functions. Indeed, mPER3 interacts with the nuclear receptor PPAR- γ via an N-terminal region including both PAS domains and a preceding predicted helix-loop-helix motive (24). This interaction represses the PPAR- γ activity and thereby inhibits the adipogenesis of mesenchymal stem cells. The importance of the *per3* gene is also shown by its implication in the delayed sleep phase syndrome and the morning or evening sleep timing preferences observed in human populations (25, 26).

To provide insights into the molecular mechanisms underlying the distinct functions and molecular interactions of the three mPER homologues, we have solved crystal structures of the PAS domain regions of mPER1 and mPER3 and compared them with our mPER2 structure (27). In addition to a conserved PAS-B/tryptophan dimer interface, mPER1- and mPER3 homodimers

Author contributions: N.K., I.S., S.H., R.Ö., H.M.S., A.K., and E.W. designed research; N.K., I.S., S.H., R.Ö., H.M.S., A.G., and C.W. performed research; A.G. and C.W. contributed new reagents/analytic tools; N.K., I.S., S.H., R.Ö., H.M.S., A.K., and E.W. analyzed data; and N.K. and E.W. wrote the paper.

The authors declare no conflict of interest.

This article is a PNAS Direct Submission.

Data deposition: The atomic coordinates have been deposited in the Protein Data Bank, www.pdb.org [PDB ID codes 4DJ2 (mPER1) and 4DJ3 (mPER3)].

¹Present address: Western Australian Institute for Medical Research Rear 50 Murray Street Perth, WA 6000 Australia.

²Present address: Novo Nordisk A/S, Novo Nordisk Park, DK-2760 Måløv, Denmark.

³Present address: Max Planck Institute for Neurological Research, Gleuelerstr. 50, 50931 Cologne, Germany.

⁴Present address: Adolf-Butenandt-Institute, Department of Physiological Chemistry, Butenandtstrasse 5, 81377 Munich, Germany.

⁵To whom correspondence should be addressed. E-mail: eva.wolf@med.uni-muenchen.de.

This article contains supporting information online at www.pnas.org/lookup/suppl/doi:10.1073/pnas.1113280109/-DCSupplemental.

are stabilized by interfaces located within the PAS-A domain (mPER1) or a predicted helix-loop-helix region N-terminal to the PAS-A domain (mPER3). These additional interfaces lead to increased affinities compared to the mPER2 PAS domain homodimers. We also provide evidence that the PAS domains of mPER1 and mPER3 might be able to bind heme. Furthermore, we show by luciferase complementation assays that the mPER homodimers observed in our crystal structures are also formed in HEK293 cells. Moreover, our fluorescence recovery after photobleaching (FRAP) analyses reveal that destabilization of the PAS-B/tryptophan dimer interface generates faster moving mPER2 containing complexes in human U2OS cells.

Results

Crystal Structures of Mouse PERIOD1 and Mouse PERIOD3. We have determined crystal structures of the fragments mPER1[191–502] and mPER3[108–411], which include the two PAS domains (PAS-A and PAS-B), the αE helix C-terminal to PAS-B and about 25 residues N-terminal to PAS-A (Fig. 1, Fig. S1, and Table S1).

Both structures revealed noncrystallographic homodimers (Fig. 1A and D). Each monomer contains two canonical PAS domains with a five-stranded antiparallel β -sheet (βA - βE) covered on one face by α -helices (αA , αA^* , αB , αC) (Fig. 1A and D, Fig. S1,

and Table S2). The mPER homodimers are stabilized by interactions between the antiparallel PAS-B β -sheet surfaces. Central to this interface are the conserved tryptophans Trp448_{mPER1} and Trp359_{mPER3} [corresponding to Trp419_{mPER2}; (27)] as well as two phenylalanines, Phe444_{mPER1}/Phe355_{mPER3} (=Phe415_{mPER2}) and Phe454_{mPER1}/Phe365_{mPER3} (=Phe425_{mPER2}) (Fig. 1A and D, Figs. S2A and S3C).

The mPER2 homodimer also involved interactions of the PAS-A domain with helix αE and the PAS-B domain of the dimerizing molecule (27) (Fig. S2B). These interactions are not observed in the mPER1 and mPER3 structures because the relative orientation of the monomers is changed in these two homologues (Fig. S3A; Table S2). Instead, a second homodimer interface is observed in the PAS-A domains of mPER1 and mPER3, which is mostly mediated by contacts between their antiparallel αC helices (Fig. 1B and E, Fig. S2B). Central to this interface is a tyrosine residue, Tyr267_{mPER1} and Tyr179_{mPER3}. In mPER1, the presence of two glycine residues (Gly264 and Gly268) allows for a close approach of the two αC helices (Fig. 1B). In mPER3, the αC helices do not approach each other as closely as in mPER1, likely due to the exchange of Gly264_{mPER1} to a bulky arginine (Arg176_{mPER3}) (Fig. 1E, Fig. S2B).

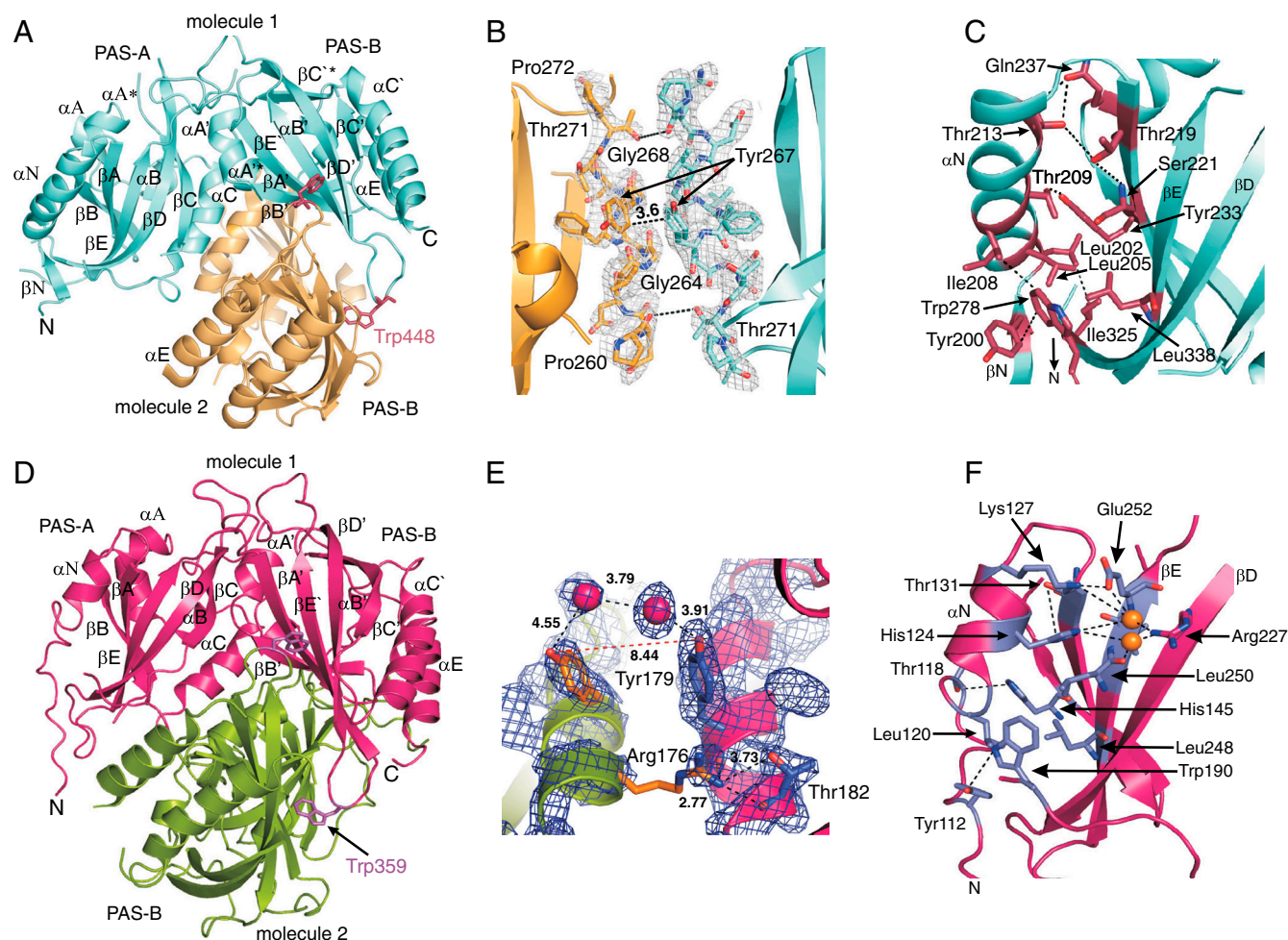


Fig. 1. Crystal structures of mPER1[191–502] and mPER3[108–411] (A) Ribbon presentation of the mPER1[191–502] homodimer with molecule 1 shown in cyan, molecule 2 in yellow. The conserved Trp448 is shown as atomic stick figure. (B) Close-up view of the mPER1 PAS-A/ αC dimer interface formed by antiparallel packing of the αC helices. The $2F_o - F_c$ electron density is shown in gray (1σ level). (C) Close-up view of the mPER1 PAS-A/N-terminal cap interface. (D) Ribbon presentation of the mPER3[108–411] homodimer with molecule 1 shown in magenta, molecule 2 in green. The conserved Trp359 is shown as atomic stick figure. (E) Close-up view of the mPER3 PAS-A/ αC dimer interface. The composite omit map is shown in blue ($2F_o - F_c$, $\sigma = 1$). (F) Close-up view of the mPER3 PAS-A/N-terminal cap interface. His124 (αN) forms main- and side chain contacts to Thr131, Leu250, and Val 251 and water mediated H-bonds to Arg227 and Glu252. Lys127 (αN) forms a salt bridge to Glu252. Leu120 makes van der Waals contacts to Trp190 and Leu248. (A)–(F) Interacting residues and water molecules are highlighted as atomic stick figures and spheres. Numbers indicate distances in Å.

In all three mPER homologues the region N-terminal to the PAS-A domain (referred to as N-terminal cap) interacts with the PAS-A domain surface intramolecularly. Whereas the N-terminal cap of mPER2 is unstructured, it folds into a long α -helix (α N) and a β -strand (β N) in mPER1 and a shorter α -helix (α N) in mPER3 (Fig. 1 *A* and *C, D* and *F*, Fig. S3 *A* and *B*). Our mPER structures revealed a conserved interaction between Tyr200_{mPER1}/Tyr171_{mPER2}/Tyr112_{mPER3} (N-terminal cap) and the PAS-A residue Trp278_{mPER1}/Trp249_{mPER2}/Trp190_{mPER3} (Fig. 1 *C* and *F*, Fig. S3*B*, and ref. 27). In mPER1, the PAS-A residue Tyr233 constitutes a central residue of this interface, which contacts Leu202, Leu205, and Thr209 of the N-terminal cap (Fig. 1*C*). Additionally, Leu205 and Ile208 (α N) form van der Waals contacts to Trp278 and Leu338 (PAS-A). Thr209 and Thr213 (α N) hydrogen bond to Thr219, Ser221, and Gln237 of PAS-A. In mPER3, Tyr233_{mPER1} is replaced by a histidine (His145_{mPER3}), which does not establish strong contacts to the N-terminal cap (shortest distance to Thr118: 4.5 Å). Instead, the N-terminal cap of mPER3 contacts the PAS-A surface via His124, Leu120, and Lys127 as detailed in Fig. 1*F*.

In the PAS-A β E-strand of mPER2 an LxxLL coactivator motif (³⁰⁶LCC³⁰⁹LL) has been identified, which plays a role in the interaction of mPER2 with REV-ERB α and possibly other nuclear receptors (23). Although the sequences are changed to ³³⁵PCC³³⁸LL in mPER1 and ²⁴⁵PCC²⁴⁸LT in mPER3, the coactivator motif regions (β E strands) of mPER1, 2, and 3 superimpose well (Fig. S3 *A* and *B*). However, Leu338_{mPER1} and Leu248_{mPER3} are buried in a hydrophobic pocket formed by Trp278_{mPER1}/Trp190_{mPER3} (PAS-A) and Leu205_{mPER1}/Leu120_{mPER3} of the N-terminal cap (Fig. 1 *C* and *F*, Fig. S3*B*). In mPER2, Leu309_{mPER2} is less covered and the β D- β E loop preceding the coactivator motif is less ordered than in mPER1 and mPER3 (Fig. S3 *A* and *B*).

The α E helix of mPER1, mPER2, and mPER3 contains a functional nuclear export signal (NES; Fig. S1), which corresponds well to the consensus sequence L-x(2,3)-[LIVFM]-x(2,3)-L-x-[LI] (28). Whereas Leu489_{mPER1}/Leu460_{mPER2}/Leu399_{mPER3}, Ile493_{mPER1}/Ile464_{mPER2}/Ile403_{mPER3}, and Leu496_{mPER1}/Leu467_{mPER2}/Leu406_{mPER3} pack against the α C' helix of PAS-B, the C-terminal residues Leu498_{mPER1}/Met469_{mPER2}/Leu408_{mPER3} point to the molecule surface (Fig. S4).

Analysis of mPER PAS Domain Interactions in Solution. In order to prove the existence of the mPER1 and mPER3 homodimers in solution and to compare their affinities with the mPER2 PAS domain fragments (27), we have analyzed the fragments mPER1 [197–502] and mPER3[108–411] by analytical gel filtration and analytical ultracentrifugation (Fig. S5). The dissociation constant of the mPER3[108–411] homodimer is 1.72 μ M, which is comparable to the equivalent mPER2[170–473] fragment ($K_D = 1.34 \mu$ M). For the mPER1[197–502] PAS domain fragment, however, we obtained a K_D of 0.15 μ M corresponding to a 10 to 15 times higher affinity than mPER2 and mPER3 (Fig. S5*G*).

We have mutated the PAS-B interface residues Phe444, Trp448, and Leu456 of mPER1 as well as Trp359, Ile367, and Pro330 of mPER3 (Fig. S3*C*) to glutamate. In our gel filtration experiments, the mutations W359E and I367E totally and P330E partially disrupted the mPER3[108–411] homodimer (Fig. S5*D*). In the mPER1[197–502] fragment only the W448E mutation completely prevented homodimer formation. The F444E mutation was partially effective (Fig. S5 *A* and *C*) and the L456E mutation (corresponding to I367E in mPER3) totally ineffective. Analytical ultracentrifugation revealed that the mPER1[197–502]F444E mutant protein population, which elutes before the wild-type protein in our gel filtration experiments, corresponds to a homodimer with an enlarged hydrodynamic radius and not to a higher oligomeric state. We reasoned that in the dimeric F444E mutant population the two monomers are loosely held

together by the remaining PAS-A/ α C dimer interface. To prove this hypothesis we generated a F444E/Y267E double mutant in order to destabilize both, the PAS-B/ β -sheet- and the PAS-A/ α C dimer interface. As expected, the double mutant totally disrupted the homodimer (Fig. S5*C*). In contrast, the Y267E single mutation left the homodimer intact suggesting the PAS-B interface to be more important.

Sequence analysis predicts the existence of a helix-loop-helix motif N-terminal to the PAS-A domain of mPER1, 2, and 3 (5, 29, 30) and secondary structure predictions suggest this N-terminal region to be mostly α -helical. To explore its potential contribution to homodimer formation, we have determined the dimer affinity of the N-terminally extended mPER3 PAS domain fragment mPER3[32–411], which includes the predicted helix-loop-helix motif (Fig. S1*B*). Indeed, the K_D for the mPER3[32–411] homodimer was 0.4 μ M corresponding to a roughly four times higher affinity compared to mPER3[108–411] (Fig. S5*G*). Moreover, none of our PAS-B dimer interface mutants disrupted the mPER3[32–411] homodimers (Fig. S5*E*). Furthermore, our CD spectra revealed an increased α -helical content of mPER3[32–411] compared to mPER3[108–411] (Fig. S6 *B–D*). Hence, our analysis suggests the presence of an additional α -helical homodimer interface between residues 32 and 107 of mPER3, which likely adopts a helix-loop-helix fold. Since mPER1 and mPER2 have also been predicted to contain a helix-loop-helix motif N-terminal to their PAS-A domain (Fig. S1*B*) (5, 29), we tested the effect of the W419E mutation, which is able to disrupt mPER2[170–473] and mPER2[128–473] PAS domain homodimers (27), in the N-terminally extended fragment mPER2[59–473]. Unlike mPER3[32–411], the mPER2[59–473] homodimers are efficiently disrupted by the W419E mutation (Fig. S5*F*).

Heme Binding of mPER1 and mPER3. To find out, if mPER1 and mPER3, like mPER2 (14, 15), are able to bind heme in their PAS domains, we have incubated our purified mPER3[108–411], mPER3[32–411], and mPER1[197–502] proteins with heme, separated the heme exposed proteins via gel filtration chromatography and assessed heme binding by UV/VIS spectroscopy. For all three fragments we observed a shift of the absorption maximum from 390 nm (free heme) to about 420 nm (protein-bound heme, Fig. S7 *A–C*), suggesting that heme binds to our mPER1 and mPER3 PAS domain fragments.

PAS Domain Interactions are Essential for mPER Homodimerization in Mammalian Cells. To investigate if the mPER crystal dimers are also present inside cells, we performed luciferase complementation experiments in HEK293 cells using wild-type and tryptophan mutant versions of the mPER proteins (Fig. 2). In our previously reported coimmunoprecipitation (Co-IP) experiments (27), mutation of the conserved Trp419_{mPER2} (W419E) efficiently disrupted mPER2[128–473] PAS domain homodimers, but only had a subtle effect on the formation of full-length mPER2 homodimers in HEK293 cells. We concluded that the full-length mPER2 homodimer is additionally stabilized via non-PAS mPER2 regions, either directly (due to mPER2-mPER2 homodimer interactions) or indirectly by other interacting molecules such as the cryptochromes. To distinguish between these two possibilities, the luciferase complementation assay was performed with a C-terminally truncated mPER2[1–1127] fragment (mPER2 Δ C), which is unable to interact with mCRY1 (Fig. 2 *A* and *B*). Compared to the wild-type mPER2 Δ C fragment, the amount of homodimers (measured as luciferase activity) was reduced to about 40% when both monomers contained the W419E mutation and to about 75% when only one monomer was mutated (Fig. 2*B*). This result suggests that the PAS-B/tryptophan interface is the predominant homodimer interface of the full-length mPER2 protein and indirect mCRY-mediated interactions masked the W419E mutant effect in our Co-IP studies with full-length mPER2.

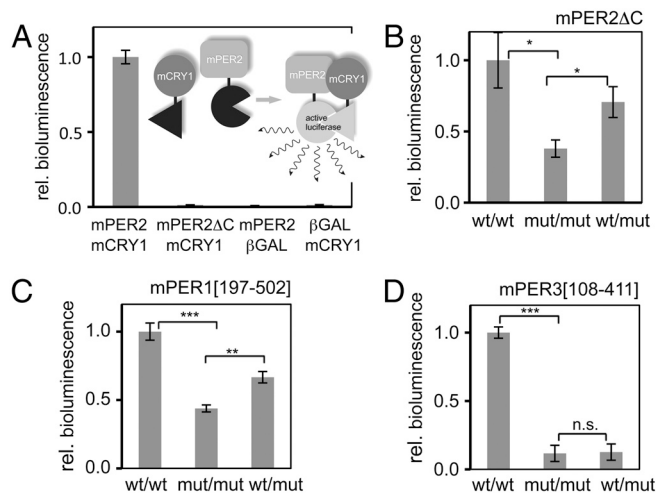


Fig. 2. Tryptophan residues within mPER-mPER interfaces are critical for mPER homodimerization in mammalian cells. (A) Luciferase complementation assay—proof-of-concept: mPER2 and mCRY1 were expressed as fusion proteins with an N-terminal or C-terminal fragment of *firefly* luciferase in HEK293 cells. Strong and specific bioluminescence signals were detected upon mPER2 and mCRY1 fusion protein coexpression, but not if a truncated version of mPER2 with a deletion of the C-terminal mCRY binding domain—mPER2 Δ C—or an irrelevant protein (β GAL) is coexpressed. Data are normalized to *renilla* luciferase activity, which was used as a transfection control. Shown are average values and error bars of two independent transfections. (B)–(D) mPER fragments were expressed as luciferase fusion proteins in HEK293 cells. The N-terminal luciferase fragment was fused to the N-terminus and the C-terminal luciferase fragment to the C-terminus of a corresponding mPER fragment. Shown are average values of four to five independent transfections with s.e.m. (*: $p < 0.05$; **: $p < 0.005$; ***: $p < 0.001$; n.s.: not significant; t-test). Each experiment was performed at least three times with similar results. (B) mPER2 without mCRY-binding domain (mPER2 Δ C = mPER2[1–1127]) was expressed either as wild-type (wt) or as W419E mutant (mut). Mutation at position 419 in both binding partners (mut/mut) severely, mutation in one partner (wt/mut) moderately reduces bioluminescence signals. (C) mPER1[197–502] fragments were expressed either as wild-type (wt) or as W448E mutant (mut). Mutation at position 448 in both binding partners (mut/mut) severely, mutation in one partner (wt/mut) moderately reduces bioluminescence signals. (D) mPER3[108–411] fragments were expressed either as wild-type (wt) or as W359E mutant (mut). Mutation at position 359 in one or both of the binding partners (wt/mut and mut/mut) severely reduces bioluminescence signals.

In our luciferase complementation assay, homodimers of the mPER3[108–411] PAS domain fragment were largely disrupted by the W359E mutation (Fig. 2D), while the corresponding W448E mutation in mPER1 efficiently weakened dimerization of the mPER1[197–502] fragment (Fig. 2C). We conclude that the PAS-B/Trp homodimer interface of mPER1 and mPER3 is also present inside HEK293 cells. In agreement with our homodimer affinity measurements, about 90% of the mPER3[108–411] dimers are disrupted when Trp359 is mutated in one or both monomers (Fig. 2D), whereas the amount of mPER1[197–502] dimers is reduced to about 45% when both monomers contain the W448E mutation and to about 65% when only one monomer is mutated (Fig. 2C). Since we have identified an additional homodimer interface between residues 32 and 107 of mPER3, which prevents the W359E mutation from disrupting mPER3[32–411] homodimers in solution (Fig. S5E), the W359E mutation is unlikely to disrupt homodimers of full-length mPER3 in our luciferase complementation assay.

Role of Homodimers in the Formation of mPER Containing Complexes.

To analyze the potential role of mPER homodimers in the formation of mPER containing clock protein complexes, we have monitored their mobility in the cytoplasm of human U2OS cells by following Venus-fused mPER proteins in FRAP (fluorescence recovery after photobleaching) experiments (Fig. 3). While the

fluorescence of tetrameric Venus-fused β -galactosidase (MW = 580 kDa) recovered within a half-time ($t_{1/2}$) of 0.56 s, mPER1 and mPER2 complexes showed a slower recovery with $t_{1/2} = 0.76$ s for mPER1 and $t_{1/2} = 1.73$ s for mPER2. The lower mobility of the cytoplasmic mPER1 and mPER2 complexes suggests, that they are larger than tetrameric Venus-fused β -galactosidase and possibly retained by interactions with other cytosolic proteins or structural elements. Mutation of the conserved Trp419_{mPER2} (W419E) leads to a significantly faster fluorescence recovery of mPER2 containing complexes ($t_{1/2} = 1.06$ s). The equivalent W448E mutation in mPER1 did not significantly affect the mobility of the mPER1 complexes, resulting in a wild-type like recovery rate with $t_{1/2} = 1.04$.

Discussion

To provide mechanistic insights into the nonredundant functions of the three PERIOD homologues mPER1, 2, and 3, we have determined crystal structures of homodimeric PAS domain fragments of mPER1 and mPER3 and compared them with the known crystal structure of mPER2 (27). While the PAS-B/tryptophan dimer interface is present in all three mPER homologues, the PAS-A-PAS-B/ α E dimer interface of mPER2 is replaced by a PAS-A-PAS-A interface in mPER1 and mPER3, which is mediated by the two antiparallel α C helices (Fig. 1, Figs. S2 and S3). The different PAS-A dimer interactions result from the changed relative orientation of the two monomers in mPER1 and mPER3 (Fig. S3A), which is likely correlated with the nonconservative amino acid exchanges in the PAS-A-PAS-B/ α E interface of mPER2 [(27) and Figs. S1B and S2B).

The center of the PAS-A/ α C interface is formed by Tyr267 in mPER1 and Tyr179 in mPER3 (Fig. 1 B and E). Interestingly, this tyrosine is replaced by an alanine (Ala287_{dPER}) in the *Drosophila* PERIOD (dPER) homologue. This substitution enables the insertion of Trp482_{dPER} (corresponding to Trp448_{mPER1}/Trp419_{mPER2}/Trp359_{mPER3}) into the PAS-A domain binding pocket of the dimerizing molecule and hence the formation of a completely different dPER homodimer (27, 31). Gly264 and Gly268 of mPER1, which allow for a close approach of the dimerizing α C helices and hence the formation of a tighter PAS-A/ α C interface than in mPER3, are conserved in mammalian PER1 homologues but not in other PER proteins or bHLH-PAS transcription factors. We propose, that the tight PAS-A/ α C interface of mPER1 is responsible for the roughly 10 times higher affinity of mPER1 PAS domain homodimers ($K_D = 0.15 \mu\text{M}$) compared to mPER2[170–473] ($K_D = 1.34 \mu\text{M}$) and mPER3[108–411] ($K_D = 1.72 \mu\text{M}$) and accounts at least partly for the lower efficiency of PAS-B/tryptophan interface mutations in disrupting mPER1 homodimers in solution [Fig. S5 A and C and ref. 27) and in human HEK293 cells (Fig. 2 C and D; Fig. 3C).

Although mPER proteins do not have known sensory functions, mPER2 has been reported to bind heme as a cofactor in its PAS domains and in its C-terminal region (13, 14). Our UV/VIS spectroscopic analyses (Fig. S7 A–C) suggest that the PAS domains of mPER1 and mPER3 might also be able to bind heme. Cys215, which has been proposed as an axial ligand for heme binding to the PAS-A domain of mPER2 (13), is conserved and ordered in mPER1 (Cys244, α A*) but changed to a serine (Ser156) in mPER3 (Fig. S7D). Cys270, another potential heme ligand of mPER2 (13), is conserved in mPER1 and mPER3 (Cys299_{mPER1}, Cys210_{mPER3}). Our mPER crystal structures will guide the design of His and Cys mutants to evaluate heme binding in vivo and in vitro.

All our mPER crystal structures contain a conserved functional NES (28) within the α E helix (Fig. S4). Interestingly, mutation of the C-terminal Met469 of mPER2 to lysine significantly affects the nuclear export activity of the NES toward a heterologous protein, whereas mutation of the equivalent C-terminal Leu408 of mPER1 to Lys has no significant effect on the activity of the mPER1-NES (28). This difference might be related to the

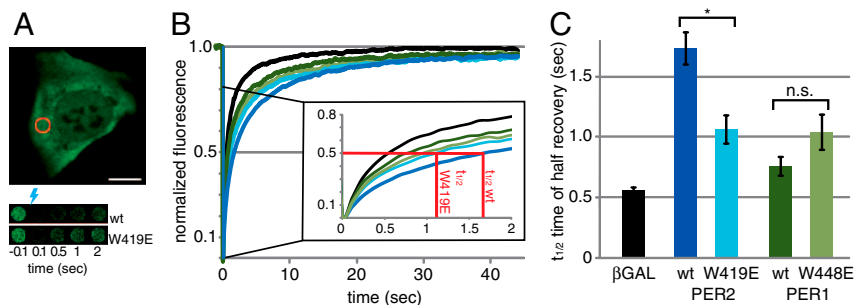


Fig. 3. mPER protein mobility in U2OS cells determined by fluorescence recovery after photobleaching (FRAP). (A) mPER proteins were stably expressed in U2OS cells as fusion proteins with the fluorescent Venus protein. They are localized in both cytoplasm and nucleus (depicted is mPER2). A representative bleach area of a FRAP experiment is indicated. The scale bar represents 10 μ m. Lower shows a representative bleaching and recovery of fluorescent molecules in the bleach areas during the first two seconds for mPER2 wild-type (wt) or the mPER2 W419E mutant fusion proteins. (B) FRAP measurements: normalized average curves of fluorescence recovery in the cytoplasm expressing mPER2 wt (dark blue), mPER2 W419E (light blue), mPER1 wt (dark green), mPER1 W448E (light green), or β GAL (a similar sized control protein; black). Data from the first two seconds of recovery (boxed area) is enlarged. Red marks show $t_{1/2}$ for mPER2 wt and mPER2 W419E. (C) Comparison of half-time of recovery ($t_{1/2} \pm$ sem; n : number of experiments with at least 10 cells per experiment): mPER2 wt ($t_{1/2} = 1.73 \pm 0.13$ s; $n = 7$) is significantly less mobile ($p < 0.001$, t -test) than the control protein β GAL ($t_{1/2} = 0.56 \pm 0.02$ s; $n = 3$). mPER2 W419E ($t_{1/2} = 1.06 \pm 0.11$ s; $n = 3$) displays a significantly increased mobility ($p = 0.016$, t -test) compared to mPER2 wt. In contrast, mPER1 mobility ($t_{1/2} = 0.76 \pm 0.08$ s; $n = 4$) is not increased upon mutation of W448E ($t_{1/2} = 1.04 \pm 0.15$ s; $n = 4$). There is a trend ($p < 0.08$, t -test), however, toward a lower mobility of mPER1 wt when compared to β GAL.

fact that Met469 is involved in mPER2 homodimer interactions, whereas the equivalent Leu residues of mPER1 and mPER3 are completely surface exposed due to the changed relative orientation of the monomers (Fig. S3A and ref. 27). Hence, homo- or heterodimer interactions of the mPER proteins are likely to modulate the function of this NES in the mammalian circadian clock.

Our mutant analyses revealed that the predicted helix-loop-helix region N-terminal to the PAS domains significantly stabilizes homodimers of mPER3 but not mPER2 (Fig. S5E and F). Due to the high sequence similarity of the mPER helix-loop-helix regions (Fig. S1B), this different behavior was somewhat unexpected. We propose, that the changed monomer orientations revealed by our crystal structures (Fig. S3A) may affect the ability of the predicted helix-loop-helix segments of mPER2 and mPER3 to approach each other for homodimer interactions. Furthermore, crude modeling exercises suggest that formation of the helix-loop-helix dimer interface requires a reorientation of at least one of the two N-terminal caps. Notably, all our mPER homodimer structures are asymmetric in a sense that the N-terminal cap is less ordered and therefore more flexible in one of the two monomers. Additionally, the different structures and PAS-A interactions of the N-terminal caps of mPER1, 2, and 3 (Fig. 1C and F, Fig. S3B) might play a role. Since the basic region that is essential for the DNA binding of basic-HLH transcription factors (32), is missing in all three mPER homologues (Fig. S1B) and mPERs have not been reported to directly bind to DNA (5, 29, 30), a regulation of mPER homo- or heterodimer formation by DNA is not to be expected. It is however possible, that (instead of homodimer interactions) the predicted helix-loop-helix region of mPER2 engages in heterodimeric interactions with other helix-loop-helix proteins. Like the ID (inhibitor of DNA binding) family of helix-loop-helix proteins, mPERs could thereby potentially compete with the formation of transcriptionally active and DNA-binding dimeric basic-HLH transcription factors (33, 34).

Based on the relatively low homodimer affinity of its PAS domains and the higher flexibility of its PAS-A domain and N-terminal cap, mPER2 seems more predisposed for heterodimeric signaling interactions than mPER1 and mPER3. Consistently, the PAS domains of mPER2, but not mPER1, have been reported to interact with the β -subunit of casein kinase 2 (35), glycogen synthase kinase 3 β (36), REV-ERB and possibly other nuclear receptors (23, 35–37). Since the mutation of the mPER1³³⁵PCLL coactivator motive to the mPER2 sequence (LCLL) did not restore mPER1 binding to REV-ERB (23), additional regions or molecular features of mPER2 appear to be required. Due to the higher flexibility of the

N-terminal cap and the β D- β E loop (Fig. S3A and B), the LxxLL motive of mPER2 is likely to be more accessible for interactions with nuclear receptors. Furthermore, the two PAS-A coactivator motives in the mPER homodimers are inappropriately positioned to jointly bind to an active nuclear receptor homodimer (38). Hence, the lower homodimer affinity and enhanced flexibility of the mPER2 PAS domains may facilitate REV-ERB binding in a nonhomodimeric conformation. Apart from the PAS domains, the C-terminal mPER2 region, which also contains an LxxLL coactivator motive (aa 1050–1054), may contribute to nuclear receptor binding.

In our luciferase complementation assay with the mPER2[1–1127] protein, we have obtained the strongest luciferase signals when the N-terminal half of the luciferase enzyme was fused to the N-terminal end and the C-terminal half to the C-terminal end of the mPER fragments. This implies that, while full-length mPER2 homodimers are predominantly stabilized by the PAS-B/tryptophan interface (Fig. 2B), their N- and C-terminal ends are near each other in a cellular context. Notably, this configuration could bring N- and C-terminal LxxLL coactivator motives into a spatial arrangement that enables binding to REV-ERB homodimers or other dimeric nuclear receptors. Furthermore, the N-terminal mPER2[1–330] fragment has been shown to interact with the C-terminal mPER2[1056–1257] fragment and with the CK2 β -subunit under Co-IP conditions, suggesting that the N- and C-terminal mPER2 regions communicate with each other and jointly provide a platform for CK2 interaction (35).

In our FRAP assays (Fig. 3), mPER1 and mPER2 showed a slower fluorescence recovery (lower mobility) than tetrameric Venus-fused β -galactosidase (MW = 580 kDa). Since Venus-mPER1- and Venus-mPER2 homodimers are only 325 kDa in size, the mPERs appear to be associated with other proteins in the cytoplasm. As mCRY1 binds directly to mPER2 in our luciferase complementation studies (Fig. 2A), the mPER complexes most likely contain mCRYs. Additional components could be the other mPER homologues and kinases such as CKI ϵ/δ , which were shown to be present in nuclear mPER1 and mPER2 complexes (17, 18). Interestingly, the mutation of Trp419 to glutamate leads to faster moving mPER2 complexes (Fig. 3). We conclude, that the PAS-B/Trp interface and hence the intact mPER2 homodimer is essential for the formation of the more slowly moving and presumably larger mPER2 complexes in mammalian cells. The fact that wild-type mPER2 complexes move more slowly and are therefore likely to be larger than wild-type mPER1 complexes, provides another example of the functional differences

between these two mPER homologues and might be correlated with the more versatile molecular interactions of mPER2 (see above). Of course we cannot exclude that interactions with other cellular structures such as cytoskeletal proteins contribute to the delayed fluorescence recovery of the mPER complexes. Such contributions become more significant as the size of the complexes increases (39) and are, if at all, more likely to affect the wild-type mPER2 complexes.

mPER3 shares some properties with mPER2 (PAS domain homodimer with similar affinity, mostly stabilized by the PAS-B/Trp interface) and others with mPER1 (homodimer structure more mPER1-like, PAS-A/ α C interface discernable). As mPER1, mPER3 possesses a second interface that raises its homodimer affinity to the sub- μ M range, but different from mPER1, mPER3 uses the helix-loop-helix motif located N-terminal to the PAS domains and not the PAS-A/ α C interface as additional stabilizing interface. These unique features of mPER3 are likely to be critical for its molecular interactions e.g. with other clock proteins (5, 7, 8) or the nuclear receptor PPAR- γ (24). They are therefore expected to affect its functions in clock- and sleep regulation and adipogenesis (25, 26) as well as other as yet not very clearly defined roles of mPER3 in peripheral tissues and within output pathways of the clock (40).

In light of the emerging picture that nontranscriptional metabolic rhythms reciprocally interact with the transcriptional oscil-

lator (3, 4), the interactions of mPERs with proteins involved in metabolic and signaling functions as well as with heme might provide possible interconnections between the cellular metabolism and the clockwork. Our PAS domain crystal structures of the three mammalian PERIOD homologues and the quantitative analyses of their homodimer interactions in solution and inside cells provide plausible explanations for their distinct molecular interactions and will guide the design of mutations or small molecule ligands to further dissect their different functions within or outside the mammalian circadian clock.

Materials and Methods

A detailed description of the materials and methods (cloning, protein expression and purification, crystallization and X-ray structure determination, biochemical, spectroscopic and cell biological studies) is provided as supplemental information.

ACKNOWLEDGMENTS. We thank the beamline staff at the SLS for excellent assistance and our colleagues at MPI Martinsried and MPI Dortmund for help with data collection. We also thank the staff of the MPI Martinsried Crystallisation Facility and the Microchemistry Core Facility as well as S. Janetzky and C. Ochs for technical assistance. mPER1 and mPER3 cDNA were generous gifts from U. Albrecht and P. Sassone-Corsi. We are very thankful to T. Korte and A. Herrmann of the Department of Biology and Molecular Biophysics at the Humboldt University Berlin for the use of the confocal microscope and technical advice. This work was supported by the Deutsche Forschungsgemeinschaft (Grants WO-695/2 and WO-695/4 to E.W.; SFB740/D2 to A.K.).

- Ko CH, Takahashi JS (2006) Molecular components of the mammalian circadian clock. *Hum Mol Genet* 15:R271–R277.
- Liu AC, et al. (2008) Redundant function of REV-ERB alpha and beta and non-essential role for BMAL1 cycling in transcriptional regulation of intracellular circadian rhythms. *PLoS Genetics* 4:e2.
- O'Neill JS, et al. (2011) Circadian rhythms persist without transcription in a eukaryote. *Nature* 469:554–558.
- O'Neill JS, Reddy AB (2011) Circadian clocks in human red blood cells. *Nature* 469:498–503.
- Zylka MJ, Shearman LP, Weaver DR, Reppert SM (1998) Three period homologs in mammals: Differential light responses in the suprachiasmatic circadian clock and oscillating transcripts outside of brain. *Neuron* 20:1103–1110.
- Field MD, et al. (2000) Analysis of clock proteins in mouse SCN demonstrates phylogenetic divergence of the circadian clockwork and resetting mechanisms. *Neuron* 25:437–447.
- Loop S, Pieler T (2005) Nuclear import of mPER3 in *Xenopus* oocytes and HeLa cells requires complex formation with mPER1. *FEBS J* 272:3714–3724.
- Yagita K, et al. (2000) Dimerization and nuclear entry of mPER proteins in mammalian cells. *Gene Dev* 14:1353–1363.
- Chen RM, et al. (2009) Rhythmic PER abundance defines a critical nodal point for negative feedback within the circadian clock mechanism. *Mol Cell* 36(3):417–430.
- Langmesser S, Tallone T, Bordon A, Rusconi S, Albrecht U (2008) Interaction of circadian clock proteins PER2 and CRY with BMAL1 and CLOCK. *BMC Mol Biol* 9:41.
- Sasaki M, Yoshitane H, Du NH, Okano T, Fukada Y (2009) Preferential inhibition of BMAL2-CLOCK activity by PER2 reemphasizes its negative role and a positive role of BMAL2 in the circadian transcription. *J Biol Chem* 284:25149–25159.
- Jin XW, et al. (1999) A molecular mechanism regulating rhythmic output from the suprachiasmatic circadian clock. *Cell* 96:57–68.
- Kitanishi K, et al. (2008) Heme-binding characteristics of the isolated PAS-A domain of mouse Per2, a transcriptional regulatory factor associated with circadian rhythms. *Biochemistry* 47:6157–6168.
- Yang J, et al. (2008) A novel heme-regulatory motif mediates heme-dependent degradation of the circadian factor period 2. *Mol Cell Biol* 28:4697–4711.
- Kaasik K, Lee CC (2004) Reciprocal regulation of haem biosynthesis and the circadian clock in mammals. *Nature* 430:467–471.
- Lukat-Rodgers GS, Correia C, Botuyan MV, Mer G, Rodgers KR (2010) Heme-based sensing by the mammalian circadian protein CLOCK. *Inorg Chem* 49:6349–6365.
- Brown SA, et al. (2005) PERIOD1-associated proteins modulate the negative limb of the mammalian circadian oscillator. *Science* 308:693–696.
- Duong HA, Robles MS, Knutti D, Weitz CJ (2011) A molecular mechanism for circadian clock negative feedback. *Science* 332:1436–1439.
- Lee C, Etchegaray JP, Cagampang FRA, Loudon ASI, Reppert SM (2001) Posttranslational mechanisms regulate the mammalian circadian clock. *Cell* 107:855–867.
- Bae K, et al. (2001) Differential functions of mPer1, mPer2, and mPer3 in the SCN circadian clock. *Neuron* 30:525–536.
- Zheng BH, et al. (1999) The mPer2 gene encodes a functional component of the mammalian circadian clock. *Nature* 400:169–173.
- Shearman LP, Jin X, Lee C, Reppert SM, Weaver DR (2000) Targeted disruption of the mPer3 gene: Subtle effects on circadian clock function. *Mol Cell Biol* 20:6269–6275.
- Schmutz I, Ripperger JA, Baeriswyl-Aebischer S, Albrecht U (2010) The mammalian clock component PERIOD2 coordinates circadian output by interaction with nuclear receptors. *Genes Dev* 24:345–357.
- Costa MJ, et al. (2011) Circadian Rhythm Gene Period 3 Is an Inhibitor of the Adipocyte Cell Fate. *J Biol Chem* 286:9063–9070.
- Ebisawa T, et al. (2001) Association of structural polymorphisms in the human period3 gene with delayed sleep phase syndrome. *EMBO Rep* 2:342–346.
- Dijk DJ, Archer SN (2009) Light, sleep, and circadian rhythms: Together again. *PLoS Biol* 7:e1000145.
- Hennig S, et al. (2009) Structural and functional analyses of PAS domain interactions of the clock proteins *Drosophila* PERIOD and mouse PERIOD2. *PLoS Biol* 7:e94.
- Vielhaber EL, Duricka D, Ullman KS, Virshup DM (2001) Nuclear export of mammalian PERIOD proteins. *J Biol Chem* 276:45921–45927.
- Sun ZS, et al. (1997) RIGUI, a putative mammalian ortholog of the *Drosophila* period gene. *Cell* 90:1003–1011.
- Takumi T, et al. (1998) A new mammalian period gene predominantly expressed in the suprachiasmatic nucleus. *Genes Cells* 3:167–176.
- Yildiz O, et al. (2005) Crystal structure and interactions of the PAS repeat region of the *Drosophila* clock protein PERIOD. *Mol Cell* 17:69–82.
- Ellenberger T (1994) Getting a grip on DNA recognition—Structures of the basic region leucine-zipper, and the basic region helix-loop-helix DNA-binding domains. *Curr Opin Struct Biol* 4:12–21.
- Duffield GE, et al. (2009) A Role for Id2 in regulating photic entrainment of the mammalian circadian system. *Curr Biol* 19:297–304.
- Ward SM, Fernando SJ, Hou TY, Duffield GE (2010) The transcriptional repressor ID2 can interact with the canonical clock components CLOCK and BMAL1 and mediate inhibitory effects on mPer1 expression. *J Biol Chem* 285:38987–39000.
- Tsuchiya Y, et al. (2009) Involvement of the protein kinase CK2 in the regulation of mammalian circadian rhythms. *Sci Signal* 2:ra26.
- litaka C, Miyazaki K, Akaike T, Ishida N (2005) A role for glycogen synthase kinase-3beta in the mammalian circadian clock. *J Biol Chem* 280:29397–29402.
- Maier B, et al. (2009) A large-scale functional RNAi screen reveals a role for CK2 in the mammalian circadian clock. *Genes Dev* 23:708–718.
- Chandra V, et al. (2008) Structure of the intact PPAR-gamma-RXR- nuclear receptor complex on DNA. *Nature* 456:350–356.
- Sprague BL, McNally JG (2005) FRAP analysis of binding: Proper and fitting. *Trends Cell Biol* 15:84–91.
- Pendergast JS, Friday RC, Yamazaki S (2010) Distinct functions of Period2 and Period3 in the mouse circadian system revealed by in vitro analysis. *PLoS One* 5:e8552.

Supporting Information

Kucera et al. 10.1073/pnas.1113280109

SI Text

SI Materials and Methods. Recombinant expression and purification.

All mouse PERIOD1 (mPER1) and PERIOD3 (mPER3) fragments were expressed as recombinant GST-fusions in the *Escherichia coli* strains BL21(DE3) using a pGEX-6P1 expression vector with a PreScission™ protease site for removal of the GST-tag. Fragments mPER1[197–502] and mPER1[191–502] were subcloned into the pGEX-6P1 vector using the restriction sites EcoRI and NotI. Tag removal yielded recombinant mPER1 proteins with an eight-residue extension (GPLGSPEF) at the N-terminus corresponding to a molecular weight of, respectively 35,061 Da and 35,706 Da. For subcloning of the mPER3 fragments 108–411 and 32–411 the restriction sites XhoI and NotI were used, yielding PreScission™ protease cleaved fragments with a 13-residue N-terminal overhang (GPLGSPEFPGRLE) and a molecular weight of respectively 35,769 Da and 44,383 Da. mPER2[59–473] was cloned into pGEX-6P2 using restriction sites BamHI and EcoRI. Removal of the GST-tag results in a construct with a five-residue N-terminal overhang (GPLGS) and a molecular weight of 47,264 Da. The proteins were purified via GSH affinity and gel filtration columns. In the case of mPER3 [108–411] an anion exchange was performed additionally. The GST-tag was cleaved and quantitatively removed.

Crystallization. Crystals of mPER3[108–411] diffracting to 2.5 Å resolution were grown at 4 °C in hanging drop setups using a reservoir solution with 100 mM MES pH 5.5, 18% PEG 6000 and a protein solution with 10 mg/ml mPER3[108–411] in 50 mM Tris pH 8.5, 200 mM NaCl, and 2 mM DTE. The mPER3 crystals belong to space group $P2_1$ with unit cell constants $a = 62.7$ Å, $b = 78.6$ Å, $c = 67.2$ Å, $\beta = 97.6^\circ$, and two molecules per asymmetric unit (solvent content 46%). For data collection at 100 K, crystals were transferred into a cryoprotecting solution containing 30% PEG400 (v/v) and shock frozen in liquid nitrogen.

Crystals of mPER1[191–502] diffracting to 2.75 Å resolution were grown at 20 °C in hanging drop setups using a reservoir solution with 100 mM Tris pH 7.5, 0.15 M NH_4OAc , 16% PEG 3350 and a protein solution with 3 mg/mL mPER1[191–502] in 50 mM Tris pH 8.5, 200 mM NaCl, and 2 mM DTT. The mPER1 crystals belong to space group $P2_1$ with unit cell constants $a = 100.3$ Å, $b = 56.9$ Å, $c = 101.1$ Å and four molecules per asymmetric unit (solvent content 39.05%). For data collection at 100 K, crystals were transferred into a cryoprotecting solution containing 20–25% Ethylene Glycol (v/v) and shock frozen in liquid nitrogen.

Data collection, structure determination and refinement. A 2.5 Å dataset of a single mPER3[108–411] crystal and a 2.75 Å dataset of a single mPER1[191–502] crystal were collected at beamline X10SA (SLS). All datasets were processed with XDS (1). The structure of mPER3[108–411] was solved by molecular replacement using MOLREP (2) with one monomer of our refined mPER2[170–473] structure (3) as search model. The structure of mPER1[191–502] was solved by molecular replacement using MOLREP with one monomer of the refined mPER3[108–411] structure as search model. In the search models, variable loop and linker regions as well as the region N-terminal to the PAS-A domain were deleted and nonconserved amino acids were mutated to alanines. The structures were refined with CNS (4) and PHENIX (5) applying several rounds of simulated annealing, positional, and B-factor refinement followed by model building into $2F_o - F_c$ and $F_o - F_c$ maps using the program Coot (6). Simulated annealing omit maps were regularly calculated in CNS and

used to verify, correct or build the model. The mPER1 model was also subjected to TLS refinement.

The final mPER3[108–411] model consists of 548 amino acids and 163 water molecules. The N-terminal amino acids 95–107 correspond to cloning artefacts. Residues 95–103, 193–202 of molecule 1 and residues 95–118, 155–162, 193–202, 215–219, 240, 390–392 of molecule 2 are not seen in the electron density due to conformational disorder. Residues 105–107, 109, 142, 176, 186, 191–192, 204, 219–220, 236, 240–242, 385, 287–388, 390–395, 401, and 409–410 of molecule 1 and residues 142, 146, 152, 153, 163–165, 204, 212–214, 221–222, 241–243, 245, 261–262, 266, 282, 321, 325, 344, 384, 394, 398, and 477 of molecule 2 are modeled as Ala due to conformational disorder of their side chains. The Ramachandran plot depicts 92.88% (509 residues) of main chain torsion angles in the most favored and allowed regions. Thirty-nine residues (7.12%) are located in disallowed regions.

The final mPER1[191–502] model consists of 1,065 amino acids and 65 water molecules. Residues 191–195, 281–293, 305–311, 328–330, and 475–482 of chain A, residues 191–195, 280–293, 306–309, 329, and 475–483 of chain B, residues 191–203, 280–294, 307–310, 327–336, and 476–481 of chain C and residues 191–211, 280–293, 304–311, 323–335, 475–482 of chain D are not seen in the electron density due to conformational disorder. Residues 198, 203, 211, 212, 214, 217, 243, 245, 247, 248, 274, 280, 294, 312, 343, 352, 411, 418, 450, 451, 468, 483, 485, 487, 488, 499, and 502 of chain A, residues 196, 198, 206, 207, 211, 212, 214, 216, 217, 243, 245, 247, 248, 274, 294, 295, 305, 311, 312, 327, 328, 343, 352, 411, 415, 450, 451, 484, 487, 488, and 502 of chain B, residues 204, 205, 206, 212, 214, 215, 225, 236, 245, 249, 256, 274, 278, 295, 306, 311, 312, 325, 326, 411, 466, 482, 483, and 491 of chain C and residues 212–216, 227, 228, 230, 231, 234, 236, 243, 245, 247, 249, 250, 256, 274, 294, 295, 312, 322, 336, 337, 342, 395, 411, 458, 462, 466, 483, 487, and 491 of chain D are modeled as Ala (in total 115 amino acids) due to conformational disorder of their side chains. The Ramachandran plot depicts 98.1% of main chain torsion angles in the most favored and allowed regions. Eighteen residues (1.9%) are located in disallowed regions. All structures exhibit good stereochemistry (Table 1). Figures were generated with Pymol v.99 (<http://www.pymol.org>). Superpositions were carried out with the SSM Superpose function from Coot (6).

Site-directed mutagenesis. Mutants were generated using the Quickchange site-directed mutagenesis kit (Stratagene) and verified by sequencing. The mutant constructs were expressed and purified to homogeneity essentially as described for the wild-type proteins.

Analytical size exclusion chromatography. Analytical size exclusion chromatography of purified GST-free mPER fragments was carried out at 4 °C on an ÄKTA Basic system using a 10/30 Superdex 75 or 200 column (Amersham Biosciences) preequilibrated with running buffers containing 50 mM Tris pH 8.5, 200 mM NaCl, and 2 mM DTT. 100 μ l protein samples containing 200–400 μ g protein were loaded onto the column. Elution from the column was monitored by measuring absorbance at 280 nm. A calibration curve was generated by measuring the elution volumes of a series of standard proteins of known molecular mass. Molecular masses of mPER proteins were estimated by interpolating their elution volumes onto the calibration curve and comparing the elution volumes of the fragments relative to each other.

Analytical ultracentrifugation and CD spectroscopy. Analytical ultracentrifugation and CD spectroscopy experiments have been performed essentially as described previously (3).

UV/VIS spectroscopy. Heme binding was determined by absorption spectra containing mPER proteins in 50 mM Tris pH 8.5, 200 mM NaCl, and 2 mM DTE and a 1.5-fold molar excess of heme (2 mM dissolved in 0.1 M NaOH). For comparison absorption spectra with heme alone were recorded. Therefore the mPER proteins were incubated with heme for 3 h or overnight at 4 °C and purified via analytical size exclusion chromatography on an ÄKTA Basic system using a 10/30 Superdex 75 column (Amersham Biosciences). Elution from the column was monitored by measuring absorbance at 280 nm, 385 nm, and 420 nm. The peak of the heme/mPER protein complex was concentrated and the absorbance spectra were recorded between 250–700 nm in a Cary 100Bio UV/VIS spectrometer using a Hellma Tray Cell.

Luciferase complementation assay. Vector construction. The split *firefly* luciferase destination vectors were constructed as follows: coding sequences for the N-terminal (amino acids 2–416 or 1–416) or C-terminal (amino acids 398–550) region of *firefly* luciferase were inserted into the XbaI site of the pcDNA-DEST40 vector (Invitrogen) to create a destination vector for expression of luciferase fragments as C-terminal fusions to the target protein. To create a destination vector for fusion proteins with N-terminally attached luciferase fragments, an AfeI site was introduced seven nucleotides 3' to the attR1 site of the pEF-DEST51 vector (Invitrogen). To create reporter vectors, open reading frames encoding clock proteins or fragments thereof were shuttled into these destination vectors using the Gateway technology (Invitrogen). Note, due to the attR-sites, short linker sequences (21 amino acids for N-terminally and 17 amino acids for C-terminally fused luciferase fragments) were generated between the *firefly* fragments and the clock proteins.

Luciferase complementation assay. HEK293 cells (approximately 175,000 cells per well in a 24-well plate) were transiently transfected with a pair of split *firefly* luciferase reporter construct (250 ng each transfection). For normalization, the *renilla* luciferase vector pRL-SV40 (1 ng; Promega) was cotransfected. At 44 h after transfection cells were lysed in 200 μ L passive lysis buffer (Promega) and frozen for 1 h at -80°C . Lysates were used to detect luciferase activity. The luciferase assay was carried out by using the Dual-Luciferase Reporter Assay System (Promega)

and a multisample plate-reading luminometer (Orion II, Berthold Detection Systems). To this end, 5 μ L of the cell extract was first mixed with 25 μ L of luciferase assay reagent II. After measurement of *firefly* luciferase activity 25 μ L of the stop & glow reagent was added and the *renilla* luciferase activity detected. For data analysis *firefly* luciferase activity was normalized to the corresponding *renilla* luciferase activity.

Fluorescence recovery after photobleaching (FRAP). Vector construction and protein expression in cultured cells. For construction of expression vectors for Venus tagged fusion proteins the coding sequence (CDS) of Venus was cloned downstream of the attR2 site into the BstBI site of the pLenti6 Gateway® destination vector (Invitrogen). Into this vector full length CDS of PER proteins lacking stop codons were shuttled. Resulting vectors were used for lentivirus production as described (7). U2OS cells (human, ATCC # HTB-96) were transfected for exogenous protein expression with lentiviral supernatant (half final volume) and 8 μ g/mL protamine sulfate (Sigma-Aldrich). Cells were put under blasticidin selection from the second day onward.

Fluorescence recovery after photobleaching (FRAP). Confocal microscopy of live cells was performed with a FluoView 1000 microscope (Olympus, Tokyo, Japan) with a $\times 60$ (1.35 numerical aperture) oil immersion objective in a climate chamber at 5% CO_2 and 37 °C. Fluorescence was measured 20 times before bleaching and then fluorescent molecules were bleached for FRAP analysis with a strong laser beam at 515 nm within a confined area in the cell (0.1 s; 15 μm^2). Exchange of bleached molecules with surrounding fluorescent molecules was measured at low laser intensity every 0.12 s for 45 s. Additionally a reference area in the same compartment of the bleached cell and a background area outside of the cells were measured.

For normalization background values were subtracted and values of the reference area were used to compensate for overall decrease of fluorescence during the measurement. For each independent experiment, at least 10 cells were measured, initial fluorescence was normalized to one, total bleached molecules were set to a hundred percent, and an average recovery curve of all cells was calculated (8). For comparison of the mobility of different fusion proteins, the half-time of recovery ($t_{1/2}$) was determined as the time, when fifty percent of the bleached molecules are exchanged; i.e., normalized fluorescence reaches half of the initial value. At least three independent experiments have been conducted for each construct.

1. Kabsch W (1993) Automatic Processing of Rotation Diffraction Data from Crystals of Initially Unknown Symmetry and Cell Constants. *J Appl Crystallogr* 26:795-800.
2. Vagin A, Teplyakov A (1997) MOLREP: an automated program for molecular replacement. *J Appl Crystallogr* 30:1022-1025.
3. Hennig S, et al. (2009) Structural and functional analyses of PAS domain interactions of the clock proteins *Drosophila* PERIOD and mouse PERIOD2. *PLoS Biol* 7:4-e94.
4. Brunger AT, et al. (1998) Crystallography & NMR system: A new software suite for macromolecular structure determination. *Acta Crystallogr D Biol Crystallogr* 54:905-921.
5. Adams PD, et al. (2002) PHENIX: Building new software for automated crystallographic structure determination. *Acta Crystallogr D Biol Crystallogr* 58(Pt 11):1948-1954.
6. Emsley P, Cowtan K (2004) Coot: Model-building tools for molecular graphics. *Acta Crystallogr D Biol Crystallogr* 60:2126-2132.
7. Brown SA, Fleury-Olela F, Nagoshi E, Hauser C, Juge C, et al. (2005) The period length of fibroblast circadian gene expression varies widely among human individuals. *PLoS Biol* 3:e338.
8. McNally JG (2008) Quantitative FRAP in analysis of molecular binding dynamics in vivo. *Methods Cell Biol* 85:329-351.
9. Krissinel E, Henrick K (2004) Secondary-structure matching (SSM), a new tool for fast protein structure alignment in three dimensions. *Acta Crystallogr D Biol Crystallogr* 60:2256-2268.
10. Woody RW, Sreerama N (2000) Estimation of protein secondary structure from circular dichroism spectra: Comparison of CONTIN, SELCON, and CDSSTR methods with an expanded reference set. *Analytical Biochemistry* 287(2):252-260.
11. Sreerama N, Venyaminov SY, Woody RW (1999) Estimation of the number of alpha-helical and beta-strand segments in proteins using circular dichroism spectroscopy. *Protein Science* 8(2):370-380.
12. Kitanishi K, et al. (2008) Heme-binding characteristics of the isolated PAS-A domain of mouse Per2, a transcriptional regulatory factor associated with circadian rhythms. *Biochemistry* 47(23):6157-6168.

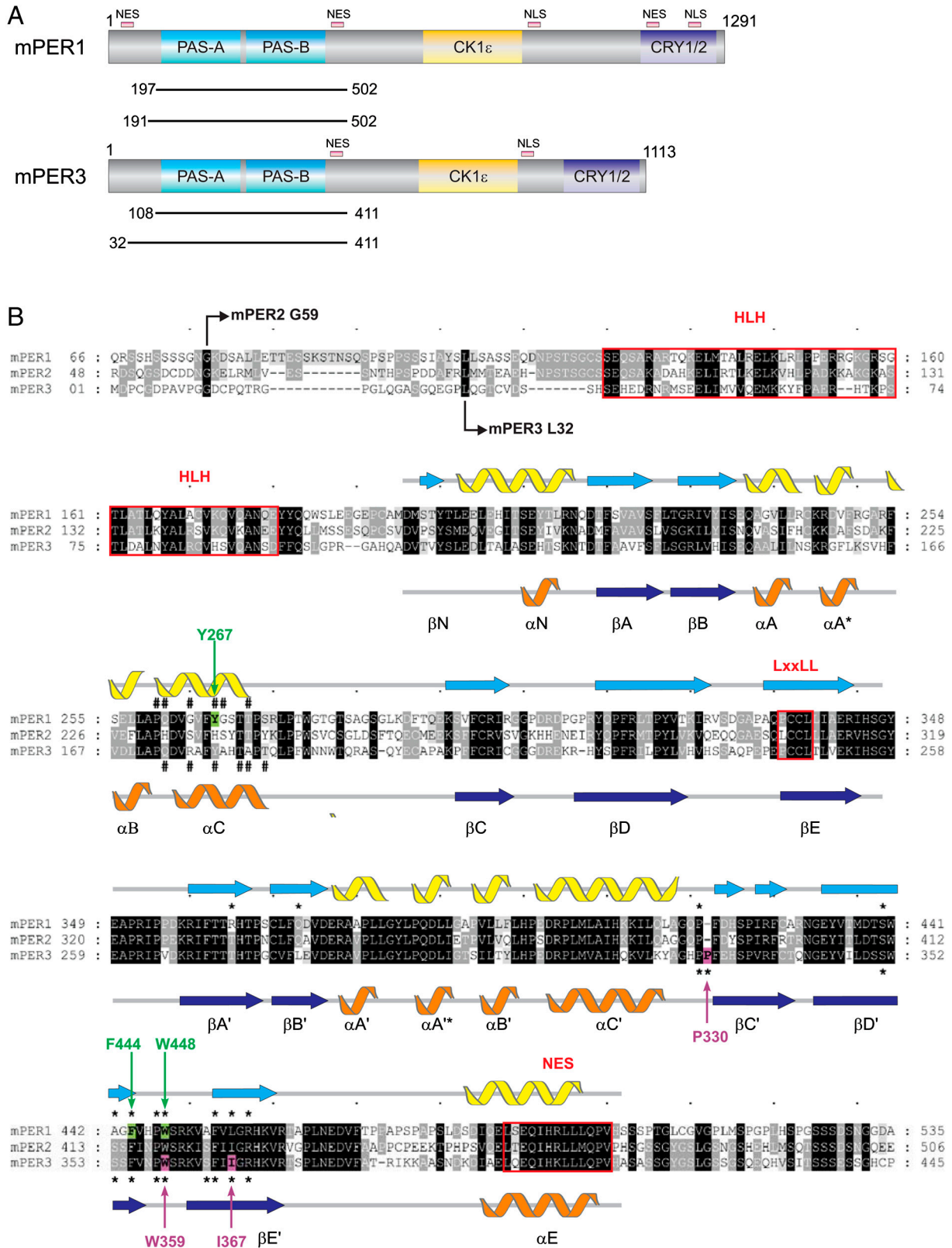


Fig. S1. Domain architecture and sequence alignment mouse PERIOD proteins. (A) Domain architecture of full-length mPER1 and mPER3. The two PAS (PER-ARNT-SIM) domains (PAS-A and PAS-B), nuclear localization signals (NLS) and nuclear export sequences (NES), and the binding domains of CK1 ϵ and mCRY1/2 are shown. The mPER fragments used for crystallization and biochemical studies are represented as black bars. (B) Sequence alignment of mouse PERIOD1, 2, and 3 [mPER 1, 2, 3, Swissprot AccNo. O35973 (1), O54943 (2), O70361 (3)]. Secondary structure elements of mPER1[191–502] (top) and mPER3[108–411] (Bottom) are shown (β N, α N; PAS-A: β A \rightarrow β E, α A \rightarrow α C; PAS-B: β A' \rightarrow β E', α A' \rightarrow α C'; α E). The alignment was generated in ClustalW (9). Mutated mPER1 residues (Trp448, Phe444, Tyr267) are highlighted by green and mutated mPER3 residues (Pro330, Trp359, Ile376) by magenta arrows. mPER1 and mPER3 residues involved in PAS-B interactions are marked with stars (*). Residues in the PAS-A/ α C dimer interface of mPER1 and mPER3 are marked with hashes (#). HLH: helix-loop-helix motive, LxxLL: coactivator motive, NES: nuclear export sequence.

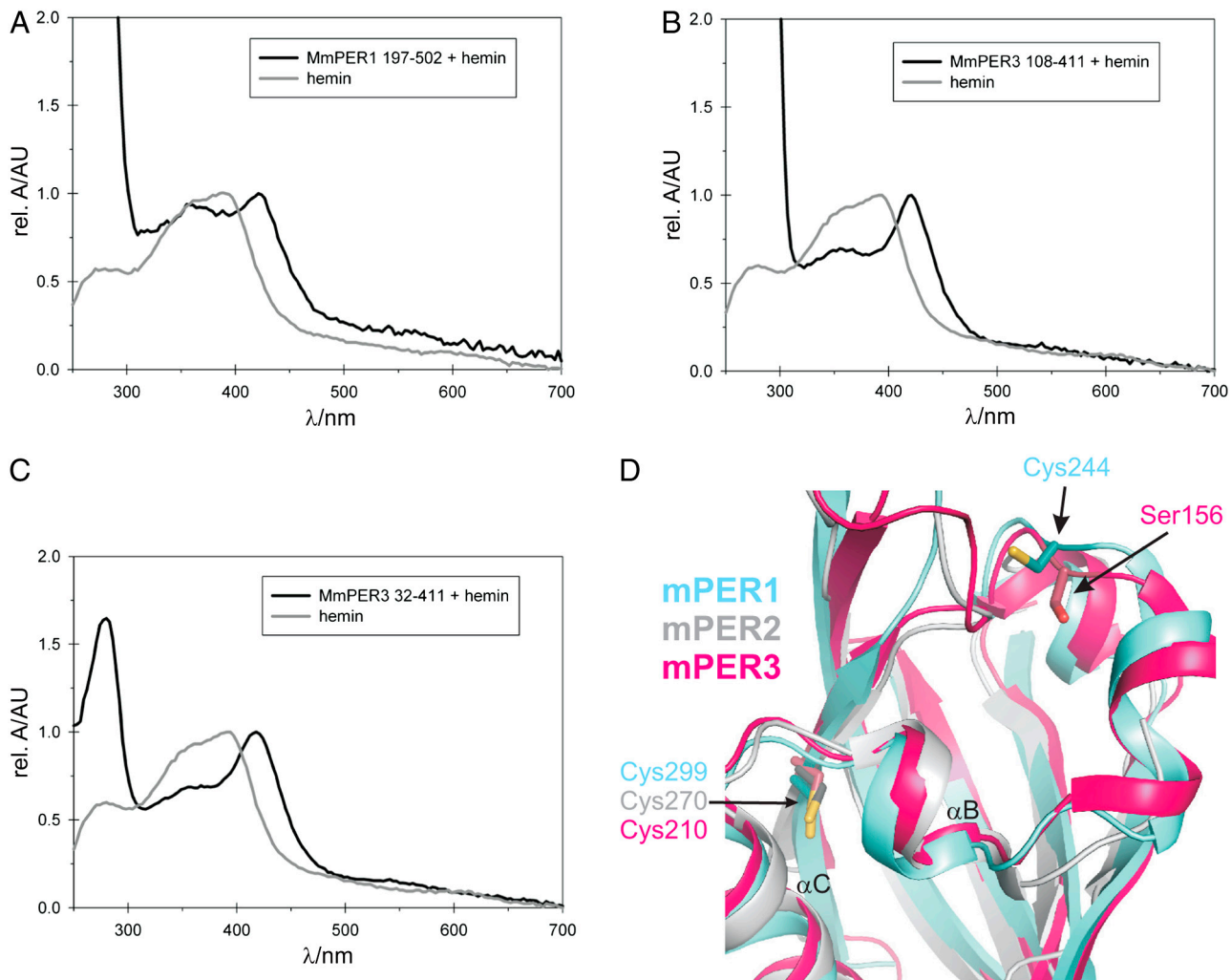


Fig. S7. Absorbance of mPER proteins in presence of heme. Absorbance spectra of (A) mPER1[197–502], (B) mPER3[108–411] and (C) mPER3[32–411] proteins, which were incubated with heme for 3 h and separated via gel filtration chromatography, were recorded between 250–700 nm (black spectrum). For comparison the absorbance spectrum of free heme was also recorded (dark gray spectrum). Heme binding did not change the elution volumes on a gel filtration column, indicating that the mPER1 and mPER3 homodimers are not disrupted. (D) Superposition of the PAS-A domains of mPER1, mPER2, and mPER3. Note, that the αA^* helix of PAS-A is disordered in mPER2 (27), but fully defined in mPER1 and in molecule 1 of mPER3. In mPER2, residues Cys215 and Cys270 have been suggested as heme ligands (12). Cys215_{mPER2} is not visible due to the conformational disorder of αA^* . The corresponding residues Cys244 and Cys299 of mPER1 and Ser156 and Cys210 of mPER3 are highlighted as atomic stick figures.

Table S1. X-ray data collection and refinement statistics

Data Collection	mPER1[191–502]	mPER3[108–411]
Wavelength (Å)	0.9807	1.0000
Resolution range (Å)*	30–2.75 (2.8–2.75)	25–2.5 (2.6–2.5)
Number of reflections		
Total	180,279	94,392
Unique	29,771	22,419
Completeness (%)*	99.0 (99.4)	99.6 (99.5)
I/σ^*	13.7 (2.3)	12.2 (2.4)
R_{sym} (%)*	9.2 (66.7)	8.3 (72.1)
Wilson plot B (Å ²)	63.1	55.9
Refinement	mPER1[191–502]	mPER3[108–411]
Resolution range (Å)	30–2.75	25–2.5
Reflections	29,744	21,297
R_{cryst} (%)	20.9	21.3
R_{free} (%) [†]	28.2	28.9
overall average B-factor (Å ²)	67.4	47.4
rmsd bond lengths (Å)	0.009	0.016
rmsd bond angles (°)	1.29	1.81

*Values in parenthesis correspond to the highest resolution shell.

[†]The Free-R factor was calculated with 5% of the data omitted from structure refinement.

Table S2. RMSD values for superposition of mPER structures

Homodimers*		
	rmsd/Å	residues
mP3- > mP1	2.04	495
mP3- > mP2	2.83	384
mP1- > mP2	3.36	392
mP1AC- > mP1BD	0.39	516
Monomers (intra) [†]		
	rmsd/Å	residues
mP3 (A- > B)	1.24	254
mP2 (A- > B)	0.73	238
mP1 (A- > B)	0.68	243
mP1 (C- > D)	0.69	248
Monomers (inter, A) [†]		
	rmsd/Å	residues
mP3- > mP1	1.64	256
mP3- > mP2	1.76	260
mP1- > mP2	1.73	244
Monomers (inter, B) [†]		
	rmsd/Å	residues
mP3- > mP1	1.24	229
mP3- > mP2	1.40	237
mP1- > mP2	1.38	226

*Larger rmsd values of homodimers reflect monomer rotations of mPER1 and mPER3 with respect to mPER2.

[†]Except for some loop and linker regions and the N-terminal extension, the mPER monomers display no significant structural differences.

Publication II

Schmalen I., Reischl S., Wallach T., Klemz R., Grudziecki A., Prabu J.R., Benda C., Kramer A., Wolf E. (2014). Interaction of circadian clock proteins CRY and PER is modulated by zinc binding and disulfide bond formation. *Cell* 157, 1203 – 1215.

➔ Crystal structure and analysis of the mCRY1/mPER2 complex

Interaction of Circadian Clock Proteins CRY1 and PER2 Is Modulated by Zinc Binding and Disulfide Bond Formation

Ira Schmalen,¹ Silke Reischl,³ Thomas Wallach,³ Roman Klemz,³ Astrid Grudziecki,³ J. Rajan Prabu,¹ Christian Benda,¹ Achim Kramer,^{3,*} and Eva Wolf^{1,2,4,*}

¹Department of Structural Cell Biology, Max Planck Institute of Biochemistry, Am Klopferspitz 18, 82152 Martinsried/Munich, Germany

²Department of Physiological Chemistry, Butenandt Institute, Ludwig Maximilians University of Munich, Butenandtstrasse 5, 81377 Munich, Germany

³Laboratory of Chronobiology, Charité Universitätsmedizin Berlin, Hessische Strasse 3-4, 10115 Berlin, Germany

⁴Present address: Institut für Allgemeine Botanik, Johannes Gutenberg-University Mainz, Johannes-von-Müllerweg 6 and Institute of Molecular Biology (IMB), 55128 Mainz, Germany

*Correspondence: achim.kramer@charite.de (A.K.), evawolf1@uni-mainz.de (E.W.)

<http://dx.doi.org/10.1016/j.cell.2014.03.057>

SUMMARY

Period (PER) proteins are essential components of the mammalian circadian clock. They form complexes with cryptochromes (CRY), which negatively regulate CLOCK/BMAL1-dependent transactivation of clock and clock-controlled genes. To define the roles of mammalian CRY/PER complexes in the circadian clock, we have determined the crystal structure of a complex comprising the photolyase homology region of mouse CRY1 (mCRY1) and a C-terminal mouse PER2 (mPER2) fragment. mPER2 winds around the helical mCRY1 domain covering the binding sites of FBXL3 and CLOCK/BMAL1, but not the FAD binding pocket. Our structure revealed an unexpected zinc ion in one interface, which stabilizes mCRY1-mPER2 interactions *in vivo*. We provide evidence that mCRY1/mPER2 complex formation is modulated by an interplay of zinc binding and mCRY1 disulfide bond formation, which may be influenced by the redox state of the cell. Our studies may allow for the development of circadian and metabolic modulators.

INTRODUCTION

In mammals, many physiological, metabolic, and behavioral processes are regulated in a daytime-dependent manner. Circadian (~24 hr) rhythms are generated by endogenous circadian clocks, which are operated by interconnected transcriptional and translational feedback loops (Young and Kay, 2001). Additionally, the cellular redox state plays an essential role in circadian clock regulation and links the clock to the cell's metabolic state (Eckel-Mahan and Sassone-Corsi, 2009). In anucleate human red blood cells, several circadian oxidation rhythms have been described, including cysteine oxidation

cycles in the H₂O₂ scavenging peroxiredoxins, the daily rhythmic transition between dimeric (mostly oxidized) and tetrameric (mostly reduced) hemoglobin, and daily nicotinamide adenine dinucleotide (NADH)/nicotinamide adenine dinucleotide phosphate (NADPH) oscillations (O'Neill and Reddy, 2011). Furthermore, circadian cycles of peroxiredoxin oxidation occur in all kingdoms of life and are interconnected with the circadian gene-regulatory transcriptional feedback loops in DNA-containing cells (Edgar et al., 2012; O'Neill and Reddy, 2011; O'Neill et al., 2011).

In the canonical gene-regulatory feedback loop of the mammalian circadian clock, the basic helix-loop-helix (bHLH)-PAS (PER-ARNT-SIM) transcription factors BMAL1 and CLOCK activate the transcription of three period (*Per1*, 2, and 3) and two cryptochrome (*Cry1* and 2) clock genes. CRY proteins repress the transcriptional activity of the CLOCK/BMAL1 complex toward the *Cry* and *Per* genes (Griffin et al., 1999; Kume et al., 1999; van der Horst et al., 1999), as well as a large number of clock-controlled genes regulating circadian physiology (Koike et al., 2012). Additionally, CRYs are involved in the regulation of glucose homeostasis, insulin secretion, and tissue-specific insulin sensitivity (Barclay et al., 2013; Lamia et al., 2011; Zhang et al., 2010).

The CRY repressor activity is determined by posttranslational modifications, as well as the daily rhythmic synthesis, nuclear translocation, and degradation of CRYs, which are controlled by interactions with PER1/2 (Yagita et al., 2002) and with the E3 ligase components FBXL3 (Gatfield and Schibler, 2007) and FBXL21 (Hirano et al., 2013; Yoo et al., 2013). The CRY tails and the most C-terminal helix (α 22) of the cryptochrome photolyase homology region (PHR) (Figure 1A) are involved in transcriptional repression of CLOCK/BMAL1 (Chaves et al., 2006) and BMAL1 binding (Czarna et al., 2011). The PHR interacts with C-terminal regions of PER1 and PER2 (Eide et al., 2002; Miyazaki et al., 2001; Ozber et al., 2010; Tomita et al., 2010; Yagita et al., 2002), with FBXL3 (Lamia et al., 2009; Xing et al., 2013), FBXL21 (Hirano et al., 2013; Yoo et al., 2013) and with the PAS domains of CLOCK (Huang et al., 2012).

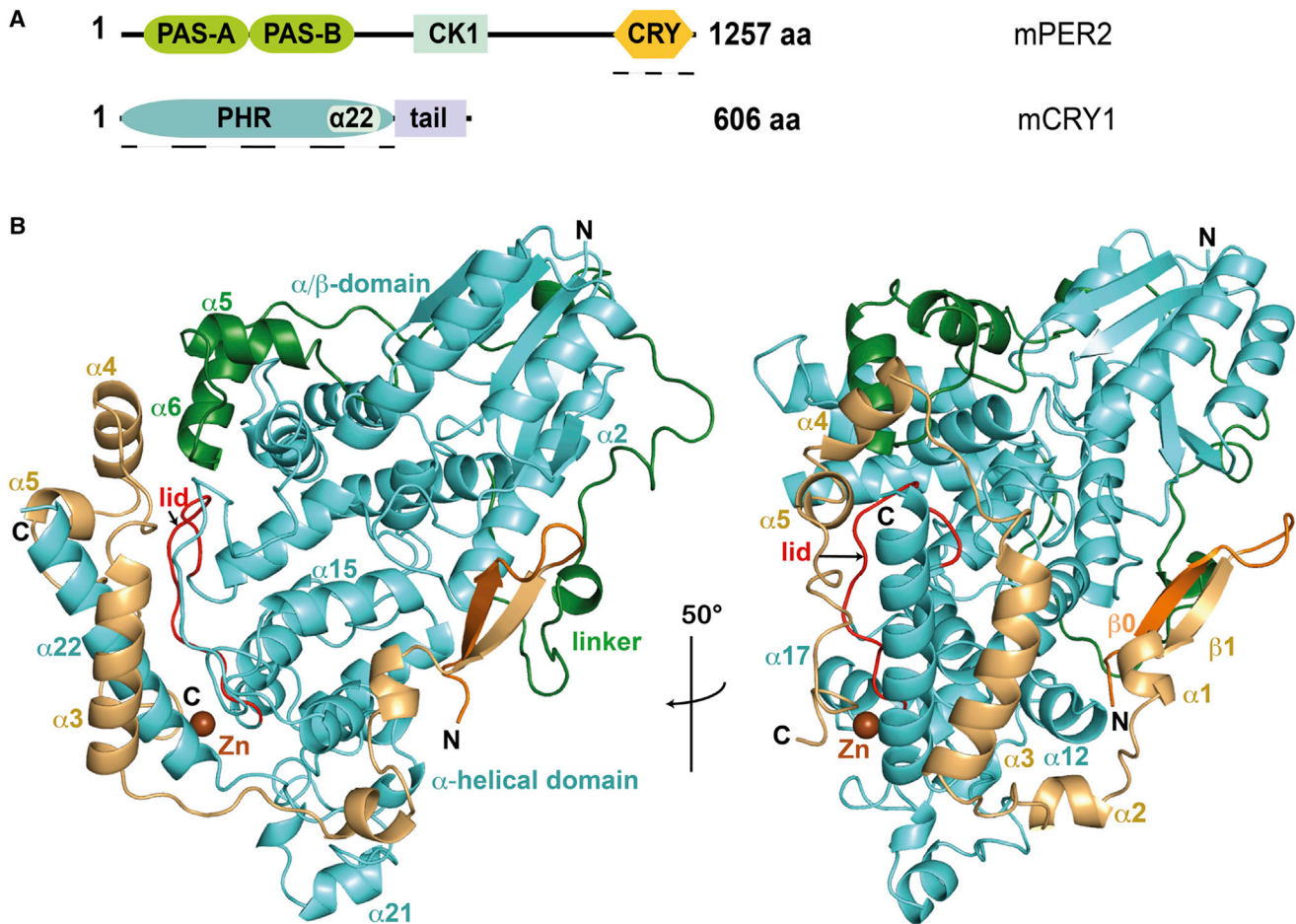


Figure 1. Domain Architecture and Crystal Structure of mCRY1/mPER2 Heterodimer

(A) Domain architecture of mouse CRY1 and PER2. Two PAS domains (PAS-A and PAS-B) and the CK1 ϵ/δ - and CRY-binding regions of mPER2 are shown. mCRY1 comprises a PHR, including helix α 22 and a nonconserved C-terminal tail. Dashed lines indicate crystallized fragments.

(B) Ribbon presentation of mCRY1[1–496] (PHR; cyan) in complex with mPER2[1132–1252] (yellow). Green, linker connecting the α/β - and α -helical domain of the mCRY1-PHR. Brown, zinc ion at the mCRY1-mPER2 interface. Red line, C-terminal lid of mCRY1.

See also [Figures S1](#) and [S2](#) and [Table S1](#).

Phosphorylation of Ser71 by AMP kinase (AMPK) in response to the cell's metabolic state reduces CRY1 stability by enhancing FBXL3 binding and weakening PER2 binding ([Lamia et al., 2009](#)). Furthermore, PER2 is reported to compete for CRY1 binding to the CLOCK/BMAL1-E-box complex ([Ye et al., 2011](#)). These data suggest that PER2 might have overlapping CRY1-binding sites with FBXL3 and CLOCK/BMAL1, which play a role in the regulation of CRY1 stability and transcriptional repression activity. Indeed, our mouse CRY1 (mCRY1) crystal structure revealed partly overlapping mCRY1 regions that are involved in mPER2 and FBXL3 interactions, as well as transcriptional repression activities of mCRY1 ([Czarna et al., 2013](#)). Consistent with our structure-based mutational analyses ([Czarna et al., 2013](#)), the mCRY2/FBXL3/SKP1 complex structure ([Xing et al., 2013](#)) showed that FBXL3 interacts with the flavin adenine dinucleotide (FAD)-binding pocket, the C-terminal helix α 22, and the C-terminal lid of the mCRY-PHR. Moreover, competition with mPER2 or FAD disrupts a preformed mCRY2/FBXL3 complex

([Xing et al., 2013](#)), and a period-lengthening small-molecule compound that competes with FAD binding stabilizes mCRY1 by inhibiting ubiquitination ([Hirota et al., 2012](#)).

Here, we have determined the crystal structure of the complex between the mCRY1-PHR and a C-terminal mPER2 fragment in order to (1) provide further insights into how alternative binding of mPER2, FBXL3, mCLOCK/BMAL1, or FAD regulates mCRY1 stability and transcriptional repression activity and (2) to advance the development of CRY-stabilizing compounds that affect clock or clock-controlled metabolic functions. mPER2 winds around mCRY1, covering extensive surface areas that significantly overlap with the binding sites of FBXL3 and mCLOCK/BMAL1. Interestingly, our complex structure revealed a jointly coordinated zinc ion that critically stabilizes full-length mCRY1-mPER2 interactions in mammalian cells. Our mutational analyses suggest that (1) formation of the Cys412-Cys363 disulfide bond, which we observed in the apo-mCRY1 structure ([Czarna et al., 2013](#)), weakens mCRY1-mPER2 interactions,

and (2) zinc facilitates formation of the reduced state of mCRY1 and stabilizes the mCRY1/mPER2 complex. The regulation of mCRY1-mPER2 interactions by zinc binding and CRY disulfide bond formation/reduction may provide a molecular link between the circadian clock and the cell's metabolic/oxidative state.

RESULTS

Crystal Structure of the Mouse CRYPTOCHROME1-PERIOD2 Complex

Using limited proteolysis, we identified a stable mCRY1/mPER2 core complex comprising the mCRY1-PHR (residues 1 to 496) and mPER2 residues 1132 to 1252 (Figures 1, S1, and S2 available online). We have determined its 2.45 Å crystal structure using molecular replacement with apo-mCRY1 (PDB ID 4K0R [Czarna et al., 2013]) as search model in combination with experimental selenium single-wavelength anomalous dispersion (Se-SAD) phasing (Table S1).

In our mCRY1/mPER2 complex structure, mCRY1 adopts the typical cryptochrome/photolyase fold (Müller and Carell, 2009) with an N-terminal α/β domain, a C-terminal α -helical domain, and a connecting linker region (Figure 1). Superposition of apo-mCRY1 and mCRY1/mPER2 reveals several differences between the two mCRY1 structures, especially in the C-terminal lid, which significantly alters its conformation (see below), the antenna recognition loop, the phosphate-binding loop, the linker region, and the C-terminal helix $\alpha 22$ (Figures S3A–S3D). The other characteristic loops of the 6-4-photolyase/animal cryptochrome family, i.e., the protrusion loop, the $\alpha 5$ - $\alpha 6$ loop, and the electron-rich sulfur loop (Hitomi et al., 2009) (Figure S2) do not change significantly upon mPER2 binding.

mPER2 winds around the α -helical domain of mCRY1 (Figure 1B). The crystallized mPER2 fragment comprises five α helices ($\alpha 1$ – $\alpha 5$, Ile1138–Thr1198) and a short N-terminal antiparallel β sheet formed by residues 1132–1136 ($\beta 1$) and part of the cloning overhang of mPER2 ($\beta 0$). Residues Gly1199 to Glu1214 following helix $\alpha 5$ adopt a well-ordered loop structure. The most C-terminal residues 1215–1252 of the crystallized mPER2[1132–1252] fragment are not seen in the electron density due to conformational disorder (Figures 1, S1B, and S1C). Our CD spectra of the mCRY1[1–496]/mPER2[1132–1252] complex support the high helical content of mCRY1-bound mPER2 in solution. CD spectra of apo-mPER2[1132–1252], however, suggest that unbound mPER2 is significantly less structured (Table S2). We therefore propose that mCRY1 binding induces α -helical folding of the C-terminal mPER2 fragment.

The mCRY1/mPER2 Complex Is Stabilized by Four Interfaces and a Zinc Ion

Several elements of the mCRY1-PHR are involved in mPER2 binding: the C-terminal helix $\alpha 22$ and its preceding connector loop, the C-terminal lid, the sulfur loop, the loop connecting helices $\alpha 5$ and $\alpha 6$, helix $\alpha 12$, and helix $\alpha 15$. Overall, the mCRY1/mPER2 complex buries a 3221 Å² solvent-accessible surface area.

Helix $\alpha 22$ constitutes a central component of the mCRY1-mPER2 interface. It is embedded between mPER2 helix $\alpha 3$ and the loop region C-terminal to mPER2 $\alpha 5$ ("C-terminal helix

interface"; Figures 2A and S1A). Notably, Arg483 and Lys485 (mCRY1 $\alpha 22$) are involved in mPER2 binding and transcriptional repression in mammalian cells (Ozber et al., 2010), as well as in interactions with purified C-terminal mBMAL1 fragments (Czarna et al., 2011). In apo- and mPER2-bound mCRY1, Arg483 forms an intramolecular salt bridge with Asp321 (sulfur loop), which likely contributes to positioning of $\alpha 22$ (Figure S3C). In the mCRY1/mPER2 complex, Arg483 forms an additional salt bridge to Asp1167 (mPER2 $\alpha 3$) (Figures 2A, right, and S3C). Furthermore, Gln486 and Gln490 ($\alpha 22$) hydrogen bond to Gln1168_{mPER2}, and Gln486 also hydrogen bonds to the backbone of Leu1164_{mPER2} (Figure 2A, left). The sulfur loop further stabilizes the position of mPER2 $\alpha 3$, mostly via hydrophobic interactions of Pro319_{mCRY1} (Figures 2A, right, and S1A). On the other side of mCRY1 $\alpha 22$, Lys485 forms a hydrophilic side-chain interaction with Asp1206 and a backbone hydrogen bond with Val1207 in the C-terminal mPER2 loop region (Figure 2A, left).

Notably, Cys1210 and Cys1213 in the C-terminal mPER2 loop region and mCRY1 residues Cys414 (lid) and His473 ($\alpha 22$) tetrahedrally coordinate a zinc ion ("zinc interface"; Figures 1B, 2B, S1A, and S4). An anomalous difference map calculated for positioning of the selenomethionines of mPER2 gave first evidence for the zinc ion in the crystal (Figures S4A and S4B). An X-ray fluorescence scan confirmed its presence (Figure S4C). Atomic absorption spectroscopy confirmed the presence of zinc in the mCRY1/mPER2 complex in solution, but not in the single proteins due to their incomplete zinc-binding sites (Figure S4D).

Another heterodimer interface is formed between mCRY1 $\alpha 12$ and mPER2 helices $\alpha 1$ and $\alpha 2$ (referred to as "mPER2($\alpha 1$ -2)-mCRY1($\alpha 12$) interface"; Figures 2C and S1A). mPER2 $\alpha 1$ additionally contacts mCRY1 $\alpha 15$, whereas mPER2 $\alpha 2$ also interfaces with Tyr466 to Met470 in the loop preceding mCRY1 $\alpha 22$. Trp1139 (mPER2 $\alpha 1$) contacts mCRY1 $\alpha 12$ and $\alpha 15$. Lys329 (mCRY1 $\alpha 12$) hydrogen bonds to backbone oxygens of Ile1149 to Tyr1153 (mPER2 $\alpha 2$) and Asn323 to the Tyr1153 side chain. The loop connecting mPER2 $\alpha 1$ and $\alpha 2$ winds tightly around Ala328 of mCRY1 $\alpha 12$.

mPER2 $\alpha 4$, which is part of a 20 amino acid stretch (1179 to 1198) reported to be essential for mCRY1 binding in cell-based assays (Tomita et al., 2010), packs against the C-terminal lid (including Phe405) and the $\alpha 5$ - $\alpha 6$ connector loop (including Leu148 and Thr149) of mCRY1 ("mPER2($\alpha 4$)-cap interface"; Figures 2D and S1A). Leu148 makes hydrophobic interactions with Leu1189 and Phe1181 of mPER2, whereas Thr149 hydrogen bonds to Glu1188 and (water mediated) to Glu1191 of mPER2 $\alpha 4$.

The mCRY C-Terminal Lid Adopts Variable Conformations and Is Involved in Disulfide Bond Formation and Zinc Coordination

The major difference between the apo-mCRY1 and mCRY1 complex structure manifests in the conformation of the C-terminal lid. Although the side chains of residues Phe406 to Phe410 are disordered in the apo structure, the loop is well defined and adopts a deviating orientation in the complex structure (Figure 3A). This is likely due to its packing against $\alpha 4$, $\alpha 5$, and the C-terminal loop of mPER2 (Figures 1B, 2D, 3B, and S3D). The

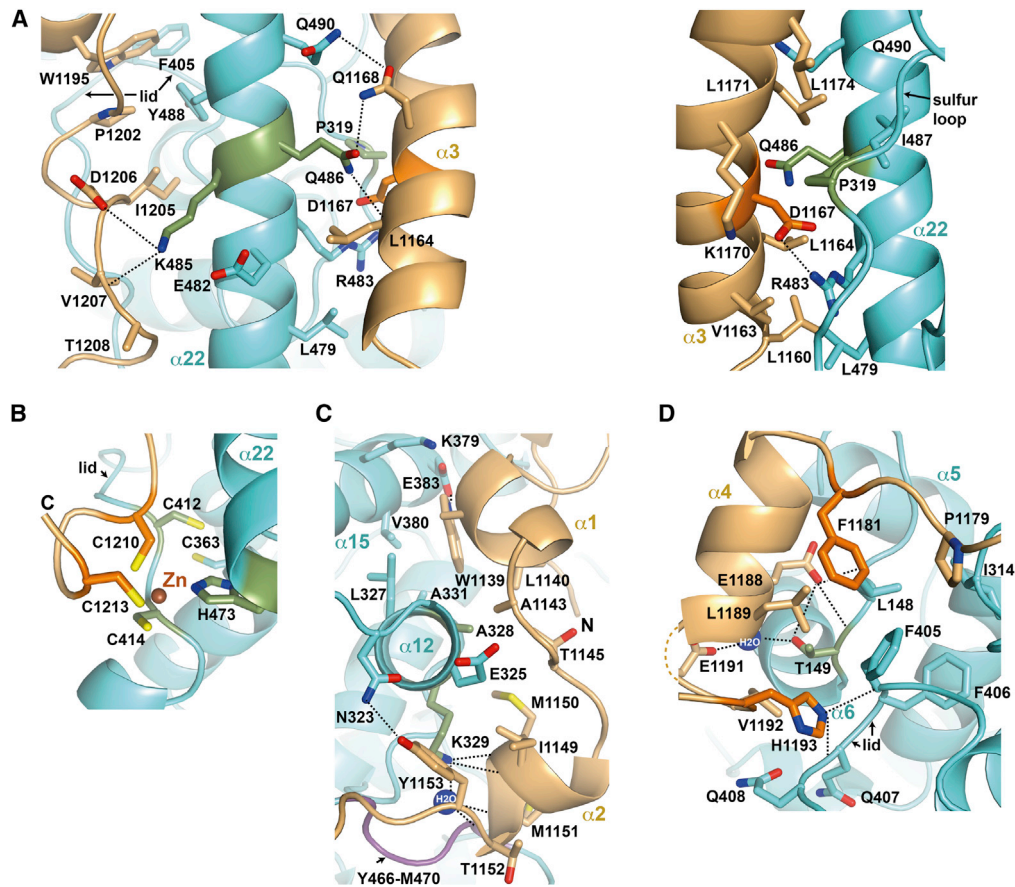


Figure 2. Close-Up View of mCRY1-mPER2 Interfaces

Crucial interface residues are shown as atomic sticks. Mutated residues are highlighted in green (CRY) and orange (PER). Dashed lines indicate salt bridges and hydrogen bonds. See [Results](#) and [Figure S1A](#) legend for a detailed description of the interactions.

(A) C-terminal helix ($\alpha 22$) interface, two orientations: mCRY1 $\alpha 22$ is clenched by mPER2 helix $\alpha 3$ and the loop connecting mPER2 $\alpha 5$ with the zinc binding motif. (B) Zinc (Zn) interface: His473 ($\alpha 22$) and Cys414 (lid) of mCRY1 and Cys1210 and Cys1213 of mPER2 tetrahedrally coordinate a zinc ion. The disulfide bridge between Cys363 and Cys412 (compare apo-mCRY1; [Figures 3A](#) and [3B](#)) is broken. This figure directly connects to [Figure 2A](#) (left) (compare Thr1208 [A] and Cys1210 [B]).

(C) mPER2($\alpha 1-2$)-mCRY1($\alpha 12$) interface: mPER2 helices $\alpha 1$ and $\alpha 2$ interact with mCRY1 helices $\alpha 12$ and $\alpha 15$ and with Tyr466-Met470 in the loop preceding $\alpha 22$. (D) mPER2($\alpha 4$)-cap interface: mPER2 helix $\alpha 4$ packs against Thr149 and Leu148 in the $\alpha 5$ - $\alpha 6$ loop and the C-terminal lid of mCRY1.

See also [Figures S1](#), [S2](#), [S3](#), and [S4](#).

apo-mCRY1 structure contains a disulfide bridge between Cys363 and Cys412, which has the potential to be a redox-dependent link to the FAD-binding pocket ([Czarna et al., 2013](#)). Located in the immediate vicinity of the zinc interface, this disulfide bridge is broken in the complex structure ([Figures 2B](#) and [3](#)). Thereby, we hypothesize that the C-terminal lid gains a higher flexibility for interaction with mPER2.

In apo-mCRY1, Phe405 is embedded in a hydrophobic pocket of the mCRY1-PHR. In the mCRY1/mPER2 complex, however, Phe406 occupies the hydrophobic pocket of apo-Phe405, whereas Phe405 projects to the surface ([Figure 3A](#)) and embeds into a huge hydrophobic pocket lined by PER and CRY residues ([Figures 2D](#), [S1A](#), and [S3D](#)). The mPER2-bound lid conformation is additionally stabilized by backbone hydrogen bonding of Phe405 and Gln407 with His1193_{mPER2} ([Figure 2D](#)) and by Phe410, which inserts into a hydrophobic pocket, including His359 and Trp399 ([Figure 3B](#)).

In apo- and FBXL3-bound mCRY2 ([Xing et al., 2013](#)), the lid adopts yet another position than in apo- and mPER2-bound mCRY1. Phe424 and Phe423 of mCRY2/FBXL3 ([Figure 3C](#)) and apo-mCRY2 (data not shown) position just as the corresponding Phe406 and Phe405 in apo-mCRY1. Phe428_{mCRY2} (corresponding to Phe410_{mCRY1}) is not embedded in the mCRY-PHR but is turned away from the mCRY2 core and mediates interactions with FBXL3. Interestingly, in both the apo-mCRY2- and the mCRY2/FBXL3 complex structure, there is no disulfide bridge between Cys381 and Cys430 (corresponding to Cys363 and Cys412 in mCRY1) ([Figures 3C](#), [S3E](#), and [S3F](#)). Instead, Cys430 forms an intermolecular disulfide bridge with Cys340 of FBXL3 in the mCRY2/FBXL3 complex structure ([Figure S3F](#)).

The FAD-Binding Pocket of mCRY1

The mCRY2/FBXL3/SKP1 complex structure ([Xing et al., 2013](#)) revealed that the C-terminal tail of FBXL3 occupies the FAD-binding

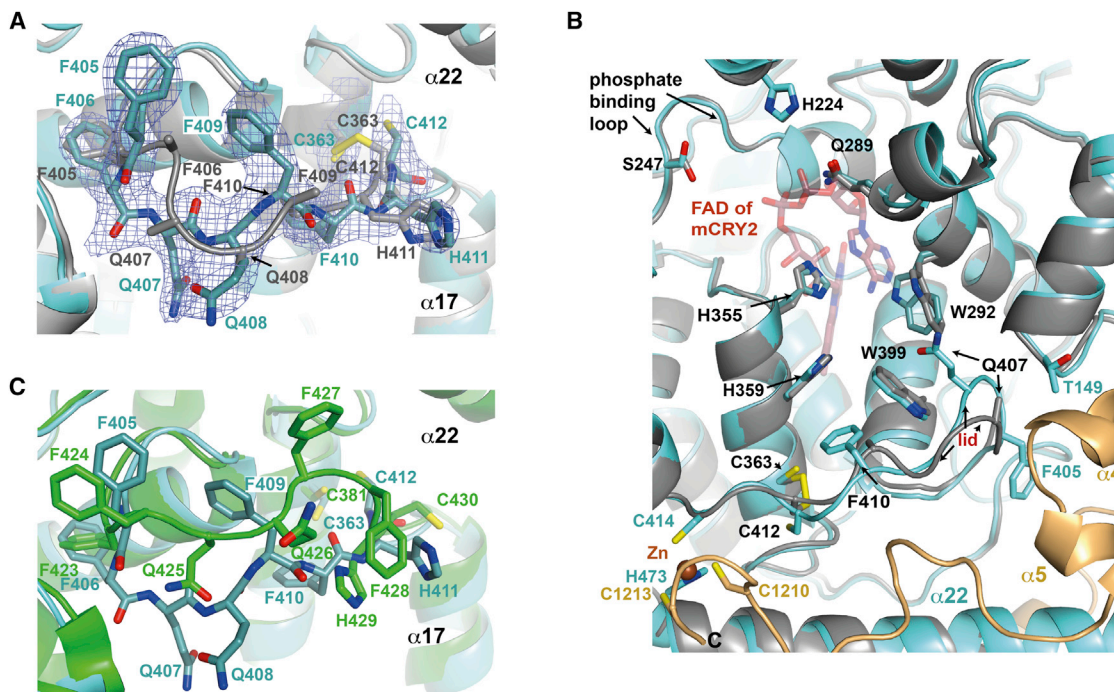


Figure 3. C-Terminal Lid and FAD-Binding Pocket of the mCRY1/mPER2 Complex

(A–C) The C-terminal lid adopts varying conformations in apo-CRY1, the mCRY1/mPER2 complex, and mCRY2. See Results for detailed comparison.

(A) Superposed C-terminal lids of mPER2-bound mCRY1 (cyan, mPER2 not shown) and apo-mCRY1 (gray). Apo-mCRY1: Phe406 to Phe410 are built as alanine. mPER2-bound mCRY1: Phe406 adopts the position of apo-Phe405 whereas Phe405 points away from the mCRY1-PHR. The Cys363-Cys412 disulfide bridge is broken. The 2Fo-Fc electron density (1σ level) of complex mCRY1 is shown in blue.

(B) Superposition of FAD-binding pocket, C-terminal lid, and zinc interface of the mCRY1/mPER2 complex (cyan/yellow) with apo-mCRY1 (gray) and FAD from the mCRY2/FAD complex (Xing et al., 2013) (red, taken from PDB ID 4I6G; mCRY2 protein not shown for clarity). Upon mPER2 binding, the C-terminal lid and its Gln407 side chain reorient. Trp292 rotates such that it would interfere with FAD binding.

(C) Superposition of C-terminal lids of mPER2-bound mCRY1 (cyan, mPER2 not shown) and FBXL3-bound mCRY2 (green, FBXL3 not shown). The disulfide bridge between Cys381 and Cys430 (corresponding to Cys363-Cys412 of apo-mCRY1) is not observed in mCRY2 (see also Figures S3E and S3F). See also Figure S3.

pocket of mCRY2. In our mCRY1/mPER2 complex structure, however, the FAD-binding pocket is accessible, unoccupied, and in a very similar conformation as in apo-mCRY1 (Figure 3B) and apo-mCRY2. Notably, the side chains of Gln289, Trp292, and His355 adopt an introverted position, which would interfere with FAD binding. mPER2 binding does not affect the conformation of His355 and Gln289, but reorientation of Trp292 is required to allow for the positioning of Gln407 in the mPER2-bound lid conformation. We therefore suggest that, although mPER2 binding to mCRY1 may somewhat negatively affect FAD binding by enforcing an unfavorable side-chain orientation of Trp292, it neither requires nor fully excludes the presence of FAD.

Structural Basis for Mutually Exclusive Binding of mPER2 and FBXL3 to mCRY

Our mCRY1/mPER2 crystal structure explains why mPER2-bound mCRY2 is completely devoid of FBXL3 in HEK293 cells and a purified C-terminal mPER2 fragment displaces mCRY2 from FBXL3 (Xing et al., 2013) (Figure 4). Whereas mPER2 α 3 blocks binding of the leucine-rich repeat (LRR) N domain of FBXL3 to helix α 22 and the sulfur loop of mCRY (Figure 4B, left), the C-terminal mPER2 loop region, including the zinc

interface, interferes with binding of the LRR C domain of FBXL3 to mCRY α 22 and the lid (Figure 4B, right). Moreover, mPER2 α 4 and α 5 completely overlap with the conserved mCRY2 C-terminal extension sequence (CCS), implying that the CCS adopts a deviating orientation in the mCRY1/mPER2 complex (Figure 4B, right).

The high sequence identity (86%) and conservation of mCRY binding residues between FBXL3 and FBXL21 (Hirano et al., 2013; Yoo et al., 2013) suggest that these two counteracting E3-ligase subunits bind to the same mCRY surface regions, and therefore, simultaneous binding of FBXL21 and mPER2 is unlikely, too.

Analyses of mCRY1-mPER2 Interactions In Vitro

To validate our mCRY1/mPER2 complex structure in solution and to assess the relative contributions of the different interfaces in vitro, we have generated mPER2[1119–1252] fragments with point mutations in the mCRY1/mPER2 interfaces. Effects of these mutations on the mCRY1-mPER2 interaction were analyzed in pull-down assays using total lysates and in native gels using purified proteins (Figures 5A, 5C, and 5D). The single H1193E mutation in the mPER2(α 4)-cap interface, which aims to

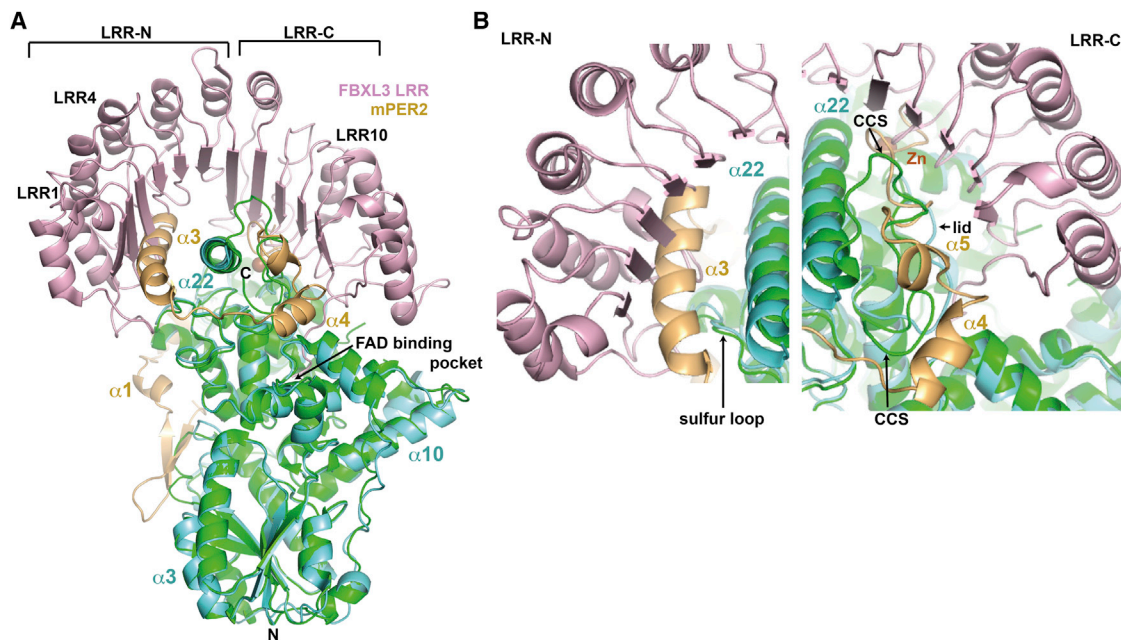


Figure 4. mPER2 and FBXL3 LRR Are Mutually Exclusive in Binding to mCRY1/2

(A) Superposition of mCRY1 (cyan) in complex with mPER2 (yellow) and mCRY2 (green) in complex with FBXL3 LRR (leucine-rich repeat domain, light pink; PDB ID 4I6J) (rmsd = 2.047 Å for 486 CRY C α positions).

(B) Close-up view: mPER2[1132–1252] and FBXL3 LRR occupy partly overlapping binding sites on mCRY (CCS, conserved cryptochrome C-terminal extension sequence).

See also Figure S3.

electrostatically interfere with binding to the mCRY1 C-terminal lid (Figure 2D), showed wild-type (WT)-like behavior in both assays. However, in combination with the D1167R mutation in the C-terminal helix interface (Figure 2A, right), the H1193E mutation further weakens mCRY1 binding. Binding of mCRY1 was even more severely impaired through the additional F1181R mutation, which also targets the interaction with the mCRY1 C-terminal lid (Figure 2D). These results suggest that both interfaces (C-terminal helix interface and mPER2(α 4)-cap interface) are of similar importance for complex formation *in vitro*. In addition, our native gel analyses imply that the mCRY1 tail is not required for mCRY1/mPER2 complex formation, as comparable results were gained with the mCRY1-PHR and full-length mCRY1 (Figures 5C and 5D).

Mutation of the zinc-coordinating residues Cys1210 and Cys1213 to alanine surprisingly did not compromise complex formation *in vitro*, neither in the total lysate (natural presence of zinc) nor in the purified system (supplied with zinc acetate) (Figures 5A, 5C, and 5D). Furthermore, no difference in complex formation was observed for WT proteins whether zinc was added to the buffer or not (Figures 5C and 5D), implying that the zinc-binding interface is of minor importance for complex formation *in vitro*. Affinity measurements (isothermal titration calorimetry, ITC) further support this result because a K_d in the lower nanomolar range was observed for the mCRY1-mPER2 interaction even in the absence of zinc ions (Figure 5B). However, zinc binding clearly stabilizes the purified mCRY1/mPER2 complex as demonstrated by the higher melting temperature of the WT

complex compared to the zinc-free mCRY1/mPER2(C1210A/C1213A) mutant complex in our thermofluor experiments (Figure 6A). Furthermore, ITC experiments revealed that the WT mCRY1/mPER2 complex binds zinc ions with a nanomolar affinity (K_d of \sim 8 nM) (Figure 6B).

mCRY1-mPER2 Heterodimer Interfaces Are Present in a Cellular Context

To validate our mCRY1/mPER2 complex structure in a cellular environment and in the context of full-length mCRY1 and mPER2 proteins, we have tested mCRY1 interface mutants for their effect on the stability of the mCRY1/mPER2 complex using a luciferase complementation assay (Figures 7A and S5A). Full-length mCRY1 and mPER2 (WT or mutants) were expressed as fusion proteins with C- and N-terminal firefly luciferase fragments in HEK293 cells (Czarna et al., 2013). mPER2-mCRY1 interactions lead to a functional luciferase whose activity was measured in cell lysates.

The mCRY1 T149E mutation was designed to sterically and electrostatically weaken interactions with mPER2 α 4 (Figure 2D). Consistent with our structure and the reported importance of mPER2 helices α 4 and α 5 for mCRY1-mPER2 interactions (Tomita et al., 2010), the T149E mutation drastically reduced mPER2 binding.

Disruption of the interaction of mCRY1 α 22 with mPER2 α 3 (Q486R) and with the loop connecting mPER2 α 5 with the zinc-binding motif (K485D) (Figure 2A, K485D/Q486R double mutant) drastically reduced mPER2 binding to below 10%. This confirms

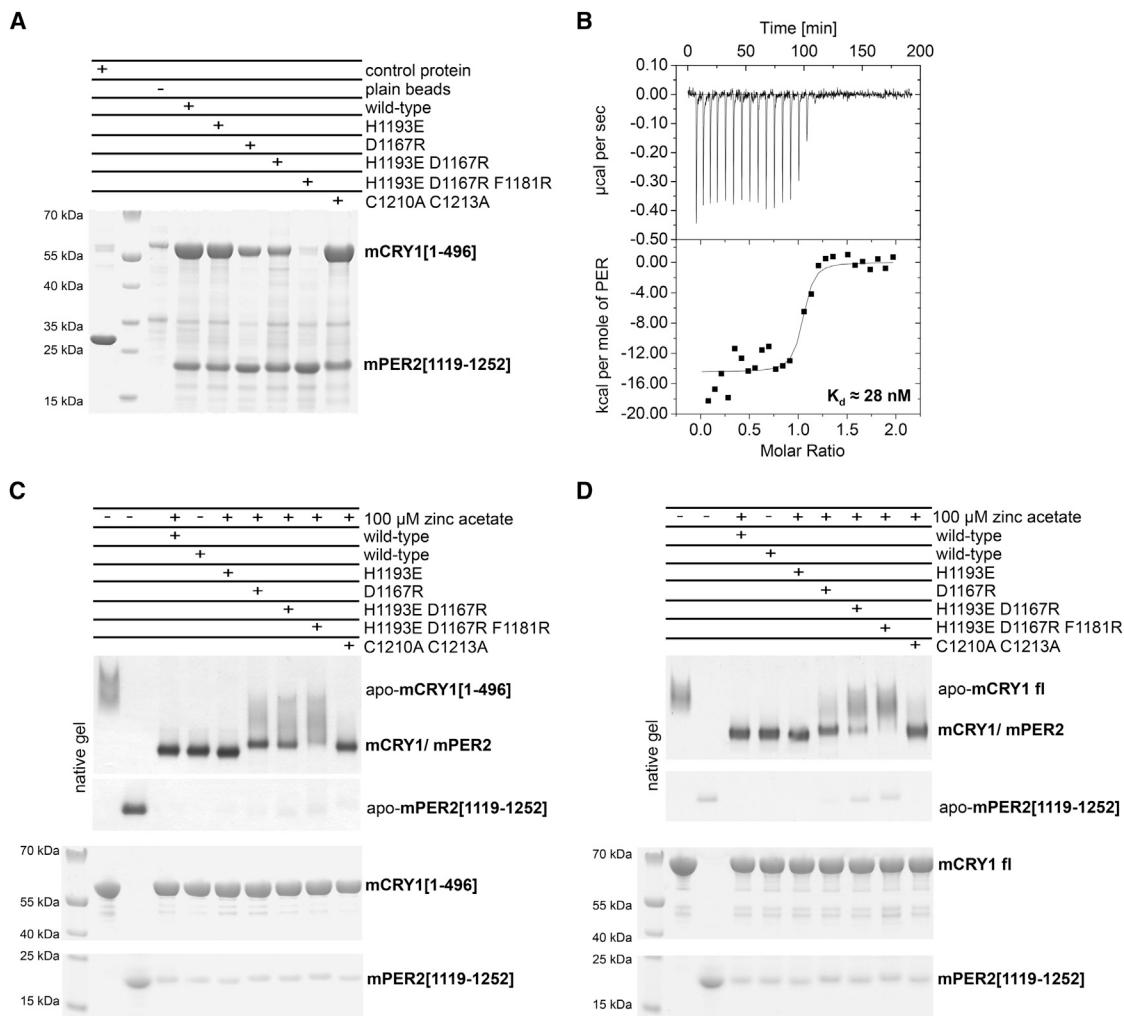


Figure 5. Biochemical Analysis of mCRY1/mPER2 Interfaces

(A) Ni^{2+} pull-down from total cell lysates testing for interactions of N-terminally His-tagged WT and mutant mPER2[1119–1252] proteins with untagged mCRY1 [1–496]. Eluates were analyzed on a Coomassie-stained 18% SDS-PAA gel. Negative controls: lane 1, pull-down of mCRY1 with a noncircadian control protein; lane 3, pull-down with plain beads.

(B) ITC profile for the interaction of mCRY1[1–496] and mPER2[1119–1252]. The binding event is exothermic. Top: time response of heat change upon addition of ligand (mPER2). Bottom: best fit obtained with a single site-binding model (best χ^2 statistic), resulting in a 1:1 stoichiometry ($n = 1.02$). The approximate K_d for the mCRY1-mPER2 interaction is 28 nM.

(C and D) Native gels (top) with purified proteins testing interactions of mPER2[1119–1252] (WT and mutants) with (C) mCRY1[1–496] (PHR) and (D) mCRY1 [1–606] (full length). Samples were also analyzed by SDS-PAGE (bottom).

See also Figure S1 and Table S2.

the existence and importance of the combined C-terminal helix interface in a cellular environment. The P319R mutation in the mCRY1 sulfur loop should also weaken the interaction with mPER2 $\alpha 3$ (Figure 2A). Whereas the P319R mutation moderately reduced binding in our luciferase complementation assay (this study), the K485D single mutation reduced binding to ~20% (Czarna et al., 2013). This finding suggests that mCRY1 binding to the mPER2 loop region (targeted by K485D) is more important than the interaction with the long mPER2 helix $\alpha 3$ (targeted by Q486R and P319R) *in vivo*.

A double mutation in the mPER2($\alpha 1$ –2)-mCRY1($\alpha 12$) interface (A328R/K329D) (Figure 2C) reduces mPER2 interactions by

about one half. We conclude that mPER2 helices $\alpha 1$ and $\alpha 2$ contribute to mCRY1 binding also in a cellular environment but are not as important for complex stability as for example helix $\alpha 4$.

Zinc Binding and Adjacent Disulfide Bond Formation Are Interdependent in a Cellular Context and *In Vitro*

To define potential roles of the zinc ion and the CRY1 Cys363–Cys412 disulfide bridge in a cellular environment, we have mutated the zinc-coordinating residues of mCRY1 (Cys414 and His473) and mPER2 (Cys1210 and Cys1213), as well as Cys363 and Cys412 to alanine. The mutants were tested for their effect on the stability of the mCRY1/mPER2 complex using a

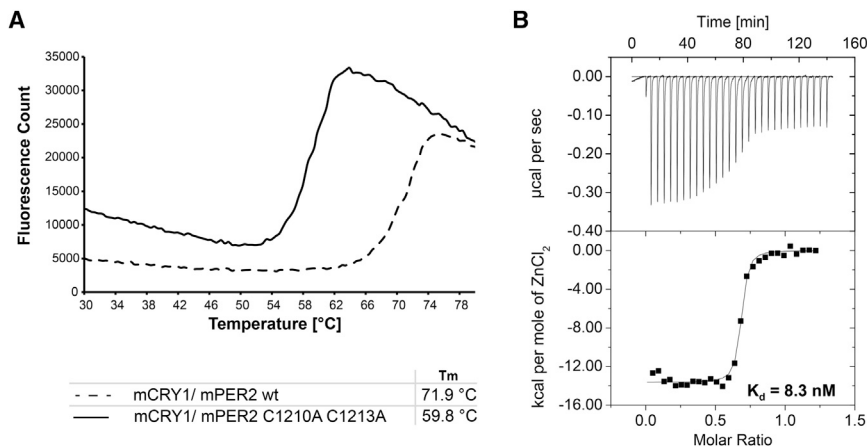


Figure 6. High-Affinity Zinc Binding Stabilizes the mCRY1-mPER2 Complex

(A) Melting temperature determination by thermofluor analysis of zinc-stabilized WT mCRY1 [1–496]/mPER2[1119–1252] complex in comparison with zinc-free mCRY1/mPER2(C1210A C1213A) mutant complex.

(B) ITC profile of zinc binding to the mCRY1 [1–496]/mPER2[1119–1252] complex. The binding event is exothermic. Top: time response of heat change upon addition of the zinc ligand. Bottom: best fit obtained with a single site-binding model (best χ^2 statistic) results in a stoichiometry of $n = 0.67$, probably because not all complexes are active in zinc binding. The approximate K_d for Zn^{2+} binding to the mCRY1/mPER2 complex is 8 nM. See also Figures S4, S6, and S7.

luciferase complementation assay in HEK293 cells (Figures 7A and S5A).

The mCRY1 single mutations C414A and H473A significantly reduced mPER2 binding, with the C414A single mutation being more effective. Furthermore, very weak interactions were observed between the mPER2(C1210A/C1213A) double-mutant protein and wild-type or C414A mutant mCRY1, indicating that zinc coordination is of vital importance for the formation of a stable complex between full-length mCRY1 and mPER2 *in vivo*.

C412A and C363A single mutations, which prevent formation of the Cys412-Cys363 disulfide bridge, slightly enhanced mPER2 binding in some of our luciferase complementation assays yet behaved wild-type like in other experiments. We propose that disruption of this disulfide bridge enhances mPER2 binding by facilitating the observed conformational changes of the mCRY1 lid (discussed above). The mild and somewhat fluctuating impact of the C412A and C363A single mutations on mPER2 binding probably depends on the redox status and hence the extent of Cys412-Cys363 disulfide bridge formation in the HEK293 cells.

To test whether mCRY1 exists in an oxidized form also in living cells, we analyzed mCRY1 disulfide bridge formation in HEK293 cells by N-Ethylmaleimide (NEM) and Maleimide-PEG (MP) modification (Figure 7B). Indeed, we found increased molecular weight forms of mCRY1 (CRY1-MP) only in lysates that were dithiothreitol (DTT) treated before MP modification, but not when lysates were either left untreated or when potential disulfide bridges were stabilized with H_2O_2 . This indicates that full-length mCRY1 also occurs in oxidized forms within cells.

Quite surprisingly, the mCRY1 C414A/C412A and the C414A/C363A double mutations only weakened mPER2 binding to ~50% in our luciferase complementation assay (Figure 7A). Furthermore, mCRY1 single- (C412A) or double (C412A/C414A)-mutant proteins showed ~50% binding activity toward mPER2 proteins containing the C1210A/C1213A double mutation. Hence, the C412A and C363A mutations partially rescue the severe weakening of the mCRY1-mPER2 interaction by the mCRY1 (C414A) and mPER2 (C1210A/C1213A) mutations, suggesting that reduction of the Cys412-Cys363 disulfide bridge and the resulting increased flexibility of the

mCRY1 C-terminal lid decrease the severity of disruption of the zinc-binding site.

To further elucidate whether the mCRY1 Cys412-Cys363 disulfide bridge forms in dependence of zinc in the mCRY1/mPER2 complex *in vitro*, we kept purified zinc-containing and zinc-free mCRY1/mPER2 complexes under reducing or non-reducing conditions and monitored the mCRY1 oxidation status by mass spectrometry (MS) (Figure S6). The presence of zinc in the complexes was analyzed in parallel by atomic absorption spectroscopy (ICP-OES) (Figure S7). Under nonreducing conditions, only a moderate amount of the putatively oxidized mCRY1 species (with the total mass reduced by ~2 Da as expected for the oxidation of a disulfide bridge) is observed in the zinc-bound WT mCRY1/mPER2 complex (Figure S6A, middle). However, in the zinc-free mCRY1/mPER2(C1210A/C1213A) mutant complex (Figure S6B), as well as when the zinc ion is removed from the WT complex through EDTA (Figure S6A, right), mCRY1 appears almost completely oxidized. To test whether the mCRY1 oxidation status is affected by disulfide bond formation between Cys412 and Cys363, we mutated Cys412 to alanine. Indeed, the C412A mutation substantially reduced mCRY1 oxidation in the zinc-free mCRY1(C412A)/mPER2(C1210A/C1213A) mutant complex (Figure S6C), indicating that Cys412 oxidation accounts for a significant fraction of the MS peak CRY_{p1} assigned to oxidized mCRY1 protein. However, we also found a moderate amount of putatively oxidized mCRY1 after aeration in the C412A mutant, suggesting additional disulfide bond formation (Figure S6C). Notably, the behavior of the purified zinc-free mCRY1(C412A)/mPER2(C1210A/C1213A) complex mirrors that of the WT mCRY1/mPER2 complex in our MS experiments (Figure S6D). This observation is consistent with the partial rescue of zinc-binding deficiency by the C412A and C363A mutations observed in our luciferase complementation experiment (Figure 7A).

In conclusion, our mutational analyses confirm the presence of all heterodimer interfaces revealed by our mCRY1/mPER2 crystal structure and indicate an interdependent role of the coordinated zinc ion and of the mCRY1 Cys412-Cys363 disulfide bridge, among others, in the positive (zinc) and negative (disulfide bridge) regulation of the mCRY1-mPER2 interaction *in vivo*.

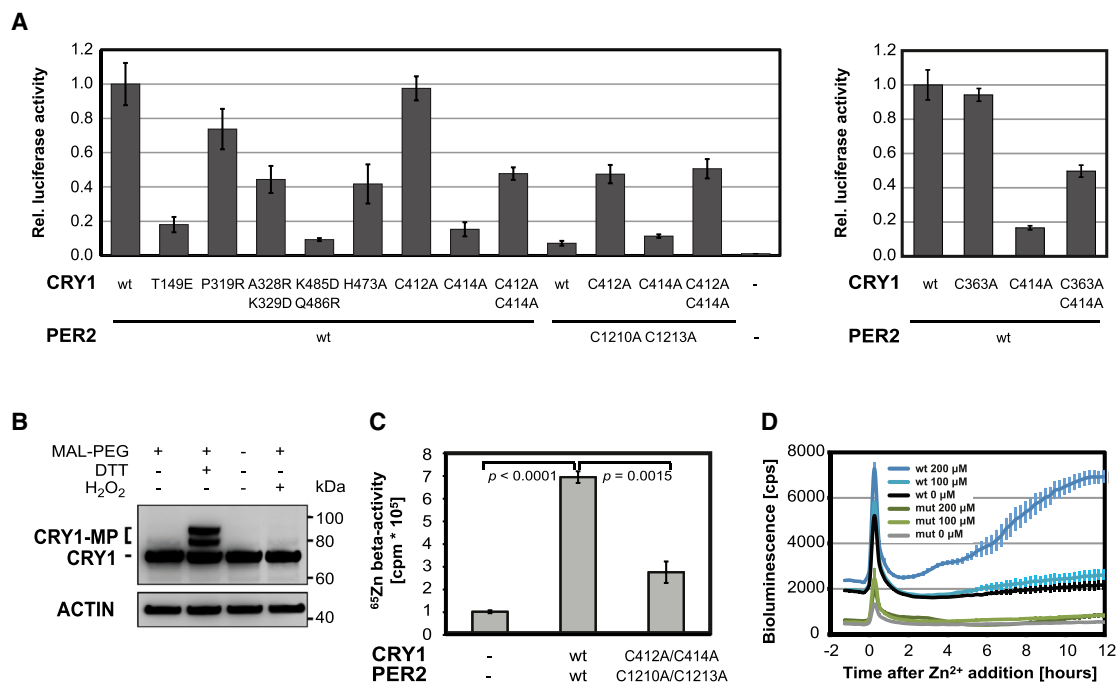


Figure 7. mCRY1/mPER2 Complex Formation Is Regulated by Four Interfaces, a Zinc Ion, and Disulfide Bridge Formation in Living Cells

(A) Luciferase complementation assay. All heterodimer interfaces revealed by the crystal structure are present in full-length mCRY1/mPER2 complexes inside cells. Disruption of the zinc interface is partially rescued by mutation of the disulfide bond forming Cys363 and Cys412. Full-length mCRY1 and mPER2 (WT or mutants) were expressed as fusion proteins with firefly luciferase fragments in HEK293 cells (Czarna et al., 2013). Approximately equal expression of fusion proteins was detected in western blot experiments (Figure S5A). Data are normalized to renilla luciferase activity (used as a transfection control) and presented relative to mCRY1(WT)-mPER2(WT) activity. Shown are mean \pm SEM of three (left) or four (right) independent transfections. Three additional experiments gave similar results.

(B) mCRY1 forms disulfide bridges in living cells: HEK293 cells transiently transfected with mCRY1 were harvested in presence of excess amounts of N-Ethylmaleimide (NEM) that immediately block all free thiol groups. Subsequently, disulfide bridges were reduced with Dithiothreitol (+DTT), and any thiol group previously oxidized was now modified with Maleimide-PEG (MP, MW 5 kDa). Increased molecular-weight forms of mCRY1 were detected in cell lysates treated with DTT, but not when lysates were not reduced (-DTT) or even oxidized with H₂O₂. This indicates that, within cells, full-length mCRY1 can occur in oxidized forms with one or more disulfide bridges.

(C) Critical cysteine residues coordinate zinc in the mCRY1/mPER2 complex in a cellular context: HEK293 cells were transiently transfected with full-length mPER2 or mCRY1 either as WT versions or with alanine mutations in the zinc-coordinating Cys414 (mCRY1), Cys1210, and Cys1213 (mPER2), as well as the disulfide bond forming Cys412 of mCRY1. Immunoprecipitated mPER2 was incubated with mCRY1-containing cell lysate in the presence of the radioactive zinc isotope ⁶⁵Zn²⁺. In this pull-down assay, WT proteins incorporated significantly (t test) more ⁶⁵Zn²⁺ than the mutants. Shown are mean \pm SEM of three independent immunoprecipitation experiments. The high expression of proteins was verified in western blot experiments (not shown).

(D) Zinc ions enhance the mCRY1-mPER2 interaction in living cells: Two U2-OS reporter cell lines, which stably express mCRY1 and mPER2 split luciferase fusion proteins either as WT or with alanine mutations in the zinc-coordinating cysteines (Cys414 of mCRY1; Cys1210, Cys1213 of mPER2) and Cys412 of mCRY1 (mut: C412A/C414A/C1210A/C1213A), were cultivated in Zn²⁺-depleted medium for about a week. Then various concentrations of Zn²⁺ were added to the medium while continuously monitoring luciferase activity. Treatment with zinc ions (but not iron ions, not shown) dose-dependently increases luciferase activity in cells expressing WT mCRY1 and mPER2 (see also Figure S5C), but not or to a much lesser extent in cells expressing mCRY1 and mPER2 with mutations of zinc-coordinating residues. Zinc has no effect on mRNA expression levels of the reporter constructs (not shown) or on luciferase activity of a control U2-OS cell expressing mCRY1-LUCIFERASE (not shown). Shown are mean \pm SEM of four independent treatments. Several additional experiments gave similar results. See also Figures S1, S2, and S5.

Zinc Ions Bind to the mCRY1/mPER2 Complex in a Cellular Context and Enhance the mCRY1-mPER2 Interaction in Living Cells

To test whether zinc can bind to the mCRY1/mPER2 complex in a cellular environment, we transiently transfected HEK293 cells with full-length mPER2 or full-length mCRY1 either as WT versions or with mutations in the three zinc-coordinating cysteines (mCRY1: C414A; mPER2: C1210A and C1213A) and the disulfide bridge forming Cys412 of mCRY1. To ensure that sufficiently stable mCRY1/mPER2 complexes are formed even without zinc coordination, we used the mCRY1 (C412A and

C414A) double mutant, which enhanced mCRY1-mPER2 interaction compared to the C414A single mutation in our luciferase complementation assays (Figure 7A). Immunoprecipitated mPER2 was incubated with mCRY1-containing cell lysate in the presence of the radioactive zinc isotope ⁶⁵Zn²⁺. A 7-fold increase in ⁶⁵Zn²⁺ radioactivity was detected when mPER2- and mCRY1-containing cell lysates were used. Mutations in the zinc coordination site led to a substantial and significant reduction of zinc binding (Figure 7C). In addition, immunoprecipitated mPER2 incubated with a control lysate did essentially not incorporate ⁶⁵Zn²⁺ (Figure S5B). Together, these results indicate

that zinc can bind to the full-length mCRY1/mPER2 complex in a cellular context, and this binding depends on critical zinc-coordinating cysteine residues in both proteins. The residual radioactivity observed for the mutant proteins could be due to $^{65}\text{Zn}^{2+}$ binding to large endogenous mCRY1/mPER2 complexes recruited via mPER PAS domain homodimer interactions (Kucera et al., 2012), as well as unspecific zinc binding.

To investigate whether zinc ions also contribute to the stabilization of the mCRY1-mPER2 interaction in living cells, we created two reporter U2-OS cell lines that stably express mPER2 and mCRY1 split luciferase fusion proteins either as WT proteins or with mutations in the zinc-coordinating residues Cys414 (mCRY1), Cys1210, and Cys1213 (mPER2), as well as the disulfide bridge forming Cys412 of mCRY1 (mut: C412A/C414A/C1210A/C1213A). Treatment with zinc (but not iron) ions dose-dependently enhances the bioluminescence in cells expressing WT mPER2 and mCRY1, but not or to a much lesser extent in cells expressing mutant mCRY1 and mPER2 proteins, indicating that zinc coordination indeed contributes to mCRY1-mPER2 interaction strength, and this effect depends on the integrity of the zinc-coordinating residues (Figures 7D and S5C).

DISCUSSION

Our crystal structure of the mCRY1/mPER2 heterodimer shows an intimate and high-affinity clock protein complex with a zinc interface that critically stabilizes the mCRY1/mPER2 complex in mammalian cells. Our cell-based and in vitro (LC-ESI-MS/ICP-OES) studies suggest that the coordinated zinc ion structurally facilitates the reduction of a nearby located disulfide bridge of mCRY1 (probably between Cys412 and Cys363, among others), which likely enhances the flexibility of the mCRY1 C-terminal lid and thereby mPER2 binding. This functionally important interplay between an intermolecular composite 3Cys/1His zinc-binding site in a heterodimer interface and one or more intramolecular disulfide bonds formed by nearby located cysteine residues has not been observed in other zinc-binding proteins (e.g., Maret, 2012; Auld, 2001). Notably, the redox-regulated chaperone Hsp33 and anti- σ factor RsrA use intramolecular cysteine-containing zinc centers as redox sensors (Ilbert et al., 2006). In both proteins, oxidative or disulfide stress leads to oxidation and, hence, disulfide bond formation of their zinc-coordinating cysteines, as well as zinc release, which induce conformational changes leading to their functional activation. On the other hand, betaine-homocysteine methyltransferase is reversibly inactivated through oxidation of its zinc-coordinating cysteines and zinc release (Evans et al., 2002).

Our LC-ESI-MS/ICP-OES experiments show that the mCRY1/mPER2 complex does not release its zinc ion under nonreducing conditions (Figure S7, number 2). Instead, the experiments suggest that zinc release supports mCRY1 oxidation (Figures S6A, top right, and S6B) and that this oxidation also involves Cys412 (Figure S6C). Using the same basic elements (i.e., a zinc ion and a nearby located highly reactive cysteine) but in a different structural arrangement, mode of action, and interplay, the CRY1/PER2 complex therefore may act as a sensor of the rhythmically changing redox state of the cell, which was

proposed to be involved in driving circadian rhythms (Edgar et al., 2012; O'Neill and Reddy, 2011; O'Neill et al., 2011; Wang et al., 2012).

In general, there are various intracellular zinc pools described such as zinc in vesicles, zinc tightly bound to macromolecules, zinc bound to metallothioneins (the major cellular zinc storage proteins), and a pool of "free" zinc (Oteiza, 2012). Although the total cellular amount of zinc is described to be in the high micromolar range, the concentration of "free" zinc is much lower (nano- to picomolar) because most zinc is bound to proteins with high affinity. However, under certain circumstances, e.g., oxidative stress, zinc may be released. Our measured K_d for zinc binding to the mCRY1/mPER2 complex in the lower nanomolar range suggests a dynamic, regulatory zinc-binding site that might be influenced by its environment within the cell.

Interestingly, the zinc-coordinating residues and most other residues mediating CRY-PER interactions are conserved in vertebrate CRY and PER2 proteins, in PER1, and, to a minor extent, in PER3, which strongly suggests the existence of homologous CRY/PER complexes (Figures S1 and S2).

Lacking the knowledge about the mCRY1-mPER2 zinc interface, Okano et al. (2009) generated a transgenic mouse line constitutively overexpressing mCRY1 with a C414A mutation. These mice showed a long 28 hr free-running period of locomotor activity rhythms and abnormal entrainment behavior, as well as symptoms of diabetes, including reduced β cell proliferation and insulin secretion (hypoinsulinemia) (Okano et al., 2009, 2010, 2013). Most likely, these dominant in vivo effects of the C414A mutation are due to disruption of the mCRY1-mPER2 zinc interface, demonstrating the importance of zinc-dependent mCRY1/mPER2 complex formation for circadian dynamics and metabolic regulation. Notably, mutations in mBMAL1 and mCLOCK also lead to hypoinsulinemia and defective β cell function, whereas mCRY1/mCRY2 double-knockout mice exhibit hyperinsulinemia and tissue-specific insulin resistance (Barclay et al., 2013; Marcheva et al., 2010). Furthermore, the mCLOCK Δ 19 mutation leads to extended circadian periods, whereas *mCry1*^{-/-} mice exhibit a period shortened by 1 hr (King et al., 1997; van der Horst et al., 1999). Hence, the circadian and metabolic phenotypes of the mCRY1 C414A mutation are more similar to those resulting from mutations in the mCLOCK/BMAL1 complex than to mCRY knockouts. Our structure suggests that the intimate interaction of mPER2 with mCRY1 α 22 interferes with repressive mCRY1 binding to the mCLOCK/BMAL1-E-box complex. Thus, we speculate that the weakened mPER2 interaction of the zinc-binding-deficient mCRY1(C414A) mutant protein (Figure 7A) leads to an enhanced transcriptional repression activity in vivo. We further propose that, in transgenic mice, the overexpressed mCRY1(C414A) mutant protein represses the mCLOCK/BMAL1 complex more strongly than endogenous WT mCRY1. This may cause the dominant phenotype of the mCRY1(C414A) mutation, which somewhat resembles the phenotypes of transgenic mice expressing weakened transcriptional activator complexes, including, for example, the mCLOCK Δ 19 mutant protein.

Our structure also shows that binding of FBXL3 or PER2 to CRY is mutually exclusive and suggests that PER2 stabilizes

CRY1 by shielding it from FBXL3. Strikingly, neither mPER2 (this study) nor FBXL3 (Xing et al., 2013) binds in close proximity of the AMPK phosphorylation site Ser71, suggesting that AMPK regulates PER2 and FBXL3 binding in a more indirect manner. Notably, Cys412 appears highly reactive in switching functions because it not only forms the intramolecular disulfide bond to Cys363 in apo-mCRY1 but also an intermolecular disulfide bond with FBXL3 in the CRY2/FBXL3 complex structure.

Taken together, our crystal structure provides a more complete understanding of how mammalian CRY and PER proteins interact, how this interaction might be sensing and be regulated by cellular redox/metabolic states, and how the interplay with other clock components drives the circadian clock and metabolic processes. This will guide the design of new mutants, experiments, and small-molecule ligands to study or target macromolecular CRY/PER containing complexes *in vivo*.

EXPERIMENTAL PROCEDURES

Protein Purification and Crystallization

mCRY1 and mPER2 proteins were recombinantly expressed as His-fusions in insect cells and *E. coli*, respectively. For purification of the mCRY1/mPER2 complex (native and selenomethionine labeled), lysates were combined and copurified via Ni²⁺ affinity, anion exchange, and heparin and size-exclusion chromatography columns. For biochemical analysis, mCRY1 proteins were purified via Ni²⁺ affinity, anion exchange, heparin and size-exclusion columns, mPER2 proteins via Ni²⁺ affinity followed by tag cleavage, anion exchange, and size-exclusion chromatography.

Crystals of the mCRY1/mPER2 complex grew at 20°C in 0.2 M MgCl₂ and 12%–13% PEG3350. They contain one complex per asymmetric unit (space group P4₃2₁2).

Data Collection, Structure Determination, and Refinement

A 2.45 Å data set of a mCRY1/mPER2 crystal and a 2.8 Å data set of a selenomethionine-labeled mCRY1/mPER2 crystal were collected at beamline PXII (SLS). The mCRY1/mPER2 complex structure was solved by molecular replacement with apo-mCRY1 (PDB ID 4K0R) as search model combined with selenium single-wavelength anomalous dispersion (SAD) phasing. Data collection and refinement statistics are summarized in Table S1.

Inductively Coupled Plasma Optical Emission Spectrometry

We performed inductively coupled plasma optical emission spectrometry (ICP-OES) using a Varian VISTA-RL spectrometer with a MicroMist nebulizer. Zinc binding was determined by measuring its specific emission at 213.857 nm.

Pull-Down Experiments

Clear lysates of *E. coli* cells expressing His-tagged mPER2 (WT and mutants) were incubated with Ni-Sepharose 6 Fast Flow beads in presence of 25 mM imidazole for 1 hr. After washing and equilibration in lysis buffer with 70 mM imidazole, mPER2-bound Ni-beads were incubated with clear lysates of insect cells expressing untagged mCRY1 for 1 hr in order to pull down mCRY1. The beads were extensively washed before elution of the bound complex with 500 mM imidazole and analysis by SDS-PAGE.

Native PAGE Analysis

Purified proteins were incubated at a 1:1 molar ratio in a BIS-Tris Propane buffer (pH 7.0) at 4°C for at least 2 hr. Samples were analyzed on a native 4%–20% Novex Tris-Glycine gel and by SDS-PAGE.

Circular Dichroism, Isothermal Titration Calorimetry, and Thermofluor

Circular dichroism (CD) spectroscopy using a Jasco J-810 spectropolarimeter and ITC experiments using a VP-ITC MicroCalorimeter were performed essen-

tially as described in Czarna et al. (2011). Thermofluor was performed as described in Weir et al. (2010).

LC-ESI MS Analysis

Purified WT and mutant mCRY1/mPER2 complexes were kept under reducing (4 mM DTT) or nonreducing (no DTT, aeration) conditions for 2 days. For removal of bound zinc, the protein complex was treated with 10 mM EDTA, and zinc-bound EDTA was removed by dialysis. LC-MS analyses were performed on a Bruker micrOTOF connected to an Agilent 1100 HPLC system equipped with a diode array detector.

Luciferase Complementation Assay

The luciferase complementation assay was performed essentially as described in Kucera et al. (2012).

Analysis of Disulfide Bridges in mCRY1

mCRY1 disulfide bridges were analyzed essentially using a combined method from Wu et al. (2000) and Templeton et al. (2010). Free thiol groups in lysates of MYC-tagged mCRY1-expressing HEK293 cells were blocked with 50 mM NEM, excess NEM was removed by methanol precipitation, and disulfide bridges were then reduced with 20 mM DTT. After removal of DTT by methanol precipitation, arosen free thiol groups were modified by incubation with 300 μM Maleimide-PEG. Samples were then analyzed by western blotting using an anti-MYC antibody.

Live-Cell Zinc-Binding Assay

Human U2-OS cells stably expressing mCRY1 and mPER2 as split-luciferase hybrid proteins were kept for at least 1 week in zinc-depleted medium prior to zinc ion addition. Bioluminescence of reconstituted luciferase was recorded for several days.

⁶⁵Zn-Binding Assay

HEK293 cells were cultured for 5 days in zinc-free medium before transfection with equal amounts of plasmid DNA encoding either WT or mutant epitope-tagged mCRY1 or mPER2. Lysates with overexpressed V5-tagged mPER2 constructs were incubated with anti-V5 antibody and equivalent amounts of Protein G PLUS-agarose beads overnight. Beads were washed, mixed with lysates overexpressing mCRY1 or control lysates, and incubated for 3 hr with 35 μM ⁶⁵ZnCl₂ radionuclide at room temperature. After washing, ⁶⁵Zn binding was determined by scintillation counting in a Wallac 1440 DSA system.

The Extended Experimental Procedures section, which provides detailed information about all experimental procedures, including protein purification, crystallization, structure determination, *in vitro* interaction studies (ITC, native gels, and pull-down), circular dichroism, thermofluor, LC-ESI-MS, and atomic absorption spectroscopy (ICP-OES), as well as cell-based studies (luciferase complementation assays, zinc-binding assays, and disulfide bond formation), is included in the Supplemental Information.

ACCESSION NUMBERS

The coordinates and structure factors have been deposited in the Protein Data Bank under the accession code 4ct0.

SUPPLEMENTAL INFORMATION

Supplemental Information includes Extended Experimental Procedures, seven figures, and two tables and can be found with this article online at <http://dx.doi.org/10.1016/j.cell.2014.03.057>.

AUTHOR CONTRIBUTIONS

I.S., S.R., T.W., R.K., A.K., and E.W. designed experiments; I.S., S.R., T.W., R.K., C.B., and A.G. performed experiments; I.S., J.R.P., and C.B. solved the structure; I.S., S.R., T.W., R.K., J.R.P., C.B., A.K., and E.W. analyzed data; and I.S., A.K., and E.W. wrote the paper.

ACKNOWLEDGMENTS

We thank the beamline staff at Swiss Light Source (SLS, Villigen) for excellent assistance and the Max Planck Institute (MPI) of Biochemistry Crystallization Facility and Biochemistry Core Facility, especially Elisabeth Wehyer-Stingl, for technical assistance and support. Further, we thank Helmut Hartl and Jaroslava Obel (Department of Chemistry and Pharmacy, LMU Munich) for ICP-OES analysis. We thank our colleagues of the Department of Structural Cell Biology at the MPI of Biochemistry for help with data collection, fruitful discussions, and critical comments. We are indebted to Claire Basquin for assistance with ITC, thermofluor, and other biophysical methods and to Michaela Rode for assistance with insect cell culture. Anna Czarna, Sebastian Falk, Kai Hell, Debora Makino, Michael Taschner, and Justine Witosch are thanked for valuable suggestions and discussions. This study was supported by DFG grants Wo695-3 (FOR526), Wo695-4, and Wo695-6 to E.W., DFG grant SFB740/D2 to A.K., and a fellowship of the Studienstiftung des deutschen Volkes to I.S.

Received: September 4, 2013

Revised: February 6, 2014

Accepted: March 17, 2014

Published: May 22, 2014

REFERENCES

- Auld, D.S. (2001). Zinc coordination sphere in biochemical zinc sites. *Biometals* *14*, 271–313.
- Barclay, J.L., Shostak, A., Leliavski, A., Tsang, A.H., Jöhren, O., Müller-Fielitz, H., Landgraf, D., Naujokat, N., van der Horst, G.T.J., and Oster, H. (2013). High-fat diet-induced hyperinsulinemia and tissue-specific insulin resistance in Cry-deficient mice. *Am. J. Physiol. Endocrinol. Metab.* *304*, E1053–E1063.
- Chaves, I., Yagita, K., Barnhoorn, S., Okamura, H., van der Horst, G.T.J., and Tamanini, F. (2006). Functional evolution of the photolyase/cryptochrome protein family: importance of the C terminus of mammalian CRY1 for circadian core oscillator performance. *Mol. Cell. Biol.* *26*, 1743–1753.
- Czarna, A., Breitzkreuz, H., Mahrenholz, C.C., Arens, J., Strauss, H.M., and Wolf, E. (2011). Quantitative analyses of cryptochrome-mBMAL1 interactions: mechanistic insights into the transcriptional regulation of the mammalian circadian clock. *J. Biol. Chem.* *286*, 22414–22425.
- Czarna, A., Berndt, A., Singh, H.R., Grudziecki, A., Ladurner, A.G., Timinszky, G., Kramer, A., and Wolf, E. (2013). Structures of *Drosophila* cryptochrome and mouse cryptochrome1 provide insight into circadian function. *Cell* *153*, 1394–1405.
- Eckel-Mahan, K., and Sassone-Corsi, P. (2009). Metabolism control by the circadian clock and vice versa. *Nat. Struct. Mol. Biol.* *16*, 462–467.
- Edgar, R.S., Green, E.W., Zhao, Y., van Ooijen, G., Olmedo, M., Qin, X., Xu, Y., Pan, M., Valekunja, U.K., Feeney, K.A., et al. (2012). Peroxiredoxins are conserved markers of circadian rhythms. *Nature* *485*, 459–464.
- Eide, E.J., Vielhaber, E.L., Hinz, W.A., and Virshup, D.M. (2002). The circadian regulatory proteins BMAL1 and cryptochromes are substrates of casein kinase I ϵ . *J. Biol. Chem.* *277*, 17248–17254.
- Evans, J.C., Huddler, D.P., Jiracek, J., Castro, C., Millian, N.S., Garrow, T.A., and Ludwig, M.L. (2002). Betaine-homocysteine methyltransferase: zinc in a distorted barrel. *Structure* *10*, 1159–1171.
- Gatfield, D., and Schibler, U. (2007). Physiology. Proteasomes keep the circadian clock ticking. *Science* *316*, 1135–1136.
- Griffin, E.A., Jr., Staknis, D., and Weitz, C.J. (1999). Light-independent role of CRY1 and CRY2 in the mammalian circadian clock. *Science* *286*, 768–771.
- Hirano, A., Yumimoto, K., Tsunematsu, R., Matsumoto, M., Oyama, M., Kozuka-Hata, H., Nakagawa, T., Lanjakornsiripan, D., Nakayama, K.I., and Fukada, Y. (2013). FBXL21 regulates oscillation of the circadian clock through ubiquitination and stabilization of cryptochromes. *Cell* *152*, 1106–1118.
- Hirota, T., Lee, J.W., St John, P.C., Sawa, M., Iwaisako, K., Noguchi, T., Pong-sawakul, P.Y., Sonntag, T., Welsh, D.K., Brenner, D.A., et al. (2012). Identification of small molecule activators of cryptochrome. *Science* *337*, 1094–1097.
- Hitomi, K., DiTacchio, L., Arvai, A.S., Yamamoto, J., Kim, S.-T., Todo, T., Tainer, J.A., Iwai, S., Panda, S., and Getzoff, E.D. (2009). Functional motifs in the (6-4) photolyase crystal structure make a comparative framework for DNA repair photolyases and clock cryptochromes. *Proc. Natl. Acad. Sci. USA* *106*, 6962–6967.
- Huang, N., Chelliah, Y., Shan, Y., Taylor, C.A., Yoo, S.-H., Partch, C., Green, C.B., Zhang, H., and Takahashi, J.S. (2012). Crystal structure of the heterodimeric CLOCK:BMAL1 transcriptional activator complex. *Science* *337*, 189–194.
- Ilbert, M., Graf, P.C., and Jakob, U. (2006). Zinc center as redox switch—new function for an old motif. *Antioxid. Redox Signal.* *8*, 835–846.
- King, D.P., Vitaterna, M.H., Chang, A.M., Dove, W.F., Pinto, L.H., Turek, F.W., and Takahashi, J.S. (1997). The mouse Clock mutation behaves as an antimorph and maps within the W19H deletion, distal of Kit. *Genetics* *146*, 1049–1060.
- Koike, N., Yoo, S.-H., Huang, H.-C., Kumar, V., Lee, C., Kim, T.-K., and Takahashi, J.S. (2012). Transcriptional architecture and chromatin landscape of the core circadian clock in mammals. *Science* *338*, 349–354.
- Kucera, N., Schmalen, I., Hennig, S., Öllinger, R., Strauss, H.M., Grudziecki, A., Wieczorek, C., Kramer, A., and Wolf, E. (2012). Unwinding the differences of the mammalian PERIOD clock proteins from crystal structure to cellular function. *Proc. Natl. Acad. Sci. USA* *109*, 3311–3316.
- Kume, K., Zylka, M.J., Sriram, S., Shearman, L.P., Weaver, D.R., Jin, X., Maywood, E.S., Hastings, M.H., and Reppert, S.M. (1999). mCRY1 and mCRY2 are essential components of the negative limb of the circadian feedback loop. *Cell* *98*, 193–205.
- Lamia, K.A., Sachdeva, U.M., DiTacchio, L., Williams, E.C., Alvarez, J.G., Egan, D.F., Vasquez, D.S., Juguilon, H., Panda, S., Shaw, R.J., et al. (2009). AMPK regulates the circadian clock by cryptochrome phosphorylation and degradation. *Science* *326*, 437–440.
- Lamia, K.A., Papp, S.J., Yu, R.T., Barish, G.D., Uhlenhaut, N.H., Jonker, J.W., Downes, M., and Evans, R.M. (2011). Cryptochromes mediate rhythmic repression of the glucocorticoid receptor. *Nature* *480*, 552–556.
- Marcheva, B., Ramsey, K.M., Buhr, E.D., Kobayashi, Y., Su, H., Ko, C.H., Ivanova, G., Omura, C., Mo, S., Vitaterna, M.H., et al. (2010). Disruption of the clock components CLOCK and BMAL1 leads to hypoinsulinemia and diabetes. *Nature* *466*, 627–631.
- Maret, W. (2012). New perspectives of zinc coordination environments in proteins. *J. Inorg. Biochem.* *111*, 110–116.
- Miyazaki, K., Mesaki, M., and Ishida, N. (2001). Nuclear entry mechanism of rat PER2 (rPER2): role of rPER2 in nuclear localization of CRY protein. *Mol. Cell. Biol.* *21*, 6651–6659.
- Müller, M., and Carell, T. (2009). Structural biology of DNA photolyases and cryptochromes. *Curr. Opin. Struct. Biol.* *19*, 277–285.
- O'Neill, J.S., and Reddy, A.B. (2011). Circadian clocks in human red blood cells. *Nature* *469*, 498–503.
- O'Neill, J.S., van Ooijen, G., Dixon, L.E., Troein, C., Corellou, F., Bouget, F.-Y., Reddy, A.B., and Millar, A.J. (2011). Circadian rhythms persist without transcription in a eukaryote. *Nature* *469*, 554–558.
- Okano, S., Akashi, M., Hayasaka, K., and Nakajima, O. (2009). Unusual circadian locomotor activity and pathophysiology in mutant CRY1 transgenic mice. *Neurosci. Lett.* *451*, 246–251.
- Okano, S., Hayasaka, K., Igarashi, M., Iwai, H., Togashi, Y., and Nakajima, O. (2010). Non-obese early onset diabetes mellitus in mutant cryptochrome1 transgenic mice. *Eur. J. Clin. Invest.* *40*, 1011–1017.
- Okano, S., Hayasaka, K., Igarashi, M., Togashi, Y., and Nakajima, O. (2013). Characterization of age-associated alterations of islet function and structure in diabetic mutant cryptochrome 1 transgenic mice. *J. Diabetes Investigation* *4*, 428–435.

- Oteiza, P.I. (2012). Zinc and the modulation of redox homeostasis. *Free Radic. Biol. Med.* 53, 1748–1759.
- Ozber, N., Baris, I., Tatlici, G., Gur, I., Kilinc, S., Unal, E.B., and Kavakli, I.H. (2010). Identification of two amino acids in the C-terminal domain of mouse CRY2 essential for PER2 interaction. *BMC Mol. Biol.* 11, 69.
- Templeton, D.J., Aye, M.-S., Rady, J., Xu, F., and Cross, J.V. (2010). Purification of reversibly oxidized proteins (PROP) reveals a redox switch controlling p38 MAP kinase activity. *PLoS ONE* 5, e15012.
- Tomita, T., Miyazaki, K., Onishi, Y., Honda, S., Ishida, N., and Oishi, K. (2010). Conserved amino acid residues in C-terminus of PERIOD 2 are involved in interaction with CRYPTOCHROME 1. *Biochim. Biophys. Acta* 1803, 492–498.
- van der Horst, G.T., Muijtjens, M., Kobayashi, K., Takano, R., Kanno, S., Takao, M., de Wit, J., Verkerk, A., Eker, A.P., van Leenen, D., et al. (1999). Mammalian Cry1 and Cry2 are essential for maintenance of circadian rhythms. *Nature* 398, 627–630.
- Wang, T.A., Yu, Y.V., Govindaiah, G., Ye, X., Artinian, L., Coleman, T.P., Sweedler, J.V., Cox, C.L., and Gillette, M.U. (2012). Circadian rhythm of redox state regulates excitability in suprachiasmatic nucleus neurons. *Science* 337, 839–842.
- Weir, J.R., Bonneau, F., Hentschel, J., and Conti, E. (2010). Structural analysis reveals the characteristic features of Mtr4, a DExH helicase involved in nuclear RNA processing and surveillance. *Proc. Natl. Acad. Sci. USA* 107, 12139–12144.
- Wu, H.H., Thomas, J.A., and Momand, J. (2000). p53 protein oxidation in cultured cells in response to pyrrolidine dithiocarbamate: a novel method for relating the amount of p53 oxidation in vivo to the regulation of p53-responsive genes. *Biochem. J.* 357, 87–93.
- Xing, W., Busino, L., Hinds, T.R., Marionni, S.T., Saifee, N.H., Bush, M.F., Pagano, M., and Zheng, N. (2013). SCF(FBL3) ubiquitin ligase targets cryptochromes at their cofactor pocket. *Nature* 496, 64–68.
- Yagita, K., Tamanini, F., Yasuda, M., Hoeijmakers, J.H.J., van der Horst, G.T.J., and Okamura, H. (2002). Nucleocytoplasmic shuttling and mCRY-dependent inhibition of ubiquitylation of the mPER2 clock protein. *EMBO J.* 21, 1301–1314.
- Ye, R., Selby, C.P., Ozturk, N., Annayev, Y., and Sancar, A. (2011). Biochemical analysis of the canonical model for the mammalian circadian clock. *J. Biol. Chem.* 286, 25891–25902.
- Yoo, S.-H., Mohawk, J.A., Siepkka, S.M., Shan, Y., Huh, S.K., Hong, H.-K., Kornblum, I., Kumar, V., Koike, N., Xu, M., et al. (2013). Competing E3 ubiquitin ligases govern circadian periodicity by degradation of CRY in nucleus and cytoplasm. *Cell* 152, 1091–1105.
- Young, M.W., and Kay, S.A. (2001). Time zones: a comparative genetics of circadian clocks. *Nat. Rev. Genet.* 2, 702–715.
- Zhang, E.E., Liu, Y., Dentin, R., Pongsawakul, P.Y., Liu, A.C., Hirota, T., Nusinow, D.A., Sun, X., Landais, S., Kodama, Y., et al. (2010). Cryptochrome mediates circadian regulation of cAMP signaling and hepatic gluconeogenesis. *Nat. Med.* 16, 1152–1156.

EXTENDED EXPERIMENTAL PROCEDURES

Recombinant Protein Expression and Purification

Recombinant mCRY1 proteins (full-length and residues 1-496) were obtained as 6xHIS-fusions (11 residue C-terminal overhang AAALHHHHHH of 1,296.3 Da) or untagged from High5 (H5) insect cells. Cells were infected at 1×10^6 cells/ml with a P3 high virus titer solution at a 1:100 (v/v) dilution and grown at 26°C for 52 hr. Cells were harvested at 2,000 rpm, frozen and lysed in a buffer containing 50 mM Tris at pH 7.1 (for complex purification and mCRY1[1-496]) or at pH 7.8 (for full-length mCRY1), 300 mM NaCl, 25 mM Imidazole, 5 mM CHAPS, 1 mM EDTA, 1 mM PMSF, cOmplete EDTA-free protease inhibitor cocktail (ROCHE), DNase and 10% glycerol.

Recombinant mPER2 fragments (residues 1132-1252 and residues 1119-1252) were overexpressed as 6xHIS-fusions in the *E. coli* strain BL21(DE3). They contain a 22 residue N-terminal overhang (MKHHHHHSAGLEVLFGPDSM, 2532.84 Da) with a PreScission protease cleavage site leaving a 5 amino acid overhang (GPDSM). Cells were harvested at 6,000 rpm, frozen and lysed in a buffer containing 50 mM Tris pH 7.5, 300 mM NaCl, 25 mM imidazole, 5 mM CHAPS, 1 mM EDTA, 1 mM PMSF and 10% glycerol.

For purification of the mCRY1/mPER2 complex lysates were combined and co-purified by Ni²⁺-affinity chromatography followed by Q Sepharose anion exchange chromatography and Heparin Sepharose chromatography (all GE Healthcare). The final purification step by size-exclusion chromatography (Superdex 200, GE Healthcare) was carried out in 25 mM HEPES pH 7.0, 100 mM NaCl and 2 mM DTT. For crystallization 5 mM TCEP was added to the concentrated protein.

For biochemical analysis mCRY1 proteins were purified via Ni²⁺-affinity, anion exchange, heparin and size-exclusion columns. mPER2 proteins were purified via Ni²⁺-affinity chromatography followed by PreScission protease tag cleavage overnight, anion exchange and size-exclusion chromatography. Selenomethionine labeling of mPER2 was carried out according to published methods (Bergfors, 2009). The selenomethionine substituted protein/complex was purified using the same protocol as for the native protein.

Crystallization

Native crystals of the mCRY1[1-496]/mPER2[1132-1252] complex were observed within 4-5 days at 20°C using hanging drop setups. They were grown mixing the complex at 20 mg/ml concentration with an equal volume of precipitant solution containing 0.2 M MgCl₂ and 12%–13% PEG 3350. mCRY1[1-496]/mPER2[1132-1252] crystals belong to space group P4₃2₁2 with unit cell constants a = 99.736 Å, b = 99.736 Å, c = 178.632 Å, $\alpha/\beta/\gamma = 90^\circ$ and one molecule per asymmetric unit (solvent content 60%). For data collection at 100 K, crystals were transferred into a cryoprotecting solution containing 20% glycerol (v/v) and shock frozen in liquid nitrogen. Crystals containing selenomethionine labeled mPER2 were grown under the same conditions, however, reducing the protein concentration to 17.5 mg/ml.

Data Collection, Structure Determination, and Refinement

A 2.45 Å data set of a single mCRY1/mPER2 crystal and a 2.8 Å data set of a single selenomethionine labeled mCRY1/mPER2 crystal were collected at the PXII (X10SA) beamline of the Swiss Light Source (SLS) (Villigen, Switzerland) and processed using XDS (Kabsch, 1993). Data were evaluated according to $I/\sigma(I)$ in the highest resolution shell. The rather high R_{sym} value obtained for the SAD data set is due to the high anomalous signal in this data set that was not corrected for when calculating R_{sym} as well as the very high redundancy of the data set. The structure of the mCRY1/mPER2 complex was solved by molecular replacement (MR) combined with selenium single-wavelength anomalous dispersion (SAD) phasing. PHASER (McCoy et al., 2007) was used for molecular replacement with the apo-mCRY1 structure as search model and PHENIX AutoSol (Terwilliger et al., 2009) for calculation of the initial electron density map using combined MR and Se-SAD phases. An anomalous difference map (PHENIX Maps) clearly located the selenomethionines within the mPER2 structure and allowed us to assign the sequence of mPER2 with certainty. Refinement was carried out with PHENIX (Adams et al., 2010) applying several rounds of positional and individual B-factor refinement followed by model building using Buccaneer (Cowtan, 2006) and Coot (Emsley and Cowtan, 2004). After initial refinement against the selenomethionine data set, the structure was refined to 2.45 Å using the native data set with a transferred R_{free} test set. The model was also subjected to simulated annealing and TLS refinement. The final model is characterized by an R_{free} of 23.31% and an R_{cryst} of 18.60% and exhibits very good stereochemistry (Table S1).

The final mCRY1/mPER2 model consists of 582 amino acids, 175 water molecules, 1 PEG molecule, 1 chloride ion and 1 zinc ion in the mCRY1-mPER2 interface. Furthermore, an X-ray fluorescence scan at the SLS beamline confirmed the presence of zinc in the crystals. Residues 1-2, 233-240 and the C-terminal overhang of the crystallized mCRY1[1-496] fragment as well as residues 1215-1252 and the N-terminal His-tag of the crystallized mPER2[1132-1252] fragment are not seen in the electron density due to conformational disorder. Residues EVLFQ in the N-terminal cloning overhang of mPER2[1132-1252] form an extra beta strand, β_0 , which packs against β strand 1 (β_1) (Figure 1B). 33 mCRY1 residues and 3 mPER2 residues are modeled as alanine due to conformational disorder of their side chains. The Ramachandran plot depicts 94.3% of main chain torsion angles in the most favored regions, no outliers are depicted according to MolProbity. Figures were generated with MacPymol (DeLano Scientific LLC, 2006). The buried surface area was calculated with PISA (Protein interfaces, surfaces and assemblies' service PISA at the European Bioinformatics Institute), http://www.ebi.ac.uk/pdbe/prot_int/pistart.html (Krissinel and Henrick, 2007).

Inductively Coupled Plasma Optical Emission Spectrometry

To analyze the zinc content of individually purified mPER2 and mCRY1 proteins and of the mCRY1/mPER2 complex in solution, we performed Inductively Coupled Plasma Optical Emission Spectrometry (ICP-OES) using a Varian VISTA-RL spectrometer with a MicroMist nebulizer. Zinc binding was determined by measuring its specific emission at 213.857 nm.

Site-Directed Mutagenesis

mPER2 mutants were generated using the QuikChange site-directed mutagenesis kit (Stratagene) and verified by sequencing. The mutant constructs were expressed and purified to homogeneity essentially as described for the wild-type proteins.

Pull-Down Experiments

His-tagged mPER2 proteins (wild-type and mutants) were expressed in *E. coli* BL21 (DE3) cells. 30 ml with OD₆₀₀ = 1 were harvested and the cell pellets lysed in 1 ml lysis buffer containing 50 mM Tris pH 7.5, 300 mM NaCl, 10% glycerol, 3 mM β-mercaptoethanol, 10 μM zinc acetate and 25 mM imidazole. After centrifugation the supernatants were incubated with 25 μl pre-equilibrated Ni-Sepharose 6 Fast Flow beads (GE Healthcare) for 1 hr to pull-down His-tagged mPER2. Beads were then extensively washed with lysis buffer to remove contaminants and finally equilibrated in lysis buffer pH 7.1 containing 70 mM imidazole. To test for pull-down capacity of mCRY1[1-496], the protein was expressed without tag in insect cells. 20 ml of cells were harvested and lysed in 1 ml lysis buffer containing 50 mM Tris pH 7.1, 300 mM NaCl, 5% glycerol, 3 mM β-mercaptoethanol, 10 μM zinc acetate and 70 mM imidazole (+ DNase and cOmplete EDTA-free protease inhibitor cocktail [ROCHE]). After centrifugation the supernatants were incubated with pre-equilibrated mPER2-Ni-beads for 1 hr to pull-down mCRY1. The beads were then extensively washed with lysis buffer to remove contaminants. Finally the bound protein was eluted from the beads using lysis buffer supplemented with 500 mM imidazole. As negative control the experiment was performed simultaneously in the absence of mPER2 and in the presence of a control protein, which does not bind mCRY1. The eluted proteins were analyzed using SDS-PAGE.

Native PAGE Analysis

For Native-PAGE analysis purified proteins were incubated at a molar ratio of 1 to 1 in 25 mM BIS-Tris Propane pH 7, 100 mM NaCl, 10 mM TCEP and ± 100 μM zinc acetate at 4°C for at least 2 hr. For sample preparation 2x Tris-Glycine Native Sample Buffer was added. Samples were loaded on a 4%–20% Novex Tris-Glycine gel and run constantly at 125 V in Tris-Glycine Native running buffer (pH 8.3). Samples were additionally subjected to SDS-PAGE analysis. In the native and SDS gels, 3 μg total protein (mCRY1/mPER2 complex or individual proteins) were loaded per lane except for lane 2 in the native gel analysis of mCRY1fl (Figure 5D), where the amount of mPER2 protein present in 3 μg mCRY1/mPER2 complex was loaded. The sharper CRY1/PER2 complex bands suggest that mPER2 binding stabilizes mCRY1.

Circular Dichroism Spectroscopy

Purified protein samples were diluted to final concentrations between 2.5 and 11 μM in a buffer containing 25 mM Tris pH 7.3, 100 mM NaCl, 2 mM DTT (racemic). CD spectra were measured by a Jasco J-810 spectropolarimeter using a 0.1 cm path length quartz cuvette and represent the mean molar ellipticity per amino acid residue after buffer correction. Measurements were performed at 4°C in a wavelength range from 195 nm to 250 nm with 0.1 nm intervals collecting data for 1 s at each point. For each measurement four spectra were accumulated. Secondary structure analysis was performed using the CONTIN algorithm (Provencher and Glöckner, 1981).

Isothermal Titration Calorimetry

The ITC experiments were performed using a VP-ITC MicroCalorimeter (MicroCal, Northampton, MA). For the interaction of mCRY1 [1-496] and mPER2[1119-1252] all reagents were extensively dialyzed against a buffer containing 25 mM HEPES pH 7.1, 100 mM NaCl, 2 mM TCEP. The protein in the cell (mCRY1) had a concentration of 10 μM, while the concentration of mPER2 in the syringe was 10 times higher. The typical titration consisted of 29 injections of 2 to 10 μl aliquots into the cell (1.4426 ml), at time intervals of 360 s at 23°C.

To study the interaction of the mCRY1[1-496]/mPER2[1119-1252] complex (both proteins untagged) with zinc, the zinc-free reconstituted protein complex was extensively dialysed against a buffer containing 25 mM Tris pH 7.1, 100 mM NaCl, 2 mM TCEP. The protein in the cell had a concentration of 10 μM, while the concentration of ZnCl₂ in the syringe was 7.5 times higher. The typical titration consisted of 29 injections of 2 to 7.5 μl aliquots into the cell (1.4426 ml), at time intervals of 280 s at 23°C.

The enthalpy changes ΔH upon binding, the association constant (K_A) and the binding stoichiometry (N) were obtained directly whereas the Gibbs energy (ΔG) - and entropy (ΔS) changes were calculated according to Equation (1).

$$\Delta G^\circ = \Delta H^\circ - T\Delta S^\circ = -RT \ln K_A \quad (1)$$

The dilution heat of the control titration, consisting of the identical titrant solution but with only buffer in the sample cell, was subtracted from each experimental titration. Enthalpy changes ΔH ≠ 0 at the end of the zinc titration (Figure 6B), which remain despite

comprehension of all necessary controls, are potentially due to nonspecific interactions of the titrant and the protein in the cell. Data analysis was performed using the ORIGIN (V7.0) software provided by the manufacturer (Microcal).

Thermofluor

For protein melting temperature determination 5 μ l of 2 mg/ml protein solution (wild-type or mutant) were mixed in a 96-well PCR plate with 45 μ l of 40 mM HEPES pH 7.5, 150 mM NaCl, 4 mM DTT and 35x SYPRO Orange (Invitrogen). The plate was sealed, heated in increments of 0.5°C in a real-time PCR system (Eppendorf) from 20°C to 80°C and the fluorescence changes were monitored. The wavelengths for excitation and emission were 470 and 550 nm, respectively. Finally, the data were fitted with a Boltzmann model to obtain the temperature midpoint of the protein unfolding transition (T_m).

Liquid Chromatography Electrospray Ionization Mass Spectrometry Analysis of Proteins Kept under Reducing and Nonreducing Conditions

Wild-type and mutant mCRY1/mPER2 complexes were purified as described before and kept under reducing conditions (+ 4 mM DTT) or non-reducing conditions (no DTT, dialysis against aerated buffer) in 25 mM HEPES pH 7.5, 100 mM NaCl for 2 days. For removal of bound zinc, the wild-type complex was treated with 10 mM EDTA for several hours in the absence of DTT and zinc bound EDTA was removed by extensive dialysis. LC-MS analyses were performed on a Bruker micrOTOF connected to an Agilent 1100 HPLC system equipped with a diode array detector. Samples were separated on a Phenomenex Aeris 3.6 μ m C4 WIDEPOR column (100 \times 2.1 mm) with a gradient of 30% to 80% acetonitrile in H₂O with 0.05% TFA over 15 min. The obtained mass spectra were deconvoluted using Maximum Entropy.

Luciferase Complementation Assays

The luciferase complementation assays were performed essentially as described in [Czarna et al. \(2013\)](#). Briefly, HEK293 cells were transiently transfected with a pair of split firefly luciferase reporter constructs, i.e., mPER2 (wild-type or mutant versions) C-terminally fused to amino acids 2-416 of firefly luciferase and mCRY1 (wild-type or mutant versions) C-terminally fused to amino acids 398-550 of firefly luciferase. For normalization, a vector expressing renilla luciferase was co-transfected. After 44 hr luciferase activities were measured in cell lysates using the Dual-Luciferase Reporter Assay System (Promega). For data analysis firefly luciferase activity was normalized to the corresponding renilla luciferase activity. Equal expression of the variants of mCRY1 and mPER2 fusion proteins was analyzed by Western Blot. The primary antibodies were anti-mCRY1 and anti-mPER2 antibodies generated in our laboratory, the secondary antibody was donkey-anti-rabbit (Santa Cruz Biotechnology). To control equal loading the blot was re-probed with an anti- α -Tubulin antibody (Sigma Aldrich).

Analysis of Disulfide Bridges in mCRY1

We used a combination of the methods described by [Wu et al. \(2000\)](#) and [Templeton et al. \(2010\)](#). Briefly, HEK293 cells transiently transfected with wild-type N-terminally MYC-tagged mCRY1 were harvested 48 hr after transfection. To this end, cells were washed with PBS buffer, scraped and pelleted. The cell pellet was immediately frozen at -80°C until further processing. The cell pellet was resuspended in MOPS-G-buffer (25 mM MOPS (pH 7.1), 5 mM EDTA, 150 mM NaCl, 0.1% Igepal, 6 M guanidine HCl) containing 50 mM N-Ethylmaleimide (NEM) immediately after removal from the freezer to avoid oxidation by aerial oxygen. The resuspended cells were sonified and the crude extract was centrifuged to remove cellular debris.

The supernatant was transferred to a new reaction tube and incubated at room temperature for two hours. To remove excess NEM, the proteins were precipitated by addition of 4 volumes methanol and incubation at -20°C for at least one hour. The precipitate was washed five times with methanol. The pellets were dried, dissolved in MOPS-G-buffer and distributed to 4 reaction tubes. Two tubes were left untreated as controls, the others were treated with 20 mM DTT or 5 mM H₂O₂ and all tubes were incubated at room temperature for one hour. To remove DTT and H₂O₂ proteins were precipitated by addition of 4 volumes methanol and incubation at -20°C for at least one hour. The precipitates were washed three times with methanol. The pellets were dried and subsequently dissolved in SEENS-buffer (0.1 M sodium phosphate (pH 6.5), 10 mM EDTA, 0.1% Nonidet P40, 3% SDS) containing 300 μ M Mal-PEG (Methoxypolyethylene glycol maleimide, Sigma Aldrich) and incubated at room temperature for one hour. One control sample was not treated with Mal-PEG. The samples were analyzed by Western blot with a neutral SDS-gel loading buffer and without boiling the samples to avoid unspecific reaction of Mal-PEG with amino-groups. The primary antibody was an anti-MYC-Antibody (9E10, Santa Cruz Biotechnology), the secondary antibody was goat-anti-rabbit (Santa Cruz Biotechnology). The blot was re-probed with an anti-Actin antibody (Sigma Aldrich).

Live-Cell Zinc-Binding Assay

Lentiviruses delivering either wild-type mCRY1 and mPER2 or the mutant versions of mCRY1 (C412A/C414A) and mPER2 (C1210A, C1213A) as split luciferase hybrids in the pLenti6 backbone (Invitrogen) were produced in HEK293T cells as previously described ([Maier et al., 2009](#)). Virus containing supernatants were cleared using Filtropur S micro filters (Sarstedt). Human U2-OS cells were transduced in the presence of 8 μ g/ μ l protamine sulfate (Sigma Aldrich) followed by positive selection with blasticidine (10 μ g/ml) (Invitrogen). U2-OS cells stably expressing mCRY1 and mPER2 split luciferase fusions (wild-type or mutant versions) were kept

for at least 1 week in zinc depleted medium prior to zinc ion addition in the range of 0 to 300 μM . Bioluminescence was recorded using a TopCount luminometer (PerkinElmer) with a stacker unit with a sampling rate of about 30 min for several days.

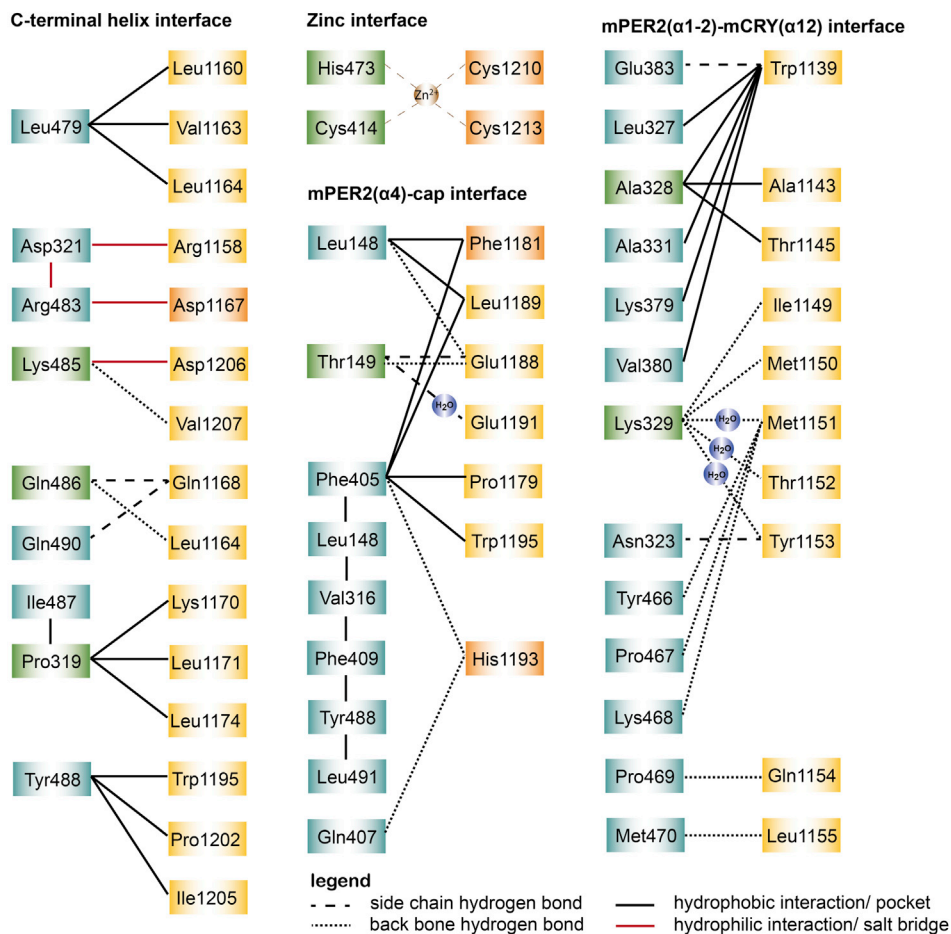
⁶⁵Zn-Binding Assay

HEK293 cells were cultured over 5 days in zinc-free DMEM (Invitrogen) supplemented with 10% of dialyzed fetal bovine serum (GIBCO, Invitrogen), 100 U/ml penicillin, 100 $\mu\text{g}/\text{ml}$ streptomycin and 25 mM HEPES. Cells were transfected with equal amounts of plasmid DNA encoding either wild-type or mutant epitope-tagged mCRY1 or mPER2 with Lipofectamine 2000 Transfection Reagent (Invitrogen) according to the manufacture's protocol. 48 hr after transfection, cells were harvested in 500 μl co-IP buffer (20 mM Tris-HCl at pH 8.0; 140 mM NaCl; 1.5 mM MgCl_2 ; 1 mM TCEP; 1% Triton X-100; 10% glycerol) containing protease inhibitor cocktail (Sigma Aldrich). Lysates with overexpressed V5-tagged mPER2 constructs were incubated with anti-V5 antibody (R960-25, Invitrogen) and equivalent amounts of Protein G PLUS-agarose beads (Santa Cruz Biotechnology) overnight at 4°C under constant agitation. Beads were washed once in washing buffer (20 mM Tris-HCl at pH 8.0; 150 mM NaCl; 0.5% Igepal CA-630), mixed with the corresponding mCRY1 overexpressing or control lysates, incubated for 3 hr with 35 μM ⁶⁵ZnCl₂ radionuclide (325 kBq per assay, PerkinElmer) at room temperature under agitation. As control for background only beads and ⁶⁵ZnCl₂ in lysis buffer were used. Beads were washed 5 times in washing buffer, 1 ml of ULTIMA Gold (PerkinElmer) was added and scintillation was counted for 1 min in a Wallac 1400 DSA system.

SUPPLEMENTAL REFERENCES

- Adams, P.D., Afonine, P.V., Bunkóczi, G., Chen, V.B., Davis, I.W., Echols, N., Headd, J.J., Hung, L.W., Kapral, G.J., Grosse-Kunstleve, R.W., et al. (2010). PHENIX: a comprehensive Python-based system for macromolecular structure solution. *Acta Crystallogr. D Biol. Crystallogr.* 66, 213–221.
- Bergfors, T.M. (2009). *Protein Crystallization: Techniques, Strategies, and Tips*, Second Edition (La Jolla, CA: International University Line).
- Cowtan, K. (2006). The Buccaneer software for automated model building. 1. Tracing protein chains. *Acta Crystallogr. D Biol. Crystallogr.* 62, 1002–1011.
- da Silva, J.J.R.F., and Williams, R.J.P. (2001). *The Biological Chemistry of the Elements* (Oxford: Oxford University Press).
- Emsley, P., and Cowtan, K. (2004). Coot: model-building tools for molecular graphics. *Acta Crystallogr. D Biol. Crystallogr.* 60, 2126–2132.
- Goujon, M., McWilliam, H., Li, W., Valentin, F., Squizzato, S., Paern, J., and Lopez, R. (2010). A new bioinformatics analysis tools framework at EMBL-EBI. *Nucleic Acids Res.* 38 (Web Server issue), W695–W699.
- Kabsch, W. (1993). Automatic processing of rotation diffraction data from crystals of initially unknown symmetry and cell constants. *J. Appl. Cryst.* 26, 795–800.
- Krissinel, E., and Henrick, K. (2007). Inference of macromolecular assemblies from crystalline state. *J. Mol. Biol.* 372, 774–797.
- Maier, B., Wendt, S., Vanselow, J.T., Wallach, T., Reischl, S., Oehmke, S., Schlosser, A., and Kramer, A. (2009). A large-scale functional RNAi screen reveals a role for CK2 in the mammalian circadian clock. *Genes Dev.* 23, 708–718.
- McCoy, A.J., Grosse-Kunstleve, R.W., Adams, P.D., Winn, M.D., Storoni, L.C., and Read, R.J. (2007). Phaser crystallographic software. *J. Appl. Cryst.* 40, 658–674.
- Palmiter, R.D., and Findley, S.D. (1995). Cloning and functional characterization of a mammalian zinc transporter that confers resistance to zinc. *EMBO J.* 14, 639–649.
- Pattison, S.E., and Cousins, R.J. (1986). Kinetics of zinc uptake and exchange by primary cultures of rat hepatocytes. *Am. J. Physiol.* 250, E677–E685.
- Provencher, S.W., and Glöckner, J. (1981). Estimation of globular protein secondary structure from circular dichroism. *Biochemistry* 20, 33–37.
- Sievers, F., Wilm, A., Dineen, D., Gibson, T.J., Karplus, K., Li, W., Lopez, R., McWilliam, H., Remmert, M., Söding, J., et al. (2011). Fast, scalable generation of high-quality protein multiple sequence alignments using Clustal Omega. *Mol. Syst. Biol.* 7, 539.
- Terwilliger, T.C., Adams, P.D., Read, R.J., McCoy, A.J., Moriarty, N.W., Grosse-Kunstleve, R.W., Afonine, P.V., Zwart, P.H., and Hung, L.W. (2009). Decision-making in structure solution using Bayesian estimates of map quality: the PHENIX AutoSol wizard. *Acta Crystallogr. D Biol. Crystallogr.* 65, 582–601.
- Waterhouse, A.M., Procter, J.B., Martin, D.M.A., Clamp, M., and Barton, G.J. (2009). Jalview Version 2—a multiple sequence alignment editor and analysis workbench. *Bioinformatics* 25, 1189–1191.

A



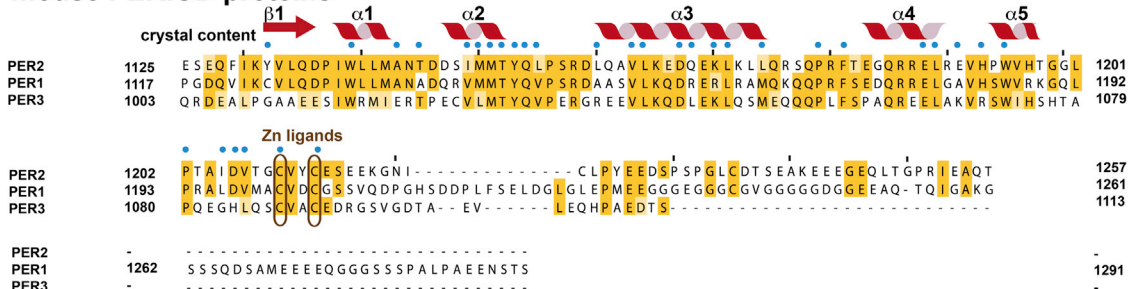
B

PER2



C

mouse PERIOD proteins



(legend on next page)

Figure S1. mCRY1/mPER2 Interactions and Sequence Alignments of mPER2, Related to Figures 1, 2, 5, and 7

(A) Schematic representation of mCRY1/mPER2 interface contacts. *C-terminal helix ($\alpha 22$) interface*: Central Interactions of Arg483, Lys485, Gln486, Gln490 (mCRY1 $\alpha 22$) and Asp321 (mCRY1 sulfur loop) are described in the main text. Asp321 also makes hydrophilic interactions to Arg1158 of mPER2. Additional hydrophobic interactions are established between Tyr488 (mCRY1 $\alpha 22$) and mPER2 residues Trp1195, Pro1202, Ile1205 and between Leu479 ($\alpha 22$) and mPER2 residues Leu1160, Val1163 and Leu1164. Pro319 (mCRY1 sulfur loop) packs into a hydrophobic pocket, which is lined by Ile487 (mCRY1 $\alpha 22$) as well as Lys1170, Leu1171 and Leu1174 of mPER2 $\alpha 3$. *Zinc interface*: Interactions are described in the main text. *mPER2($\alpha 4$)-cap interface*: Phe405 of the mCRY1 C-terminal lid is embedded in a hydrophobic pocket composed of Pro1179, Phe1181, Leu1189, Trp1195 of mPER2 and Leu148, Val316, Phe409, Tyr488 and Leu491 of mCRY1. Additionally, His1193_{mPER2} hydrogen bonds to the backbone of Phe405 and Gln407. Leu148 (mCRY1 $\alpha 5$ - $\alpha 6$ connector loop) makes hydrophobic interactions with Leu1189 and Phe1181 of mPER2. The side chain of Thr149 forms a direct hydrogen bond to Glu1188 and a water mediated hydrogen bond to Glu1191 of mPER2 $\alpha 4$. The backbones of Thr149 and Leu148 hydrogen bond to the Glu1188 side chain. *mPER2($\alpha 1$ -2)-mCRY1($\alpha 12$) interface*: The backbones of Tyr466 to Met470 in the loop preceding mCRY1 $\alpha 22$ as well as Lys329 and Asn323 (mCRY1 $\alpha 12$) are critical for positioning of mPER2 $\alpha 2$. Lys329 forms direct or water mediated hydrogen bonds to backbone oxygens of Ile1149 to Tyr1153 (mPER2 $\alpha 2$), while Asn323 forms a hydrogen bond to the Tyr1153 side chain. Ala328 is positioned opposite Thr1145 and Ala1143 in the loop connecting mPER2 helices $\alpha 1$ and $\alpha 2$. Trp1139 (mPER2 $\alpha 1$) hydrogen bonds to Glu383 (mCRY1 $\alpha 15$) and inserts into a hydrophobic cave, which is lined by Leu327, Ala328, Ala331 ($\alpha 12$) and Lys379, Val380 ($\alpha 15$) of mCRY1.

(B) Secondary structure assignment of mouse PER2 (mPER2) and alignment of its orthologs from *Homo sapiens*, *Gallus gallus*, *Xenopus laevis* and *Danio rerio*. Conserved residues are colored in dark yellow. Blue dots indicate mCRY1 interacting residues. Zinc coordinating residues are highlighted with brown boxes. Residues that were mutated for further analysis of the mCRY1/mPER2 interaction are labeled with black letters (Asp1167, Phe1181, His1193, Cys1210, Cys1213).

(C) Alignment of mPER2 and its homologs mPER1 and mPER3. The zinc coordinating residues Cys1210 and Cys1213 are conserved in mPER1 and mPER3. The alignments in Figures S1 and S2 were generated in ClustalOmega (Goujon et al., 2010; Sievers et al., 2011) and modified in Jalview (Waterhouse et al., 2009).

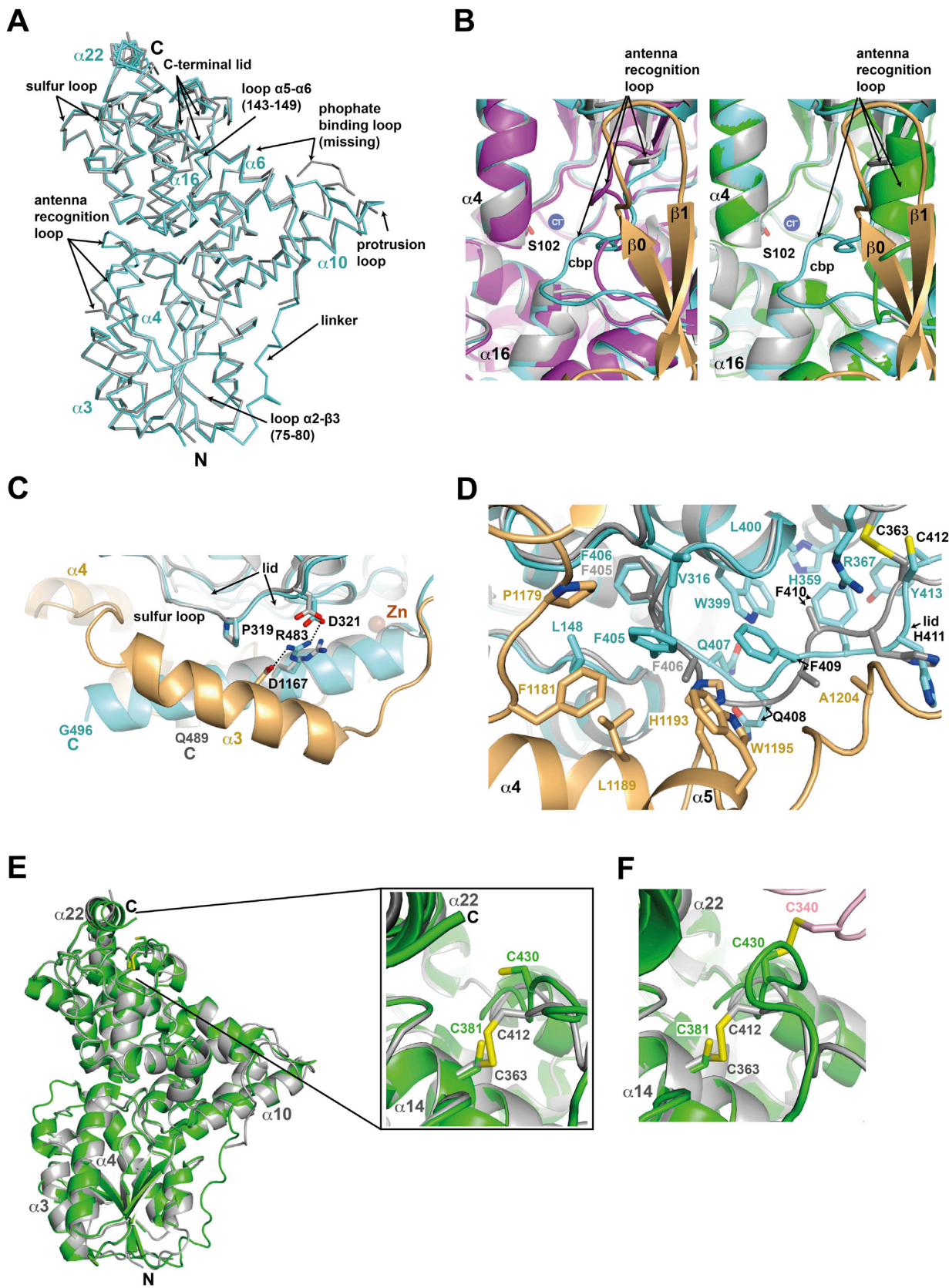
CRY



(legend on next page)

Figure S2. Sequence Alignment and Structural Elements of mCRY1, Related to Figures 1, 2, and 7

Secondary structure assignment of mouse CRY1 (mCRY1) and alignment of its homolog mouse CRY2 (mCRY2) and its orthologs from *Homo sapiens*, *gallus gallus*, *Xenopus laevis* and *danio rerio*. Conserved residues are colored in dark cyan. Green dots indicate mPER2 interacting residues. Zinc coordinating residues are highlighted with brown boxes. Residues that were mutated for further analysis of the mCRY1/mPER2 interaction are labeled with black letters (Thr149, Pro319, Ala328, Lys329, Cys363, Cys412, Cys414, His473, Lys485, Gln486).



(legend on next page)

Figure S3. Comparison of mPER2-Bound mCRY1 Structure with apo-CRY1, mCRY2, and dCRY, Related to Figures 2, 3, and 4

(A) Ribbon presentation of superposed apo-mCRY1-PHR (gray) and mCRY1-PHR (cyan) from the mCRY1/mPER2 complex structure (rmsd = 0.886 Å for 457 CRY C α positions). The antenna recognition loop (residues 39–46) as well as residues 167–177 in the linker region are unordered in the apo-mCRY1 structure, but well defined in the mCRY1/mPER2 complex. The C-terminal lid (Cys402 to Pro415) alters its conformation and the phosphate binding loop is less defined in the mPER2-complex structure. No significant changes are observed in the protrusion loop, the α 5- α 6 connector loop and the electron-rich sulfur loop.

(B) Superposition of the antenna recognition loop in the mCRY1/mPER2 complex (cyan/yellow) with (left) apo-mCRY1 (gray; pdb 4K0R [Czarna et al., 2013]) and dCRY (magenta; pdb 4JZY [Czarna et al., 2013]; rmsd = 1.427 Å for 439 CRY C α positions) and with (right) apo-mCRY2 (green, pdb 4I6E [Xing et al., 2013]). The ordered antenna recognition loop of the mCRY1/mPER2 complex reaches into the antenna chromophore binding pocket (cbp), but in a different position than the dCRY antenna recognition loop. mPER2 strands β 0 and β 1 are located nearby and may therefore influence the conformation of the antenna loop. Potentially, the coordination of a chloride ion (Cl⁻) by Ser102, which is located in the vicinity of the antenna chromophore binding pocket and which is a predicted phosphorylation site of mCRY1 (Lamia et al., 2009), affects the antenna recognition loop conformation in the mCRY1/mPER2 complex. Furthermore, a PEG molecule from the crystallization solution is located in the vicinity of the cbp (not shown). In apo-mCRY2 and FBXL3-bound mCRY2 (only apo-mCRY2 is superimposed for clarity) the antenna recognition loop forms a surface exposed α -helix that superimposes with β 0 and β 1 of mPER2 in our mCRY1/mPER2 complex structure (right).

(C) Superposition of the C-terminal helix α 22 of apo-mCRY1 (gray) and the mCRY1/mPER2 complex (cyan/yellow). Helix α 22 could be built to completeness in the complex structure. Arg483 forms a salt bridge to Asp321 in the sulfur loop, in the mPER2 complex additionally to Asp1167 (mPER2 helix α 3). Pro319 (sulfur loop) also interacts with mPER2 α 3.

(D) mCRY1-mPER2 (cyan/yellow) interface at the C-terminal lid with apo-mCRY1 (gray) superimposed. In the complex, Phe405 points away from the mCRY1-PHR body and embeds into a huge hydrophobic pocket composed of Pro1179, Phe1181, Leu1189, Trp1195 of mPER2 and Leu148, Val316, Phe409, Tyr488 and Leu491 of mCRY1 (Leu491 and Tyr488 are not shown for clarity.) In the apo-mCRY1 structure, Phe406 to Phe410 are built as alanine due their unordered side chains. In the complex, Gln407 and Gln408 are well defined and reorient to allow for backbone hydrogen bonding of His1193_{mPER2}. Phe410 embeds into a hydrophobic pocket composed of His359, Trp399, Leu400 and Try413 and forms a backbone hydrogen bond with the Arg367 side chain. His411 moves away from the mCRY1 body and forms a hydrogen bond with the backbone of Ala1204_{mPER2}.

(E) Superposition of apo-mCRY1-PHR (gray) and apo-mCRY2-PHR (green, pdb 4I6E [Xing et al., 2013]) (rmsd = 1.031 Å for 445 CRY C α positions). In contrast to the apo-mCRY1 structure, the disulfide bridge between Cys381 and Cys430 (corresponding to Cys363 and Cys412 of mCRY1) is broken in the apo-mCRY2 structure.

(F) Superposition of apo-mCRY1-PHR (gray) and mCRY2/FBXL3 (pdb 4I6J [Xing et al., 2013]; mCRY2 in green, FBXL3 LRR in light pink) (rmsd = 1.434 Å for 459 CRY C α positions). In the mCRY2/FBXL3 structure, Cys430 is in disulfide bridge distance to Cys340 of FBXL3 LRR.

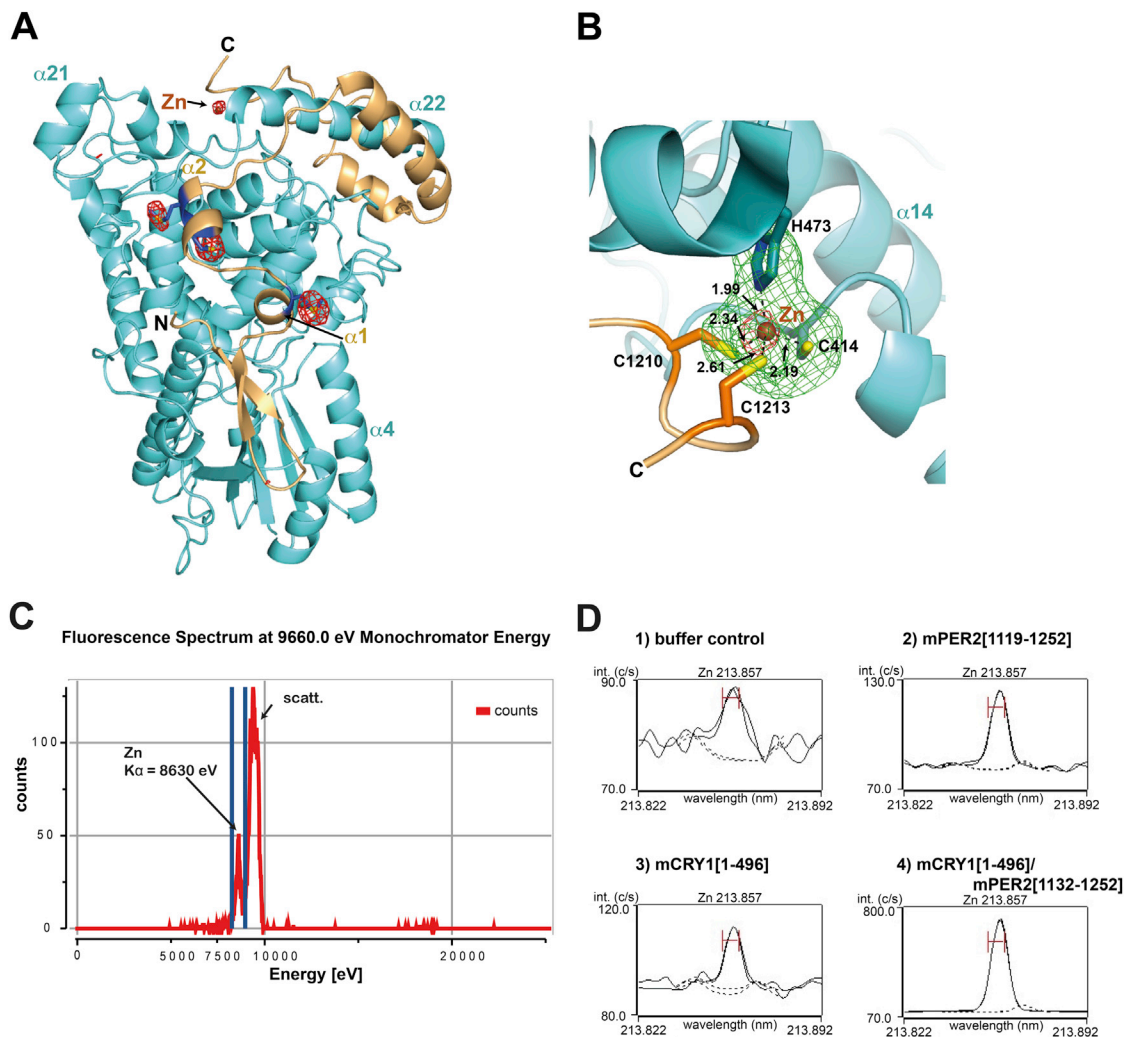


Figure S4. mCRY1/mPER2 Heterodimer Binds Zinc in the Crystal and in Solution, Related to Figures 2 and 6

(A) mCRY1/mPER2 complex (cyan/yellow) with selenium anomalous difference map. (Seleno)methionine residues of mPER2 (blue) are shown as atomic sticks. The selenium anomalous difference map (red, 4σ level) was calculated at 2.8 \AA resolution using anomalous differences of the peak wavelength ($\lambda_{\text{peak}} = 0.9763\text{ \AA}$). The N-terminal methionine as well as a methionine in the cloning overhang of mPER2 are disordered. An unexpected additional peak gave first evidence for the presence of a zinc ion (Zn, brown, see arrow) at the interface of CRY and PER.

(B) Close-up view of the zinc interface: The Fo-Fc omit map (2.8σ level, green) was calculated omitting the side chains of Cys414 and His473 (mCRY1) and Cys1210 and Cys1213 (mPER2) as well as the tetrahedrally coordinated zinc ion. The 2.8 \AA selenium anomalous difference map (λ_{peak}) showed density for Zn (4σ level, red).

(C) Identification of zinc in the mCRY1/mPER2 crystal by X-ray fluorescence spectroscopy. Zinc is unambiguously identified by its $\text{K}\alpha$ emission line at $8,630\text{ eV}$.

(D) Presence of zinc in mPER2, mCRY1 and the mCRY1/mPER2 complex in solution. 1) Control, buffer (25 mM HEPES pH 7.0, 100 mM NaCl, 2 mM DTT), 2) mPER2[1119-1252] individually purified from *E. coli*, 3) mCRY1[1-496] individually purified from insect cells, 4) mCRY1[1-496]/mPER2[1132-1252] complex, copurified from mixed lysates. Buffer and proteins were subjected to inductively coupled plasma optical emission spectrometry (ICP-OES) analysis. The signal intensities at the zinc-specific wavelength of 213.857 nm are shown. Only copurified mCRY1[1-496]/mPER2[1132-1252] complex binds zinc (strong signal), while single mCRY1 and mPER2 proteins are zinc-free in solution (weak signal).

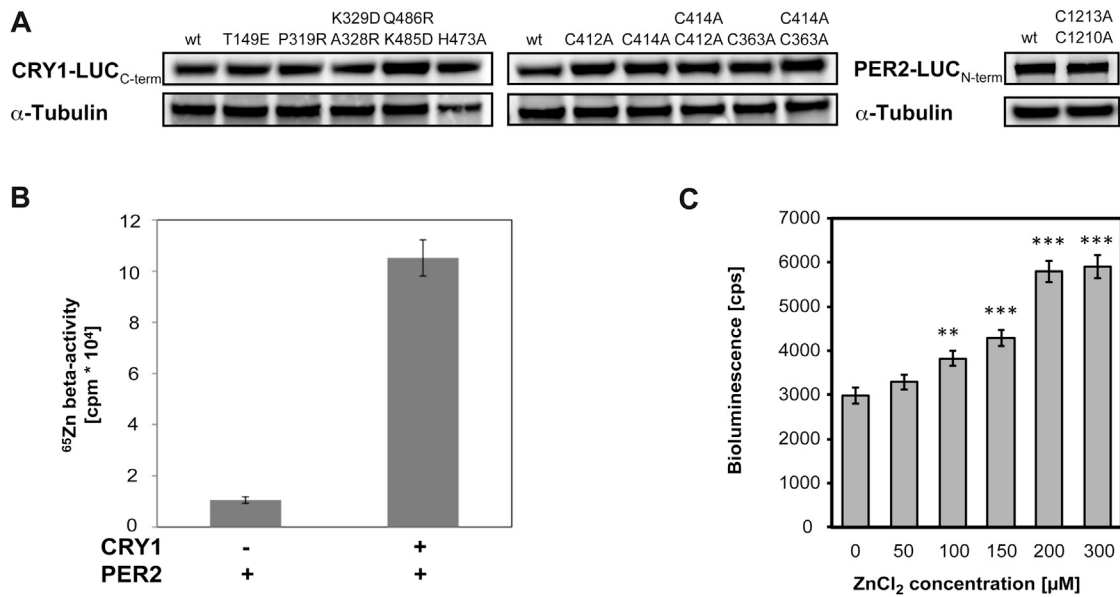


Figure S5. Zinc-Dependent mCRY1-mPER2 Interaction in Living Cells, Related to Figure 7

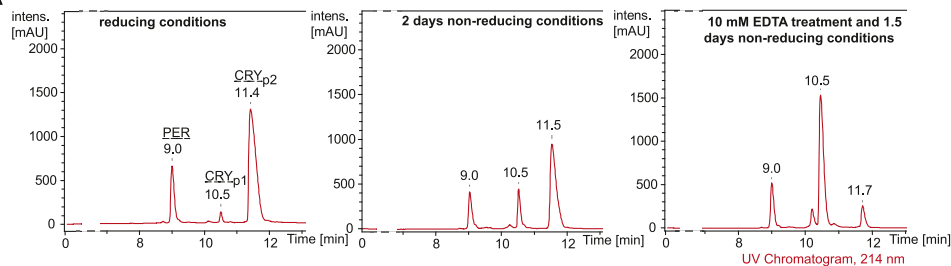
(A) Approximately equal expression of mCRY1 and mPER2 fusion protein variants in HEK293 cells demonstrated in western blot experiments.

(B) Incorporation of the radioactive zinc isotope $^{65}\text{Zn}^{2+}$ is dependent on the presence of both mPER2 and mCRY1. HEK293 cells were transiently transfected with full-length mPER2 or full-length mCRY1. Immunoprecipitated mPER2 was incubated with mCRY1-containing cell lysate or control cell lysate in the presence of the radioactive zinc isotope $^{65}\text{Zn}^{2+}$. mPER2 containing lysate alone incorporated significantly ($p < 0.0001$; t test) less radioactive $^{65}\text{Zn}^{2+}$ than when incubated with mCRY1 containing lysate. Shown are mean \pm SEM of four independent immunoprecipitation experiments. The high expression of proteins was verified in western blot experiments (not shown).

(C) Zinc ions dose-dependently enhance the mCRY1-mPER2 interaction in living cells. An U2-OS reporter cell line stably expressing mCRY1 and mPER2 split luciferase fusion proteins was cultivated in Zn^{2+} -depleted medium for about a week. Then various concentrations of Zn^{2+} were added to the medium and bioluminescence was analyzed after 10 hr. Shown are mean \pm SEM (** $p < 0.005$; *** $p < 0.0001$; t test; $n = 16$).

The Zn^{2+} concentration dependence of the split-luciferase signal with a half-maximal concentration around $150 \mu\text{M}$ probably reflects the replenishment of total cellular zinc ($100\text{--}500 \mu\text{M}$) (da Silva and Williams, 2001; Palmiter and Findley, 1995) in our previously zinc depleted cells. In addition, the observed kinetics are consistent with the observation that the rate of total zinc exchange is very slow (reported for hepatocytes to be ~ 30 hr by Pattison and Cousins [1986]).

A



ratio, area under peak:

CRY_{p2}/CRY_{p1}: 29.9

CRY_{wt}/PER_{wt}: 4.2

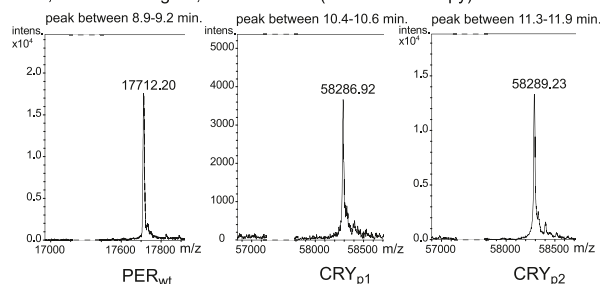
CRY_{p2}/CRY_{p1}: 4.1

CRY_{wt}/PER_{wt}: 4.7

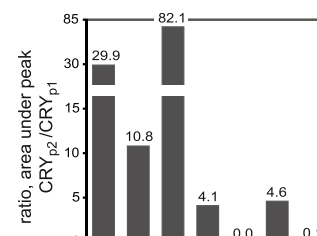
CRY_{p2}/CRY_{p1}: 0.1

CRY_{wt}/PER_{wt}: 4.4

+MS, -Constant Bkgrnd, Deconvoluted (maximum entropy)



D



CRY_{wt}/PER_{wt}

CRY_{wt}/PER_{CACA}

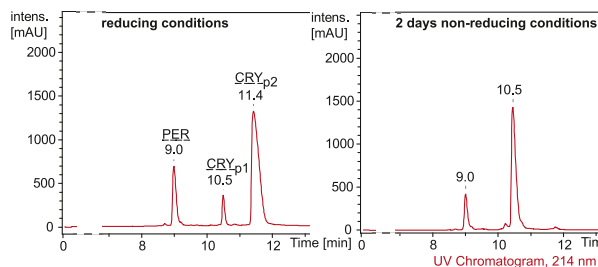
CRY_{C412A}/PER_{CACA}

red. cond.

non-red. cond.

EDTA + non-red. cond.

B



ratio, area under peak:

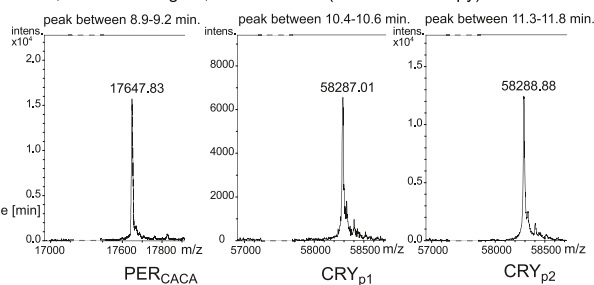
CRY_{p2}/CRY_{p1}: 10.8

CRY_{wt}/PER_{CACA}: 4.3

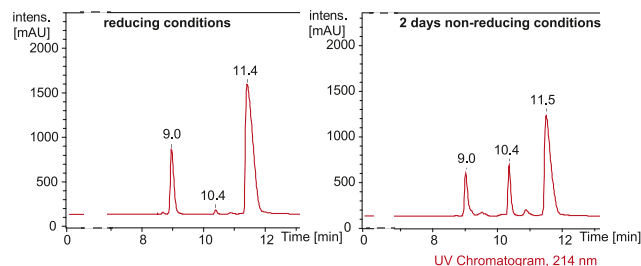
CRY_{p2}/CRY_{p1}: 0.0

CRY_{wt}/PER_{CACA}: 4.7

+MS, -Constant Bkgrnd, Deconvoluted (maximum entropy)



C



ratio, area under peak:

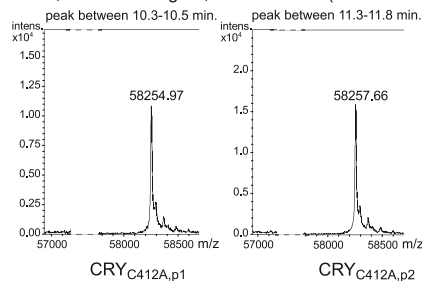
CRY_{p2}/CRY_{p1}: 82.1

CRY_{C412A}/PER_{CACA}: 4.2

CRY_{p2}/CRY_{p1}: 4.6

CRY_{C412A}/PER_{CACA}: 5.3

+MS, -Constant Bkgrnd, Deconvoluted (maximum entropy)



Footnote 1: the precision of mass analysis lies in the range of ± 1 Da

Footnote 2: mCRY1 is missing its N-terminal methionine, it was posttranslationally cleaved off

(legend on next page)

Figure S6. Liquid Chromatography Electrospray-Ionization Mass Spectrometry Analysis of WT and Mutant mCRY1[1–496]/mPER2[1119–1252] Complexes in Reducing and Nonreducing Conditions, Related to Figure 6

(A) HPLC chromatograms (top) and deconvoluted LC-MS spectra (bottom) for wild-type mCRY1/mPER2 complex. *Top*: HPLC chromatograms for the wild-type mCRY1/mPER2 complex. Left: reducing conditions (in presence of 4 mM DTT); middle: after 2 days in non-reducing conditions (no DTT, aerated buffer); right: after zinc removal by 10 mM EDTA treatment followed by 1.5 days in non-reducing conditions. Two mCRY1 species are observed with a retention time of 10.5 min (CRY_{p1}, putatively oxidized) and 11.4 min (CRY_{p2}, putatively reduced), respectively. While only a moderate increase in CRY_{p1} (p1 = peak 1) is observed after 2 days in non-reducing conditions, removal of zinc by EDTA almost completely shifts mCRY1 to peak 1. The third peak with the retention time of 9.0 min contains mPER2. (A–C) The ratios between the areas under mCRY1 peak 2 and peak 1 (CRY_{p2}/CRY_{p1}) are presented as a measure for the interconversion of the two mCRY1 species upon changing redox conditions or zinc removal. The ratios between the peak areas for total mCRY1 (sum of peaks p1 and p2) and total mPER2 (peak at 9.0 min) remain constant within the accuracy of the method. *Bottom*: Deconvoluted LC-MS spectra of the peaks detected for the wild-type mCRY1/mPER2 complex with (left) wild-type mPER2 (peak at 9.0 min retention) and (middle, right) wild-type mCRY1. A ~2 Da mass difference (as expected for the oxidation of a disulfide bridge) is determined for the two CRY species corresponding to the peaks with retention times of 10.5 (CRY_{p1}) and 11.4 (CRY_{p2}) minutes.

(B) HPLC chromatograms and deconvoluted LC-MS spectra for the zinc-free mCRY1/mPER2(C1210A/C1213A) complex. HPLC chromatogram for the mCRY1/PER2(C1210A/C1213A) complex under reducing conditions (left) and after 2 days in non-reducing conditions (2nd from left). After 2 days in non-reducing conditions, wild-type mCRY1 completely shifts to peak 1 (CRY_{p1}, putatively oxidized). Three right panels: Deconvoluted LC-MS spectra for the mPER2(C1210A/C1213A) mutant protein (PER_{CACA}, peak at 9.0 min retention time) and for the two wild-type mCRY1 species in peak 1 (CRY_{p1}) and peak 2 (CRY_{p2}).

(C) HPLC chromatograms and deconvoluted LC-MS spectra for the zinc-free mCRY1/mPER2 complex with alanine mutations in the zinc binding Cys1210 and Cys1213 of mPER2 and in the disulfide bond forming Cys412 of mCRY1. HPLC chromatogram for mCRY1(C412A)/PER2(C1210A/C1213A) complex under reducing conditions (left) and after 2 days in non-reducing conditions (2nd from left). The mCRY1(C412A) mutant protein only shows a moderate increase of CRY peak 1 (CRY_{C412A,p1}) after 2 days in non-reducing conditions. Two right panels: Deconvoluted LC-MS spectra for the two mCRY1(C412A) mutant species in peak 1 (CRY_{C412A,p1}) and peak 2 (CRY_{C412A,p2}). We postulate that the CRY_{C412A,p1} peak observed under non-reducing conditions in the mCRY1(C412A) mutant protein is due to the presence of an additional disulfide bridge.

(D) Histogram displaying the ratios between the areas under peak 2 (CRY_{p2}, assigned to reduced mCRY1) and peak 1 (CRY_{p1}, assigned to oxidized mCRY1) obtained for wild-type and mutant mCRY1[1–496]/mPER2[1119–1252] complexes under different conditions (Figure S6 A–C). The redox state of mCRY1 is influenced by the presence of zinc in the complex. The behavior of the zinc-free mCRY1(C412A)/mPER2(C1210A/C1213A) complex mirrors that of the wild-type mCRY1/mPER2 complex, suggesting that Cys412 is involved in zinc-dependent redox changes in mCRY1.

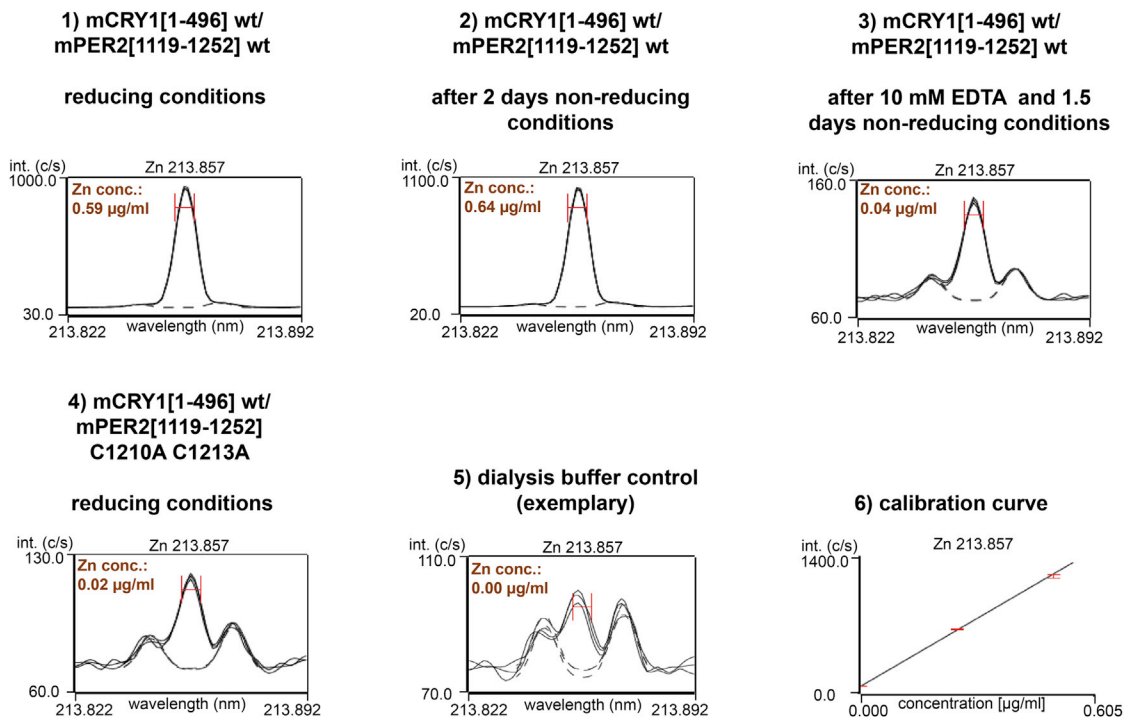


Figure S7. Zinc Content of the mCRY1/mPER2 Complex in Solution, Related to Figure 6

(1) Wild-type mCRY1[1-496]/mPER2[1119-1252] complex (8.8 μ M), copurified from mixed lysates and kept under reducing conditions (4 mM DTT), 2) mCRY1[1-496]/mPER2[1119-1252] complex (9.5 μ M), copurified from mixed lysates and kept under non-reducing conditions for 2 days (no DTT, aerated buffer), 3) mCRY1[1-496]/mPER2[1119-1252] complex (7.65 μ M), copurified from mixed lysates, treated with 10 mM EDTA for several hours and kept under non-reducing conditions for additional 1.5 days (no DTT, aerated buffer), 4) mCRY1[1-496]/mPER2[1119-1252] complex with alanine mutations in mPER2 Cys1210 and Cys1213 (8.8 μ M) copurified from mixed lysates and kept under reducing conditions (4 mM DTT), 5) Control, dialysis buffer (25 mM HEPES pH 7.5, 100 mM NaCl). Buffers and proteins were subjected to inductively coupled plasma optical emission spectrometry (ICP-OES) analysis. The signal intensities at the zinc-specific wavelength of 213.857 nm are shown. Copurified wild-type mCRY1[1-496]/mPER2[1119-1252] complex contains zinc in a \sim 1:1 molar ratio. After extensive dialysis in aerated buffer over 2 days, zinc is still bound to the wild-type complex. 10 mM EDTA treatment followed by extensive dialysis almost completely depleted the wild-type complex from zinc. mCRY1/mPER2 complex with alanine mutations in mPER2 Cys1210 and Cys1213 does not bind zinc. Zinc concentrations were calculated based on a calibration curve (6).

Table S1. X-Ray Data Collection and Refinement Statistics,
Related to Figure 1

Data collection	Native	SAD
	mCRY1 [1-496]/ mPER2 [1132-1252]	mCRY1 [1-496]/ mPER2* [1132-1252]
Beamline	SLS PXII	SLS PXII
Space group	P4 ₃ 2 ₁ 2	P4 ₃ 2 ₁ 2
<u>Cell dimensions</u>		
a, b, c (Å)	99.74, 99.74, 178.63	99.53, 99.53, 178.66
α, β, γ (°)	90, 90, 90	90, 90, 90
Wavelength (Å)	0.9716	0.9763
Resolution range (Å) ^a	45.50 – 2.45 (2.55 – 2.45)	30.00 – 2.80 (2.85 - 2.80)
Number of reflections		
Total	853563	2375575
Unique	33988	42277
Completeness (%) ^a	100 (100)	100 (100)
I/σ ^a	35.0 (3.6)	25.9 (2.2)
R _{sym} (%) ^a	5.7 (105.3)	20.9 (242.1)
Wilson plot B (Å ²)	68.4	66.7
Refinement		
Resolution range (Å)	45.50 – 2.45	
Reflections	33913	
R _{cryst} (%)	18.60	
R _{free} (%) ^b	23.31	
Ramachandran values		
Favored region (%)	94.3	
Allowed region (%)	100	
Overall average B factor (Å ²)	69.8	
R.m.s.d bond lengths (Å)	0.009	
R.m.s.d. bond angles (°)	1.125	

* selenomethionine labelled

^a Values in parenthesis correspond to the highest resolution shell.

^b The Free-R factor was calculated with 5 % of the data omitted from structure refinement.

Table S2. CD Spectra Suggest That the Unbound C-Terminal mPER2 Region Is Mainly Unstructured; upon Binding to mCRY1-PHR, It Adopts a Helical Fold, Related to Figure 5

Fractions Protein	H (dis- torted)	S (dis- torted)	Turn	Unordered	RMSD	NRMSD
mPER2 [1132-1252]	0.15 (0.12)	0.21 (0.11)	0.25	0.38	0.10	0.032
mCRY1 [1-496]/ mPER2 [1132-1252]	0.50 (0.22)	0.05 (0.04)	0.20	0.25	0.13	0.036
mCRY1 [1-500]*	0.31	0.17	0.22	0.30	0.06	0.025

(N)RMSD = (normalized) root mean square deviation
H = helices, include regular and distorted α -helices
S = strands, include regular and distorted β -strands
* = values were determined by Czarna et al., 2013

4 Extended Discussion

Crystal structure analysis in combination with single particle electron microscopy (EM), small angle X-ray scattering (SAXS) and complementary biochemical methods unraveled the clock mechanism in cyanobacteria, which is governed by the Kai proteins, KaiA, KaiB and KaiC. Crystal structures visualized not only the single Kai proteins but also their interaction in subcomplexes as well as regulatory phosphorylation sites. EM and SAXS allowed the real-time quantification of evolving Kai subcomplexes in the course of a circadian cycle. The combined model now shows that the circadian cycle is driven by conformational changes in KaiC through sequential interaction with KaiA and KaiB as well as ATP dependent auto-phosphorylation and dephosphorylation of KaiC, respectively (Egli and Johnson, 2013; Johnson et al., 2011). Although the power of structural analysis to provide explanations for biological mechanisms was also proven for many other processes before, structural analysis of circadian clocks is only slowly evolving and still particularly missing multicomponent complex structures. In the case of mammalian clock proteins, the crystal structure of the CLOCK/BMAL1 heterodimer visualizes the stable and active interaction of the two transcription factors mediating rhythmic transcription of clock-and clock controlled genes (Huang et al., 2012). Apart from that, the recently solved mCRY2-FBXL3-SKP1 complex structure shows how FBXL3 targets mCRY2 for degradation (Xing et al., 2013). The crystal structure of the mPER2 PAS domains did not only visualize and explain important mPER2 residues reported in literature but also shed light on the mPER2 dimerization surface and its impact on a functional clock (Hennig et al., 2009). Recently, the apo-mCRY1 structure allowed for first insight into the FBXL3/CLOCK-BMAL1/PER2 binding to CRY1 through structure-based mutagenesis (Czarna et al., 2013).

The crystal structures of the mouse PER1 PAS domains and the core mouse CRY1/PER2 complex, which were solved in the course of this study, will further advance the structural reconstruction of the mammalian clock and will allow to design future experiments. For now, they allow a complete and detailed structural description of two essential interaction sites of mammalian PERIOD proteins; the homo- and heterodimerising PAS domains and the CRY interaction domain. Results from complementary biochemical, biophysical and cell based assays as well as the analysis of already known PER structures and literature helps I) to identify and understand the differences between the three mammalian PER proteins PER1, 2 and 3, II)

to illustrate potential mechanisms for CRY/PER complex formation and regulation for clock transcriptional feedback repression and III) to speculate on mechanisms driving the circadian cycle. The following sections discuss novel observations and results in the context of the circadian clock and speculate on their significance for the mammalian oscillator. The final section names open questions and gives an outlook on questions to be addressed in the future (section 5).

4.1 *In Vitro* Characterization of Mammalian PERIOD Proteins

Stable full-length mouse PERIOD protein expression and purification for crystallization is currently neither possible in *E. coli* nor in insect cell culture most likely because they contain long, unfolded regions which do not adopt a stable tertiary structure. However, rational design of protein fragments based on sequence alignment and secondary structure prediction permitted the expression and purification of the N-terminal PAS domains of mPER1 (and nearby residues) as well as the \approx 500 C-terminal residues of mPER2 which were, in complex with full-length mCRY1, further processed by limited proteolysis for definition of the mCRY1/mPER2 core complex. The PAS domains of mPER2 were described elsewhere before (Hennig et al., 2009). The PAS domains of mPER3 were examined in a parallel study (see (Kucera et al., 2012)). In solution both the mPER1 PAS domains and mCRY1-mPER2 form a stable homo- and heterodimer, respectively.

4.2 A Conserved Tryptophan as Mediator of Clock PAS Interactions

The crystal structure of the PAS domains of mPER1 reveals that the PAS-B domains are aligned in an antiparallel manner in the mPER1 homodimer. Mutational analysis confirms that mPER1 homodimer is essentially stabilized by symmetric interactions of the antiparallel PAS-B β -sheet surfaces and the connecting loops, one of which includes Trp448_{mPER1} (PAS-B Trp (tryptophan) interface), which is highly conserved among PER proteins. Trp448_{mPER1} stabilizes the homodimer mainly through hydrophobic interactions. A similar interface is present in the mPER2 and mPER3 PAS homodimer. This is not surprising as not only the central tryptophan (Trp419_{mPER2}, Trp359_{mPER3}) is conserved among PER1-3 but most PER residues in PAS-B (Figure 3.1_S1/S3).

Luciferase complementation assays in HEK293 cells (performed in collaboration with the group of Prof. Dr. Achim Kramer, Charité, Berlin) support the importance of this PAS-B Trp interface for the homodimerization of mPER1, 2 and 3 (Figure 3.1_2) in mammalian cells. Our preliminary *in vitro* data (not shown) imply that the PAS-B Trp interface is probably also important for PER heterodimer formation. PER dimerization and the CRY-PER interaction have been described to be decisive for the determination of the subcellular localization of the repressor complex. Therefore, it would be interesting to examine the effects of the W448E (or corresponding mutations in mPER2/3) mutation on subcellular localization of mPER1 (mPER2/3, respectively) and consequently CRY. Similarly, we speculate that the PAS-A - PAS-B/ α E interface in mPER2, which is absent from mPER1, modulates an active NES, which is conserved in all PER paralogs in the α E helix (Figure 3.1_S1). This would explain why the mutation of the interaction stabilizing methionine to lysine within the NES of mPER2 alters its nuclear export activity in fusion with a non-related protein, whereas mutation of the equivalent solvent exposed leucine to lysine in mPER1 has no significant effect (Vielhaber et al., 2001). Accordingly, heterodimerization of mPER3 has been implicated with nuclear localization of PERs by masking the active CLD (cytoplasmic localization domain) of mPER3. As the CLD of mPER3 comprises the PAS-B Trp interface, heterodimerisation with mPER1 and PER2 via the PAS-B Trp interface would explain this masking effect.

Interestingly, the structure based analysis of the mCLOCK/mBMAL1 heterodimer by Huang et al. confirms not only that Trp448_{mPER1} is conserved in the PAS domains of BMAL1 (Trp427_{BMAL1}), but also reveals an apparently conserved, hydrophobic interaction mediating role of Trp427_{BMAL1} (corresponds to Trp448_{PER1}) as it binds to CLOCK (Huang et al., 2012). However, Trp427_{BMAL1} in the PAS-B domain of BMAL1 mediates a compositionally different interface with PAS-B of CLOCK as the PAS domains of CLOCK and BMAL1 encompass a parallel structural arrangement of their PAS-B domains. The corresponding tryptophan in CLOCK (Trp362_{CLOCK}) was implied to be involved in the interaction with cryptochromes (Sato et al., 2006); NPAS2, the mammalian CLOCK homolog, also contains the conserved Trp. Moreover, a tryptophan is conserved at the same position in dPER (Trp482_{dPER}) and in dCYCLE, the functional homolog of BMAL1, but not in dCLOCK. In the crystal structure of the dPER PAS domains (Yildiz et al., 2005), Trp482_{dPER} is involved in a PAS-A – PAS-B homodimer interface residing in a hydrophobic pocket (compare Figure 7). As the PAS-B β -sheet surface, which is part of the PAS-B Trp interface in mPER and which supposedly mediates dPER-dTIM interaction

in *Drosophila* (Hennig et al., 2009), is in close proximity to Trp482_{dPER}, it is possible that Trp482_{dPER} switches to regulate homo- and heterodimerization of dPER. Likewise, heterodimerisation of dTIM with dPER probably covers the CLD in PAS-B β -sheet surface of dPER (Saez and Young, 1996) and promotes nuclear import of the complex (functional homologue of mammalian CRY/PER complex).

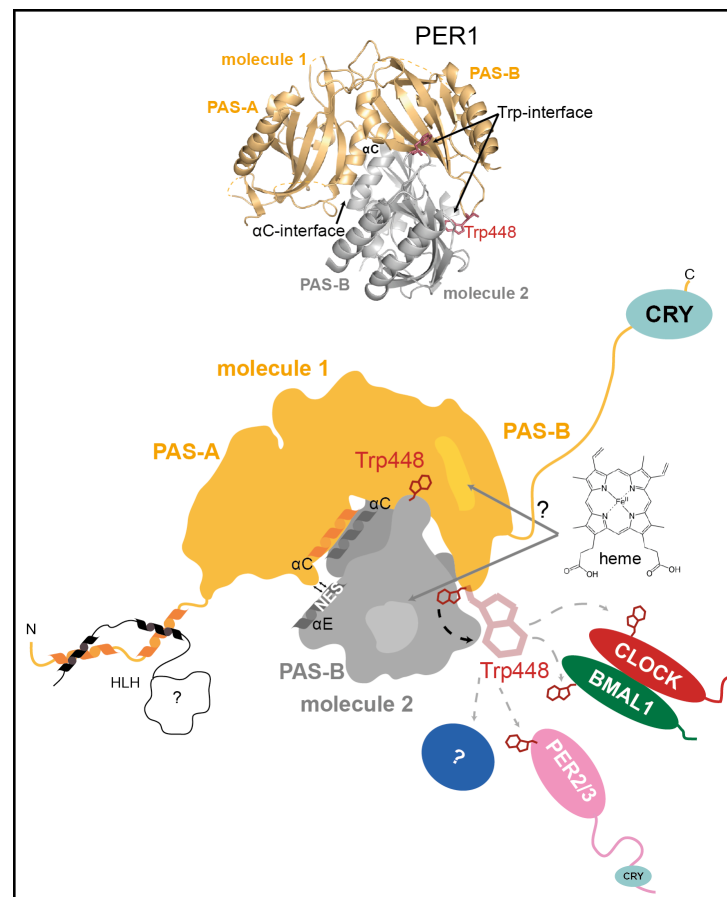


Figure 13: The PAS domains of PER1 and its potential protein interactors and ligands. The conserved Trp448 might allow for interaction with other clock (PAS) proteins. Whether PER1 coordinates heme in its PAS domains *in vivo* is not clear, yet.

This shows that Trp448_{mPER1} is conserved among the core mammalian PAS clock proteins and to most extent among the PAS clock proteins in the related *Drosophila* oscillator. However, it is not generally conserved among (HLH-) PAS proteins. It mediates PAS-PAS and maybe PAS-protein interactions in different conformations and interfaces. In the case of dPER this results in an obviously different open ring like homodimer PAS conformation compared to the perpendicularly stacked domains in the mPER homodimer. Thus, the conserved tryptophan of

mammalian clock PAS proteins could be a common interaction mediator of clock PAS proteins. More importantly, as mPER2 supposedly interacts with the PAS domains of BMAL1, the conserved tryptophan is a good candidate interaction site. The similar spatial arrangement of the single PAS-AB domains of BMAL1 compared to those of mPER further supports this idea (first noticed by (Huang et al., 2012)) (summarized in Figure 13).

4.3 Mammalian PER - a Heme Bound Signal Sensor or not?

The activity of the clock protein NPAS2 (and REV-ERB α/β , section 1.3) was shown to be regulated through binding of a heme cofactor in its PAS domains. In NPAS2, heme senses carbon monoxide, a degradation product of heme, and supposedly induces the dissociation of the NPAS2/BMAL1 transcription factor complex from DNA and consequently repression of protein expression (Dioum et al., 2002). Like REV-ERB, NPAS2 has been implicated with the regulation of *Alas-1* expression, the key enzyme of heme biosynthesis, i.e. NPAS regulates the expression of its own ligand in a negative feedback loop and modifies the clock according to heme metabolism. Recently, it was demonstrated that both PAS domains of PER2 bind to heme, too. Heme is suggested to modulate the effect of mPER2 (and to lesser extent of mPER1) on NPAS2 transcriptional regulation (Kaasik and Lee, 2004) possibly through heme exchange between NPAS2 and mPER2 (Kitanishi et al., 2008). The structure of the mPER1 PAS domains also allows to assess the chances of heme binding to mPER1. In mPER2 PAS-A Cys215 and Cys270 have been identified as two potential heme coordinating residues. Both residues are present and conserved in mPER1 (Cys244, Cys299). In mPER3 Cys215, however, is changed to serine (Ser156). Structure overlay of mPER1 (and mPER2) with FixL and EcDOS, two known heme binding PAS proteins, suggest that heme binding to PER PAS domains is generally possible but needs rearrangement of the α C helix, the β C sheet and their interjacent loop (Figure 3.1_S1) though co-coordination of heme by Cys244 and Cys299 seems structurally unlikely. For the PAS-B domain of mPER2 a methionine/histidine or bis-histidine coordination of heme was suggested, which is not investigated in detail and thus cannot be related to mPER1 (Yang et al., 2008). As the mPER2 PAS fold is more flexible, heme binding is most likely occurring in and stabilizing the PER2 PAS domains. Nevertheless, our UV/VIS spectroscopic analysis suggests heme binding for mPER1 PAS and mPER3 PAS as well (Figure 3.1_S7).

In contrast, Airola et al. question specific heme binding to the core of the PER PAS domains.

Most of the evidence for PER PAS heme binding provided in literature is based on *in vitro* experiments. Their experimental comparison of known heme binding proteins with non-heme binding proteins for their heme binding capacity as well as a mutational analysis convincingly indicates that common *in vitro* assays like UV/Vis spectral analysis do not allow to differentiate between specific and non-specific binding. Moreover, in contrast to mammalian PERs, NPAS2 and REV-ERB copurify with their heme ligand from the *E. coli* expression system (Airola et al., 2010). No *in vivo* data underlining heme binding to and importance for PER was published so far.

Apart from heme binding to the PER2 PAS domains, at least one HRM (heme regulatory motif) was suggested in the C-terminal domain of hPER2 (conserved in mPER2) which contains the cryptochrome binding site (Figure 5). HRMs are thought to regulate the activity of proximate domains in dependence of heme binding. For instance, Bach-1, which is the transcriptional repressor of heme oxygenase-1, is modulated according to heme binding to its HRMs (Suzuki et al., 2004) or the heme-regulated eIF2 kinase which regulates translation to balance synthesis of heme and globulins during erythroid differentiation (Chen, 2007). HRMs usually consist of a Cys-Pro dipeptide at position two and three, in which the cysteine essentially ligates heme, and a preferred hydrophobic residue at position 4. Two HRMs have been identified in hPER2 which are mainly conserved in mPER2 but not in mPER1 and mPER3 (SC⁸⁴¹PA (hPER2) = SC⁸³⁰PS (mPER2) and AC⁹⁶²PA (hPER2) = AC⁹⁵⁶PV (mPER2)), while only SC⁸⁴¹PA (hPER2), which is located in a conserved patch of hPER2, was described to effectively influence hPER2 function. Binding of heme to Cys⁸⁴¹ (hPER2) supposedly inhibits cryptochrome binding and stabilization of hPER2. Consequently, hPER2 is ubiquitinated and degraded. Thereby, heme binding to the HRM of hPER2 was implied to influence circadian gene expression, too. Different from the PAS domains, the HRMs of hPER2 exclusively bind ferric heme and thus potentially act as a redox sensor (Yang et al., 2008). Strikingly, our structural analysis of mCRY1/mPER2 revealed that amino acids 1132-1214 of mPER2 mediate interaction with mCRY1² (section 3.2). The stable expression of a protein fragment comprising the SC⁸³⁰PS HRM of mPER2 failed, however, affinity measurements and limited proteolysis of a mPER2 fragment comprising residues 849-end with full-length mCRY1 suggest that, if at all, residues 849-1132

² As sequence analysis of hPER2 and mPER2 depicts a total sequence identity of 80 % which strongly suggests the existence of homologous CRY1/PER2 complexes in human and mouse, the mouse CRY1/PER2 structure can be applied for evaluation of data from human protein analysis.

are, like residues 1215-1257, only weakly in contact with mCRY1 (data not shown). That means that the HRM of mPER2 probably regulates mPER2 binding to mCRY1 in an indirect manner but not through a heme associated changed conformational state of mPER2 which was already excluded by CD (circular dichroism) analysis earlier (Yang et al., 2008).

Moreover, Yang et al. found evidence for a third binding heme binding site located between residues 1121-1255 (1123-1257 mPER2) of hPER2 which comprise the core CRY1 binding site of PER2. Interestingly, the only cysteine residues within this amino acids stretch are those cysteines, that are involved in zinc coordination in the CRY1/PER2 complex (Cys1210 and Cys1213 (section 3.2 and 4.4)). Strikingly, Cys414, which is one of the two opposite zinc coordinating residues of mCRY1, is residing in the amino acid stretch HCYC⁴¹⁴PVG, which also contains the typical heme coordinating cysteine-proline motif (first notified by (Okano et al., 2009)). As the zinc interface critically stabilizes CRY1-PER2 interaction, it is well possible that binding of heme to the zinc coordinating residues interferes with PER2 binding to CRY1. However, it remains to be answered whether heme binding to the C-terminus of PER2 is specific or not like in case of the PER PAS domains. Since the HRMs are not conserved in mPER1 and mPER3 and heme binding to the PER PAS domain most likely occurs in mPER2, heme binding would distinguish mPER2 from mPER1 and mPER3 within the circadian oscillator and establish it as a cellular redox sensor.

4.4 Zinc Binding and Disulfide Bond Formation Regulates the mCRY1/mPER2 Core Complex

The PER PAS domains are most probably not directly involved in CRY/PER core complex formation, although there is a hint that the N- and C-terminus of PER2 approach each other in a cellular context (section 3.1) (Tsuchiya et al., 2009). PER2 binds to CRY via its C-terminal 100 amino acids. Limited proteolysis readily allowed to crystalize the photolyase homology region of mCRY1 (mCRY1[1-496]) (PHR) in complex with mPER2[1132-1252] and to solve the structure at 2.45 Å resolution. The mCRY1/mPER2 crystal structure (Figure 3.2_1) shows an intimate and high affinity protein complex, in which the C-terminal residues 1132-1214 of mPER2 literally wind around the α -helical domain of mCRY1 adopting a stable, mainly helical fold. mCRY1 sustains its typical photolyase homology fold which was already described for the apo-protein (Czarna et al., 2013). However, mPER2 binding substantially stabilizes its fold as depicted e.g. in

the C-terminal helix $\alpha 22$ and the lid as well as in the antenna recognition loop, the phosphate-binding loop and the linker region of mCRY1 (Figure 3.2_S3A). The C-terminal, non-conserved tail of CRY is not involved in interaction with mPER2 (Figure 3.2_5). Interaction of mCRY1 and mPER2 is established by four main interfaces (C-terminal helix interface, mPER2($\alpha 4$)-cap interface, mPER2($\alpha 1-2$)-mCRY1($\alpha 12$) interface, zinc interface, Figure 3.2_2). These include amino acids of 1179–1198 in mPER2 helix $\alpha 4$ as well as mCRY1 helix $\alpha 22$, which have been reported to be essential for interaction in cell-based assays before (Ozber et al., 2010; Tomita et al., 2010).

Strikingly, structural analysis revealed a novel zinc interface in which residues Cys414 and His473 of mCRY1 and residues Cys1210 and Cys1213 of mPER2 co-coordinate a zinc ion which, according to our biochemical and structural analysis, probably structurally facilitates the reduction of a nearby located disulfide bond and thereby essentially stabilizes the mCRY1/mPER2 complex. Indeed, our results suggest that zinc release favors disulfide bond formation in CRY which probably weakens the mCRY1/mPER2 complexes (Figure 3.2_S6/S7). Despite several potential proximate cysteines, the disulfide bond that is most likely to be formed is the disulfide bond between Cys363 and Cys412 of mCRY1, which was already observed in the crystal structure of apo-mCRY1 (Czarna et al., 2013). Both the coordination of a zinc ion between two different proteins as well as the stabilizing effect of zinc coordination on the reduced state of nearby cysteines are unusual. Although speculative, the zinc coordination site and the nearby located disulfide bond possibly act as a redox sensitive switch for regulation of the mCRY1/mPER2 complex in a mode different and yet unclear from traditional protein zinc redox switches.

Usually oxidative or disulfide stress leads to disulfide bond formation of the zinc coordinating cysteine residues in intramolecular zinc binding and redox sensing proteins. This is followed by zinc release and reversible activation or inactivation of the proteins (redox zinc switch) (Maret, 2006). For instance, the C-terminal zinc coordinating domain of chaperone Hsp33 unfolds as a result of cysteine oxidation. This probably uncovers a homodimerisation interface and its substrate binding site. Hsp33 dimers are active and hold proteins off from oxidative stress induced inactivation or aggregation (Ilbert et al., 2006). Opposite to that, betaine-homocysteine methyltransferase, which catalyzes the conversion of homocysteine into methionine during methionine biosynthesis, is inactivated upon ROS mediated zinc release

(Evans et al., 2002). By trapping cysteines with high molecular weight reagents we could demonstrate that CRY1 indeed can contain one or more disulfide bonds in a cellular environment (Figure 3.2_7, NEM/Mal-PEG experiment). This finding is insofar vexing in the first place as CRYs and PERs are located either in the cytoplasm or in the nucleus, two cellular compartments which have a highly reducing environment which disfavors disulfide bond formation.

Reactive oxygen species (e.g. superoxide anions, hydroxyl radicals, hydrogen peroxide) usually are signs for an abnormal cellular redox state and harmful oxidative stress, however, there is evidence that ROS specifically modulate protein activities and signaling cascades, e.g. with regard to prevention of oxidative damage, in cell cycle progression (Iiyama et al., 2006) or in growth factor response, too. In the latter case it was suggested that the activity of tyrosine phosphatases can be negatively regulated through modification of a cysteine, the common target of ROS, in their reactive center by hydrogen peroxide (Salmeen et al., 2003). ROS can be derived from numerous exogenous or endogenous sources. Mitochondria during aerobic respiration or generally NADPH oxidases, cytochrome P450 enzymes or other enzymes produce reactive oxygen species within the cell (Finkel, 2011). These specifically target and posttranslationally modify cysteines of redox sensitive proteins by formation of intra- or intermolecular disulfide bonds, sulfenic/sulfinic/sulfonic acid formation or glutathionylation amongst others (Wang et al., 2012b). For instance, the ataxia-telangiectasia mutated (ATM) protein kinase is activated in response to DNA double strand breaks and other stresses through formation of its disulfide linked homodimer which can be catalysed by H₂O₂ (Guo et al., 2010).

Controversially, classical cellular antioxidants like thioredoxins are also suggested to specifically bind to target proteins and trigger protein signaling cascades depending on the cellular redox state. For example, thioredoxin 1 reduces HDAC1, which contains a disulfide bond in response to ROS resulting from hypertrophic stimuli, and thereby influences its subcellular localization and consequently its preventive function in cardiac hypertrophy (Ago et al., 2008). Notably, oxidation and reduction of antioxidant peroxiredoxins oscillates in a circadian manner independently of transcription in anucleate erythrocytes. The redox cycles show typical characteristics of circadian rhythms including temperature compensation and entrainment. This shows on the one hand that oxidants are interconnected with cellular regulation and on the other hand that they are able to drive circadian rhythms (O'Neill and Reddy, 2011).

It is well possible that ROS trigger oxidation of mCRY1 and thereby weakens its interaction with mPER2 and probably impact both CRY-PER nuclear co-localization as well as transcriptional repression. It is further conceivable that mCRY1 oxidation and weakened mPER2 binding destabilizes CRY and targets it for degradation via the FBXL3 ubiquitin pathway, however, there is no experimental evidence for this. Alternatively, increasing oxidative pressure could result in oxidation of zinc coordinating cysteines within existing CRY/PER complexes, zinc release (like in classical zinc redox switches) and oxidation of intramolecular CRY cysteines. This study could not reveal evidence for this scenario as non-reducing/(mild) oxidative conditions did not result in zinc release (Figure 3.2_S7). Thereby, ROS are a potential source for CRY/PER to sense the current metabolic state of the cell (negative regulation), either via disulfide bond formation or as earlier speculated via the redox state of heme (section 4.3), and maybe to adopt the circadian clock. Similarly, Nemoto et al. describe an acute negative feedback regulation on glycogen synthase kinase 3 and glycogen synthase through ROS after excessive metabolism (Nemoto et al., 2000). Opposite to that zinc binding stabilizes the CRY/PER complex and thereby positively regulates it.

Nevertheless, it remains to be elucidated whether and how the observed interconnection of a zinc interface and a nearby located disulfide bond in detail influence negative feedback repression in the dependence of metabolism. What triggers the potential redox change of CRY/PER and is it a universal mechanism of circadian CRY/PER regulation or rather a specificity of e.g. metabolic organs like the liver or subcellular compartments (e.g. redox state of CRY/PER influence their nuclear localization)? Interestingly, NAD^+ in the mouse liver (Peek et al., 2013) and NADH/NADPH in red blood cells (O'Neill and Reddy, 2011) show a rhythmic abundance. Moreover, Wang et al. determined oscillations in the redox state of FAD and NADPH in organotypic slices of the rat SCN (Wang et al., 2012a). As redox cofactors they might just as well as ROS be the basis for a redox change in CRY/PER.

Usually zinc is bound to proteins with a high affinity (picomolar range (Maret, 2009)). Therefore, the concentration of free, exchangeable zinc in the cell is low (nano- or picomolar concentration) while the total amount of cellular zinc is in the micromolar range. Cellular zinc sources include, free zinc, zinc bound to metallothioneins or macromolecules as well as zinc in vesicles (Oteiza, 2012). Generally, zinc can be either structurally, catalytically or regulatory important for proteins. Thereby, zinc impacts many physiological aspects amongst others as regulator of cellular “redox balance” (Oteiza, 2012). As already mentioned above zinc can be

released under certain circumstances like oxidative stress.

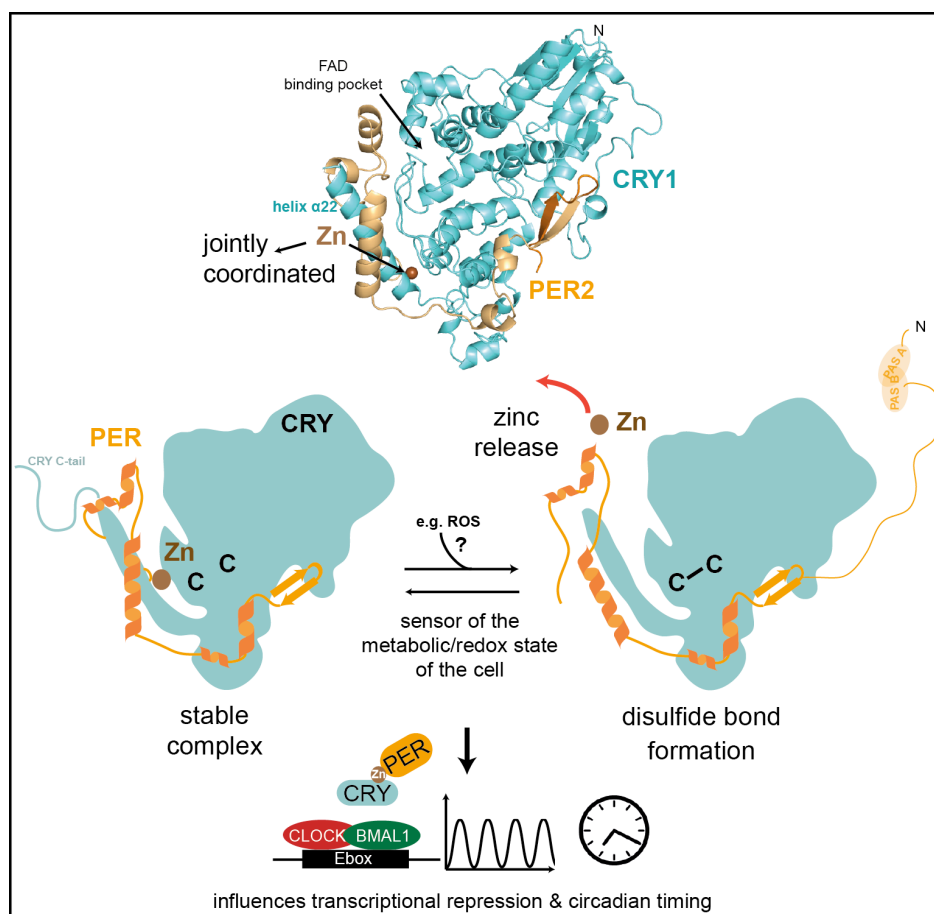


Figure 14: Regulation of the mCRY1/mPER2 complex. mCRY1 and mPER2 co-coordinate a zinc ion in one of their interfaces. Analysis suggests that zinc binding stabilizes the active, reduced state of CRY as well as CRY-PER interaction. Disulfide bond formation within CRY potentially allows the CRY/PER complex to sense the metabolic/ redox state of the cell which thereby impacts the circadian clock; (modified graphical abstract from (Schmalen et al., 2014)).

This study suggests a zinc binding affinity of mCRY1/mPER2 in the low nanomolar range (Figure 3.2_6B). This speaks for an exchangeable zinc ion and would fit a presumably dynamic CRY-PER interaction which underlies multiple regulatory inputs and structural rearrangement during negative feedback repression. Moreover, the CRY-PER interaction is probably further modulated by additional protein interactors which could influence the zinc interface, too. Examples of zinc stabilized homo- and heterodimers, in which two coordinating residues are provided from each protomer, have been described like the tyrosine kinase Lck and T-cell coreceptor CD4/CD8 heterodimer (Kim et al., 2003). It, however, remains unclear, also for the CRY/PER complex, how the zinc ion is recruited during dimerisation and released at complex

disassembly. Fluctuations in cellular zinc levels as well as local high zinc concentrations could be involved, however there is the risk of non-specific interactions (e.g. with free histidines or cysteines) and cytotoxic effects. Additionally, certain proteins could provide specific zinc delivery. Likewise, metal ion binding metallochaperones are involved in the delivery of Ni^{2+} and Cu^{2+} to their targets and e.g. the enzyme ferrochelatase delivers Fe^{2+} for insertion into porphyrin during heme synthesis (Kuchar and Hausinger, 2004). Metallothioneins, which keep zinc homeostasis in the cell, are able to readily exchange zinc ions with other proteins which would avoid free zinc and its adverse effects (Auld, 2001; Maret, 2012; Maret and Li, 2009).

Interestingly Okano et al. generated a transgenic mouse constitutively overexpressing CRY1 with a cysteine-alanine mutation in the zinc coordinating residue Cys414. While overexpressing of wild-type mCRY1 did not visibly impact the animals behavior and physiology, mutant mice show an abnormal entrainment behavior, a prolonged 28 hrs free running locomotor activity period as well as symptoms of diabetes like a reduced β -cell proliferation and hypoinsulinemia (Okano et al., 2009; 2010). The results of this study suggest that the observed mouse phenotypes are a result of disruption of the zinc interface within the mCRY1/mPER2 complex underlying its importance for circadian regulation. Interestingly, *mBmal1*^{-/-} and *mClock* ^{$\Delta 19/\Delta 19$} mutant mice are arrhythmic and show a prolonged free-running period, respectively (Bunger et al., 2000; Vitaterna et al., 1994). Additionally these mice suffer from hypoinsulinemia and defective β -cell function, whereas the *mCry1*^{-/-}/*mCry2*^{-/-} double knockout results in hyperinsulinemia and tissue-specific insulin resistance (Barclay et al., 2013; Marcheva et al., 2010). Furthermore, *mCry1*^{-/-} and *mPer2* mutant mice show a shorter free-running period (section 1.4 and 1.5). Thus, the metabolic and behavioral phenotypes of the mCRY1 C414A mutation rather resemble those phenotypes from mutations in the CLOCK/BMAL1 complex (weakened transcription activator complex) than those from *mCry1/Per2* knockouts (weakened transcription repressor complex). It is possible that attenuated mPER2 binding to mCRY1, due to disruption of the zinc interface, favors binding of mCRY1 to the mCLOCK/BMAL1 complex and consequently enhanced transcription inhibition, especially since mPER2 and mBMAL1 probably occupy interfering binding sites on mCRY1 (section 1.5). This would underline the dominant role of CRY1 as transcriptional repressor and explains why transgenic mice which express weakened transcriptional CLOCK/BMAL1 activator complexes show similar phenotypes.

4.5 Helix α 22 Determines CRY Stability and Function

Essential for mCRY1-mPER2 interaction is the C-terminal helix α 22 of mCRY1 (Figure 3.2_1/2), which is covered from both sites by mPER2 during interaction as revealed by the mCRY1/mPER2 crystal structure. Mutation of helix α 22 residues Lys485 and Gln486 almost completely abolished interaction with mPER2 in our luciferase complementation assay (Figure 3.2_7A). For inhibition of the CLOCK/BMAL1 complex CRY was described to interact with the C-terminus of BMAL1 not only via its C-terminal tail but also with helix α 22 (Chaves et al., 2006; Czarna et al., 2011). Thereby, the BMAL1 interaction with CRY would crucially overlap with the interaction site of mPER2. This would support a competition of mPER2 for mCRY1 binding to the CLOCK/BMAL1/DNA complex (Ye et al., 2011). *In vivo* PER could shuffle CRY towards and regulate its interaction with CLOCK/BMAL1 through this competitive binding site. However, it remains unclear how PER is released and BMAL1 attached to CRY especially since mCRY1 binds the C-terminus of mPER2 with a nanomolar affinity while for the C-tail CRY-BMAL1 interaction an affinity in the lower micromolar range is reported (Czarna et al., 2013). Either there is a second interaction site between CRY and BMAL1 and/or posttranslational modifications like phosphorylation or acetylation for instance of CRY or BMAL1, as already suggested, modulate the interaction (Hirayama et al., 2007; Sanada et al., 2002). Alternatively, CLOCK could have a direct (through interaction with CRY (Huang et al., 2012)) or indirect (through modulation of BMAL1 (Kiyohara et al., 2006)) stabilizing effect on the CRY-BMAL1 interaction. Nevertheless, without the crystal structure of CRY/BMAL1 it is not yet for sure that CRY and BMAL1 form a subcomplex. Interestingly, Chen et al. report that mPER2 and not mCRY1 directly binds to CLOCK/BMAL1. The presence of mPER2 enhances mCRY1 binding to CLOCK/BMAL1 in their co-immunoprecipitation assays, while simultaneous overexpression of the CRY binding domain of mPER2 reduces the amount of CRY pulled by CLOCK/BMAL1 and disrupts circadian rhythms in cell assays (Chen et al., 2009). mPER2 supposedly interacts with BMAL1 (and maybe CLOCK) via its PAS domains. A simultaneous binding of PER and CRY with CLOCK/BMAL1 cannot be excluded at that time, too.

Apart from BMAL1, comparison of the crystal structure of mCRY1/mPER2 with the recently published structure of the mCRY2/FBXL3/SKP1 complex further confirms that mPER2 and the F-box-type E3 ubiquitin ligase FBXL3 are mutually exclusive in their binding to CRY. FBXL3

interacts with the FAD binding pocket, the C-terminal helix $\alpha 22$ and the C-terminal lid of CRY (Xing et al., 2013). It clashes not only with mPER2 binding to helix $\alpha 22$ and the cryptochrome lid but also with formation of the zinc interface. Hence, mPER2 is able to clear mCRY2 (and mCRY1³) from FBXL3 as observed in pull-downs from HEK cells and with purified proteins (Xing et al., 2013). Interaction with PER stabilizes CRY *in vitro*, as observed in biochemical assays (data not shown), and *in vivo* (Chen et al., 2009; Yagita et al., 2002) probably both through reinforcing the photolyase fold and shielding of CRY from FBXL3. Opposite to that FBXL3 assigns CRY for proteasomal degradation in the nucleus, i.e. FBXL3 destabilizes CRY.

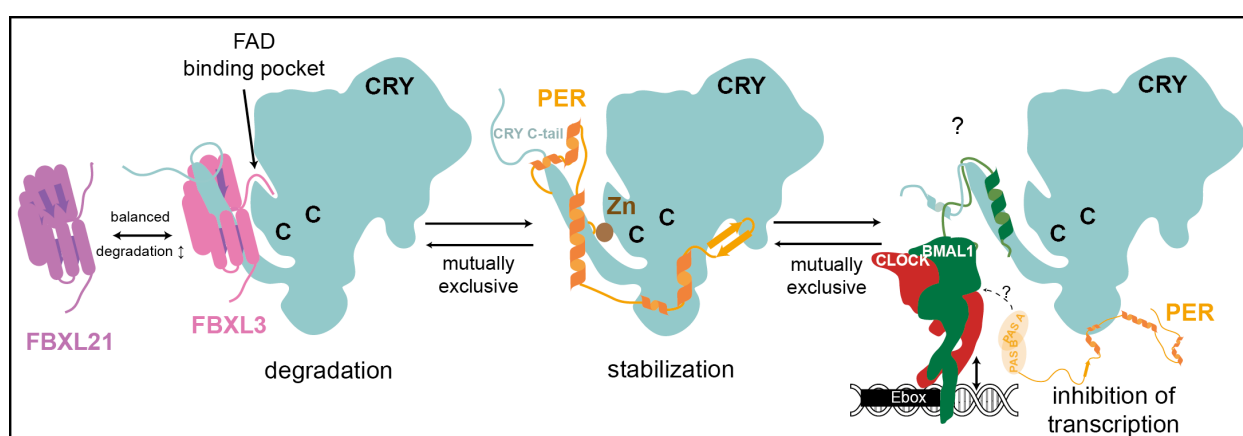


Figure 15: Overview of the mutually exclusive interaction partners of CRY which competitively bind to helix $\alpha 22$ amongst others. Thereby, FBXL3/21, PER and BMAL1 determine CRY stability and allow for its transcriptional repression function; (modified graphical abstract from (Schmalen et al., 2014)).

Interestingly, FBXL21 which has 86% sequence identity with FBXL3 was described to competitively counteract FBXL3 activity by stabilizing CRY in the nucleus but slowly targeting CRY for degradation in the cytoplasm (Hirano et al., 2013; Yoo et al., 2013). It is very likely that FBXL21 forms a similar complex with CRY like FBXL3 and thereby would also have overlapping binding sites with PER on CRY. Phosphorylation of Ser71 by AMPK was suggested to regulate binding of either mPER2 or FBXL3 to mCRY1. However, neither mPER2 nor FBXL3 bind close to the AMPK phosphorylation site which implies that AMPK regulates mPER2 and FBXL3 binding to CRY in an indirect manner. Phosphorylation of Ser557 and Ser553 in the c-tail of mCRY2 by GSK3 β was also reported to negatively regulate mCRY2 stability. However, it could not be shown that it impacts on the stabilizing binding of FBXL21 to mCRY2 (Hirano et al., 2013) and probably also does not directly impact on mPER2 binding as the C-tail of CRY is not involved in

³ mCRY1 and mCRY2 show a very high sequence identity and mainly differ in their tails; a sequence alignment is shown in Figure 3.2_S2 .

CRY-PER interaction (Figure 3.2_5C/D). Thus, it remains unclear how FBXL3 targets CRY for degradation especially since both FBXL21 and mPER2 reportedly have a higher affinity for CRY than FBXL3 (Xing et al., 2013; Yoo et al., 2013) (Figure 3.2_5B). C-terminal helix α 22 of CRY, however, operates in several important interactions of CRY in dependence of yet unknown regulatory influences (Figure 15).

4.6 FAD and the mCRY1/mPER2 Complex

In insect type I animal cryptochromes (e.g. *Drosophila* CRY) FAD is by now established as the photoreactive cofactor which is important for CRYs' functionality. An increasing number of reports suggest that mammalian type II cryptochrome (e.g. mouse CRY) also binds to FAD, undergoes photoreduction and light favoured degradation in cell culture and transgenic flies (Hoang et al., 2008). The structural elements for FAD binding, the FAD binding pocket and its FAD coordinating residues, are conserved among insect and mammalian cryptochromes, however, the mammalian FAD binding pocket is more open. In contrast to plant or insect cryptochromes, mammalian CRY does not copurify with FAD *in vitro* from insect cell expression systems. Nevertheless, Xing et al. were recently able to solve the FAD bound structure of mCRY2 through FAD crystal soaking of apo-mCRY2. In addition, they showed that FAD displaces the E3 ubiquitin ligase FBXL3 from a preformed complex with mCRY2 in an *in vitro* competition assay (Xing et al., 2013). On the one hand this makes sense since FBXL3 penetrates with its C-terminal tail into the FAD binding pocket of mCRY2 to establish essential interactions as revealed by analysis of the mCRY2/FBXL3 crystal structure. On the other hand, however, this finding is unexpected since mCRY2 reportedly binds FAD_{ox} with a dissociation constant of only 40 μ M and FAD_{red} with even less affinity. We see similar FAD binding affinities in our studies, too (data not shown). Although experimental evidence still has to be provided I here speculate on FAD as a regulator of CRY in its subsequent interactions with PER, BMAL1 and FBXL3 *in vivo*. While the study of Xing et al. confirms that FBXL3 and FAD are mutually exclusive in their binding to CRY, the structure based analysis of the FAD binding pocket in the mCRY1/mPER2 complex structure neither excludes nor supports the simultaneous binding of both FAD and mPER2 to mCRY1 (Figure 3.2_4). Strikingly, the FAD binding pocket is in direct proximity to the potential disulfide bond between Cys363 and Cys412 of mCRY1. Thereby, the FAD binding pocket and the zinc interface could be linked in a redox dependent manner. FAD could for

instance impact on the mCRY1/mPER2 interaction through modulation of the flexibility of the C-terminal lid of CRY, which is involved in mCRY1-mPER2 interaction and includes disulfide bond forming (Cys412) and zinc binding (Cys414) cysteines, or through induction of a redox change in the zinc interface or the disulfide bond. As known so far, FAD is only suggested to undergo a light-mediated reduction in cryptochromes. In oxidoreductases, which usually bind FAD as catalytically active cofactor, or other proteins which depend on a flavin redox switch, FAD can undergo redox changes upon electron transfer in dependence of an electron acceptor/donor and its environment (Becker et al., 2011). Thereby, FAD either mediates different redox reactions and/or protein conformational changes, respectively. It is not known whether FAD bound cryptochromes are able to undergo a redox change by sensing the redox state of the cell as well and how such a reaction could be triggered or mediated. Mammalian cryptochromes are found in many places of the body. Light activation of FAD could happen for instance in the eye or other surface close tissues and thereby present a tissue specific regulation of CRY. Alternatively, FAD could regulate CRY functions as already suggested by the FAD-FBXL3 interplay for CRY binding, in a light- and redox independent but rather structural manner by on- and off-binding. At least the FAD binding pocket is of importance for CRY. KL001, an artificial carbazol compound which binds to the FAD binding pocket, stabilizes CRY by inhibiting its FBXL3- and ubiquitin-dependent degradation. Interestingly, KL001 binding to CRY also appears to weaken CRY-PER interaction (Hirota et al., 2012). Mutation of conserved FAD coordinating residues in the FAD binding pocket attenuate CLOCK/BMAL1 inhibition of CRY1 (Hitomi et al., 2009).

4.7 Composition and Dynamics of the CRY/PER Repressor Complex

Negative transcriptional feedback repression is essential for the generation of circadian rhythms. The interaction of CRY and PER is presumably required for nuclear localization of both proteins in the first place and more important for the formation of a functionally active repressor complex in the second place. The C-terminal region of mPER2 interacts with mCRY1 (Figure 3.2_1). The C-tail of mCRY1 does not appear to be involved this interaction (Figure 3.2_5C/D). mCRY1 and mCRY2 essentially differ in their C-terminal tail (Figure 11 & 3.2_S2), thus mPER2 probably forms a very similar complex with the mCRY2-PHR. Sequence analysis further shows that the mPER2 residues, which are crucial for the interaction with mCRY1

including the zinc interface forming cysteines, are conserved in mPER1 and to less extent in mPER3. This suggests that homologous CRY/PER complexes can also be formed. As target of posttranslational modifications, the CRY C-tail could be involved in mCRY1-mPER2 interaction regulation.

In the nucleus PER proteins supposedly recruit, next to CRY, numerous other proteins to the site of CLOCK/BMAL1 mediated transcription for feedback repression. The PAS domains of PER are assumed to not only mediate interactions with the transcription factors but also homo- and heterodimeric PER-PER and other PER-protein interactions. Thereby, they might be important for formation of the repressor complex. Probably, it is both the interaction site with CRY as well as the PAS domains and other interaction sites on PER that shape PER complexes. Likewise, on the one hand our luciferase complementation assays show that mPER2 homodimers are formed through PAS-PAS interactions and influenced by the PAS-B Trp interface, however, on the other hand these results also suggest that at least full-length PER homodimers are indirectly but essentially stabilized by CRY mediated interactions (Figure 3.1_2).

Although mammalian PERs and CRYs likely form CRY-PER complexes in all possible combinations, it cannot not be excluded that one combination e.g. the PER2/CRY1 complex is preferentially formed or underlies different regulations. Similarly, the homodimers of the mPER1, mPER2 and mPER3 PAS domains show unique features next to their generally conserved fold and their common PAS-B Trp interface. For instance, mPER1 is additionally stabilized by a α C-interface formed by the two PAS-A domains in the homodimer. The α C-interface probably accounts for the higher affinity of the mPER1 PAS dimer and supports its generally less flexible fold. This probably explains why mPER1 has fewer known interactors. Nevertheless, the here described crystal structures of PER only envision small parts of the PER proteins. Especially central parts of the mammalian PER proteins are not well conserved both among species and among the three mammalian PER paralogs and might well impact on the PAS and C-terminal domain of PER.

Strikingly, PER2 associates with association DNA regulatory elements with a delay of several hours compared to PER1 (Duong and Weitz, 2014). Similarly CRY1 lags behind PER1, PER2 and CRY2, respectively, according to ChIP-seq data (Koike et al., 2012). Thereby, the transcription low phase was suggested to be split into a transcription “repressed phase” mediated by PER1/PER2 and CRY2 in which CLOCK/BMAL1 are released from the DNA and a

follow-up “poised phase” in which CRY1 binds to CLOCK/BMAL1/DNA and puts transcription on “hold” before a new circadian cycle starts (Koike et al., 2012). Accordingly, Duong et al. observe a temporally different and sequential recruitment of the histone modifiers HDAC1 and Suv39h1 to the sites of transcriptional repression (Duong and Weitz, 2014). Our FRAP motility assay in U2O2 cells shows that mPER2 and mPER1 complexes move with different speed and consequently potentially have different sizes within the cell (Figure 3.1_3). Still this might not be due to distinct mPER1 and mPER2 complexes since the overall composition of isolated mPER1 and mPER2 complexes at circadian time of transcriptional repression appears to be identical and including the respectively other PER (Padmanabhan et al., 2012). However, Duong and Weitz speculate that the precise stoichiometry and dynamics of PER1/PER2 complexes as well as their interaction with CLOCK/BMAL1 is temporally varying from the beginning to the end of transcriptional feedback repression and probably depending on posttranslational modifications. This would allow for the sequential recruitment of the different co-repressors of CLOCK/BMAL1 transcriptional activity. I here speculate that the difference among the mammalian PER and their combinations not only shape the repressor complex but also add another level of complexity and specificity to the recruitment of CRY1 and CRY2 and other co-repressors. This is potentiated through the timed degradation of PER and CRY and the impact of the cellular redox state. The latter might critically influence both the CRY-PER interaction and the activity of the NAD⁺ dependent deacetylase SIRT1, which modulates PER2 stability and BMAL1 interaction with CRY (section 1.2). Together this accounts for negative transcriptional feedback repression and consequently circadian rhythms.

5 Outlook

The crystal structures of the mPER1 PAS domains and especially the mCRY1/mPER2 core complex are an important step towards the structural reconstitution of the mammalian clock. We gained a more complete understanding of the mechanisms underlying the different functions of the PER proteins and their interactors and how the PER complexes might sense the metabolic state of their environment.

Future directions now include the definition and comparative analysis of homologous CRY/PER and heterodimeric PER/PER complexes. Interaction studies will show whether and how these complexes are formed and regulated. Moreover, the role of FAD or other cofactors in regulation of mammalian CRY interactions, for instance with PER, and functions will be defined. Especially spectroscopic methods will support the decoding of the underlying (photo)chemistry.

Although we found evidence for the formation of disulfide bounds in mCRY1, this observation has to be further examined since CRY is located in a reducing environment in the cell. Our results suggest that disulfide bond formation involves Cys363 and Cys412 of mCRY1. Additional disulfide bonds in mCRY1, that might play a role in redox sensing or redox regulation of the circadian clock, will be identified and carefully examined concerning their appearance *in vivo*.

We will unravel whether oxidative or metabolic stress indeed impacts on the CRY/PER complex composition, localization and functionality in a cellular context. Moreover, the interplay between mCRY1 disulfide bonds and zinc binding within the CRY/PER complex for clock regulation should be analyzed in more detail. Although our crystallized CRY/PER interface does not cover any known posttranslational modification sites a future task also includes shedding more light on the influence and mechanism underlying nearby modification sites e.g. phosphorylation of mCRY1 Ser71 by AMPK which supposedly targets mCRY1 for degradation (see section 1.5), on CRY/PER complex regulation.

Identification of yet unknown components of the multi-protein PER repressor complex in the nucleus and precise mapping of their interaction sites, for instance on PER or among each other, will support the complete structural analysis of PER and PER repressor subcomplexes. This also includes the structural characterization of CRY or PER subcomplexes with CLOCK and

BMAL1 which will allow to understand how CRY and/or PER directly interfere with the CLOCK/BMAL1 transcription activator complex. In the long term this will not only help to understand transcriptional feedback repression but might also help to identify a potential metabolic modulator function of the CRY/PER complex. This might finally result in a mechanism for CRY sensing the metabolic state of the cell. However, in a long term only mouse models targeting the potential disulfide bonds of CRY and the zinc interface of the CRY/PER complex will show whether the interplay of disulfide bond formation and the zinc interface is important for the mammalian circadian clock *in vivo*.

References

- Ago, T., Liu, T., Zhai, P., Chen, W., Li, H., Molkentin, J.D., Vatner, S.F., and Sadoshima, J. (2008).** A redox-dependent pathway for regulating class IIHDACs and cardiac hypertrophy. *Cell* *133*, 978–993.
- Agostino, P.V., Golombek, D.A., and Meck, W.H. (2010).** Unwinding the Molecular Basis of Interval and Circadian Timing. *Front Integr Neurosci* *5*, 64.
- Airola, M.V., Du, J., Dawson, J.H., and Crane, B.R. (2010).** Heme binding to the Mammalian circadian clock protein period 2 is nonspecific. *Biochemistry* *49*, 4327–4338.
- Akashi, M., and Takumi, T. (2005).** The orphan nuclear receptor RORalpha regulates circadian transcription of the mammalian core-clock Bmal1. *Nature Structural & Molecular Biology* *12*, 441–448.
- Albrecht, U., and Eichele, G. (2003).** The mammalian circadian clock. *Curr Opin Genet Dev* *13*, 271–277.
- Albrecht, U., Sun, Z.S., Eichele, G., and Lee, C.C. (1997).** A differential response of two putative mammalian circadian regulators, mper1 and mper2, to light. *Cell* *91*, 1055–1064.
- Anand, S.N., Maywood, E.S., Chesham, J.E., Joynson, G., Banks, G.T., Hastings, M.H., and Nolan, P.M. (2013).** Distinct and separable roles for endogenous CRY1 and CRY2 within the circadian molecular clockwork of the suprachiasmatic nucleus, as revealed by the Fbxl3(Afh) mutation. *J Neurosci* *33*, 7145–7153.
- Anantharaman, V., and Aravind, L. (2000).** Cache - a signaling domain common to animal Ca(2+)-channel subunits and a class of prokaryotic chemotaxis receptors. *Trends Biochem. Sci.* *25*, 535–537.
- Antoch, M.P., Song, E.J., Chang, A.M., Vitaterna, M.H., Zhao, Y., Wilsbacher, L.D., Sangoram, A.M., King, D.P., Pinto, L.H., and Takahashi, J.S. (1997).** Functional identification of the mouse circadian Clock gene by transgenic BAC rescue. *Cell* *89*, 655–667.
- Asher, G., Gatfield, D., Stratmann, M., Reinke, H., Dibner, C., Kreppel, F., Mostoslavsky, R., Alt, F.W., and Schibler, U. (2007).** SIRT1 Regulates Circadian Clock Gene Expression through PER2 Deacetylation. *Cell* *134*, 317–328.
- Asher, G., Reinke, H., Altmeyer, M., Gutierrez-Arcelus, M., Hottiger, M.O., and Schibler, U. (2010).** Poly(ADP-Ribose) Polymerase 1 Participates in the Phase Entrainment of Circadian Clocks to Feeding. *Cell* *142*, 943–953.
- Auld, D.S. (2001).** Zinc coordination sphere in biochemical zinc sites. *Biometals* *14*, 271–313.
- Bae, K., Jin, X., Maywood, E.S., Hastings, M.H., Reppert, S.M., and Weaver, D.R. (2001).** Differential functions of mPer1, mPer2, and mPer3 in the SCN circadian clock. *Neuron* *30*, 525–536.

- Balsalobre, A., Brown, S.A., Marcacci, L., Tronche, F., Kellendonk, C., Reichardt, H.M., Schütz, G., and Schibler, U. (2000).** Resetting of circadian time in peripheral tissues by glucocorticoid signaling. *Science* **289**, 2344–2347.
- Balsalobre, A., Damiola, F., and Schibler, U. (1998).** A serum shock induces circadian gene expression in mammalian tissue culture cells. *Cell* **93**, 929–937.
- Barclay, J.L., Shostak, A., Leliavski, A., Tsang, A.H., Jöhren, O., Müller-Fielitz, H., Landgraf, D., Naujokat, N., van der Horst, G.T.J., and Oster, H. (2013).** High-fat diet-induced hyperinsulinemia and tissue-specific insulin resistance in *Cry*-deficient mice. *AJP: Endocrinology and Metabolism* **304**, E1053–E1063.
- Becker, D.F., Zhu, W., and Moxley, M.A. (2011).** Flavin Redox Switching of Protein Functions. *Antioxid Redox Signal* **14**, 1079–1091.
- Bell-Pedersen, D., Cassone, V.M., Earnest, D.J., Golden, S.S., Hardin, P.E., Thomas, T.L., and Zoran, M.J. (2005).** Circadian rhythms from multiple oscillators: lessons from diverse organisms. *Nat. Rev. Genet.* **6**, 544–556.
- Benedetti, F., Dall'aspezia, S., Colombo, C., Pirovano, A., Marino, E., and Smeraldi, E. (2008).** A length polymorphism in the circadian clock gene *Per3* influences age at onset of bipolar disorder. *Neuroscience Letters* **445**, 184–187.
- Berndt, A., Kottke, T., Breitkreuz, H., Dvorsky, R., Hennig, S., Alexander, M., and Wolf, E. (2007).** A novel photoreaction mechanism for the circadian blue light photoreceptor *Drosophila* cryptochrome. *J Biol Chem* **282**, 13011–13021.
- Bersten, D.C., Sullivan, A.E., Peet, D.J., and Whitelaw, M.L. (2013).** bHLH-PAS proteins in cancer. *Nat. Rev. Cancer* **13**, 827–841.
- Brown, S.A., Zimbrunn, G., Fleury-Olela, F., Preitner, N., and Schibler, U. (2002).** Rhythms of mammalian body temperature can sustain peripheral circadian clocks. *Curr. Biol.* **12**, 1574–1583.
- Brown, S.A., Fleury-Olela, F., Nagoshi, E., Hauser, C., Juge, C., Meier, C.A., Chicheportiche, R., Dayer, J.-M., Albrecht, U., and Schibler, U. (2005a).** The period length of fibroblast circadian gene expression varies widely among human individuals. *PLoS Biol.* **3**, e338.
- Brown, S.A., Ripperger, J., Kadener, S., Fleury-Olela, F., Vilbois, F., Rosbash, M., and Schibler, U. (2005b).** *PERIOD1*-associated proteins modulate the negative limb of the mammalian circadian oscillator. *Science* **308**, 693–696.
- Bunger, M.K., Wilsbacher, L.D., Moran, S.M., Clendenin, C., Radcliffe, L.A., Hogenesch, J.B., Simon, M.C., Takahashi, J.S., and Bradfield, C.A. (2000).** *Mop3* is an essential component of the master circadian pacemaker in mammals. *Cell* **103**, 1009–1017.
- Camacho, F., Cilio, M., Guo, Y., Virshup, D.M., Patel, K., Khorkova, O., Styren, S., Morse, B., Yao, Z., and Keesler, G.A. (2001).** Human casein kinase I delta phosphorylation of human circadian clock proteins period 1 and 2. *FEBS Lett* **489**, 159–165.
- Cantó, C., Gerhart-Hines, Z., Feige, J.N., Lagouge, M., Noriega, L., Milne, J.C., Elliott, P.J.,**

- Puigserver, P., and Auwerx, J. (2009). AMPK regulates energy expenditure by modulating NAD(+) metabolism and SIRT1 activity. *Nature* *458*, 1056–U1140.
- Cashmore**, A.R.A., Jarillo, J.A.J., Wu, Y.J.Y., and Liu, D.D. (1999). Cryptochromes: blue light receptors for plants and animals. *Science* *284*, 760–765.
- Cermakian**, N., Monaco, L., Pando, M.P., Dierich, A., and Sassone-Corsi, P. (2001). Altered behavioral rhythms and clock gene expression in mice with a targeted mutation in the *Period1* gene. *The EMBO Journal* *20*, 3967–3974.
- Chaves**, I., Yagita, K., Barnhoorn, S., Okamura, H., van der Horst, G.T.J., and Tamanini, F. (2006). Functional Evolution of the Photolyase/Cryptochrome Protein Family: Importance of the C Terminus of Mammalian CRY1 for Circadian Core Oscillator Performance. *Molecular and Cellular Biology* *26*, 1743–1753.
- Chaves**, I., Pokorny, R., Byrdin, M., Hoang, N., Ritz, T., Brettel, K., Essen, L.-O., van der Horst, G.T.J., Batschauer, A., and Ahmad, M. (2011). The Cryptochromes: Blue Light Photoreceptors in Plants and Animals. *Annu. Rev. Plant Biol.* *62*, 335–364.
- Chen**, J.-J. (2007). Regulation of protein synthesis by the heme-regulated eIF2 alpha kinase: relevance to anemias. *Blood* *109*, 2693–2699.
- Chen**, R., Schirmer, A., Lee, Y., Lee, H., Kumar, V., Yoo, S.-H., Takahashi, J.S., and Lee, C. (2009). Rhythmic PER abundance defines a critical nodal point for negative feedback within the circadian clock mechanism. *Mol. Cell* *36*, 417–430.
- Costa**, M.J., So, A.Y.-L., Kaasik, K., Krueger, K.C., Pillsbury, M.L., Fu, Y.-H., Ptáček, L.J., Yamamoto, K.R., and Feldman, B.J. (2011). Circadian rhythm gene period 3 is an inhibitor of the adipocyte cell fate. *J Biol Chem* *286*, 9063–9070.
- Crosson**, S., Rajagopal, S., and Moffat, K. (2003). The LOV domain family: Photoresponsive signaling modules coupled to diverse output domains. *Biochemistry* *42*, 2–10.
- Curtis**, A.M., Seo, S.B., Westgate, E.J., Rudic, R.D., Smyth, E.M., Chakravarti, D., FitzGerald, G.A., and McNamara, P. (2004). Histone acetyltransferase-dependent chromatin remodeling and the vascular clock. *J Biol Chem* *279*, 7091–7097.
- Czarna**, A., Berndt, A., Singh, H.R., Grudziecki, A., Ladurner, A.G., Timinszky, G., Kramer, A., and Wolf, E. (2013). Structures of *Drosophila* cryptochrome and mouse cryptochrome1 provide insight into circadian function. *Cell* *153*, 1394–1405.
- Czarna**, A., Breitkreuz, H., Mahrenholz, C.C., Arens, J., Strauss, H.M., and Wolf, E. (2011). Quantitative analyses of cryptochrome-mBMAL1 interactions: mechanistic insights into the transcriptional regulation of the mammalian circadian clock. *286*, 22414–22425.
- Damiola**, F., Le Minh, N., Preitner, N., Kornmann, B., Fleury-Olela, F., and Schibler, U. (2000). Restricted feeding uncouples circadian oscillators in peripheral tissues from the central pacemaker in the suprachiasmatic nucleus. *Genes Dev* *14*, 2950–2961.
- Dardente**, H., Fortier, E.E., Martineau, V., and Cermakian, N. (2007). Cryptochromes impair phosphorylation of transcriptional activators in the clock: a general mechanism for circadian

repression. *Biochem J* 402, 525–536.

De Bacquer, D., Van Risseghem, M., Clays, E., Kittel, F., De Backer, G., and Braeckman, L. (2009). Rotating shift work and the metabolic syndrome: a prospective study. *Int J Epidemiol* 38, 848–854.

Dioum, E.M., Rutter, J., Tuckerman, J.R., Gonzalez, G., Gilles-Gonzalez, M.-A., and McKnight, S.L. (2002). NPAS2: a gas-responsive transcription factor. *Science* 298, 2385–2387.

Doi, M., Hirayama, J., and Sassone-Corsi, P. (2006). Circadian regulator CLOCK is a histone acetyltransferase. *Cell* 125, 497–508.

Dunlap, J.C. (1998). Molecular Bases for Circadian Clocks. *Cell* 96, 271–290.

Duong, H.A., and Weitz, C.J. (2014). Temporal orchestration of repressive chromatin modifiers by circadian clock Period complexes. *Nature Structural & Molecular Biology* 21, 126–132.

Duong, H.A., Robles, M.S., Knutti, D., and Weitz, C.J. (2011). A molecular mechanism for circadian clock negative feedback. *Science* 332, 1436–1439.

Ebisawa, T., Uchiyama, M., Kajimura, N., Mishima, K., Kamei, Y., Katoh, M., Watanabe, T., Sekimoto, M., Shibui, K., Kim, K., et al. (2001). Association of structural polymorphisms in the human period3 gene with delayed sleep phase syndrome. *EMBO Rep* 2, 342–346.

Eckel-Mahan, K., and Sassone-Corsi, P. (2009). Metabolism control by the circadian clock and vice versa. *Nature Structural & Molecular Biology* 16, 462–467.

Egli, M., and Johnson, C.H. (2013). A circadian clock nanomachine that runs without transcription or translation. *Curr Opin Neurobiol* 23, 732–740.

Eide, E.J., Woolf, M.F., Kang, H., Woolf, P., Hurst, W., Camacho, F., Vielhaber, E.L., Giovanni, A., and Virshup, D.M. (2005). Control of mammalian circadian rhythm by CKI epsilon-regulated proteasome-mediated PER2 degradation. *Molecular and Cellular Biology* 25, 2795–2807.

Eide, E.J., Vielhaber, E.L., Hinz, W.A., and Virshup, D.M. (2002). The circadian regulatory proteins BMAL1 and cryptochromes are substrates of casein kinase Iepsilon. 277, 17248–17254.

Eskin, A. (1979). Identification and physiology of circadian pacemakers. Introduction. *Fed. Proc.* 38, 2570–2572.

Etchegaray, J.P., Lee, C., Wade, P.A., and Reppert, S.M. (2003). Rhythmic histone acetylation underlies transcription in the mammalian circadian clock. *Nature* 421, 177–182.

Evans, J.C., Huddler, D.P., Jiracek, J., Castro, C., Millian, N.S., Garrow, T.A., and Ludwig, M.L. (2002). Betaine-homocysteine methyltransferase: zinc in a distorted barrel. *Structure* 10, 1159–1171.

Finkel, T. (2011). Signal transduction by reactive oxygen species. *J Cell Biol* 194, 7–15.

Foley, L.E., Gegear, R.J., and Reppert, S.M. (2011). Human cryptochrome exhibits light-dependent magnetosensitivity. *Nat Commun* 2, 356.

- Fu, L., Pelicano, H., Liu, J., Huang, P., and Lee, C. (2002).** The circadian gene *Period2* plays an important role in tumor suppression and DNA damage response in vivo. *Cell* *111*, 41–50.
- Fujihashi, M., Numoto, N., Kobayashi, Y., Mizushima, A., Tsujimura, M., Nakamura, A., Kawarabayasi, Y., and Miki, K. (2007).** Crystal structure of archaeal photolyase from *Sulfolobus tokodaii* with two FAD molecules: Implication of a novel light-harvesting cofactor. *J. Mol. Biol.* *365*, 903–910.
- Gallego, M., and Virshup, D.M. (2007).** Post-translational modifications regulate the ticking of the circadian clock. *Nat. Rev. Mol. Cell Biol.* *8*, 139–148.
- Gao, P., Yoo, S.-H., Lee, K.-J., Rosensweig, C., Takahashi, J.S., Chen, B.P., and Green, C.B. (2013).** Phosphorylation of the cryptochrome 1 C-terminal tail regulates circadian period length. *J Biol Chem* *288*, 35277–35286.
- Gegear, R.J., Foley, L.E., Casselman, A., and Reppert, S.M. (2010).** Animal cryptochromes mediate magnetoreception by an unconventional photochemical mechanism. *Nature* *463*, 804–807.
- Gekakis, N.N., Staknis, D.D., Nguyen, H.B.H., Davis, F.C.F., Wilsbacher, L.D.L., King, D.P.D., Takahashi, J.S.J., and Weitz, C.J.C. (1998).** Role of the *CLOCK* protein in the mammalian circadian mechanism. *Science* *280*, 1564–1569.
- Gery, S., Virk, R.K., Chumakov, K., Yu, A., and Koeffler, H.P. (2007).** The clock gene *Per2* links the circadian system to the estrogen receptor. *Oncogene* *26*, 7916–7920.
- Gery, S., Komatsu, N., Baldjyan, L., Yu, A., Koo, D., and Koeffler, H.P. (2006).** The circadian gene *per1* plays an important role in cell growth and DNA damage control in human cancer cells. *Mol. Cell* *22*, 375–382.
- Golombek, D.A., and Rosenstein, R.E. (2010).** Physiology of circadian entrainment. *Physiol. Rev.* *90*, 1063–1102.
- Green, C.B., Takahashi, J.S., and Bass, J. (2008).** The Meter of Metabolism. *Cell* *134*, 728–742.
- Griffin, E.A., Jr (1999).** Light-Independent Role of *CRY1* and *CRY2* in the Mammalian Circadian Clock. *Science* *286*, 768–771.
- Grimaldi, B., Nakahata, Y., Kaluzova, M., Masubuchi, S., and Sassone-Corsi, P. (2009).** Chromatin remodeling, metabolism and circadian clocks: The interplay of *CLOCK* and *SIRT1*. *Int J Biochem Cell Biol* *41*, 81–86.
- Guillaumond, F., Dardente, H., Giguère, V., and Cermakian, N. (2005).** Differential control of *Bmal1* circadian transcription by *REV-ERB* and *ROR* nuclear receptors. *J. Biol. Rhythms* *20*, 391–403.
- Guo, Z.Z., Kozlov, S.S., Lavin, M.F.M., Person, M.D.M., and Paull, T.T.T. (2010).** ATM activation by oxidative stress. *Science* *330*, 517–521.
- Harada, Y., Sakai, M., Kurabayashi, N., Hirota, T., and Fukada, Y. (2005).** Ser-557-phosphorylated *mCRY2* is degraded upon synergistic phosphorylation by glycogen synthase kinase-3 beta. *J Biol Chem* *280*, 31714–31721.

- Hardin, P.E.** (2011). Molecular genetic analysis of circadian timekeeping in *Drosophila*. *Adv Genet* 74, 141–173.
- Hasan, S., van der Veen, D.R., Winsky-Sommerer, R., Dijk, D.-J., and Archer, S.N.** (2011). Altered sleep and behavioral activity phenotypes in PER3-deficient mice. *Am. J. Physiol. Regul. Integr. Comp. Physiol.* 301, R1821–R1830.
- Hastings, M., O'Neill, J.S., and Maywood, E.S.** (2007). Circadian clocks: regulators of endocrine and metabolic rhythms. *Journal of Endocrinology* 195, 187–198.
- Hastings, M.H., and Herzog, E.D.** (2004). Clock Genes, Oscillators, and Cellular Networks in the Suprachiasmatic Nuclei. *J. Biol. Rhythms* 19, 400–413.
- Hennig, S., Strauss, H.M., Vanselow, K., Yildiz, O., Schulze, S., Arens, J., Kramer, A., and Wolf, E.** (2009). Structural and functional analyses of PAS domain interactions of the clock proteins *Drosophila* PERIOD and mouse PERIOD2. *PLoS Biol.* 7, e94.
- Henry, J.T., and Crosson, S.** (2011). Ligand-Binding PAS Domains in a Genomic, Cellular, and Structural Context. *Annu Rev Microbiol* 65, 261–286.
- Hirano, A., Yumimoto, K., Tsunematsu, R., Matsumoto, M., Oyama, M., Kozuka-Hata, H., Nakagawa, T., Lanjakornsiripan, D., Nakayama, K.I., and Fukada, Y.** (2013). FBXL21 regulates oscillation of the circadian clock through ubiquitination and stabilization of cryptochromes. *152*, 1106–1118.
- Hirayama, J., Sahar, S., Grimaldi, B., Tamaru, T., Takamatsu, K., Nakahata, Y., and Sassone-Corsi, P.** (2007). CLOCK-mediated acetylation of BMAL1 controls circadian function. *Nature* 450, 1086–1090.
- Hirota, T., Lee, J.W., St John, P.C., Sawa, M., Iwaisako, K., Noguchi, T., Pongsawakul, P.Y., Sonntag, T., Welsh, D.K., Brenner, D.A., et al.** (2012). Identification of small molecule activators of cryptochrome. *Science* 337, 1094–1097.
- Hirota, T., Okano, T., Kokame, K., Shirotani-Ikejima, H., Miyata, T., and Fukada, Y.** (2002). Glucose down-regulates Per1 and Per2 mRNA levels and induces circadian gene expression in cultured Rat-1 fibroblasts. *J Biol Chem* 277, 44244–44251.
- Hitomi, K., DiTacchio, L., Arvai, A.S., Yamamoto, J., Kim, S.T., Todo, T., Tainer, J.A., Iwai, S., Panda, S., and Getzoff, E.D.** (2009). Functional motifs in the (6-4) photolyase crystal structure make a comparative framework for DNA repair photolyases and clock cryptochromes. *Proc Natl Acad Sci U S A* 106, 6962–6967.
- Hoang, N., Schleicher, E., Kacprzak, S., Bouly, J.-P., Picot, M., Wu, W., Berndt, A., Wolf, E., Bittl, R., and Ahmad, M.** (2008). Human and *Drosophila* cryptochromes are light activated by flavin photoreduction in living cells. *PLoS Biol.* 6, e160.
- Huang, N., Chelliah, Y., Shan, Y., Taylor, C.A., Yoo, S.-H., Partch, C., Green, C.B., Zhang, H., and Takahashi, J.S.** (2012). Crystal structure of the heterodimeric CLOCK:BMAL1 transcriptional activator complex. *Science* 337, 189–194.
- Huang, Y., Baxter, R., Smith, B.S., Partch, C.L., Colbert, C.L., and Deisenhofer, J.** (2006). Crystal

structure of cryptochrome 3 from *Arabidopsis thaliana* and its implications for photolyase activity. *Proc Natl Acad Sci U S A* *103*, 17701–17706.

Iitaka, C., Miyazaki, K., Akaike, T., and Ishida, N. (2005). A role for glycogen synthase kinase-3 β in the mammalian circadian clock. *J Biol Chem* *280*, 29397–29402.

Iiyama, M., Kakihana, K., Kurosu, T., and Miura, O. (2006). Reactive oxygen species generated by hematopoietic cytokines play roles in activation of receptor-mediated signaling and in cell cycle progression. *Cell. Signal.* *18*, 174–182.

Ilbert, M., Graf, P., and Jakob, U. (2006). Zinc center as redox switch-new function for an old motif. *8*, 835–846.

Jin, X., Shearman, L.P., Weaver, D.R., Zylka, M.J., De Vries, G.J., and Reppert, S.M. (1998). A Molecular Mechanism Regulating Rhythmic Output from the Suprachiasmatic Circadian Clock. *Cell* *96*, 57–68.

Johnson, C.H., Moore, R.Y., and Morin, L.P. (1988). Loss of Entrainment and Anatomical Plasticity After Lesions of the Hamster Retinohypothalamic Tract. *Brain Res.* *460*, 297–313.

Johnson, C.H., Stewart, P.L., and Egli, M. (2011). The Cyanobacterial Circadian System: From Biophysics to Bioevolution. *Annu Rev Biophys* *40*, 143–167.

Kaasik, K., and Lee, C.C. (2004). Reciprocal regulation of haem biosynthesis and the circadian clock in mammals. *Nature* *430*, 467–471.

Kim, P.W., Sun, Z., Blacklow, S.C., Wagner, G., and Eck, M.J. (2003). A zinc clasp structure tethers Lck to T cell coreceptors CD4 and CD8. *Science* *301*, 1725–1728.

Kitanishi, K., Igarashi, J., Hayasaka, K., Hikage, N., Saiful, I., Yamauchi, S., Uchida, T., Ishimori, K., and Shimizu, T. (2008). Heme-binding characteristics of the isolated PAS-A domain of mouse Per2, a transcriptional regulatory factor associated with circadian rhythms. *Biochemistry* *47*, 6157–6168.

Kiyohara, Y.B., Tagao, S., Tamanini, F., Morita, A., Sugisawa, Y., Yasuda, M., Yamanaka, I., Ueda, H.R., van der Horst, G.T.J., Kondo, T., et al. (2006). The BMAL1 C terminus regulates the circadian transcription feedback loop. *Proc Natl Acad Sci U S A* *103*, 10074–10079.

Klar, T., Kaiser, G., Hennecke, U., Carell, T., Batschauer, A., and Essen, L.-O. (2006). Natural and non-natural antenna chromophores in the DNA photolyase from *Thermus thermophilus*. *ChemBiochem* *7*, 1798–1806.

Ko, C.H., and Takahashi, J.S. (2006). Molecular components of the mammalian circadian clock. *Hum Mol Genet* *15 Spec No 2*, R271–R277.

Koike, N., Yoo, S.-H., Huang, H.-C., Kumar, V., Lee, C., Kim, T.-K., and Takahashi, J.S. (2012). Transcriptional Architecture and Chromatin Landscape of the Core Circadian Clock in Mammals. *Science Signaling* *338*, 349–354.

Kojima, S., Sher-Chen, E.L., and Green, C.B. (2012). Circadian control of mRNA polyadenylation dynamics regulates rhythmic protein expression. *Genes Dev* *26*, 2724–2736.

- Kramer, A.**, and Merrow, M. (2013). *Circadian Clocks* (Heidelberg: Springer).
- Kucera, N.**, Schmalen, I., Hennig, S., Öllinger, R., Strauss, H.M., Grudziecki, A., Wieczorek, C., Kramer, A., and Wolf, E. (2012). Unwinding the differences of the mammalian PERIOD clock proteins from crystal structure to cellular function. *Proc Natl Acad Sci U S A* *109*, 3311–3316.
- Kuchar, J.**, and Hausinger, R.P. (2004). Biosynthesis of metal sites. *Chem Rev* *104*, 509–525.
- Kume, K.**, Zylka, M.J., Sriram, S., Shearman, L.P., Weaver, D.R., Jin, X.W., Maywood, E.S., Hastings, M.H., and Reppert, S.M. (1999). mCRY1 and mCRY2 are essential components of the negative limb of the circadian clock feedback loop. *Cell* *98*, 193–205.
- Kurabayashi, N.**, Hirota, T., Sakai, M., Sanada, K., and Fukada, Y. (2010). DYRK1A and glycogen synthase kinase 3beta, a dual-kinase mechanism directing proteasomal degradation of CRY2 for circadian timekeeping. *Molecular and Cellular Biology* *30*, 1757–1768.
- Lamia, K.A.**, Papp, S.J., Yu, R.T., Barish, G.D., Uhlentaut, N.H., Jonker, J.W., Downes, M., and Evans, R.M. (2011). Cryptochromes mediate rhythmic repression of the glucocorticoid receptor. *Nature* *480*, 552–556.
- Lamia, K.A.**, Sachdeva, U.M., DiTacchio, L., Williams, E.C., Alvarez, J.G., Egan, D.F., Vasquez, D.S., Juguilon, H., Panda, S., Shaw, R.J., et al. (2009). AMPK regulates the circadian clock by cryptochrome phosphorylation and degradation. *326*, 437–440.
- Langmesser, S.**, Tallone, T., Bordon, A., Rusconi, S., and Albrecht, U. (2008). Interaction of circadian clock proteins PER2 and CRY with BMAL1 and CLOCK. *BMC Mol Biol* *9*, 41.
- Lee, C.**, Etchegaray, J.P., Cagampang, F.R., Loudon, A.S., and Reppert, S.M. (2001). Posttranslational mechanisms regulate the mammalian circadian clock. *Cell* *107*, 855–867.
- Lee, Y.**, Lee, J., Kwon, I., Nakajima, Y., Ohmiya, Y., Son, G.H., Lee, K.H., and Kim, K. (2010). Coactivation of the CLOCK-BMAL1 complex by CBP mediates resetting of the circadian clock. *J Cell Sci* *123*, 3547–3557.
- LeSauter, J.**, Hoque, N., Weintraub, M., Pfaff, D.W., and Silver, R. (2009). Stomach ghrelin-secreting cells as food-entrainable circadian clocks. *Proc Natl Acad Sci U S A* *106*, 13582–13587.
- Liu, A.C.**, Lewis, W.G., and Kay, S.A. (2007a). Mammalian circadian signaling networks and therapeutic targets. *Nat Chem Biol* *3*, 630–639.
- Liu, A.C.**, Welsh, D.K., Ko, C.H., Tran, H.G., Zhang, E.E., Priest, A.A., Buhr, E.D., Singer, O., Meeker, K., Verma, I.M., et al. (2007b). Intercellular coupling confers robustness against mutations in the SCN circadian clock network. *Cell* *129*, 605–616.
- Liu, C.**, Li, S., Liu, T., Borjigin, J., and Lin, J.D. (2007c). Transcriptional coactivator PGC-1alpha integrates the mammalian clock and energy metabolism. *Nature* *447*, 477–481.
- Loop, S.**, and Pieler, T. (2005). Nuclear import of mPER3 in *Xenopus* oocytes and HeLa cells requires complex formation with mPER1. *Febs J.* *272*, 3714–3724.
- Loop, S.**, Katzer, M., and Pieler, T. (2005). mPER1-mediated nuclear export of mCRY1/2 is an important element in establishing circadian rhythm. *EMBO Rep* *6*, 341–347.

- Loros, J.J., and Dunlap, J.C. (2000).** Genetic and molecular analysis of circadian rhythms in *Neurospora*. *Annu. Rev. Physiol.* *63*, 757–794.
- Lowrey, P.L., and Takahashi, J.S. (2004).** Mammalian circadian biology: Elucidating genome-wide levels of temporal organization. *Annu Rev Genomics Hum Genet* *5*, 407–441.
- Lowrey, P.L., and Takahashi, J.S. (2011).** Genetics of Circadian Rhythms in Mammalian Model Organisms. *Adv Genet* *74*, 175–230.
- Malhotra, K., Kim, S.T., Batschauer, A., Dawut, L., and Sancar, A. (2001).** Putative Blue-Light Photoreceptors From *Arabidopsis Thaliana* and *Sinapis Alba* with a High Degree of Sequence Homology to DNA Photolyase Contain the 2 Photolyase Cofactors but Lack DNA Repair Activity. *Biochemistry* *34*, 6892–6899.
- Marcheva, B., Ramsey, K.M., Buhr, E.D., Kobayashi, Y., Su, H., Ko, C.H., Ivanova, G., Omura, C., Mo, S., Vitaterna, M.H., et al. (2010).** Disruption of the clock components CLOCK and BMAL1 leads to hypoinsulinaemia and diabetes. *Nature* *466*, 627–631.
- Maret, W. (2006).** Zinc coordination environments in proteins as redox sensors and signal transducers. *Antioxid Redox Signal* *8*, 1419–1441.
- Maret, W. (2009).** Molecular aspects of human cellular zinc homeostasis: redox control of zinc potentials and zinc signals. *Biometals* *22*, 149–157.
- Maret, W. (2012).** New perspectives of zinc coordination environments in proteins. *Journal of Inorganic Biochemistry* *111*, 110–116.
- Maret, W., and Li, Y. (2009).** Coordination Dynamics of Zinc in Proteins. *Chem Rev* *109*, 4682–4707.
- Menet, J.S., Abruzzi, K.C., Desrochers, J., Rodriguez, J., and Rosbash, M. (2010).** Dynamic PER repression mechanisms in the *Drosophila* circadian clock: from on-DNA to off-DNA. *Genes Dev* *24*, 358–367.
- Menet, J.S., Rodriguez, J., Abruzzi, K.C., and Rosbash, M. (2012).** Nascent-Seq reveals novel features of mouse circadian transcriptional regulation. *Elife* *1*, e00011.
- Meng, Q.-J., Logunova, L., Maywood, E.S., Gallego, M., Lebiecki, J., Brown, T.M., Sládek, M., Semikhodskii, A.S., Glossop, N.R.J., Piggins, H.D., et al. (2008).** Setting clock speed in mammals: the CK1 epsilon tau mutation in mice accelerates circadian pacemakers by selectively destabilizing PERIOD proteins. *Neuron* *58*, 78–88.
- Miyazaki, K., Mesaki, M., and Ishida, N. (2001).** Nuclear Entry Mechanism of Rat PER2 (rPER2): Role of rPER2 in Nuclear Localization of CRY Protein. *Molecular and Cellular Biology* *21*, 6651–6659.
- Moore, R.Y., and Eichler, V.B. (1972).** Loss of a circadian adrenal corticosterone rhythm following suprachiasmatic lesions in the rat. *Brain Res.* *42*, 201–206.
- Möglich, A., Ayers, R.A., and Moffat, K. (2009).** Structure and signaling mechanism of Per-ARNT-Sim domains. *Structure* *17*, 1282–1294.

- Nakahata, Y., Kaluzova, M., Grimaldi, B., Sahar, S., Hirayama, J., Chen, D., Guarente, L.P., and Sassone-Corsi, P. (2007).** The NAD⁺-Dependent Deacetylase SIRT1 Modulates CLOCK-Mediated Chromatin Remodeling and Circadian Control. *Cell* *134*, 329–340.
- Nakahata, Y., Sahar, S., Astarita, G., Kaluzova, M., and Sassone-Corsi, P. (2009).** Circadian control of the NAD⁺ salvage pathway by CLOCK-SIRT1. *Science* *324*, 654–657.
- Nakashima, A., Kawamoto, T., Honda, K.K., Ueshima, T., Noshiro, M., Iwata, T., Fujimoto, K., Kubo, H., Honma, S., Yorioka, N., et al. (2008).** DEC1 modulates the circadian phase of clock gene expression. *Molecular and Cellular Biology* *28*, 4080–4092.
- Nemoto, S., Takeda, K., Yu, Z.X., Ferrans, V.J., and Finkel, T. (2000).** Role for mitochondrial oxidants as regulators of cellular metabolism. *Molecular and Cellular Biology* *20*, 7311–7318.
- O'Neill, J.S., and Reddy, A.B. (2011).** Circadian clocks in human red blood cells. *Nature* *469*, 498–503.
- Okamura, H., Miyake, S., Sumi, Y., Yamaguchi, S., Yasui, A., Muijtjens, M., Hoeijmakers, J.H., and van der Horst, G.T. (1999).** Photic induction of mPer1 and mPer2 in cry-deficient mice lacking a biological clock. *Science* *286*, 2531–2534.
- Okano, S., Akashi, M., Hayasaka, K., and Nakajima, O. (2009).** Unusual circadian locomotor activity and pathophysiology in mutant CRY1 transgenic mice. *Neuroscience Letters* *451*, 246–251.
- Okano, S., Hayasaka, K., Igarashi, M., Iwai, H., Togashi, Y., and Nakajima, O. (2010).** Non-obese early onset diabetes mellitus in mutant cryptochrome1 transgenic mice. *European Journal of Clinical Investigation* *40*, 1011–1017.
- Oster, H., Yasui, A., van der Horst, G., and Albrecht, U. (2002).** Disruption of mCry2 restores circadian rhythmicity in mPer2 mutant mice. *Genes Dev* *16*, 2633–2638.
- Oteiza, P.I. (2012).** Zinc and the modulation of redox homeostasis. *Free Radical Biology and Medicine* *53*, 1748–1759.
- Ozber, N., Baris, I., Tatlici, G., Gur, I., Kilinc, S., Unal, E.B., and Kavakli, I.H. (2010).** Identification of two Amino Acids in the C-terminal Domain of Mouse CRY2 Essential for PER2 Interaction. *BMC Mol Biol* *11*, 69.
- Ozgur, S., and Sancar, A. (2003).** Purification and properties of human blue-light photoreceptor cryptochrome 2. *Biochemistry* *42*, 2926–2932.
- Ozturk, N., Selby, C.P., Annayev, Y., Zhong, D., and Sancar, A. (2011).** Reaction mechanism of Drosophila cryptochrome. *Proc Natl Acad Sci U S A* *108*, 516–521.
- Padmanabhan, K., Robles, M.S., Westerling, T., and Weitz, C.J. (2012).** Feedback regulation of transcriptional termination by the mammalian circadian clock PERIOD complex. *Science* *337*, 599–602.
- Panda, S., Antoch, M.P., Miller, B.H., Su, A.I., Schook, A.B., Straume, M., Schultz, P.G., Kay, S.A., Takahashi, J.S., and Hogenesch, J.B. (2002).** Coordinated transcription of key pathways in the mouse by the circadian clock. *Cell* *109*, 307–320.

- Peek, C.B., Affinati, A.H., Ramsey, K.M., Kuo, H.-Y., Yu, W., Sena, L.A., Ilkayeva, O., Marcheva, B., Kobayashi, Y., Omura, C., et al. (2013).** Circadian clock NAD⁺ cycle drives mitochondrial oxidative metabolism in mice. *Science* *342*, 1243417.
- Pendergast, J.S., Niswender, K.D., and Yamazaki, S. (2012).** Tissue-specific function of Period3 in circadian rhythmicity. *PLoS One* *7*, e30254.
- Peschel, N., Chen, K.F., Szabo, G., and Stanewsky, R. (2009).** Light-dependent interactions between the *Drosophila* circadian clock factors cryptochrome, jetlag, and timeless. *Curr. Biol.* *19*, 241–247.
- Preitner, N., Damiola, F., Damiola, F., Zakany, J., Duboule, D., Albrecht, U., and Schibler, U. (2002).** The Orphan Nuclear Receptor REV-ERB α Controls Circadian Transcription within the Positive Limb of the Mammalian Circadian Oscillator. *Cell* *110*, 251–260.
- Quintero, J.E., Kuhlman, S.J., and McMahan, D.G. (2003).** The biological clock nucleus: A multiphasic oscillator network regulated by light. *J Neurosci* *23*, 8070–8076.
- Ralph, M.R., Foster, R.G., Davis, F.C., and Menaker, M. (1990).** Transplanted suprachiasmatic nucleus determines circadian period. *Science* *247*, 975–978.
- Reppert, S.M., and Weaver, D.R. (2001).** Molecular analysis of mammalian circadian rhythms. *Annu. Rev. Physiol.* *63*, 647–676.
- Ripperger, J., and Schibler, U. (2006).** Rhythmic CLOCK-BMAL1 binding to multiple E-box motifs drives circadian Dbp transcription and chromatin transitions. *Nat Genet* *38*, 369–374.
- Ripperger, J.A., and Albrecht, U. (2011).** The circadian clock component PERIOD2: from molecular to cerebral functions. *Prog Brain Res* *199*, 233–245.
- Rodgers, J.T., Lerin, C., Haas, W., Gygi, S.P., Spiegelman, B.M., and Puigserver, P. (2005).** Nutrient control of glucose homeostasis through a complex of PGC-1 α and SIRT1. *Nature* *434*, 113–118.
- Rutter, J., Reick, M., Wu, L.C., and McKnight, S.L. (2001).** Regulation of clock and NPAS2 DNA binding by the redox state of NAD cofactors. *Science* *293*, 510–514.
- Saez, L., and Young, M.W. (1996).** Regulation of Nuclear Entry of the *Drosophila* Clock Proteins Period and Timeless. *Neuron* *17*, 911–920.
- Sahar, S., Zocchi, L., Kinoshita, C., Borrelli, E., and Sassone-Corsi, P. (2010).** Regulation of BMAL1 Protein Stability and Circadian Function by GSK3 β -Mediated Phosphorylation. *PLoS One* *5*, e8561.
- Salmeen, A., Andersen, J.N., Myers, M.P., Meng, T.-C., Hinks, J.A., Tonks, N.K., and Barford, D. (2003).** Redox regulation of protein tyrosine phosphatase 1B involves a sulphenyl-amide intermediate. *Nature* *423*, 769–773.
- Sanada, K., Okano, T., and Fukada, Y. (2002).** Mitogen-activated protein kinase phosphorylates and negatively regulates basic helix-loop-helix-PAS transcription factor BMAL1. *J Biol Chem* *277*, 267–271.

- Sato, T.K., Yamada, R.G., Ukai, H., Baggs, J.E., Miraglia, L.J., Kobayashi, T.J., Welsh, D.K., Kay, S.A., Ueda, H.R., and Hogenesch, J.B. (2006).** Feedback repression is required for mammalian circadian clock function. *Nat Genet* **38**, 312–319.
- Schmalen, I., Reischl, S., Wallach, T., Klemz, R., Grudziecki, A., Prabu, J.R., Benda, C., Kramer, A., and Wolf, E. (2014).** Interaction of Circadian Clock Proteins CRY1 and PER2 Is Modulated by Zinc Binding and Disulfide Bond Formation. *Cell* **157**, 1203–1215.
- Schmutz, I., Ripperger, J.A., Baeriswyl-Aebischer, S., and Albrecht, U. (2010).** The mammalian clock component PERIOD2 coordinates circadian output by interaction with nuclear receptors. *Genes Dev* **24**, 345–357.
- Selby, C.P., and Sancar, A. (2012).** The second chromophore in *Drosophila* photolyase/cryptochrome family photoreceptors. *Biochemistry* **51**, 167–171.
- Shearman, L.P., Jin, X., Lee, C., Reppert, S.M., and Weaver, D.R. (2000a).** Targeted disruption of the mPer3 gene: subtle effects on circadian clock function. *Molecular and Cellular Biology* **20**, 6269–6275.
- Shearman, L.P., Sriram, S., Weaver, D.R., Maywood, E.S., Chaves, I., Zheng, B., Kume, K., Lee, C.C., van der Horst, G.T., Hastings, M.H., et al. (2000b).** Interacting molecular loops in the mammalian circadian clock. *Science* **288**, 1013–1019.
- Shearman, L.P., Zylka, M.J., Weaver, D.R., Kolakowski, L.F., and Reppert, S.M. (1997).** Two period homologs: circadian expression and photic regulation in the suprachiasmatic nuclei. *Neuron* **19**, 1261–1269.
- Shirogane, T., Jin, J., Ang, X.L., and Harper, J.W. (2005).** SCF β -TRCP controls clock-dependent transcription via casein kinase 1-dependent degradation of the mammalian period-1 (Per1) protein. *J Biol Chem* **280**, 26863–26872.
- Stephan, F.K., and Zucker, I. (1972).** Circadian rhythms in drinking behavior and locomotor activity of rats are eliminated by hypothalamic lesions. *Proc Natl Acad Sci U S A* **69**, 1583–1586.
- Storch, K.-F., Lipan, O., Leykin, I., Viswanathan, N., Davis, F.C., Wong, W.H., and Weitz, C.J. (2002).** Extensive and divergent circadian gene expression in liver and heart. *Nature* **417**, 78–83.
- Sun, Z.S., Albrecht, U., Zhuchenko, O., Bailey, J., Eichele, G., and Lee, C.C. (1997).** RIGUI, a putative mammalian ortholog of the *Drosophila* period gene. *Cell* **90**, 1003–1011.
- Suzuki, H., Tashiro, S., Hira, S., Sun, J., Yamazaki, C., Zenke, Y., Ikeda-Saito, M., Yoshida, M., and Igarashi, K. (2004).** Heme regulates gene expression by triggering Crm1-dependent nuclear export of Bach1. *The EMBO Journal* **23**, 2544–2553.
- Takano, A., Shimizu, K., Kani, S., Buijs, R.M., Okada, M., and Nagai, K. (2000).** Cloning and characterization of rat casein kinase 1epsilon. *FEBS Lett* **477**, 106–112.
- Takano, A., Isojima, Y., and Nagai, K. (2004).** Identification of mPer1 phosphorylation sites responsible for the nuclear entry. *J Biol Chem* **279**, 32578–32585.
- Tei, H., Okamura, H., Shigeyoshi, Y., Fukuhara, C., Ozawa, R., Hirose, M., and Sakaki, Y. (1997).**

Circadian oscillation of a mammalian homologue of the *Drosophila* period gene. *Nature* 389, 512–516.

Thresher, R.J.R., Vitaterna, M.H.M., Miyamoto, Y.Y., Kazantsev, A.A., Hsu, D.S.D., Petit, C.C., Selby, C.P.C., Dawut, L.L., Smithies, O.O., Takahashi, J.S.J., et al. (1998). Role of mouse cryptochrome blue-light photoreceptor in circadian photoresponses. *Science* 282, 1490–1494.

Toh, K.L., Jones, C.R., He, Y., Eide, E.J., Hinze, W.A., Virshup, D.M., Ptáček, L.J., and Fu, Y.H. (2001). An hPer2 phosphorylation site mutation in familial advanced sleep phase syndrome. *Science* 291, 1040–1043.

Tomita, T., Miyazaki, K., Onishi, Y., Honda, S., Ishida, N., and Oishi, K. (2010). Conserved amino acid residues in C-terminus of PERIOD 2 are involved in interaction with CRYPTOCHROME 1. *Biochim. Biophys. Acta* 1803, 492–498.

Tsuchiya, Y., Akashi, M., Matsuda, M., Goto, K., Miyata, Y., Node, K., and Nishida, E. (2009). Involvement of the protein kinase CK2 in the regulation of mammalian circadian rhythms. *Science Signaling* 2, ra26.

Ueda, H.R., Hayashi, S., Chen, W., Sano, M., Machida, M., Shigeyoshi, Y., Iino, M., and Hashimoto, S. (2005). System-level identification of transcriptional circuits underlying mammalian circadian clocks. *Nat Genet* 37, 187–192.

Ukai-Tadenuma, M., Yamada, R.G., Xu, H., Ripperger, J.A., Liu, A.C., and Ueda, H.R. (2011). Delay in Feedback Repression by Cryptochrome 1 Is Required for Circadian Clock Function. *Cell* 144, 268–281.

van der Horst, G.T.J., Muijtjens, M., Kobayashi, K., Takano, R., Kanno, S.-I., Takao, M., Wit, J. de, Verkerk, A., Eker, A.P.M., Leenen, D.V., et al. (1999). Mammalian Cry1 and Cry2 are essential for maintenance of circadian rhythms. *Nature* 398, 627–630.

Vanselow, K., Vanselow, J.T., Westermarck, P.O., Reischl, S., Maier, B., Korte, T., Herrmann, A., Herzog, H., Schlotter, A., and Kramer, A. (2006). Differential effects of PER2 phosphorylation: molecular basis for the human familial advanced sleep phase syndrome (FASPS). *Genes Dev* 20, 2660–2672.

Vielhaber, E.L., Duricka, D., Ullman, K.S., and Virshup, D.M. (2001). Nuclear export of mammalian PERIOD proteins. *J Biol Chem* 276, 45921–45927.

Viola, A.U., Archer, S.N., James, L.M., Groeger, J.A., Lo, J.C.Y., Skene, D.J., Schantz, von, M., and Dijk, D.-J. (2007). PER3 polymorphism predicts sleep structure and waking performance. *Curr. Biol.* 17, 613–618.

Vitaterna, M.H., King, D.P., Chang, A.M., Kornhauser, J.M., Lowrey, P.L., McDonald, J.D., Dove, W.F., Pinto, L.H., Turek, F.W., and Takahashi, J.S. (1994). Mutagenesis and Mapping of a Mouse Gene Clock, Essential for Circadian Behavior. *Science* 264, 719–725.

Vitaterna, M.H., Selby, C.P., Todo, T., Niwa, H., Thompson, C., Fruechte, E.M., Hitomi, K., Thresher, R.J., Ishikawa, T., Miyazaki, U., et al. (1999). Differential regulation of mammalian period genes and circadian rhythmicity by cryptochromes 1 and 2. *Proc Natl Acad Sci U S A* 96, 12114–12119.

- Wang, T.A., Yu, Y.V., Govindaiah, G., Ye, X., Artinian, L., Coleman, T.P., Sweedler, J.V., Cox, C.L., and Gillette, M.U. (2012a).** Circadian Rhythm of Redox State Regulates Excitability in Suprachiasmatic Nucleus Neurons. *Science* **337**, 839–842.
- Wang, X., Mozhui, K., Li, Z., Mulligan, M.K., Ingels, J.F., Zhou, X., Hori, R.T., Chen, H., Cook, M.N., Williams, R.W., et al. (2012).** A promoter polymorphism in the *Per3* gene is associated with alcohol and stress response. *Transl Psychiatry* **2**, e73.
- Wang, Y., Yang, J., and Yi, J. (2012b).** Redox Sensing by Proteins: Oxidative Modifications on Cysteines and the Consequent Events. *Antioxid Redox Signal* **16**, 649–657.
- Wu, N., Yin, L., Hanniman, E.A., Joshi, S., and Lazar, M.A. (2009).** Negative feedback maintenance of heme homeostasis by its receptor, Rev-erb α . *Genes Dev* **23**, 2201–2209.
- Xing, W., Busino, L., Hinds, T.R., Marionni, S.T., Saifee, N.H., Bush, M.F., Pagano, M., and Zheng, N. (2013).** SCFFBXL3 ubiquitin ligase targets cryptochromes at their cofactor pocket. *Nature* **496**, 64–68.
- Xu, Y., Toh, K.L., Jones, C.R., Shin, J.-Y., Fu, Y.H., and Ptáček, L.J. (2006).** Modeling of a Human Circadian Mutation Yields Insights into Clock Regulation by *PER2*. *Cell* **128**, 59–70.
- Yagita, K., Tamanini, F., van der Horst, G.T., and Okamura, H. (2001).** Molecular mechanisms of the biological clock in cultured fibroblasts. *Science* **292**, 278–281.
- Yagita, K., Yamaguchi, S., Tamanini, F., van der Horst, G., Hoeijmakers, J., Yasui, A., Loros, J.J., Dunlap, J.C., and Okamura, H. (2000).** Dimerization and nuclear entry of mPER proteins in mammalian cells. *Genes Dev* **14**, 1353–1363.
- Yagita, K., Tamanini, F., Yasuda, M., Hoeijmakers, J.H.J., van der Horst, G.T.J., and Okamura, H. (2002).** Nucleocytoplasmic shuttling and mCRY-dependent inhibition of ubiquitylation of the mPER2 clock protein. *The EMBO Journal* **21**, 1301–1314.
- Yakir, E., Hilman, D., Harir, Y., and Green, R.M. (2006).** Regulation of output from the plant circadian clock. *Febs J.* **274**, 335–345.
- Yamaguchi, S., Isejima, H., Matsuo, T., Okura, R., Yagita, K., Kobayashi, M., and Okamura, H. (2003).** Synchronization of cellular clocks in the suprachiasmatic nucleus. *Science* **302**, 1408–1412.
- Yamajuku, D., Shibata, Y., Kitazawa, M., Katakura, T., Urata, H., Kojima, T., Takayasu, S., Nakata, O., and Hashimoto, S. (2011).** Cellular DBP and E4BP4 proteins are critical for determining the period length of the circadian oscillator. *FEBS Lett* **585**, 2217–2222.
- Yang, J., Kim, K.D., Lucas, A., Drahos, K.E., Santos, C.S., Mury, S.P., Capelluto, D.G.S., and Finkielstein, C.V. (2008).** A novel heme-regulatory motif mediates heme-dependent degradation of the circadian factor period 2. *Molecular and Cellular Biology* **28**, 4697–4711.
- Yang, X., Downes, M., Yu, R.T., Bookout, A.L., He, W., Straume, M., Mangelsdorf, D.J., and Evans, R.M. (2006).** Nuclear receptor expression links the circadian clock to metabolism. *Cell* **126**, 801–810.
- Ye, R., Selby, C.P., Ozturk, N., Annayev, Y., and Sancar, A. (2011).** Biochemical analysis of the

canonical model for the mammalian circadian clock. *286*, 25891–25902.

Yildiz, O., Doi, M., Yujnovsky, I., Cardone, L., Berndt, A., Hennig, S., Schulze, S., Urbanke, C., Sassone-Corsi, P., and Wolf, E. (2005). Crystal structure and interactions of the PAS repeat region of the *Drosophila* clock protein PERIOD. *Mol. Cell* *17*, 69–82.

Yoo, S.-H., Mohawk, J.A., Siepkka, S.M., Shan, Y., Huh, S.K., Hong, H.-K., Kornblum, I., Kumar, V., Koike, N., Xu, M., et al. (2013). Competing E3 Ubiquitin Ligases Govern Circadian Periodicity by Degradation of CRY in Nucleus and Cytoplasm. *Cell* *152*, 1091–1105.

Yoo, S.-H., Yamazaki, S., Lowrey, P.L., Shimomura, K., Ko, C.H., Buhr, E.D., Siepkka, S.M., Hong, H.-K., Oh, W.J., Yoo, O.J., et al. (2004). PERIOD2::LUCIFERASE real-time reporting of circadian dynamics reveals persistent circadian oscillations in mouse peripheral tissues. *Proc Natl Acad Sci U S A* *101*, 5339–5346.

Zhang, E.E., and Kay, S.A. (2010). Clocks not winding down: unravelling circadian networks. *Nat. Rev. Mol. Cell Biol.* *11*, 764–776.

Zhang, E.E., Liu, Y., Dentin, R., Pongsawakul, P.Y., Liu, A.C., Hirota, T., Nusinow, D.A., Sun, X., Landais, S., Kodama, Y., et al. (2010). Cryptochrome mediates circadian regulation of cAMP signaling and hepatic gluconeogenesis. *Nat Med* *16*, 1152–1156.

Zheng, B., Albrecht, U., Kaasik, K., Sage, M., Lu, W., Vaishnav, S., Li, Q., Sun, Z.S., Eichele, G., Bradley, A., et al. (2001). Nonredundant roles of the *mPer1* and *mPer2* genes in the mammalian circadian clock. *Cell* *105*, 683–694.

Zheng, B., Larkin, D.W., Albrecht, U., Sun, Z.S., Sage, M., Eichele, G., Lee, C.C., and Bradley, A. (1999). The *mPer2* gene encodes a functional component of the mammalian circadian clock. *Nature* *400*, 169–173.

Zylka, M.J., Shearman, L.P., Levine, J.D., Jin, X.W., Weaver, D.R., and Reppert, S.M. (1998a). Molecular analysis of mammalian *timeless*. *Neuron* *21*, 1115–1122.

Zylka, M.J., Shearman, L.P., Weaver, D.R., and Reppert, S.M. (1998b). Three period homologs in mammals: differential light responses in the suprachiasmatic circadian clock and oscillating transcripts outside of brain. *Neuron* *20*, 1103–1110.

Acknowledgements

Finally, I would like to name and thank all people who supported me the last 4.5 years.

I acknowledge Prof. Dr. E. Wolf for giving me the chance to work on circadian clocks, for supervising this thesis and the trust in me. I am very grateful to Prof. Dr. E. Conti for hosting me in the outstanding department of Structural Cell Biology at the Max Planck Institute of Biochemistry, for being member of my TAC committee and her never ending support and advice. I would like to thank Prof. Dr. J. Soll for the chance to defend my thesis at the Faculty of Biology at the Ludwig-Maximilians-Universität München, for being member of my TAC and his scientific suggestions. In addition, I would like to thank the members of my committee, Prof. Dr. C. David, Prof. Dr. W. Enard and Prof. Dr. H. Jung, the German National Academic Foundation (“Studienstiftung des deutschen Volkes”) and the International Max Planck Research School for Molecular and Cellular Life Sciences (IMPRS-LS).

Very special thanks to the whole Wolf, Conti, Lorentzen, Biertümpfel and Mizuno labs for creating a unique atmosphere in the department, which I very much enjoyed working in, for scientific ideas and discussions and the great time we spend together.

Particularly I would like to thank Justine for being my friend and fellow lab member in all these years. Thank you for sharing knowledge, for your support, for listening, for cheering me up, ... for everything!

Furthermore, I greatly thank Lena, Regina, Janina, Felice, Rajan, Manu, Marina, Mela, Krissy, Taschi, Marc, Sibylle, Eva, Ingmar, Christian, Sebastian and Bahram for being amazing friends and making me laugh; I am so lucky that we have met!

Zu guter Letzt möchte ich mich bei meiner Familie bedanken, die mich in all den Jahren meines Studiums und meiner Promotion geduldig unterstützt hat und mir immer mit Rat und Tat zur Seite gestanden ist. Sie hat mich daran erinnert hat, dass das die wichtigen Dinge des Lebens nicht im Labor stattfinden. Ohne Christa, Klaus, Hanna, Christoph, Gracia, Felix und Maria hätte ich es nicht bis hierhin geschafft!